FUNDAMENTAL STUDIES ON IONOMER GLASSES

BY

DAVID JOHN WOOD

A thesis submitted for the degree of

Doctor of Philosophy

in the

DEPARTMENT OF BIOLOGICAL AND CHEMICAL

SCIENCES

UNIVERSITY OF GREENWICH

May 1993

University Of Greenwich
Woolwich, London

This thesis is dedicated to the memories of my Father and Grandmother

ACKNOWLEDGEMENTS

I would like to thank all my supervisors, especially Robert Hill for his endless patience and guidance. I would also like to thank all the technicians at the University of Greenwich and the staff at the Laboratory of the Government Chemist for the help they gave in various aspects of the work. I would finally like to thank my friends and especially my mum for their continued support and encouragement.

This work was funded on a CASE award by SERC and the Laboratory of the Government Chemist.

FOREWORD

Much of the content of this thesis has been presented in journals or at conferences. A list of publications is given in Appendix B, at the back of this thesis.

Since this project was conceived, glass-ionomer cements have been promoted commercially as bone substitute materials for ridge augmentation operations in maxillofacial surgery, as ear bones and as bone plates for the repair of cranial defects.

ABSTRACT

Composition-structure-property relationships were studied in glasses of the type used to produce glass ionomer dental cements. These materials are currently being developed as a bone cement in joint replacement surgery.

Initially, a simple quaternary ($2SiO_2$-Al_2O_3-CaO-CaF_2) glass was produced and was found to undergo minimal fluorine loss. This results in a glass whose composition is reproducible between batches.

This composition, however, was too reactive to form a glass ionomer cement. A glass-ceramic approach was pursued to deactivate the glass and following heat treatments, cements were produced whose properties varied depending upon the precise heat treatment used.

The heat treatments above the glass transition temperature resulted in amorphous phase separation, probably by a spinodal decomposition mechanism, followed by a two stage crystallization of calcium fluoride (fluorite) and anorthite. The anorthite phase crystallized from fluorite nuclei and, in effect, crystallization occurred by a bulk nucleation mechanism.

The glass will also undergo significant crystallization to fluorite below the glass transition temperature, with surface nucleation the dominant mechanism. This explains the deactivation of ionomer glasses used commercially to control the setting properties of dental glass ionomer cements.

The structural role of fluorine in these glasses was also investigated. It seems that fluorine is present in the glass network, rather than existing as a discreet entity bonded to a modifying cation. There is evidence that the fluoride ions are bonded only to aluminium sites and act to disrupt network connectivity.

A commercial glass was examined and was found to be clearly phase separated. This glass was found to crystallize to apatite and mullite. Apatite is the mineral phase of bone and enamel and this may explain the excellent biocompatability of glass ionomer cements .

Glasses containing sodium and phosphate ions have also been produced. The sodium containing glasses were all found to crystallize from the melt to calcium fluoride. The phosphate containing glasses formed cements without any subsequent modification, and following a simple heat treatment, all of the phosphate containing glasses were found again to crystallize initially to an apatite phase.

Selected compositions additionally crystallized to mullite. These glass-ceramics were tougher than the base glasses and this is attributed to the presence of interlocking needles of the two phases. Some of the glasses were easily castable to produce optically clear glasses, and in addition the glasses underwent bulk nucleation via prior amorphous phase separation, to give needles of apatite and mullite. These glass-ceramics thus show tremendous potential for use as a bioactive bone substitute material or as a castable crown.

Contents Page

1.INTRODUCTION

Over the last 25 years, joint replacement operations have become an established and routine part of orthopaedic surgery. Prior to this time, however, many different materials were tried by surgeons in an attempt to achieve clinical success in arthroplasty. It was not until Charnley[1] developed the low friction hip prosthesis that the first breakthrough was achieved.

Early attempts at joint replacements failed not only because of the inadequate properties of the materials, but also because of the difficulties in obtaining a secure and reliable fixation to bone[2]. This was overcome by the introduction of poly(methylmethacrylate), which has now been successfully used as an orthopaedic cement for a number of years. PMMA is used as a fixation agent for arthroplasties in general, but finds particular use in cementing the acetabular and femoral components of the total hip joint arthroplasty.

1.1 THE HIP JOINT ARTHROPLASTY

Replacement of the hip joint is the most commonly performed arthroplasty, and the one which achieves the highest success rate of all artificial joints. The great majority of replacements are carried out in patients with rheumatoid arthritis and similar inflammatory joint diseases such as osteoarthritis or ankylosing spondylitis.

Other conditions treated by arthroplasty include osteoporosis, Pagets disease and Stills disease. More rarely, a replacement operation may be carried out to treat avascular necrosis following a fracture of the femoral head or to treat a malignant tumour. Tumours may either be primary (i.e. they arise from the bone itself) or secondary (i.e. they are metastatic deposits from tumours of other tissues).

The conventional Charnley hip arthroplasty consists of a plastic (ultra high molecular weight polyethylene) acetabular cup and a metal stemmed femoral component as shown below in Figure 1.

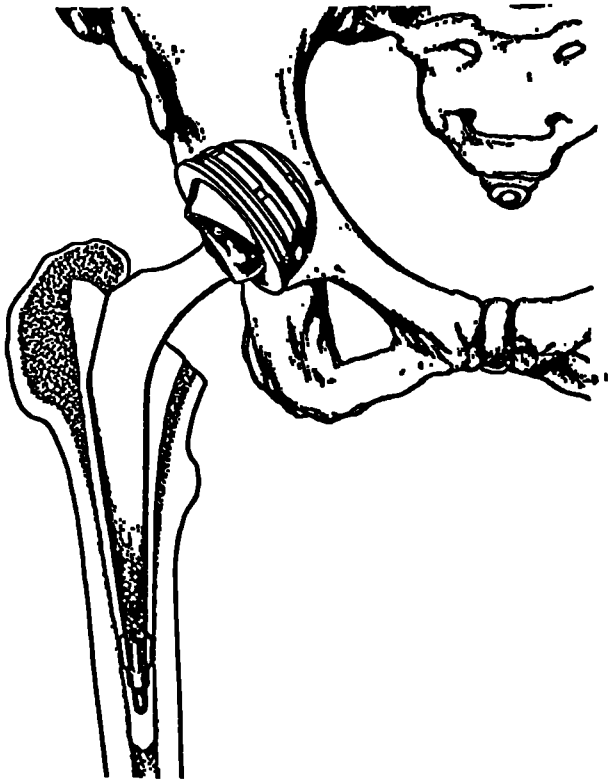

Figure 1
The Charnley Hip Joint

In a typical operation, the femoral head is removed and the medullary cavity reamed to accommodate the prosthesis. Bone cement is then placed in the cavity and

an *in situ* polymerisation of the PMMA bone cement.

PMMA has a number of attractive properties which makes it the accepted material for these applications[3]; these include acceptable biocompatibility and biodurability, ease of handling (setting time approx. 8 mins), low water absorption and good dimensional stability.

There remain, however, reservations about the suitability of PMMA in these situations. Despite being called a bone cement, PMMA is no more than a mechanical plug to fill the space between the bone and the implant; it is adhesive to neither. It achieves its supportive function merely by being tightly packed around the prosthetic component and interlocking into the cancellous bone immediately adjacent to the cortex.

The polymerisation reaction to form PMMA is very exothermic and can result in thermal necrosis of the adjacent bone tissue. It is suggested that provided the maximum temperature at the cement-tissue interface is below 50°C, there is little chance of such necrosis occurring. The exotherm during PMMA polymerisation can reach 110°C, although the temperature upon placement in the body will probably be less than this.

The unreacted bone cement actually consists of a mixture of poly(methylmethacrylate) powders and methylmethacrylate monomer liquid. After polymerisation, the resulting cement structure is heterogeneous and contains voids and inclusions which act as stress concentrators and consequently, sites for nucleation and

propagation of cracks through the bone cement.

Additionally, if the polymerisation is not taken to completion, there can also be a systemic effect caused by residual methylmethacrylate monomer units. The free monomer can enter the bodies' circulatory system and can lead to reduced blood pressure and an increase in the risk of heart attack.

Other problems are related to the low values for mechanical stiffness and strength, relative to those of bone. This results in poor or uneven stress transfer from the high modulus prosthesis to the much lower modulus bone. In order for bone growth to occur, the bone must be subject to a stress otherwise it will resorb from the implant and cause failure. This phenomenon is known as stress shielding.

Another important concern is post surgical, aseptic loosening of the cemented joint. Into this category come the problems caused by the patients' age, weight, activity, surgical technique, host tissue rejection of the implant and cement preparation. The most common cause of aseptic loosening, however, is failure of the cement itself (cohesive failure) or failure of the cement-bone (biomechanical) or cement-implant (mechanical) interfaces. It has been suggested that[4] creep may have a great significance in this phenomena. This problem coupled with the lack of adhesion and thermal necrosis of acrylic cements is thought to be the major cause of bone resorption and corresponding implant loosening and eventual failure,

which typically takes place after approximately 10-15 years.

Given that, worldwide, there are some 450,000 total hip replacements[5] carried out annually (~42,500 in the UK alone), a conservatively estimated failure rate of typically 10% has important implications in terms of the need for revision surgery, which can be an arduous task involving the retrieval of the primary prosthesis and cement.

Furthermore, many surgeons are reluctant to use acrylic cement in younger patients. In these cases, even the most optimistic predicted lifetimes for a prosthesis fall well short of the life expectancy of the patient; revision surgery will usually be necessary at a later date. In addition, these patients will generally put greater demands on the implant, due to a more active lifestyle. This will lead to greater mechanical stresses on the implant, which, in turn, will make the prognosis less certain in the long term. If you also take into account the need for a long term solution in replacing other joints such as the knee, improvements both in materials and surgical technique have great implications.

There is thus intense interest in developing new cements; and indeed cementless prostheses.

1.1.1 Cementless Prostheses

These prostheses are being developed based on the concept that the implant material should play an active role in the tissue forming processes. The prosthesis should also promote the formation of a coherent interface, capable of carrying the stresses which occur at the insertion site[6]. Such prostheses consist of either implants which are themselves made from surface-porous materials[7,8] or metal implants which have a suitable porous surface coating, such as a bioceramic[9,10] (see section 1.12). The role of such surfaces is to hopefully stimulate bone growth up to and into the prosthesis, a process called osteointegration.

The porous coating can be achieved via minute balls or loosely wound wire which are either cast with the prosthesis or applied afterwards. However, osteointegration with this system is incomplete, often occurring in only 2-5% of the porous coating and to a depth varying from 20 angstroms to a few microns.[11]

Ideally, the prosthesis should preserve the anatomical dynamics of the hip joint, i.e. proximal load transfer of bodyweight through the leg. However, in the femoral canal, with a cementless system, load is only transferred where the component is in contact with cortical bone. Uneven load transfer at the distal end of the prosthesis can thus lead to stress shielding with bone being resorbed. A good fit of implant to bone is therefore more critical in a cementless system; this requires careful preparation of the acetabulum and femur to achieve the best fit.

Furthermore, from a materials standpoint, neither the long term stability nor the optimum physical or chemical properties of such materials has been established.

1.1.2 Cemented Prostheses

Alternative cements which have been or are currently being investigated include: epoxy resins[12], fibre[13] or particle[14] reinforced PMMA cements to achieve better strength or PMMA cement coupled with hydroxyapatite granules to promote biocompatibility; a so called 'interface bioactive bone cement'[15]. There is also interest in developing protein based adhesives[16], such as fibrin which currently finds use as an adhesive in cartilage/bone grafting. Kokubo et al [17] have recently developed a 'bioactive' bone cement based on the reaction between a $CaO-SiO_2-P_2O_5$ glass and a phosphate ion-containing aqueous solution, but this cement sets too quickly to be of practical use. Behiri et al[18] are working on PEMA cements containing up to 40 % of silane-coated hydroxyapatite particles which improve the Youngs modulus and compliant nature of the cement.

One potentially attractive solution to the problem of bone cements is the use of the glass-ionomer cement (GIC)[19]. [N.B. The correct name for a glass ionomer cement is a glass polyalkenoate cement, the term 'ionomer' is misleading in that the polymer used in the cement is not an ionomer. However, the name has persisted over the years and is still the more commonly used term.] This is a material

which has its origins in the field of restorative dentistry where it currently finds use as a tooth filling material. Indeed, the properties required of a dental cement and a bone cement are very similar.

Smiths' design criteria[20] for an adhesive dental cement apply equally well for a bone cement and can thus be rewritten that 'an adhesive bone cement should

(i) wet and spread on the prepared bone surface *and*

(ii) react chemically with the mineral and/or protein phases in the bone surface.'

In addition to those mentioned, Hastings[12], and more recently, Perek and Pilliar[21], have postulated that the following characteristics should be shown by a (hard) tissue adhesive:

(i) rapid but controllable hardening

(ii) high initial tack to give primary fixation with possibility of manipulation before setting

(iii) setting without additional chemical catalysts is ideal but not always obtainable

(iv) must harden in wet environment

(v) should give adequate bond strength to tissues

(vi) long term stability *in vivo*

(vii) maintenance of bond strength in the presence of water

(viii) absence of toxic ingredients (including carcinogens and allergens) with regard to the quantities of adhesive to be used

(ix) ease of preparation for use in operating theatre, including short but adequate working time if mixing is needed

(x) must be sterilizable by recognised methods

(xi) packaged in a form allowing aseptic handling and transfer

(xii) adequate shelf life under range of ambient conditions

(xiii) ease of production on a large scale

The glass-ionomer cement fulfils all of these criteria. In particular, the excellent chemical adhesion of the glass-ionomer cement to stainless steel and other prosthetic alloys and to bone offers a major advantage over PMMA.

Another advantage is that there is no exotherm during the setting reaction and thus no thermal necrosis of bone tissue. A further problem resulting from this exotherm is that it limits the choice of antibiotics which can be 'loaded' into the PMMA cement to help post-operative recovery. Glass-ionomers, having no exotherm and a hydrophillic matrix, should provide a far better medium for the release of antibiotics or growth hormones.

In addition, the glass-ionomer undergoes minimal shrinkage, *in situ* and its' modulus can be matched to that of bone enabling good stress transfer to occur. This should reduce stress shielding. Glass-ionomers have been shown to be biocompatible in the bone environment. Indeed, Jonck et

al[22,23] claim they are bioactive in the bone environment; that is, they actively promote bone growth. Brook et al [24,25] have recently looked at existing glass ionomer cements for use as bone substitute materials in maxillofacial surgery. These gave promising biocompatibility results in both *in vitro* and *in vivo* studies, but there was a slight cytotoxicity in vitro associated with a leachate from fluorine and phosphate containing glass, that was not present in a simpler system. This response has also been seen by other workers[26]. However, fluorine containing Bioglasses suggest fluorine ions may have a beneficial effect[27] and Jonck et al have shown that fluorine containing glass-ionomer cements induce bone formation in vivo and are superior to fluorine and phosphate free materials. It is likely that low levels of fluoride ion release are beneficial whilst high levels may lead to a local toxic response. Fluoride ion release is probably not only dependant on the fluorine content of the glasses but also on the presence of soluble and insoluble counter ions within the glass. The excellent biocompatibility of glass-ionomer cements is not perhaps surprising since ionomer glasses are similar in many ways to Bioglass[28], which releases Ca^{2+}, PO_4^{2-} and F^- ions across the glass-bone interface.

The glass-ionomer cement has been used in dentistry for over twenty years, but can trace its development further back to dental silicate cements[29] and zinc polycarboxylate cements[20]. Indeed, glass-ionomers can to a

large extent be regarded as a logical progression from these earlier materials; combining the high compressive strength of the dental silicate, together with the adhesion and blandness of the zinc polycarboxylate. It is thus useful to comment on these materials and their role in the development of the glass -ionomer cement.

1.2 DENTAL SILICATE CEMENTS

The first record of a 'silicate cement' was in 1878 when T. Fletcher took out a patent for making a translucent dental material. The cement was formed by dissolving aluminium phosphate or pyrophosphate in phosphoric or pyrophosphoric acid, to form a pasty mass. This mass, when mixed with hydrate of alumina, zinc oxide or magnesium oxide, a basic zinc silicate, or other materials of 'similar nature' set to give a hard material, similar in appearance to unglazed porcelain.

Fletcher claimed that this material "*offered a singularly great resistance to the action of the fluids of the mouth*", although clinical practice tended to disprove this. Indeed, in a paper before the Odonto-Chirurgical Society in 1907, R.S. Sanderson[30] reported that practically every tooth filled with the Fletcher cement had to be replaced within the space of a few months. As other dentists were experiencing similar problems, the cement was roundly condemned and withdrawn from sale.

The problems with the cement led to a 25 year break in the development of these materials and the next generation

of cements did not appear until 1904-1907[31,32]; these have largely remained unchanged since that time. The cement still consisted of a glass powder which was reacted with a liquid containing ortho phosphoric acid[33]. The cement paste set and hardened within a few minutes to give a translucent material which could attain a compressive strength of 300 MN/m^2 in twenty four hours.

The glass compositions usually contained a large fluorine content and this is believed to endow dental silicates with a cariostatic nature due to progressive leaching of fluorine from the set cement paste[18]. However, the set cement was prone to staining and even eroded and fell apart in the oral environment. In addition, the cement was not particularly adhesive and cannot, therefore, be regarded as a permanent filling material.

1.2.1 The Glass Component

The composition of the glass powder varied from manufacturer to manufacturer. The powders all basically consisted of a combination of any of the following; silica (SiO_2), alumina (Al_2O_3), lime (CaO), sodium fluoride (NaF), calcium fluoride (CaF_2), cryolite (Na_3AlF_6) and phosphorus pentoxide (P_2O_5). Some typical glass compositions are given in Table 1[29,34]. A typical dental silicate glass is characterised by a Si:Al ratio close to unity and a high fluorine content, which usually results in the glass being phase separated.

	SiO_2	Al_2O_3	CaO	Ca	F	Na_2O	Na	P_2O_5
A	47.2	33.1	10.4			8.7		
B	39.9	27.1		5.9	15.4		6.6	4.0
C	39.7	35.8		3.2	11.0		6.4	3.4
D*	41.6	28.2	8.8		13.3	7.7		3.3
E**	31.5	27.2	9.0		22.0	11.2		5.3

* less 5.6% oxygen for fluorine

** less 9.3% oxygen for fluorine

Table 1 - Dental Silicate Glass Compositions

1.2.2 The Liquid Component

The concentration of phosphoric acid in commercial liquids is typically around 50%. All liquids additionally contain metals, usually aluminium and zinc, which are soluble in phosphoric acid. Whilst Zn^{2+} retards the setting reaction, and Al^{3+} may accelerate the final set, the combined effect of introducing *both* metals into the liquid at suitable concentrations is to increase the strength and hardness of the cement. Some typical liquid compositions are shown in Table 2.

	H_3PO4	Al	Zn	Mg	H_2O*
1	48.3	2.3	4.9		44.5
2	55.5	2.0	9.1		33.4
3	65.0	1.4	1.5	0.4	31.7
4	57.9	2.4	3.1	0.8	35.8
5	49.6	1.9	4.4		44.1

* water calculated by difference

Table 2 - Dental Silicate Liquid Compositions

1.2.3 The Setting Reaction

When the glass powder and acid are mixed, the acid degrades the glass network and ions are released into solution. The cement sets by precipitation of an amorphous, insoluble aluminium phosphate complex, which acts as a matrix phase. Other species are co-precipitated, including calcium fluoride. The precipitation results in the concentration of soluble (Na^+, Ca^{2+}, Al^{3+} and F^-) ions decreasing as the cement sets.

The precipitation is initially very rapid; the cement may attain ~65 percent of its total compressive strength after only thirty minutes, but the strength continues to increase long after the cement has set. The glass powder is only attacked at the surface, which degrades to a siliceous hydrogel. Little or no silica migrates into the matrix. Wilson[34] postulates that Al^{3+}, PO_4^{3-} and OH^- ions undergo a solution set polymerisation in which Al^{3+} ions are bridged by PO_4^{3-} and OH^- radicals, as shown in Figure 2 below:

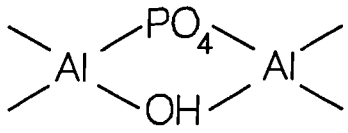

Figure 2 - $AlPO_4$ complex

It was also found that Ca^{2+} and F^- ions associate preferentially in the matrix. Indeed, there is evidence of calcium fluoride crystallites present in the matrix phase; these should improve the compressive strength of the cement. The overall setting reaction can thus be regarded as that shown overleaf in Figure 3.

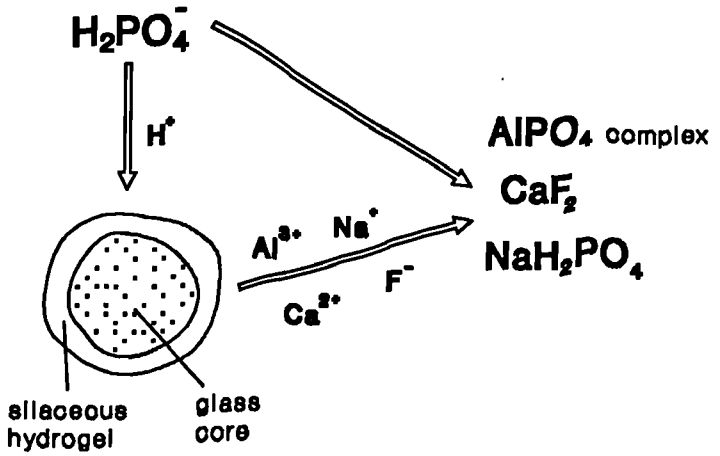

Figure 3 - Setting Reaction of Dental Silicate Cement

1.3 ZINC POLYCARBOXYLATE CEMENT

The zinc polycarboxylate cement was invented by D.C. Smith [20] in 1968. It was specifically developed as a dental adhesive, superior to both zinc phosphate and zinc eugenol cements which had remained virtually unchanged in the previous thirty years. It is a true adhesive and has the advantage of being bland towards pulpal tissue.

The zinc polycarboxylate is an acid-base reaction cement; zinc oxide, ZnO, is mixed with a solution of poly(acrylic acid). The working properties of the cement paste can be controlled through deactivating the ZnO by sintering with MgO.

Poly(acrylic acid) was chosen as the acid component because it was a water soluble polymer containing a large number of suitable chelating groups. It should, therefore, form stable chelates with calcium in tooth material and with zinc ions to form a cement.

1.3.1 The Setting Reaction

On mixing the ZnO and poly(acrylic acid), metal ions (Zn^{2+} and Mg^{2+}) are released and react with the polyacid chains, crosslinking them and causing the cement to set. As with dental silicates, the setting reaction only involves metal ions being released from the surface of the particles. The bond between the zinc ions and polyions is believed to be a mixture of both ionic and covalent (chelate) bonding; the covalent bonding progressively increasing as the cement ages. Adhesion to enamel is believed to be via a similar reaction in which calcium and phosphate ions are displaced from the enamel surface; a possible mechanism for the adhesion of poly(acrylic acid) to enamel is shown in Figure 4 below and to collagen (and hence to bone) in Figure 5 overleaf..

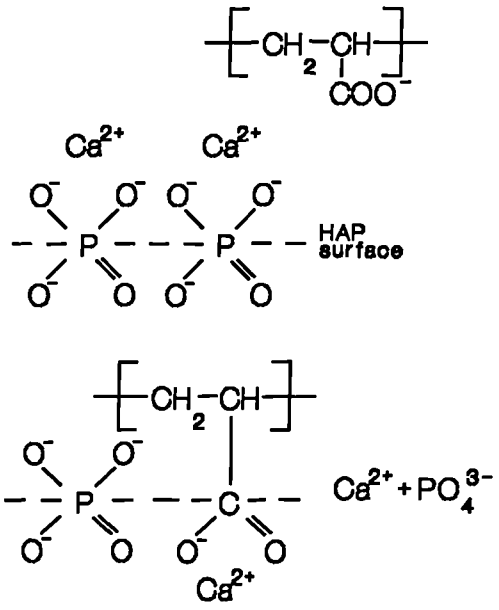

Figure 4 - Adhesion of Poly(acrylic acid) to enamel

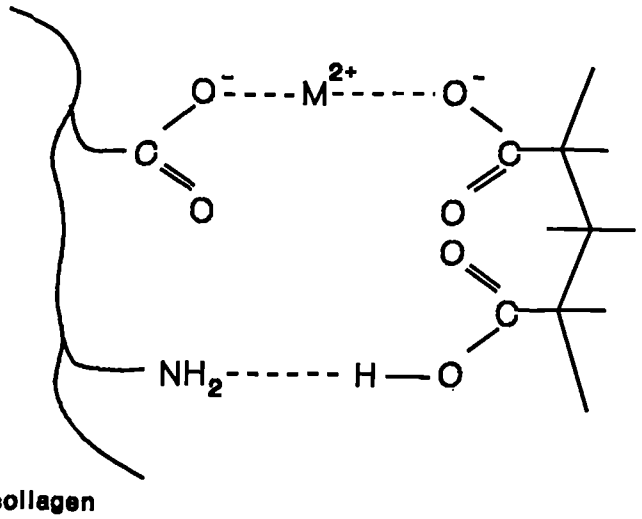

Figure 5 - Adhesion of poly(acrylic acid) to collagen

1.4 THE GLASS-IONOMER CEMENT

It would be far too simplistic to say that the glass-ionomer cement was merely a hybrid between these earlier materials. The differences in the relative acid strengths of phosphoric acid and poly(acids) meant that the proportions of the components in the glass compositions had to be altered. Indeed, it was only by developing new glass formulations that cements with useful properties were produced. The composition of the first successful ionomer glass, G200, developed in 1969 is given in Table 3. The glass-ionomer cement incorporating this glass and a fifty percent solution of poly(acrylic acid) was called ASPA I (AluminoSilicate PolyAcrylate). This cement was far from ideal, having poor setting properties and a low translucency which limited its use in cosmetic dentistry.

The key discovery in 1972 which led to *practical*

glass-ionomers[35] was that the incorporation of (+) tartaric acid improved the overall setting characteristics of the cement; the working time was extended and the setting rate sharpened. The modified glass-ionomer was called ASPA II, the liquid component of which now contained approx. 5 percent (+) tartaric acid and 45 percent poly(acrylic acid).

Research has continued into changing or modifying both the liquid[36-38] and the glass components[39-41]. Copolymers of acrylic and itaconic acids are now commonly used, and the composition of the glasses used by most commercial manufacturers are also different to G200. Two compositions used in commercial formulations are given in Table 3, along with that of G200. The values quoted are weights of components in grams. The glasses have essentially the same components as the dental silicates, but differ in the relative proportions of each.

Component	G200	Glass X	G338
SiO_2	175	175	175
Al_2O_3	100	100	100
CaF_2	207	100	90
Na_3AlF_6	30	30	135
AlF_3	32	32	32
$AlPO_4$	60	60	170

Table 3 - Compositions of Ionomer Glasses

1.4.1 The Setting Reaction

The nature of the setting reaction was established by Crisp and Wilson [e.g. 35,42-45]. Essentially, protons from the

carboxylic acid groups on the polyacid degrade the glass network, releasing metal cations which then serve to crosslink the polyacrylate chains. The glass again plays a dual role; acting both as a cation source and as a filler. The proposed setting reaction is shown schematically in Figure 6 below:

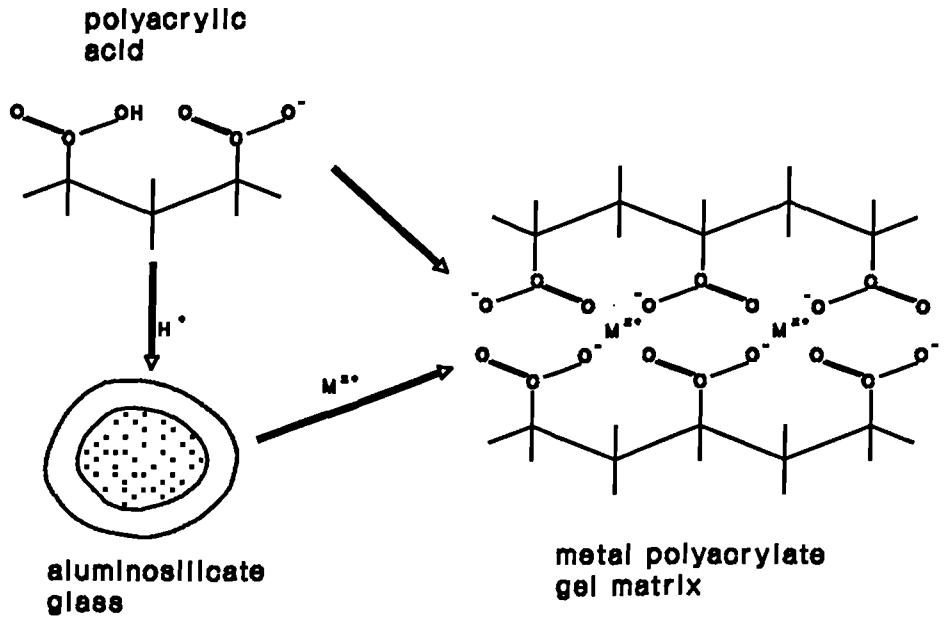

Figure 6 - Setting Reaction of the Glass-Ionomer Cement

Initially, the cement sets largely through the formation of calcium polyacrylate, but as the cement ages, aluminium polyacrylate salt bridges are formed resulting in the strength and hardness of the cement increasing with age. Leaching of the cations occurs from the surface to leave a cation-depleted silica gel around the unreacted core of the glass particle; the particles sitting in an insoluble polyacrylate matrix.

Recent studies[46], however, have indicated that the setting reaction may be more complex than previously thought. Ion leaching studies have indicated that there is no sequential release of calcium and aluminium ions; rather there is wholesale dissolution of a proportion of the glass, resulting in all species present in the glass being present throughout the matrix of the cement. Cement formation is postulated by the authors as occurring partly due to the formation of a hydrated silicate structure in addition to simple salt formation.

1.4.2 Present Uses of Glass-ionomer Cement

Current glass-ionomer cements find use in restorative dentistry, due to their excellent adhesion to tooth materials and metals. Unlike amalgams, which are merely 'fillers' ,no healthy tooth material need be removed when placing the cement, reducing cavity excavation. In addition, because of the adhesion, there is an intimate seal between the cement and cavity wall reducing the incidence of secondary caries. As with dental silicates, fluorine ions which have a cariostatic effect in the mouth are leached from the set cement .

In addition, the glass-ionomer is used as a fast setting splint bandage material. The bandage is impregnated with glass powder and freeze-dried poly(acrylic acid), and then soaked in water which causes the cement to set in the appropriate location.

1.4.3 Development of a Glass-Ionomer Bone Cement

In spite of the problems previously identified with PMMA bone cement, it still has a fracture toughness and flexural strength superior to those of glass-ionomers and will thus still find use in arthroplasty.

The currently used ionomer-glasses (see Table 3) produce uniformly fast setting cements, which whilst ideal for many dental applications, have not been developed for use in orthopaedics. For example, the dental ionomer glasses are so designed as to provide the cement with a translucency similar to tooth material; this restricts the range of glasses which can be used.

The cariostatic benefits of fluorine release from the cement are also not a factor, although some studies on fluorine containing bioglass[47] and on glass-ionomers[22-25,48] do show that limited fluorine release in the bone environment may be beneficial in promoting bone growth. In addition, fluorine is used in the treatment of both osteoporosis (loss of bone mass) and of Pagets Disease[49] (alternating phases of rapid bone resorption and formation resulting in bone bending and fracture)

One way to improve the generally poor mechanical properties of the glass-ionomers may be by controlling the composition of the glass component, without the constraints imposed by translucency, working time, etc.

To do this systematically requires a knowledge of the processes which govern a glasses' formation and how the structure of the glass effects its' subsequent properties.

1.5 GLASS

Of the various definitions of glass which have been proposed over the years, the one which has been generally accepted is that of the A.S.T.M:

'a glass is an inorganic product of fusion which has cooled to a rigid condition without crystallizing.'

This definition restricts glasses to those materials specifically made by the freezing of supercooled liquids. It excludes glasses made by evaporation methods, or by precipitation techniques (sol-gel glasses), etc.. The term 'inorganic' is also unnecessarily restrictive since many organic materials (e.g. glucose) form glasses.

Zarzycki[50] has recently proposed an alternative definition which states that:

'a glass is a non-crystalline solid exhibiting the phenomenon of glass-transition.'

This definition encompasses all methods of preparation whether the glass is organic or inorganic and additionally separates conveniently non-crystalline materials into the categories of glasses and amorphous materials.

Since this thesis concerns the production of inorganic glasses by the conventional route of cooling from the melt, this will be the only method of production discussed in depth.

1.5.1 Vitrification and the Glass Transition

Glass forming or vitrifiable substances are not common, being restricted to those materials which when melted form very viscous liquids (10^5 - 10^7 poise). If such a liquid is held for a time at a temperature just less than the freezing point, it will have a tendency to slowly crystallize. This is because the crystalline phase is then more thermodynamically stable than the supercooled liquid.

If, however, such a liquid is cooled from a temperature *above* the freezing point, crystallization may or may not occur depending upon the cooling rate. If the rate of cooling is slow enough, and nuclei are present, the liquid may crystallize. If, however, the cooling rate is sufficiently high, it may be possible to cool the liquid to temperatures well below the freezing point without any crystallization occurring. The viscosity of the liquid increases as the temperature is lowered until the final material has all the characteristics of a solid. Such materials are called glasses.

The transformation of a liquid to either a glassy or crystalline material is best shown by looking at how a convenient thermodynamic property (e.g. specific volume or enthalpy) changes with temperature as shown overleaf in Figure 7[51]

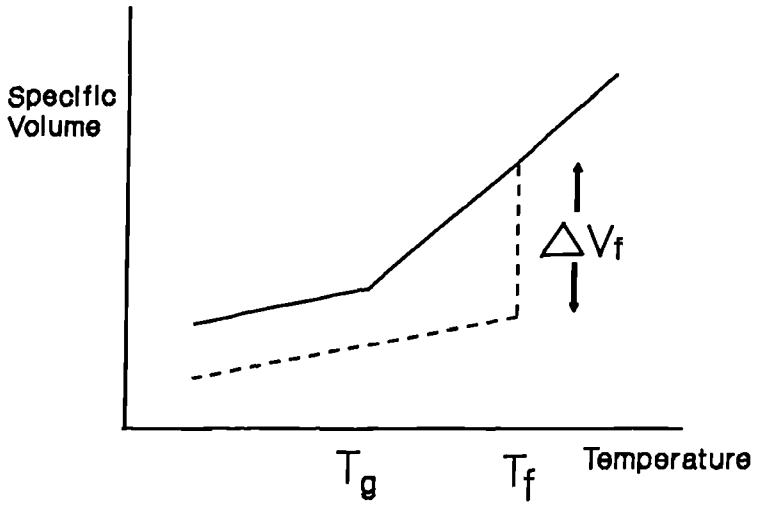

Figure 7 - Plot of Specific Volume vs Temperature

For a liquid which crystallises upon cooling, there is a sharply defined freezing point (T_f) at which solidification occurs by the formation of crystals. At this temperature there is a discontinuous volume change and an evolution of heat as the free energy of the system is reduced.

For a substance which can be cooled to the glassy state, at and below T_f, there appear neither a discontinuous volume change nor an evolution of heat. This is because the cooling results in a contraction of the supercooled liquid with a coefficient identical to that of the original liquid, hence the slope remains constant.

This situation continues until at a certain temperature, the slope of the volume-temperature curve undergoes a dramatic decrease so as to be roughly parallel to that of the crystalline form. This point marks the transition of the material from supercooled liquid to glass

and is referred to as the glass transition temperature (T_g). At T_g, the viscosity of the material is very high (10^{13} poise).

For any given fixed pressure, the glass transition varies with the rate of cooling. Very high cooling rates tend to raise the temperature at which T_g is observed whilst a slower cooling rate displaces T_g towards lower temperatures. Any value of T_g obtained by experiment is thus a function of the cooling rate of the glass.

1.5.2 Theories for the Glass Transition

The glass transition is a very complex process, not clearly understood even now. Two ways of interpreting the glass transition are by considering the phenomenon in terms of relaxation behaviour and free volume.

1.5.2.1 Relaxation Behaviour

For a liquid, the change in volume, V (or enthalpy, H), with temperature can be considered in terms of vibrational and configurational terms, i.e.

$$\alpha_l = \frac{dV_l}{dT} = \left(\frac{\delta V}{\delta T}\right)_{vib} + \left(\frac{\delta V}{\delta T}\right)_{con}$$

(where α_l = thermal expansion coefficient)

Considering each term separately, it can be seen that for both liquid and crystal, the vibrational term must be very nearly the same, since both have a similar short-range order. However, the configurational term for a liquid can

be much higher than that of the crystal.

Upon cooling from the melt, at any given temperature, the liquid will attempt to reach its lowest free energy at that temperature. This equilibrium state is obtained by a configurational change, provided that the cooling rate is low enough for these changes to occur. This configurational change to achieve equilibrium occurs over a period of time called the relaxation time, τ_r.

In glass forming materials, the configurational changes that cause the relaxation of the supercooled liquid become increasingly slower with decreasing temperature. Above T_g, the relaxation times are still short compared to the experimental time of observation, ($\tau_r < t_o$) and the material is still liquid like.

However, at a given temperature, T_g, due to an increase in viscosity, the relaxation time to reach equilibrium configuration increases suddenly and the material changes from liquid-like to solid-like behaviour. For any glass, therefore, T_g is merely the result of equality between the relaxation time and the time-scale of the experiment, i.e. T_g occurs when $\tau_r \approx t_o$.

For temperatures below T_g, the relaxation times are too long for equilibrium to be obtained by even the slowest of experiments, i.e. ($\tau_r > t_o$) and the positions of the structural units can be considered frozen. This implies that a glass is a liquid in which the configurational arrangement is no longer able to attain a minimum in free energy. Glasses, therefore, can not be regarded as being in

thermodynamic equilibrium with regard to the configuration of the structural units of the system and are hence non-equilibrium materials.

1.5.2.2 Free Volume Effect

Fox and Flory[52-54] advanced the hypothesis that the glass transition (for organic polymers) resulted from the reduction of the free volume of the amorphous phase below a certain characteristic value.

Cohen and Turnbull[55] explained this in terms of a system of molecules which are able to move, but which are confined most of the time inside cages formed by their immediate neighbours. Occasionally, by virtue of a fluctuation, a hole is formed in the cage allowing a molecule to be displaced. This can lead to diffusion if another molecule occupies the vacant hole before the original molecule returns to its site. Diffusion thus occurs by molecular jumps in the free space (holes) formed at the expense of excess volume present in the liquid. Such jumps are only allowed if the hole has a greater volume than a critical value v^* formed by the distribution of the free volume, v_f, defined as that part of the excess volume which can be redistributed without expending energy.

The amount of free volume is dependant on temperature; at low temperatures, all thermal expansion arises from the disparity of the vibratory movement of the molecules. The redistribution of energy is significant and the added volume, $\Delta\hat{v}$, tends to be distributed uniformly amongst the

different sized cages. In this case the added volume is approximately equal to the expansion of the crystalline solid, and the free volume negligible.

At higher temperatures, the major part of the added volume will be free for redistribution. A random distribution reduces the free energy of the amorphous phase by increasing the configurational entropy of the system. Such a random distribution is not possible for a crystalline phase but is for an amorphous phase. The consequence of this is that there can be an amorphous phase which is more stable than a crystalline phase of the same volume provided that the added volume is above a certain characteristic value. Thus, the glass transition temperature can be considered as the approximate temperature at which the excess volume attains a critical value and free volume starts to appear.

1.6 THEORIES FOR THE STRUCTURE OF GLASS

There have been many different theories and models postulated for the structure of inorganic glasses. A comprehensive review of all such models would be difficult; rather, this thesis concerns itself principally with four structural models which reflect the wide spectrum of thought regarding glass structure.

1.6.1 The Random Network Theory

This model was first proposed by Zachariasen[56] in a seminal paper in 1932. Previously, Goldschmidt[57] had observed that for simple oxides (M_xO_y) there was a correlation between the ability to form a glass and the relative sizes of the cation M and the oxygen anion O. To satisfy packing requirements, Goldschmidt believed that a glass former should have four O anions around each cation, with the anions being situated in the corners of a tetrahedron.

Zachariasen pointed out that the Goldschmidt criteria were not fully satisfactory even as an empirical model; BeO will permit oxygen tetrahedra around the beryllium ion, and yet can not be obtained in the glassy form. This led him to develop his own model of glass structure. He argued that since the mechanical properties of an oxide glass and its corresponding crystal were so similar then the interatomic forces must also be similar between the two forms.

It followed that, since the atoms in a crystal formed extended three-dimensional networks, then so must those in glass. However, X-ray diffraction on glasses produced a diffuse pattern showing that the networks in glass were not periodic as in crystals, but rather were random throughout the glass (i.e. the glass possessed no long range order).

This randomness produces M-O bonds of different strengths which upon heating would progressively be broken, resulting in the gradual reduction in viscosity seen in glasses. A further consequence of the randomness of the

network is that the glass has a higher internal energy than the corresponding crystal.

Zachariasen argued that this energy difference between the glass and crystalline form could not be too large, otherwise there would be a strong driving force for the material to reduce free energy by devitrifying to the crystalline form. From this it followed that the glass must contain polyhedra of the same type as the crystal and they must be joined in a similar way. For example, if the crystalline forms of silica (quartz, cristobalite, tridymite, etc.) consisted of SiO_4 tetrahedra joined at their corners, then so must vitreous silica, the only difference being that, in the glassy form, the mutual orientation of neighbouring tetrahedra would be random.

Based on his structural energy considerations, Zachariasen laid down a number of criteria which he felt an oxide must satisfy if it was to be a glass former. They are:

1. An oxygen atom must not be linked to more than two M atoms
2. The number of oxygen atoms around M must be small
3. The oxygen polyhedra must share corners with each other, not edges or faces
4. For a three-dimensional network, at least three corners of each polyhedra must be shared

Oxides of the formulae MO and M_2O are not able to fulfil these criteria and are thus not able to form glasses. Oxides of the type M_2O_3 can form glasses if the

oxygens form triangles around the M atoms as shown below in Figure 8.

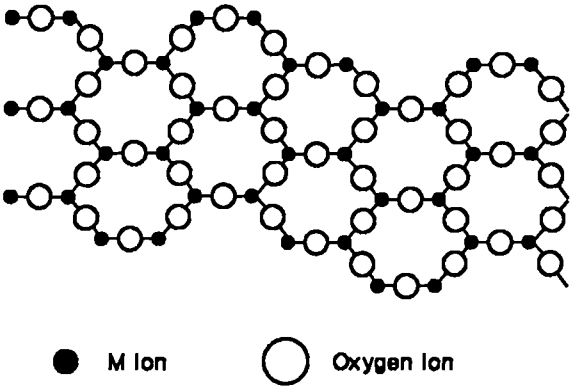

Figure 8a - Crystalline Form

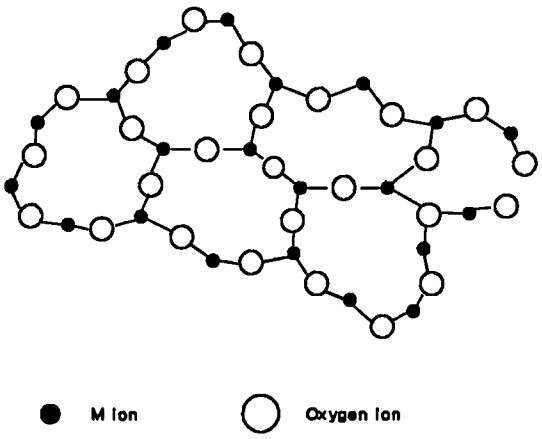

Figure 8b - Glassy Form

Zachariasen's criteria are also satisfied by the oxides MO_2 and M_2O_5 when the oxygens form tetrahedra and by the oxides MO_3 and M_2O_7 when they form octahedra. Goldschmidt had noted that BeF_2 formed a glass and this can be included in Zachariasen's list because the glass consists of BeF_4 tetrahedra.

1.6.2 Applications to Complex Oxides

Zachariasen termed the above group *network forming oxides*. However, most practical glass forming systems are a mixture of different oxides , many of which do not fall into the above category. To accommodate these oxides, Zachariasen next looked at more complex oxide glasses and this resulted in a modification of the criteria. To form a *complex* oxide glass it was necessary that:

1. the sample contained a large proportion of cations which were surrounded by oxygen triangles or tetrahedra.
2. these tetrahedra shared only corners with each other.
3. some oxygen atoms are only linked to two cations and do not form bonds with any other cations.

As well as network forming oxides, Zachariasen identified two other types of oxide present in complex glasses; these are the *network modifying oxide* and the *intermediate oxide*.

Network modifying oxides are those oxides which contain cations that are incapable of taking part in the glass network; these are essentially the alkali metal and alkaline earth oxides. The introduction of such oxides, e.g. Na_2O, results in a weakening of the glass network due to the formation of non-bridging oxygens within the glass. This effect is shown overleaf in Figure 9 for a sodium silicate glass.

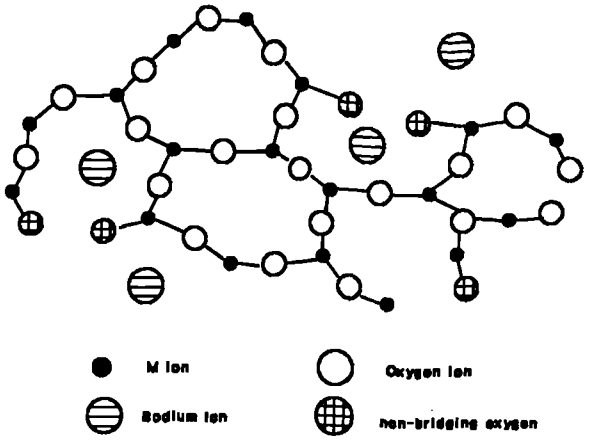

Figure 9 - Effect of Network Modifier on Glass Network

Each molecule of Na_2O added to the glass results in the rupture of a Si-O-Si bond and the formation of two $Si-O^-$ species. To maintain network charge neutrality, sodium ions are present nearby to balance the negative charges on the non-bridging oxygens. As can be seen from the figure, the overall effect is to loosen the glass network. For the case of divalent cations, e.g. CaO, one Ca^{2+} cation is enough to maintain network neutrality. The modifying cations were postulated by Zachariasen as sitting randomly within 'holes' in the glass network. The result of the addition of a network modifier is that the glass would have a lower melting point, a lower viscosity etc., which reduces with increasing modifier content. The glass is also more susceptible to acid attack which results in the exchange of modifying cations in the glass for protons from the acid; the glass is thus progressively degraded.

Intermediate oxides are those oxides which, whilst being able to replace network formers isomorphically in the glass, can not form extended networks on their own. Al_2O_3 is a typical example found in many natural feldspars and zeolites. The aluminium can either be four or six fold co-ordinated; i.e. present as tetrahedral AlO_4 or octahedral AlO_6. Appen[58] has looked at the properties of several alumino-silicates and concluded that in alkali containing glasses, aluminium was tetrahedrally coordinated, with octahedral coordination arising in only specific rare conditions. Large cations, e.g. K^+, Na^+, Ca^{2+}, etc. favoured isomorphic substitution, as in comparable crystals, but small cations, e.g. Mg^{2+}, Fe^{2+} impeded this process, favouring octahedral coordination. However, the ability of aluminium to enter the glass in one coordination state or another must be determined not only by the nature of the metal oxide (MeO) component, but also by the ratio:

$$R = \frac{a_{Me_2O} + a_{MeO}}{a_{Al_2O_3}}$$

where a = number of moles

For isomorphic substitution, this ratio should not be less than unity (i.e. $R \geq 1$). In an aluminosilicate glass, the AlO_4 tetrahedra can replace the SiO_4 tetrahedra as shown overleaf in Figure 10.

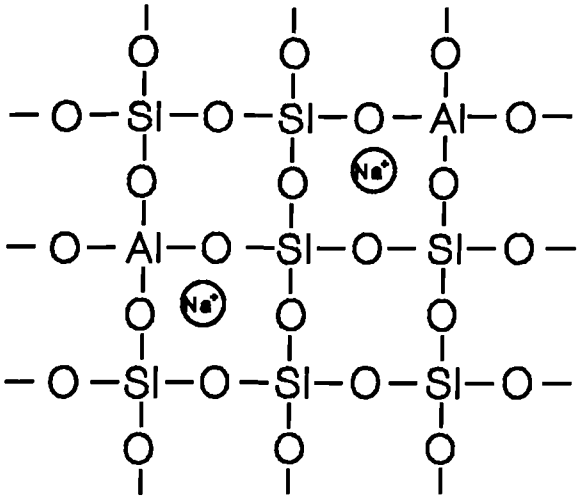

Figure 10

Schematic Diagram of an Aluminosilicate Glass

Each Si has a charge of 4+; replacement by an Al^{3+} ion results in the network having an overall negative charge. To balance this, an extra positive charge is necessary and this is commonly supplied by network modifying cations which must be present to maintain electroneutrality. To fulfil this criterion requires the presence of one alkali metal or 'half' an alkaline earth ion for each AlO_4 tetrahedron in the network. Use of alkaline earth oxides, however, presents a problem in that the 2+ charge of the calcium ion may force a clustering, at least of pairs, of AlO_4 tetrahedra which only supply a net -1 charge each[59]. The occurrence of Al-O-Al bonds in aluminosilicates is thought unlikely because of electrostatic instability. Lowenstein's aluminium avoidance principle[60] states that for two tetrahedra joined by a bridging oxygen, only one of the cations at the centre of one of the tetrahedra can be

an aluminium.

If there are insufficient modifier cations present, then the aluminium will take up other co-ordination states and the glass will have a complex structure.

When phosphorus pentoxide is also present in the glass, the $[AlO_4]$ group can achieve electroneutrality by becoming linked to a $[PO_4]$ group. In this case, the -1 charge of the tetrahedral $[AlO_4]$ group is neutralised by the excess +1 charge associated with the $[PO_4]$ group, without the need for the presence of a modifier. In addition, the radii of the aluminium and phosphorus ions (0.50 Å and 0.34 Å respectively) are such that when these ions occupy neighbouring tetrahedra, the overall atomic distance is similar to that of a pair of adjacent silicon ions in neighbouring $[SiO_4]$ groups (0.41 Å).

To study the effects of intermediates and modifiers, Engelhardt et al[61] have looked at nearly fifty glasses from the $CaO-Al_2O_3-SiO_2$ system using high resolution solid state ^{29}Si and ^{27}Al magic angle spinning nuclear magnetic resonance. They represented the calcium aluminosilicate glasses as being described by distinct sets of coexisting structural units, Q_n^m, containing different numbers of non-bridging oxygens (4-m) and tetrahedral aluminium atoms (n). In glasses of the composition range $CaO \geq Al_2O_3 \leq 0.5SiO_2$ all the aluminium was found to be incorporated in the glass network as AlO_4 tetrahedra linked to SiO_4 tetrahedra. The glass of composition $CaO = Al_2O_3 \leq 0.5SiO_2$ was found to be a fully polymerised, three dimensional network of Q_n^4 units.

It was also found that as the CaO content increased to exceed the Al_2O_3 concentration, i.e. $CaO > Al_2O_3 \leq 0.5SiO_2$, increasing amounts of non-bridging oxygens were created and a stepwise depolymerisation of the glass network was observed (i.e. $Q_n^4 \rightarrow Q_n^3 \rightarrow Q_n^2 \rightarrow Q_n^1 \rightarrow Q^0$).

The Al-O-Si groupings are vulnerable to acid attack, compared to Si-O-Si links. This is because the Al^{3+} ion has a weaker field than the Si^{4+} ion. As a result, it interacts less strongly with the electron clouds of the oxygen anions leaving them with enough residual polarizability to be susceptible to acid attack.

Although Zachariasen only considered oxide glasses, it is apparent from the above arguments that halides are also very powerful modifiers since addition of a fluoride to, for instance, an ionomer glass results in disruption of the glass network and the formation of non-bridging fluorines, as shown in Figure 11.

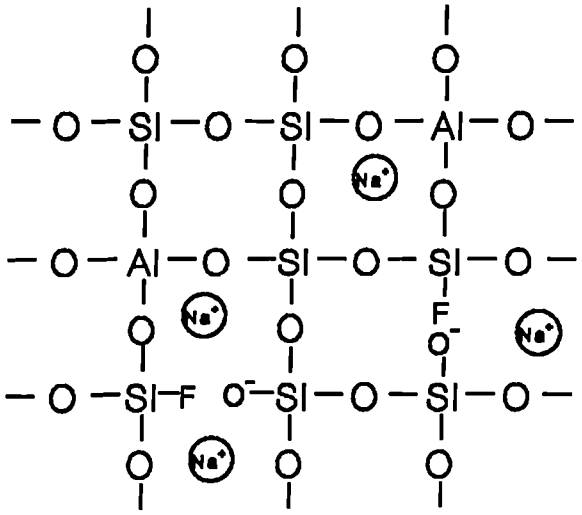

Figure 11 - Effect of a Fluoride Network Modifier

A fluoroaluminosilicate glass is then thought to consist of (SiO_3F) and $(AlO_3F)^-$ tetrahedra in addition to those already mentioned[40].

Zachariasen's hypothesis was essentially empirical, but was supported strongly with X-ray diffraction results by Warren et al[62] shortly afterwards. It is now thought, however, that there is a longer range order in glass than Zachariasen's hypothesis would allow.

1.6.3 Glasses as Inorganic Polymers

This approach owes much to the ideas of Holliday and Ray[63]. Ray defines an inorganic polymer as a substance with giant molecules composed of atoms other than carbon and linked together by mainly covalent bonds. Compared to organic polymers, inorganic polymers are generally stronger, harder, more brittle and usually insoluble. They generally do not burn and only soften or melt at high temperatures. These properties are typical of polymers with a highly cross-linked network.

By extending the ideas of Zachariasen and Warren and considering glasses as inorganic polymers, it is possible to model their physical and chemical properties in terms of the 'cross-link density' of the glass. The model proposed principally by Stevels[64] considers that the glass network consists of [-Si-O-Si-O-Si-] chains crosslinked by so-called bridging oxygens (-O-). During the transition from quartz glass, SiO_2, to silicate glasses the ratio R of the

number of oxygen atoms to the number of silicon atoms becomes greater than two. As a result the continuous network structure depolymerises which results in a loosening of the network. This loosening corresponds to an increase in the number of non-bridging oxygens compared to bridging oxygens. Stevels introduced an additional set of parameters to accommodate this change. X was the average number of non-bridging oxygen ions in the tetrahedron, Y was the average number of bridging oxygens (i.e. oxygens bonded to two network formers) and Z, the average number of all oxygens in the tetrahedron. The parameters are linked via the equations:

$$Z = X + Y, \qquad R = X + 1/2\ Y$$

The effect of cross-link density upon glass transition for organic polymers has been studied by Gibbs and Di Marzio[65] who showed that the two parameters were related by the equation:

$$T_x / T_o = 1 / (1 - Kx)$$

where:

x is the cross link density, corresponding to R from the arguments by Stevels

T_x is the glass transition temperature of the cross-linked polymer

T_o is the glass transition temperature of the corresponding linear polymer

K is an independent constant

1.6.4 Crystallite Hypotheses

This first of these models was proposed by Lebedyev[64]. As early as 1921 he expressed the opinion that glass was an alloy consisting of highly dispersed crystals. The proposal was developed by Randall et al[66-68]. They found a correspondence between the diffraction maxima in X-ray photographs of glasses and the most intense Debye lines in X-ray photographs of the crystalline phase of the same material. Line broadening is inversely proportional to the size of the scattering phase. By making assumptions about the size of the crystals, it was possible to calculate intensity curves and compare them to actual data.

The results showed a good agreement between actual and calculated curves and Randall concluded that glass consisted of exceptionally small crystals which for some reason had not grown. Randall calculated a value of 15-20 Å for crystallite size, but more sophisticated X-ray techniques have since shown that for the model to hold for SiO_2, the crystallite size can not exceed 8 Å which is comparable to the dimensions of one unit cell of cristobalite (7.1 Å); to talk about crystallites on such a scale is thus meaningless.

However, there still exists the possibility of local variation in the degree of order within the glass. Zarzycki[50] refers to microdomains in which the centre of the domain is regarded as being more ordered than the periphery. Taking as extremes the ideas of perfect crystallites and of a perfect random network, a localized

change in order from one to the other can be envisaged, i.e. a change from an ordered to a disordered state on a local scale, as shown in Figure 12.

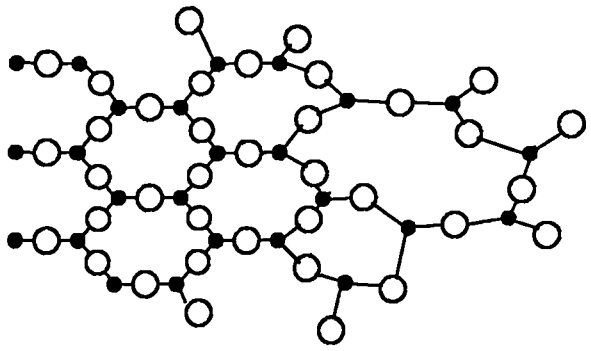

Figure 12

Local Change from Ordered to Disordered State in a Glass

Such an approach can be used to explain how the various crystallites are linked together, which was previously ascribed to the existence of 'interstitial tissue'. Such local changes could not be determined by scattering methods.

Goodman[69] has recently proposed another model for glass structure based on a phase diagram approach. He noted that most glass forming systems have as a major or minor component a material that exists in two or more polymorphic forms differing only slightly in free energy. He suggested that above T_g transient clusters of all possible polymorphs existed simultaneously at sizes below that required to form a self sustaining nucleus.Upon cooling, the clusters become bonded across their surfaces and the resulting mixed cluster will have a strained interface. Eventually, a random strained cluster network could be envisaged as

existing throughout the entire volume of liquid. At this point, the liquid matrix containing clusters changes to a solid framework of clusters containing residual liquid; this point corresponds to T_g. The residual liquid is distributed within the interstices of the clusters. Upon further cooling, the residual liquid would deposit on cluster surfaces. At these lower temperatures, the strain would be expected to be higher because of thermal expansion mismatch within the mixed cluster network, either between clusters of different type or orientation.

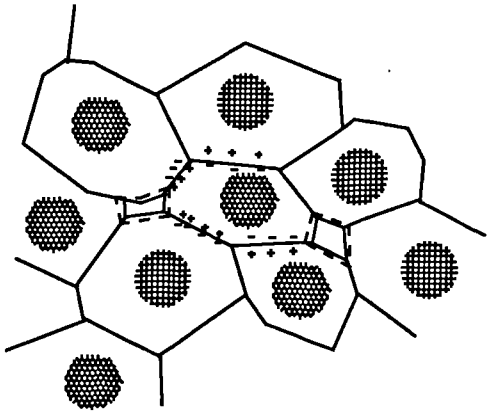

Figure 13

Goodmans Strained Mixed Cluster Model

Goodman thus proposes a random network of strained quasi-crystalline clusters as shown above in Figure 13. Each cluster is postulated as being surrounded by a random close packing of other clusters. Strain is distributed randomly within the structure; some of the clusters are strained in tension and some in compression. As a result the outside of any cluster will not be coherent with its' core in terms of scattering properties. This model again

can be seen as a microcrystalline model but refined to include a strain term which in hindsight is implicit in all such models.

1.6.5 Medium Range Order in Glasses

The most recent structural model for glass structure has been proposed by Gaskell et al[70]. They postulate a degree of order longer than that allowed by the Zachariasen - Warren model which envisaged the modifying cations, such as calcium, as sitting randomly within interstices in the glass network. Gaskell et al have shown using a neutron scattering technique that the distribution of calcium ions in a calcium silicate glass ($CaSiO_3$) is non-random, but has features which indicate the presence of medium range structural order within the glass. They propose a structure of glasses described in terms of a nearly close-packed arrangement of oxygen ions. Cations fill the appropriate octahedral and tetrahedral sites in the O sublattice, resulting in a glass that contains sheets of interconnected CaO_6 octahedra interleaved with linked SiO_4 tetrahedra. As in crystals, the octahedra are edge-linked, and a domain is regarded as a region in which the sheets of CaO_6 are essentially parallel.

As well as structural models, the formation of glasses can also be considered in terms of the kinetics of the processes governing glass formation.

1.7 KINETIC THEORY OF GLASS FORMATION

Glasses are metastable materials; the increase in viscosity with decreasing temperature effectively prevents the material from reaching its equilibrium state, i.e. the crystalline form. Vitrification can thus be thought of as *non-crystallization* and the kinetic theory aims to define the boundaries at which a liquid will not crystallise. Much of the work to develop this model was done by Turnbull and Cohen[71-73]. The difference between the liquid and crystal forms is mainly that of degree of long range order. Crystallization therefore requires the transformation from short to long range order within the material. For liquids which form glasses upon cooling, this transformation is relatively difficult.

Crystallization is neither an instantaneous nor homogenous transformation; rather it occurs by the growth of crystals at a *finite* rate from a *finite* number of nuclei distributed throughout the material. Two distinct stages are therefore observed; crystal nucleation and crystal growth.

The rate at which a liquid can be transformed into a crystal is given by the relationship:

$$X_t = 1 - \exp\left(-\frac{\pi}{3} u^3 I t^4\right)$$

where:

X_t is the volume fraction crystallised after time t

u is the crystal growth rate

I is the nucleation rate

Thus, according to kinetic theories, the failure of liquids to crystallise, but rather to form glasses, is due to either a very small nucleation rate, I, or a low rate of growth of crystals, u, (or a combination of both). Uhlmann[74] assumes a limiting value for the volume fraction, X_t of 10^{-6}, arguing that volume fractions smaller than this could not be detected. Materials for which X_t is less than 10^{-6} are thus glass forming.

1.7.1 Temperature Dependence of Nucleation and Growth Rates

Both nucleation and growth are temperature dependant as shown in Figure 14 overleaf.[50]

For a liquid to form a glass, it must be cooled rapidly to avoid crystallization. Upon cooling a liquid from its temperature of fusion, T_f, crystal growth is theoretically possible between T_f and T_3. However, formation of nuclei, the necessary precursor to growth, occurs between T_2 and T_4. The critical region for crystallization is thus between T_2 and T_3.

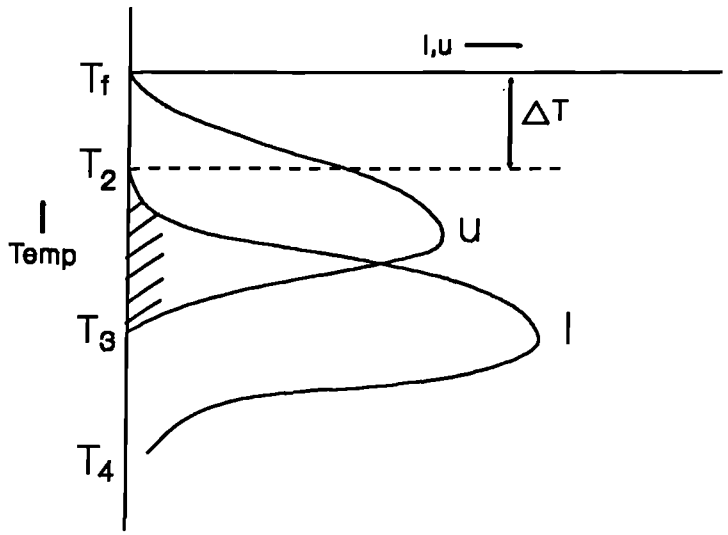

Figure 14

Dependence of Nucleation and Growth on Temperature

The chance of crystallization thus depends upon how the curves overlap and on the absolute values of I and u in the overlap region. If I and u are large (and the curves overlap substantially) then the material will crystallise fully. If I is low and u high, then the material will consist of gross crystals grown from only a small number of centres. If I is high and u is low then the material will be partially crystalline with a fine grained microstructure; i.e a glass-ceramic (see section 1.9). If both I and u are low, however, a glass can be formed.

N.B. Below T_4 the viscosity is so high that diffusion is effectively prevented and the material can be regarded as stable.

1.7.2 NUCLEATION

Nucleation initially involves the formation of embryos in which there is a longer range order present than that of the liquid. The embryos form and disappear with thermal agitations and have different and constantly fluctuating sizes. Some embryos reach a critical minimum size to be self sustaining and are then known as nuclei.

Nucleation may be either homogenous, in which case the nuclei have the same composition as the crystals which grow upon them, or heterogeneous, in which case the nuclei and crystal phase may be chemically quite different.

1.7.2.1 Homogeneous Nucleation

In this case, embryos arise from local fluctuations in the structure of the liquid phase. The embryos are assumed to have the same structure, composition and properties as the crystal phase and differ only in form and size. In the following discussion, the embryos are assumed to be spherical with size being a function of the conditions of thermodynamic stability.

The change from supercooled liquid to the crystal is accompanied by a change in free energy, which is made up of two opposing factors.

There is a reduction in free energy per unit volume, $4/3\pi r^3\Delta g_v$, due to the arrangement of atoms within the embryo being more ordered than that in the surrounding phase. However, the creation of an embryo also involves the formation of a liquid-crystal interface which results in a

gain in free energy, $4\pi r^2 \Delta g_s$ due to an increase in interfacial energy (in practice, $\Delta g_s \approx {}^s\gamma_l$). The overall change in free energy from a spherical embryo of radius, r can thus be represented by the equation:

$$\Delta g_r = \frac{4}{3}\pi r^3 \Delta g_v + 4\pi r^2 {}^s\gamma_l$$

The effect of both factors is shown in Figure 15. For an embryo of radius $r < r^*$, the ratio of surface area to volume is large and the Δg_s term dominates which results in the embryo requiring an increase in free energy to grow larger; such an embryo will be unstable.

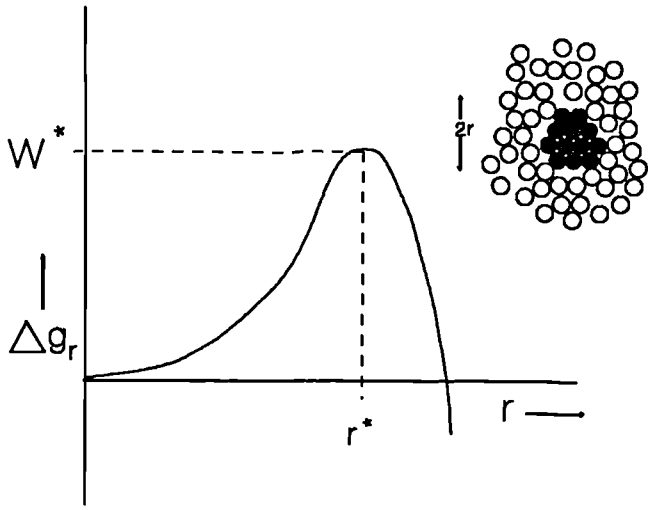

Figure 15

Free Energy as a function of Embryo Radius

For values of $r > r^*$ further growth results in a decrease in free energy; such embryos will form stable nuclei. We can therefore define r^* as the size of an embryo beyond which it can be called a nucleus. Corresponding to

the size r^* is the critical value, W^*, of change in free energy, known as the thermodynamic barrier to nucleation and given by the expression:

$$W^* = \Delta g_r^* = \frac{16\,\pi\,(^s\gamma_l)^3}{3\,(\Delta g_v)^2}$$

Assuming that the formation and size distribution of nuclei are governed by statistical fluctuations, at equilibrium, the number of nuclei per unit volume is approximately equal to:

$$n_r^* = n \exp \frac{-W^*}{k\,T}$$

where:

n_{r*} = number of nuclei per unit volume

n = number of atoms or molecules per unit volume

k = Boltzmann's constant

The growth of a nucleus results from the addition of one or more structural units from the liquid to the nucleus across an interface. This may involve a diffusion process or a re-orientation of molecules into a preferred alignment. Associated with this rearrangement process is a free energy of activation, $\Delta G'$, required if a unit, near the embryo-liquid surface, is to cross the interface and join the surface of the embryo. The term $\Delta G'$ is known as kinetic barrier to nucleation. The probability of a unit crossing the interface is given by the expression:

$$P = \upsilon_o \exp\left(\frac{-\Delta G'}{k\,T}\right)$$

where:

P = probability of an atom crossing the interface

υ_o = vibrational frequency of atoms at the nucleus-liquid interface

The rate of nucleus formation, I, is thus given by:

$$I = n\upsilon_o \exp\left(\frac{-NW^*}{RT}\right) \exp\left(\frac{-\Delta G'}{RT}\right)$$

where:

I = number of stable nuclei formed per second per unit volume

N = Avogadro's number

R = Gas constant

The first exponential term gives the probability at a given temperature, T, of forming a nucleus larger than the critical size. The second exponential term governs the rate at which the structure of the material can be changed during the formation of the nucleus. The equation shows that the rate of nucleus formation is sensitive to changes in temperature, since T is contained within the exponential term.

The rate of nucleus formation, initially governed by the first exponential term, does not increase indefinitely as the temperature falls. Rather, it achieves a maximum corresponding to the two terms achieving parity, after which the second term dominates resulting in the rate of nucleation decreasing with decreasing temperature. This accounts for the shape of the I-T curve shown earlier in Figure 14.

1.7.2.2 Heterogeneous Nucleation

Since glasses are formed as a result of the supercooled liquid having a large energy barrier to homogenous nucleation, it is not surprising that heterogeneous nucleation is the larger problem when trying to form glasses. This is because any surfaces in contact with the liquid, (whether the surface be the walls of the container or a foreign particle present in the melt), will reduce the energy barrier for nucleation W^* by reducing the surface energy between the liquid and the crystal. The effect of any foreign surface is influenced by the degree to which the surface is wetted by the crystal which precipitates in the presence of the liquid. The change in energy, W^*_{het} for heterogeneous nucleation can be expressed as:

$$W^*_{het} = W^* f(\theta)$$

where $f(\theta)$ is a function of the contact or wetting angle, θ, at the impurity-liquid-crystal junction, such that:

$$f(\theta) = \left[\frac{(2 + \cos\theta)(1 - \cos\theta)^2}{4}\right]$$

For any contact angle, θ, less than 180°, the free energy barrier is less for nucleus formation on a foreign surface than for homogeneous nucleation. For the case of a nucleus in the shape of a spherical segment, formed on a solid impurity surface, P, suspended in the liquid (see Figure 16 overleaf), there are three interfacial energy terms to consider when determining θ.

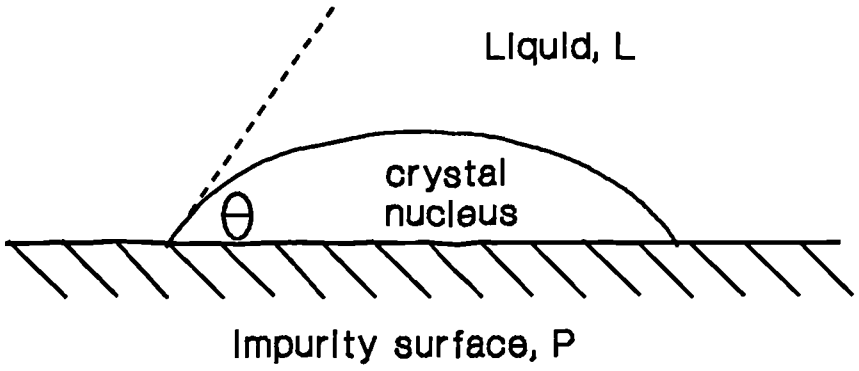

Figure 16 - Nucleus Formation on an Impurity Surface

As well as the interfacial energy of the crystal-liquid interface, ${}^{s}\gamma_{l}$, there are in addition the interfacial energies of the impurity-crystal interface, ${}^{s}\gamma_{p}$ and the impurity-liquid interface, ${}^{l}\gamma_{p}$. For a contact angle, θ, at the liquid-crystal-impurity junction, at equilibrium, the balance of surface tensions is given by:

$$ {}^{l}\gamma_{p} = {}^{s}\gamma_{p} + {}^{s}\gamma_{l}\cos\theta $$

These considerations are crucial in considering the production of glass ceramics (see section 1.9), where impurities are deliberately introduced into the glass in attempt to bring about crystallization.

1.7.3 Crystal Growth

Once a stable nucleus has formed, it will continue to grow at a rate determined by both the speed with which the required atoms are able to diffuse towards the crystal surface *and* by the manner in which they cross the interface. The work presented below is again after

Turnbull[75]. The crystal-liquid interface is regarded as being represented by two potential wells separated by a jump distance a_o, as shown in Figure 17 below:

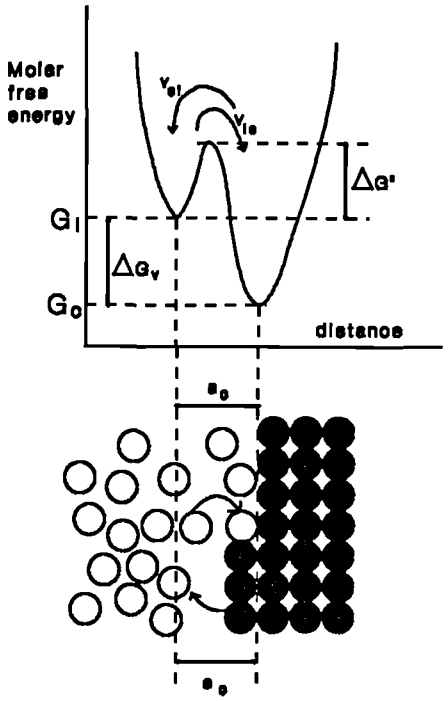

Figure 17

Free Energy as a Function of Jump Distance

The disordered atoms in the liquid state possess a higher free energy than that of atoms in the crystal.The change in molar free energy corresponding to the crystallization is:

$$\Delta G_v = G_c - G_l \quad (\Delta G_v < 0)$$

where:

G_c = free energy of atoms in crystal

G_l = free energy of atoms in liquid

To cross the interface from liquid to crystal, an atom must overcome a fee energy barrier equal to ΔG^*; to cross

from crystal to liquid, the free energy barrier is ($\Delta G'' + \Delta G_v$). The *net* rate of crystal growth will be proportional to the difference between the frequencies of the liquid-solid and solid-liquid transitions, given by v_{ls} and v_{sl} respectively, where:

$$v_{ls} = v \exp\left(\frac{-\Delta G''}{RT}\right)$$

and

$$v_{sl} = v \exp\left[\frac{-(\Delta G'' + \Delta G_v)}{RT}\right]$$

If the fraction of sites available for growth is given by f, such that $0 < f < 1$, then the growth rate is given by:

$$u = f a_o (v_{ls} - v_{sl})$$

Expanding the terms for v_{ls} and for v_{sl}:

$$u = f a_o v \exp\left(\frac{-\Delta G''}{RT}\right)\left[1 - \exp\left(\frac{\Delta G_v}{RT}\right)\right]$$

Turnbull and Cohen[71] suggest that for simple substances at least, a reasonable assumption would be that the activation energy, $\Delta G''$, for crystal growth was close to that for viscous flow. The above equation may thus be rewritten as:

$$u = f \frac{RT}{3\pi a_0^2 \eta N}\left[1 - \exp\left(\frac{\Delta G_v}{RT}\right)\right]$$

where:

η = viscosity

Both nucleation and growth rates of crystals are thus dependant on activation energy terms, $\Delta G'$ and $\Delta G''$ respectively. In general, these energies will not be equal and may even differ in order of magnitude. Nucleation is affected only by diffusion on a very local level in the area around the nucleus centre, but the rate of growth may be affected by the rate of diffusion of atoms a considerable distance from the surface of the crystal.

Having now obtained kinetic expressions for I and u, it is possible to give a more quantitative formulation of the conditions required for glass formation. The problem is thus to determine the minimum values of $\Delta G'$ and $\Delta G''$ necessary for glass formation. Values for I_{max} and u_{max} must also be assumed. These values can not be exceeded in the course of cooling and are thus somewhat arbitrary, since they are dependant on cooling rate. Turnbull and Cohen[71] take :

I_{max} = 1 nucleus cm^{-3} s^{-1}

u_{max} = 10^{-5} interatomic distances s^{-1}.

The conditions for glass formation can thus be regarded as:

1. Upon cooling from the melt, there must be no temperature T' (< T_f) at which the nucleation rate exceeds I_{max}.
2. Or, if such a temperature exists, the growth rate always remains less than u_{max}.

This kinetic treatment is more likely to be valid when in the course of vitrification, the atomic movements are closely related to viscous flow processes or interdiffusion. The formation of glasses is easier in complex oxide systems (e.g. oxide glasses containing a variety of cations) because in addition to lowering the melting point, there has to be a redistribution by interdiffusion of diverse constituents prior to crystallization.

The models described above have generally been postulated for simple glasses. The structure and properties of complex glasses are still to an extent unresolved, and may be affected by other factors, such as amorphous phase separation which would obviously affect the kinetics of nucleation and crystal growth.

1.8 AMORPHOUS PHASE SEPARATION (APS)

Many glass forming systems do not produce homogeneous glasses; rather the glass is observed to consist of two non-crystalline phases, produced as a result of phase separation. This results in a change in the physical and chemical properties of the glass and in addition, the appearance or texture of the glass will be altered to an extent governed by the system and how rapidly it is cooled.

Barry et al[76,77] have observed phase separation of ionomer glasses into two phases; one of which is more reactive. The extent and scale of any phase separation will clearly effect the susceptibility of the glass to acid

attack. Indeed, Hill and Wilson[78] have shown there is a quite marked effect in both the appearance of the glass and the properties of the glass ionomer cement as a result of phase separation.

1.8.1 Metastable Phase Separation

If phase separation takes place above the liquidus, it is known as stable immiscibility, whereas phase separation at temperatures below the liquidus is known as metastable or glass-in-glass phase separation. A comprehensive review of phase separation has been written by James[79].

Phase separation will occur in a glass if the system can reduce its' free energy by unmixing. There are two possible routes for phase separation to occur below the liquidus; by a nucleation and growth process or by spinodal decomposition. The former parallels closely the kinetic theories for crystal nucleation and growth, whilst the latter has principally been characterised by Cahn and co-workers[80-85].

That phase separation occurs can best be shown by considering the two possible ways in which free energy varies with composition for a mixture of components A and B at a temperature T. The curves arise due to the fact that the change in free energy of mixing is related to both enthalpy and entropy by the equation:

$$\Delta G_m = \Delta H_m - T\Delta S_m$$

This relationship is shown schematically below in Figure 18. The entropy term will always favour mixing at any temperature and any combination of A and B. The difference in the two curves below is due to the contribution of the enthalpy term ΔH_m.

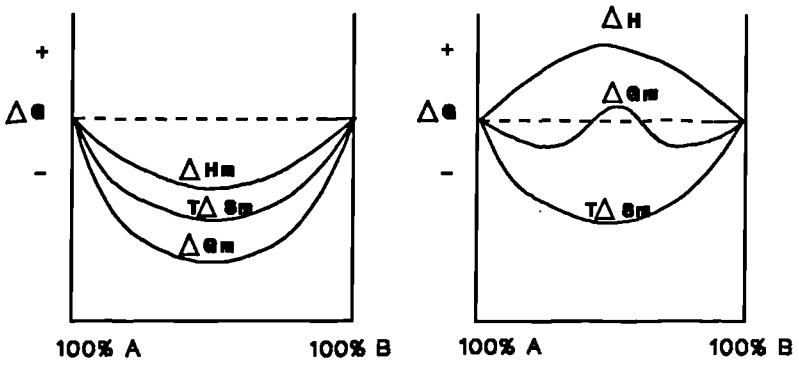

Figure 18 - Variation of Free Energy with Composition

If ΔH_m is also negative,as shown in the first figure, then ΔG_m is very negative and mixing is highly favoured as the way to reduce free energy; there could be no phase separation at any temperature or composition. If, however, ΔH_m is positive, as shown by the second figure, then mixing is unfavourable and the equation predicts that phase separation will occur for compositions which will reduce free energy by unmixing, i.e. compositions between x_1 and x_2 in Figure 19 overleaf:

Points x_3 and x_4 represent inflections in the ΔG curve at which the second differential of free energy with respect to composition is zero, i.e., $d^2G / dx^2 = 0$.

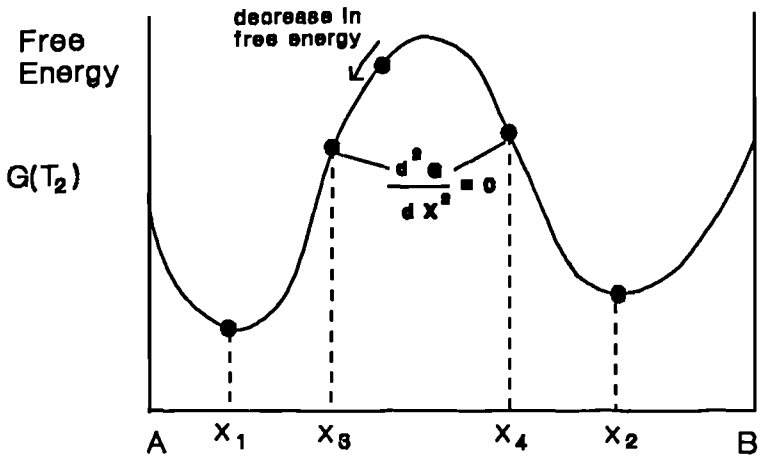

Figure 19 - Variation of Free Energy with Composition

Between x_3 and x_4 d^2G / dx^2 is negative and any fluctuation of any size would result in the reduction of free energy. The system is thus unstable to any fluctuation and separation will occur spontaneously and be accompanied by a constantly decreasing free energy. The system is controlled entirely by diffusion in a direction opposite to the concentration gradient, until the limiting compositions of the separate phases are reached. Phase separation thus occurs without an activation energy and is known as spinodal decomposition.

In the regions between (x_1 and x_3) and (x_2 and x_4), small fluctuations would increase the free energy. The single phase is thus stable with respect to such fluctuations which would tend to spontaneously dissolve. Growth would only be possible if the fluctuations attained

a critical size. There is thus a kinetic barrier to phase separation outside the spinodal. In this region, phase separation takes place by a nucleation and growth process, nuclei being fluctuations which are large enough to cause a free energy decrease.

At low temperatures, the boundaries where phase separation occurs, x_1 and x_2, are widely separated but move closer as the temperature is increased. The loci of the minima thus trace out an immiscibility dome as shown in Figure 20 below. Eventually, the two minima coincide at T_c, the upper consolute temperature. Likewise, the points of inflection move close together with increasing temperature and also meet at T_c. Thus the loci of these points also trace out an inner dome, defining the spinodal region.

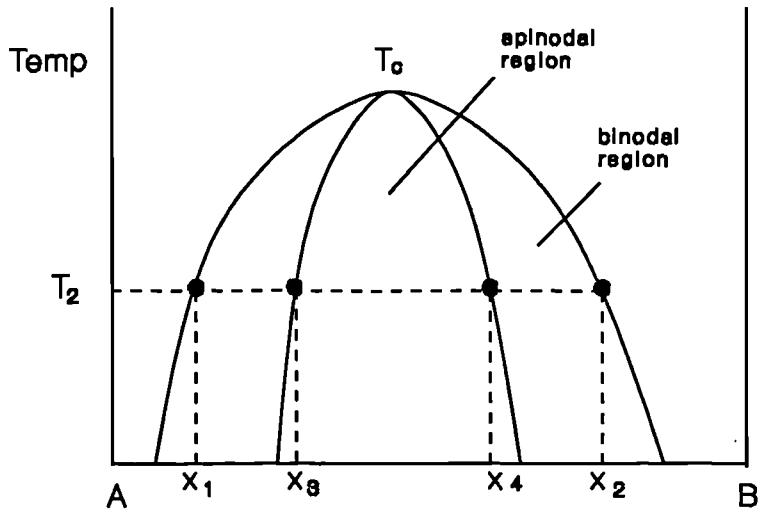

Figure 20 - Immiscibility Dome showing Spinodal Region

Because phase separation in the two regions occurs by

different processes, the morphology of the separated phases in each region is also distinctly different. These differences are shown in Figures 21 and 22, which represents how the composition of a component varies as a function of time. In the case of spinodal decomposition, there is a continuous change in composition around the starting composition, c_o up to a point where equilibrium is attained. The interface between the two phases is initially diffuse but ultimately becomes sharp, when the separated phases attain their limiting concentrations, c_a and c_a'. The separated phases are generally non-spherical and have a high degree of connectivity. The distribution of the second phase is characterised by a geometric spacing, which can be regarded as a set of sinusoidal concentration waves with constant wavelength but variable orientation, phase and amplitude. This gives the characteristic interconnected structure represented below in Figure 21. Eventually the interconnected structure breaks down to give a droplet in matrix morphology.

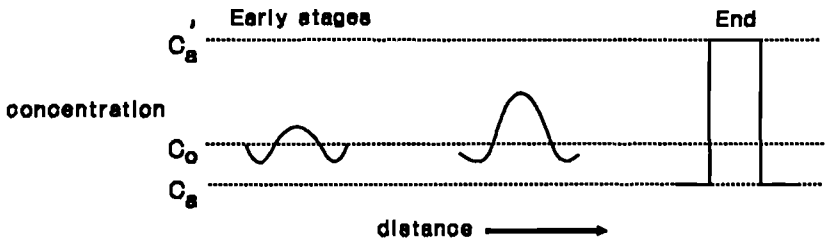

Figure 21 - Morphology following spinodal decomposition

In contrast, for phase separation by nucleation and

growth, the composition of the second phase does not vary with time and the interface remains distinct throughout the process; only the size scale changes (see Figure 22). In this case, there is a tendency towards a random distribution of both the size and position of the phases. The minor phase tends to consist of spherical particles exhibiting low connectivity to give a microstructure of distinct droplets randomly distributed in a matrix phase.

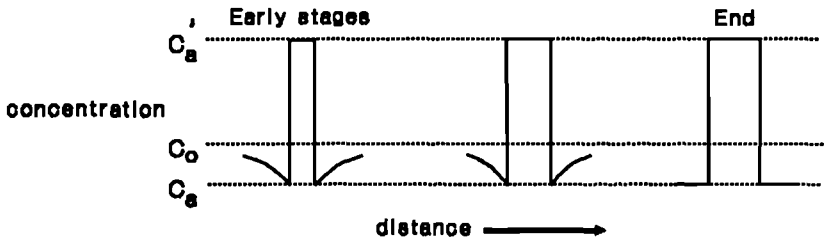

Figure 22 - Morphology following Nucleation and Growth

In addition to phase separation occurring upon cooling from the melt, phase separation can be *induced* in a glass by means of a subsequent heat treatment. Such phase separation has been widely used in the production of opaque enamels [essentially, glassy emulsions containing dispersed phases in the form of fine droplets] and many opal glasses. Metastable phase separation can also occur as a precursor to the formation of many glass-ceramics.

1.9 GLASS-CERAMICS

These are fine grained polycrystalline materials which are obtained from an initially vitreous phase following a

heat treatment cycle. The large number of fine crystals limits the propagation of Griffith flaws through the glass-ceramic which consequently has far superior mechanical properties compared to the base glass. The final properties depend directly upon the nature of the precipitated phases, the degree of crystallinity and the size of the crystallites, etc..

To obtain the fine microstructure which characterises a glass-ceramic requires bulk nucleation from a large number of sites. This occurs if the nucleation rate, I, is high within the glass. In general, this can not be achieved by homogenous nucleation but rather is brought about by the addition of suitable nucleating agents.

These are materials which are soluble in the molten glass, but which upon cooling or upon subsequent reheating, take part in or promote structural changes within the glass, leading to the development of a high density of internal nucleation sites. As one way of achieving this, the nucleating agent may precipitate out of the glass by homogenous nucleation in a finely dispersed form.

For such nucleating agents the rate of homogenous nucleation must be high (requiring a low free energy of activation for nucleation). This depends upon there being a high degree of supersaturation and a low interfacial energy between the nuclei and the glass. Furthermore, the activation energy for diffusion of the units which make up the nuclei must be low enough to allow embryos to reach critical size.

Another method by which nucleating agents facilitate crystallization is by promoting phase separation below the liquidus, which results in the kinetics of nucleation becoming more favourable. Uhlmann[86] believes that phase separation occurring prior to nucleation and growth could influence the behaviour of the glass during reheating in various ways.

Phase separation has the result of producing two vitreous phases. The contact angle, θ, defined previously, between two vitreous phases is generally lower than that between a vitreous and crystalline phase. There is thus good wetting between the phases and the contact angle tends to zero. This implies that $f(\theta)$ will also tend to zero and that the activation energy for nucleation would be negligible. There is thus a larger driving force for nucleation than existed in the base glass.

In addition, the formation of a significant interface during phase separation can serve as a preferential site for nucleation. Atomic mobility may be enhanced and in the interfacial regions between the two phases, there may be an enrichment in some component providing a local increase in the driving force for nucleation.

The changes in structure and mobility of various units that result from amorphous phase separation may increase the probability of homogenous nucleation within one or both of the phases and nuclei arising this way may serve to provide heterogeneous nucleation of other crystalline phases.

The efficiency of a nucleating agent in promoting growth of crystalline phases is dependant on factors such as the interfacial energy and the matching of lattice parameters between the nucleating particle and the phase being crystallised.

To promote a fine grained microstructure, the growth rate, u, can not be too high. With a high growth rate, once growth is initiated at a nucleation site, the crystal growth front could move so rapidly as to prevent initiation of growth at nearby sites. The resulting microstructure would tend to be coarse. Growth should therefore proceed at a rate compatible with crystallising the bulk of the glass in a reasonable timescale.

An idealised heat treatment schedule is shown in the Figure 23 below.

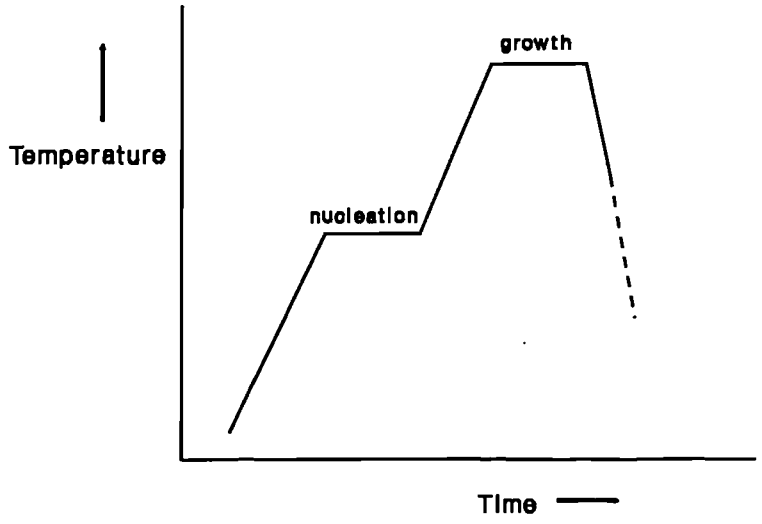

Figure 23 - Idealised Heat Treatment for a Glass-ceramic

The heating rate should be low enough to prevent the occurrence of thermal gradients within the glass;this results in stresses within the material and possibly cracking. The optimum nucleation temperature generally seems to lie within the range of viscosities of 10^{11} to 10^{12} Poise; to a first approximation the optimum nucleation temperature corresponding to these viscosities lies between (T_g) and (T_g + 50°C)

Following the nucleation stage the glass is further heated (at a low rate) to the optimum growth temperature, selected to provide maximum growth of the crystalline phase without deformation of the material by viscous flow. Cooling may or may not involve a subsequent annealing step, depending upon the system.

1.10 FLUORINE IN GLASSES AND GLASS-CERAMICS

Ionomer glasses are unique in that they have fluorine as a major component in the glass. Generally, lower amounts of fluorine have historically been used in glasses for a number of purposes; as an opacifying agent in opal glasses, as a fining agent in glass melts and also as a nucleating agent in many glass-ceramic systems. A comprehensive review of fluorine containing glasses and glass ceramics has been carried out by Singer and Tomozawa[87-89].

Kumar et al[90] have looked at the effect of fluorine on silicate and phosphate melts. They concluded that fluorine was lost as HF in the presence of water and as SiF_4 when no water was present in the air. The weight loss was strongly

dependant on the basicity of the glass; the greater the basicity of the glass, the less the weight loss observed. They postulated that in basic melts, above a certain metal oxide content, there was little tendency to form Si-F bonds; rather, fluorine was present as free F^- species. Below this metal oxide content, fluorine was present both as F^- ions and also replacing oxygens coordinated with silicon to form Si-F bonds.

Rabinovich[91] has looked at the structural role of fluorine in silicate glasses in terms of the relative abilities of oxygen and fluorine to screen silicon cations. He argued that oxygen will generally screen silicon preferentially because of its greater polarisability compared to fluorine. Not all the oxygens surrounding a silicon screen the cation equally, e.g. non-bridging oxygens are always polarised in a way that provides the best screening to silicons.

At high temperatures, thermal vibrations may result in a situation where three (bridging and non-bridging) oxygens provide relatively good screening.If a fluorine ion then provides a better screening to the silicon cation than the fourth oxygen, then the fluorine ion may replace the fourth oxygen resulting in the formation of the $[SiO_3F]$ tetrahedron. Further substitution of fluorine into such a tetrahedron to give $[SiO_2F_2]$, $[SiOF_3]$ and eventually volatile SiF_4 molecules is less likely because such substitution will reduce the overall screening of the silicon cation. The tendency to further substitution is greatest in high silica

(i.e. acidic) glasses.

Because non-bridging oxygens provide such good screening, is unlikely that fluorine will successfully replace them. Therefore, the more non-bridging oxygens there are in the glass, i.e. the more basic is the glass network, then the less may fluorine ions be incorporated in the glass network. The fluorine ions are then postulated as remaining within the co-ordination spheres of other cations. The chance of forming SiF_4 molecules in such melts is slight and the volatilisation of fluorine from such melts would be expected to be low. The fluorine ions which have moved into the spheres of M^+ and M^{2+} ions are postulated as leading to the formation of crystalline fluorides in glass.

Parker and West[92] have carried out a model study of SiF_4 volatilisation from Na_2O-CaO-SiO_2 glasses containing up to 6 wt% fluorine. They described the glasses precipitating CaF_2 and giving a charactistically white product consisting of spherical crystals of diameter approximately 1μm. Upon heating in a dry atmosphere to temperatures of 900-1000°C, SiF_4 was reported to be the major species lost. In addition, they quote vapour pressures of various fluorides at 1425°C, shown overleaf, which show that SiF_4 has by the far the greatest vapour pressure. It is thus not surprising that volatilization of SiF_4 is so common.

Fluoride species	Vapour Pressure (mm Hg)
SiF_4	4×10^7
AlF_3	8100
NaF	98
CaF_2	0.1
(SiO_2	<0.01)
(Al_2O_3	<0.01)

Shelby and Coon [93,94] have proposed a model for the structural role of fluorine in lead fluorosilicates. They suggest that at low F^- contents, fluorine ions are bonded to the Pb^{2+} ions. As a result of the relative field strengths of Pb^{2+} and Si^{4+} ions, they assume that the Pb-F bond is relatively weak, explaining the high mobility of fluorine ions within this system and the low activation for conduction seen in these glasses. At high fluorine contents, the fluorine is postulated as switching sites and bonding to silicon rather than lead, and not contributing to conduction. Shelby et al[95,96] have also looked at CaO-CaF_2-Al_2O_3 glasses. They found that the structure of these glasses was analogous to the similar fluoroaluminosilicate glasses[93,94], with tetrahedral aluminium ions occupying the silicon sites. The addition of fluorine led to the same trends in behaviour which supported the idea that fluorine entered these structures as a nonbridging species in the form of AlO_3F tetrahedra.

Fluorides can crystallise out of glasses with considerable ease; this is attributed to fluorine

disrupting the network[97]. Even if a clear glass has been produced upon cooling a fluorine-containing melt, reheating of the glass to a temperature within or just above the annealing range often results in the formation of crystalline fluoride nuclei. This is due to atomic rearrangements within the glass being relatively easy because of the weak network. The nuclei are formed at a temperature where the crystal growth rate, u,is low resulting in fluorides being precipitated as a large number of very fine crystals, giving a high density of nucleation sites.

By weakening the glass structure, fluorine modifies the kinetic barriers for nucleation and growth which can then take place at lower temperatures. Vogel and Höland[98], for instance, found when studying $MgO-Al_2O_3-SiO_2$ glasses that addition of fluorine lowered the temperature for crystallization from 1130°C to 960°C. The fluorine containing glass also showed more advanced phase separation as a precursor to nucleation. Glass-in-glass phase separation prior to crystallization was also seen by Mukherjee and Rogers[99] in $Na_2O-CaO-Al_2O_3-SiO_2-CaF_2$ glasses; the phase separation took place more readily as the fluorine content was increased and was found to be the rate determining step in the formation of nuclei.

Roginskaya et al[100] investigating the crystallization of glasses in the $CaO-Al_2O_3-SiO_2-R_2O$ system containing fluorine, determined that the crystallization of fluorosilicate phases took place from a droplet phase

enriched in Ca^{2+} and F^- ions.

A calcium fluoride rich droplet phase was also observed by Gutzow et al[101] in boro-silicate enamels to which 10 to 30 wt% calcium fluoride had been added. During the subsequent heat treatment of the phase separated glass, cubic microcrystallites of fluorite were formed between the droplets.

Has and Stelian[102] produced glass-ceramics for potential use as hard or household porcelain or stoneware. They found that during heat treatment, formation of silicate crystals took place on nuclei of fluoride microcrystals which appeared in the material at the beginning of the heat treatment. They looked at a complex glass containing SiO_2, Al_2O_3, MgO, CaO, BaO, ZnO, PbO, Na_2O and K_2O into which was substituted 8-20 % by weight of a corresponding fluoride.

1.11 GLASS-CERAMICS AS BIOMATERIALS

Bioceramics (including bioglasses and bioglass-ceramics) are a new class of materials which are designed to be used for surgical implants. The common requirement of these materials is therefore that they show no adverse tissue reactivity, that is that they are biocompatible.

Biocompatibility is defined after Williams[103] as

'the ability of a material to perform with appropriate host response in a specific application'.

In considering biocompatibility we must consider both the host response and the response of the biomaterial.

Ceramics make good biomaterials because, due to the wide range of glass and ceramic compositions which can be used, the ceramic can be tailored to achieve:

1. similarity of physical properties to those of bone
2. corrosion resistance to body fluids
3. tissue adherence
4. high compressive strength
5. compatibility with the musculo-skeletal system

etc.,etc..

However, ceramics are not ideal biomaterials. There are a number of problems associated in particular with the brittle nature of ceramics, including a lack of ductility, low static strength and impact resistance and a generally low flexural strength. They also suffer from environmental stress cracking in the relatively aggressive conditions encountered in the body.

Bioceramics fall into three general categories, (i) nearly bioinert, (ii) bioactive and (iii) resorbable. Each type has a different tissue response and means of attaching the prosthesis to the musculo-skeletal system (see Table 4 below) and find use in diverse applications including heart valves, bone plates, tooth implants, and hip and knee implants.

Table 4 - Tissue attachments of bioceramics[103]

Type of attachment	example
Dense, nonporous, nearly inert ceramics attach by bone growth into surface irregularities by cementing the device into the tissues or by press fitting into a defect (morphological fixation)	Al_2O_3 (single crystal and poly-crystalline)

For porous, inert implants bone ingrowth occurs, which mechanically attaches the bone to the material (biological fixation)	Al_2O_3 (porous, poly-crystalline) Hydroxyapatite coated porous metals
Dense, nonporous, surface reactive ceramics, glasses and glass-ceramics attach directly by chemical bonding with the bone (bioactive fixation)	**Bioactive glasses** **Bioactive glass-**ceramics Hydroxyapatite
Dense nonporous (or porous) resorbable ceramics are designed to be slowly replaced by bone	Calcium sulphate Tricalcium phosphate

1.12 BIOGLASSES AND GLASS-CERAMICS

Hench et al[28] have developed a surface active glass of the formula Na_2O-CaO-CaF_2-P_2O_5-SiO_2. Many of the glasses in this system are based on the composition 45S5 in which there is 45% SiO_2 and a 5 to 1 molar ratio of Ca to P. Such a composition has a highly reactive surface when exposed to an aqueous medium. The surface forms a biologically active hydroxycarbonate apatite (HCA) layer which provides the bonding interface with tissues; such a layer seems to be common amongst successful bioglasses and glass-ceramics. The addition of as little as 3% Al_2O_3 to Bioglass, however, results in a complete loss of bone-bonding ability.

There are a large number of bioglass-ceramics containing apatite as a crystal phase. The materials fall into two distinct groups, the apatite-wollastonite (A-W) glass-ceramics developed by Kokubo et al[104] and the mica based materials that were originally developed by Beall[105] and Grossman[106]. This latter group includes the Bioverit materials developed by Vogel et al[107] and the Ceravital materials[108].

In the A-W glass ceramics it is the needle shaped wollastonite crystallites that impart the high strength and fracture toughness to the final material[109]. The processing route for A-W glass-ceramics, however, is not a classic two stage nucleation and growth process, but involves sintering a glass-ceramic powder. This is due to the fact that wollastonite undergoes surface nucleation to produce a very coarse microstructure of needles growing in from the surface to the bulk of the material. Rather, the glass is quenched, ground into a fine powder and then sintered and crystallised in one stage. Such a material is unlikely to have an optimum microstructure and strength.

In the other type, the mica phase imparts machinability and strength. However, the mica containing glass-ceramics generally contain a high proportion of alkali metal ions, which results in *in vivo* degradation of mechanical properties. Furthermore, the strength and machinability of these materials is always compromised at the expense of sufficient bioactivity.

1.13 THE GLASS COMPONENT OF THE GLASS IONOMER CEMENT

From early on, Kent et al[110] realised that a completely systematic study could not be mounted on a six component glass system. Instead, they varied the amount of each component in turn and looked for an effect from each.

They looked at several series of glasses varying the Al_2O_3:SiO_2 ratio, the $AlPO_4$ content, the AlF_3 content and the CaO:Na_2O ratio respectively. As the Al_2O_3:SiO_2 ratio was

increased so the hydrolytic stability and the rate of set of the cements was increased. It was also found that the presence of Na^+ ions reduced the hydrolytic stability of the cement.

During this study, the loss of fluorine from the melt was neglected which limits some of the value of this work. In addition, the quenching conditions were not controlled and this resulted in some of the glasses being phase separated and crystalline. Quenching conditions play a very important part in the subsequent properties of the glass. Barry et al[76,77] observed phase separation of ionomer glasses into two phases; one of which was more reactive. The rate of quench will clearly affect the degree of phase separation and hence the susceptibility of the glass to acid attack. Indeed, Hill and Wilson[78] have shown there is a quite marked effect in both the appearance of the glass and the properties of the cement, depending upon the precise quenching regime.

The same criticisms can also be applied to parallel work carried out by Wilson et al[40]. They examined a series of simple ternary and quaternary ionomer glasses in which the amounts of each component were systematically altered. The glasses they looked at fell into five basic types:

i. SiO_2-Al_2O_3-CaO

ii. SiO_2-Al_2O_3-CaF_2

iii. SiO_2-Al_2O_3-CaO-CaF_2

iv. SiO_2-Al_2O_3-CaO-P_2O_5

v. SiO_2-Al_2O_3-CaF_2-P_2O_5

The glasses were again quenched onto a metal plate prior to being quenched in water and fluorine loss was again neglected in the study. In spite of this, Wilson drew some useful general conclusions. With regard to the ternary glasses, it was found that glasses containing CaO produced weaker cements than those which contained CaF_2; these cements were also hydrolytically less stable.

In both systems a high silica content prevented cement formation and in both systems the critical Si/Al ratio for cement formation was 2:1, below which glasses yielded fast setting cements and above which useful cements were not formed. This ratio can not be considered in isolation, however, since the mole fraction of network modifying cations largely determines the structural role of aluminium within the glass network.

It was found that in order to obtain four coordinate aluminium, the Ca:Al ratio had to be greater than 1:2 and the Si:Al ratio had to be greater than 1:1.

The four component (SiO_2, Al_2O_3, CaO, CaF_2) glasses produced cements which were either very fast setting or indeed unworkable. The setting time of the cement is related to the acid susceptibility of the glass; this is determined by the number of bridging oxygen atoms in the glass network, i.e. the cross-link density of the glass. The greater the number of bridging oxygen atoms in the glass, the more cross-linked is the glass network and the less susceptible will be the glass to acid attack (and the slower will be the cement to set).

This model also explains the role of calcium fluoride within the glass. Calcium fluoride is found to act as a powerful network modifier; as well as introducing a network dwelling cation, it also provides a non-bridging fluorine which reduces the cross-link density of the glass. The presence of calcium fluoride in the glass thus accounts for the high reactivity and acid susceptibility shown by these quaternary glasses.

The glasses containing P_2O_5 and CaO would not form hydrolytically stable cements whilst those glasses containing P_2O_5 and CaF_2 contained such an excess of calcium fluoride that they had all crystallized to fluorite.

2. AIMS

There are a number of problems which can be readily identified with regards to the current ionomer glasses. In both current dental and proposed orthopaedic applications, consistent setting times and mechanical properties are essential, but in practice it has been found that there are marked batch to batch variations in the properties of the glasses.

During the melting procedure, fluorine is lost from the melt in an uncontrolled manner, largely as HF. This results in variable composition between batches. Another problem is that fluorides are corrosive towards elements and furnace linings; this can be a real problem when scaling up to commercial production.

Upon quenching, some of the more complex glasses are

known to liquid-liquid phase separate[76,77] into two phases,one of which is rich in calcium and fluorine; this phase is attacked preferentially by the polyacid and thus plays the major role in the setting reaction. These glasses may subsequently crystallise to one or more crystalline phases, typically calcium fluoride (fluorite). The rate of quenching, therefore, strongly influences glass properties. Commercial manufacturers often subject the glass to a series of corrective heat treatments until a glass batch gives acceptable properties. The effect of these heat treatments is not clear.

Because of these problems, it was decided to develop new glass compositions. Also, by designing new glass compositions, it was hoped to understand the fundamental processes governing the behaviour of the glasses. This should enable a *systematic* development of glasses to be possible, with the aim of optimising properties. In order to do this, it is first necessary to eliminate fluorine loss from the melt so that glasses of defined composition can be made. It is also important to gain an understanding of the processes of amorphous phase separation and crystallization.

It was decided to initially investigate a reactive glass from the quaternary (SiO_2-Al_2O_3-CaO-CaF_2) system studied by Wilson et al[40] and by means of a subsequent heat treatment, to crystallize out the calcium fluoride in a controlled manner. In effect a glass-ceramic[97,111] would be

produced in which the network modifying ions were incorporated into a crystalline phase, to leave a less reactive residual glassy phase which would take part in the cement forming reaction. To achieve a suitable degree of control over the removal of the network modifier a completely amorphous glass was needed.

A glass, generically named G280, was initially chosen from the paper by Wilson. This glass has the composition $2SiO_2.Al_2O_3.CaO.CaF_2$; the Ca:Al ratio is greater than 1:2 and the Si:Al ratio equals 1:1. All the aluminium ions would, therefore, be expected to take up four-fold coordination in the glass network. In addition, the glass has a relatively low fusion temperature and was reported as not attacking the crucible to any great degree; which is important from a practical view.

Glasses containing systematic additions of sodium oxide and phosphorus pentoxide were also investigated. {These compositions are similar in many ways to various bioglasses[28] and bioglass-ceramics[104].}

3. EXPERIMENTAL

3.1 MATERIALS

$CaCO_3$	FSA Laboratory Supplies, Bishop Meadow Road,Loughborough
Na_3AlF_6	FSA Laboratory Supplies, Bishop Meadow Road, Loughborough
P_2O_5	FSA Laboratory Supplies, Bishop Meadow Road, Loughborough
Al_2O_3	BDH Ltd., Merck House, Poole, Dorset
SiO_2	TSL Group plc., PO Box 6, Wallsend, Newcastle
CaF_2	Riedel-de Haën, AG D-3016 Seelze 1, Germany
Poly(acrylic acid)	Allied Colloids, Bradford
(+) Tartaric acid	BDH Ltd., Merck House, Poole, Dorset

3.2 METHODS

3.2.1 Preparation of Glasses

The glass components were weighed out in the appropriate quantities to give a 500g batch of pre-fired powders. After being mixed for 2 hours in a ball-mill, the mixture was transferred to a sillimanite crucible and a lid put on. The crucible and contents were vacuum dried to eliminate as much moisture as possible prior to firing. The crucible and charge were heated at temperatures between 1350°C and 1550°C depending upon the composition in an electric furnace. To protect the elements from fluorine attack, the elements were not located in the furnace

chamber but were within the walls of the furnace. After typically 90 min. the glass melt was quenched either directly into water to produce a frit or poured into a pre-heated graphite mould, as required. Glass frit was subsequently ground in a vibratory mill to produce a fine powder.

3.2.2 Thermal Analysis

3.2.2.1 Differential Thermal Analysis (DTA)

This is a sensitive method for evaluating the thermal properties of samples covering both exothermic and endothermic energies. A DTA trace is a graph of the differential temperature between the sample and a reference material plotted against the actual temperature.

Alumina was used as the reference material and sample and reference were placed in matched platinum/rhodium crucibles. Temperature changes are measured by two thermocouples in contact with the crucibles. The thermocouples are connected back to back so that their e.m.f.s are opposed; the net e.m.f. is therefore a measure of the temperature difference between the two.

DTA experiments were performed on a Stanton Redcroft DTA 673-4, and a standard heating rate of 10°C was employed.

3.2.2.2 Nucleation Efficiency

A given mass of glass particles of a size, for instance, of <45 μm have a large surface area compared to

the same mass of larger particles (e.g. >125 μm). If crystallization is occurring from the bulk of the glass, particle size would be relatively unimportant since surface crystallization would make only a small contribution to the overall crystallization rate. If surface crystallization is the dominant mechanism, then different particle sizes would be expected to undergo different degrees of crystallization. This would be seen by DTA since the crystallization peak temperatures would be different for different particle sizes. By performing DTA on a series of different sized particles, it is thus possible to look at whether a glass crystallises by a surface or bulk mechanism.

3.2.2.3 Activation Energy Determination

Activation energies of crystallisation can also be determined by DTA. The activation energy measured is a combination of both nucleation and growth terms. Both nucleation and growth are temperature dependant as shown previously in Figure 14.

By heating the samples at various rates, the amount of time at which the glass is at its maximum nucleation and growth rates will be different. This difference will be reflected in the temperatures of peak crystallization shown on the DTA trace. The method thus involves DTA runs performed at different heating rates. Marotta et al[112] derived a relationship between heating rate and crystallization temperature :

$$\ln 1/T = Ea/RTp + \text{constant}$$

where, Tp = crystallization peak temperature

$\dot{T}$ = heating rate

Ea = activation energy

R = gas constant

This method makes no allowance for different crystallization mechanisms and is effected both by nucleation and growth processes.

Matusita et al[113,114] have developed another method which requires a prior knowledge of crystallization mechanism. The method is also based on the relationship between heating rate and peak crystallization temperatures.

They argued that the rate of change of the volume fraction of crystals precipitated in the glass could be expressed as:

$$\frac{dx}{dt} = A\alpha^{-(n-1)}\ (1-x)^{k} \exp\left(-\frac{mE}{RT}\right)$$

where:

x = volume fraction of crystals

A = a constant

α = heating rate

n, k and m = numerical factors depending upon mechanism of crystallization

E = activation energy for crystal growth

The rate of change of x reaches its maximum at a temperature of T_0. Solving the above equation for

(d/dt)(dx/dt) = 0, the following equation is derived:

$$\frac{\alpha^n}{T_0^2} = \frac{AkR}{mE}(1-x_0)^{k-1}\exp^{\left(-\frac{mE}{RT_0}\right)}$$

where:

x_0 = volume fraction of crystals at T_0

The term k is equal to 1 for bulk nucleation. Therefore, the term $(1-x_0)^{k-1}$ is always 1 for bulk nucleation. For surface nucleation, the term k is equal to 2/3 and the term $(1-x_0)^{k-1}$ can be regarded as a constant compared to the exponential term. The above equation can thus be rewritten as:

$$\ln\left(\frac{\alpha^n}{T_0^2}\right) = -\frac{mE}{RT_0} + constant$$

Unidirectional surface dominated crystallization can be represented by n = m = 1; whilst the activation energy for bulk crystallization from a constant number of nuclei can be obtained by setting n = m = 3.

Therefore, as long as the crystallization mechanism is known, a plot of ln (α^n / T_0^2) versus $1/T_0$ will yield a value for activation energy which is a function of the gradient of the line, as determined by linear regression.

3.2.2.4 Thermogravimetric Analysis (TGA)

TGA was used to monitor how the mass of a sample changed with increasing temperature upto 1000°C, relative to that of an inert material, the weight of which is constant. TGA was carried out on two glasses using a Stanton Redcroft STA 1500, employing a heating rate of 10°C/min and a nitrogen atmosphere.

3.2.3 X-Ray Powder Diffraction (XRD)

X-ray powder diffraction was carried out on a Rigaku Miniflex Diffractometer, modified to permit step counting and interfaced to a microcomputer[115], as shown overleaf in Figure 24. By using step counting, the number of counts is kept constant and the time to detect them is measured. This then allows a count rate to be calculated. Because the number of counts is constant for each step, the standard deviation will also be constant and therefore independent of peak intensity.

The step counting parameters were : starting angle 60°, finishing angle 10°, interval angle 0.1°, counts per step 5000.

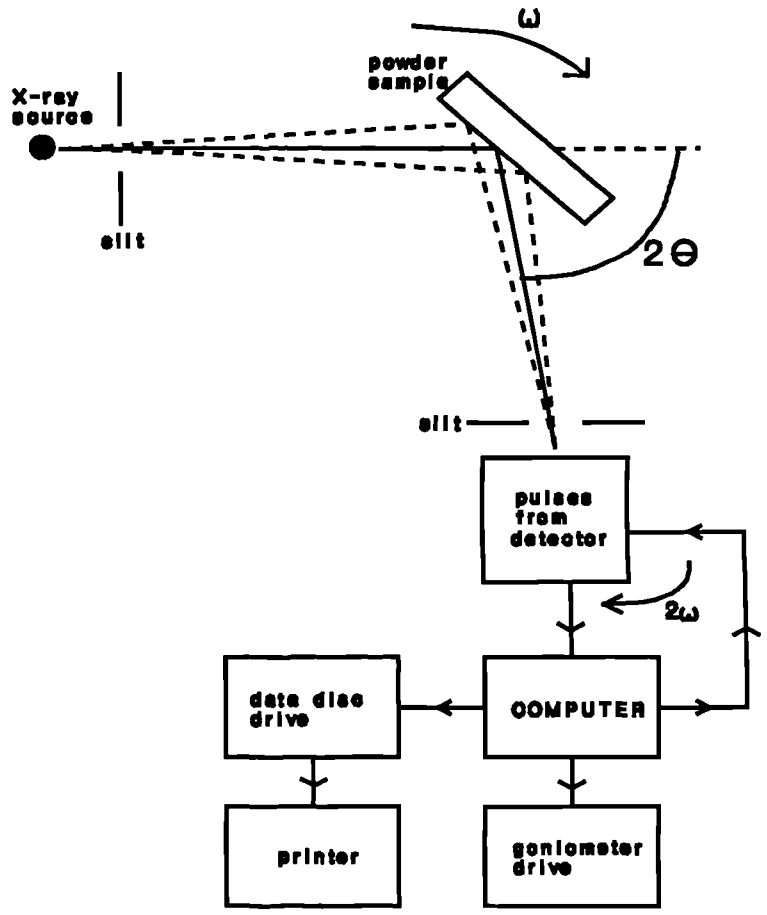

Figure 24 - Modified X-ray Diffractometer

A 5000 count has a standard deviation of 71 and a maximum likely error of 1.4%.

In order to determine the amount of crystalline calcium fluoride in any glass, a quantitative X-ray diffraction method was used.

In a mixture of two phases, α and β, the intensity of a selected line of the α phase can be written as:

$$I_\alpha = \frac{K_1 C_\alpha}{\mu_m}$$

where: I_α = intensity of a line of the α phase

K_1 = a constant

c_α = volume fraction of α in the mixture

μ_m = linear absorption coefficient of the mixture

The value of K_1 is unknown because the value of the intensity of the incident beam, I_0, is generally unknown. However, K_1 will cancel out if the ratio of I_α to the intensity of some standard reference line is measured. The approach taken was to use indirect analysis by means of an internal standard following the method of Klug and Alexander[116]. This involves "spiking" the glass with a crystalline phase whose diffraction lines do not overlap with those of the sample.

Suppose that the intensity of phase A in a mixture of phases (A, B, etc.) in a sample is unknown. To a known amount of the sample, a known amount of a standard substance, S, is added to form a new composite material. Let c_A and c'_A be the volume fractions of phase A in the original and composite samples respectively. In addition, let c_S be the volume fraction of S in the composite sample. If a diffraction pattern is now prepared from the composite sample, then from the previous equation:

$$I_A = \frac{K_2 c'_A}{\mu_m} \qquad I_S = \frac{K_3 c_S}{\mu_m}$$

where: I_A = intensity of a particular line of the phase A

I_S = intensity of a particular line of the standard S

Division of one expression by the other gives:

$$\frac{I_A}{I_S} = \frac{K_2 C_A'}{K_3 C_S} = K_4 \frac{C_A'}{C_S}$$

The volume fractions of phase A and the standard S can be expressed in terms of weight fractions by using the equations:

$$C_A' = \frac{w_A' / \rho_A}{w_A' / \rho_A + w_B' / \rho_B + \ldots\ldots + w_S / \rho_S}$$

and

$$C_S = \frac{w_S / \rho_S}{w_A' / \rho_A + w_B' / \rho_B + \ldots\ldots + w_S / \rho_S}$$

where: w_A' = weight fraction of phase A in composite sample

ρ_A = density of phase A

etc., etc.

Therefore,

$$\frac{I_A}{I_S} = K_4 \frac{C_A'}{C_S} = K_4 \frac{w_A' \rho_S}{w_S \rho_A}$$

Now, the densities of the phases are constant and if the weight fraction of the standard, w_S is kept constant in all composite samples, then:

$$\frac{I_A}{I_S} = K_5 w_A'$$

The relationship between the weight fractions of A in the original and composite samples is:

$$w_A' = w_A (1-w_S)$$

Combining the last two equations:

$$\frac{I_A}{I_S} = K_6 w_A$$

The intensity ratio of a line from phase A and a line from the standard S is therefore a linear function of w_A, the weight fraction of A in the original sample. A calibration line for fluorite was constructed by adding standard amounts (2, 5, 10, 20, 40, 80, 100%) of calcium fluoride to an amorphous glass and adding to this mixture an accurately weighed known amount, w_s, of the spiking agent (NaF). The ratio of CaF_2/NaF intensities was determined for each standard and a calibration line constructed.

Peak areas, rather than peak heights were used in calculations as the area method is less susceptible to crystallite size effects. The step counting procedure was further modified to enable a low or high count per step to be used over regions of little or specific interest respectively.

3.2.4 Scanning Electron Microscopy (SEM)

Glass frit was examined before and after heat treatment with a Cambridge Stereoscan 90 scanning electron

microscope. The frit was etched in 0.5% hydrofluoric acid for 15 seconds prior to examination of an internal cleaved surface and were sputter coated with gold to allow conduction.

3.2.5 Transmission Electron Microscopy (TEM)

TEM was carried out on glass samples both using an AEI EM802 TEM machine. Carbon replicas were taken from both powder and bulk samples.

3.2.6 Hydropyrolysis

This is a method to quantitatively determine the amount of fluorine present in the glass. It is based, after Newman[117] on a technique for analysing minerals.

Samples of glass powder were ground thoroughly with a flux mixture and subject to hydropyrolysis. In this method, steam is passed over the powdered sample at 1000 °C and the resulting hydrogen fluoride bubbled with the steam through a buffered sodium hydroxide solution. The amount of fluorine is determined using a fluorine electrode and a series of calibrated standards.

3.2.7 Preparation of Glass-Ionomer Cements

Cements were prepared by mixing the glass and an aqueous solution of poly(acrylic acid). The glass powder

was weighed and placed on a ceramic or PTFE mixing slab. An appropriate volume of poly(acrylic acid) was then pipetted next to the powder and the powder worked into the liquid using a dental mixing spatula, until a smooth homogeneous paste was obtained. The powder to liquid ratio was kept constant at three to one (by weight) and a standard solution of 40% (m/m) poly(acrylic acid) of M_w 2.27 * 10^4 was used throughout. (+) tartaric acid was added for the phosphate free glasses.

3.2.8 Determination of Working Time

Working times were determined from rheograms obtained from the Wilson Rheometer[118]. The apparatus was turned on at the same time as the powder and liquid were first brought together. The setting cement was then rapidly transferred to the apparatus and placed between the two ridged plates, approximately 4mm part, as shown in Figure 25.

One plate was fixed whilst the other oscillated under the action of an eccentrically driven spring.

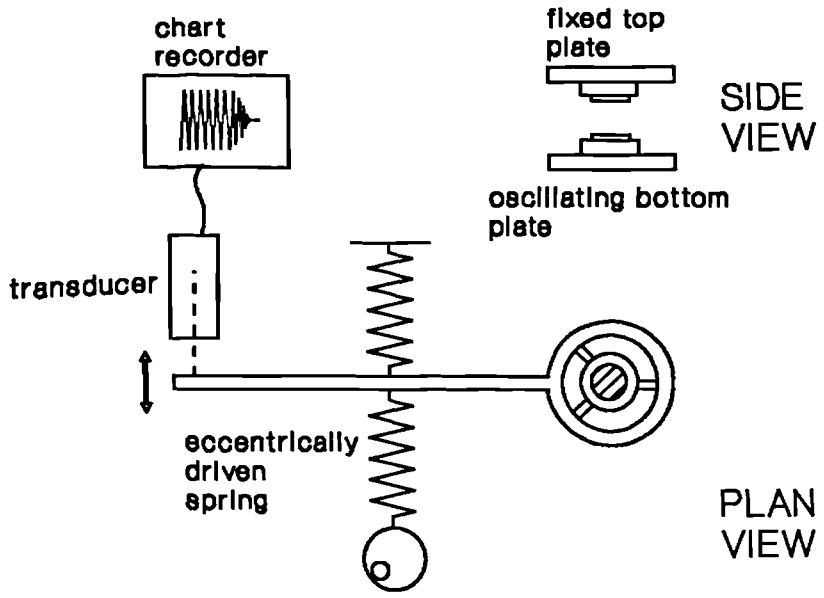

Figure 25 - Wilson Oscillating Rheometer

The amount of oscillation was recorded as a voltage induced by a rod moving in and out of a transducer. With fresh cement between the plates, the rod moved freely. However, upon setting, the cement stiffened and the amount of oscillation was progressively damped, restricting the movement of the rod within the transducer and giving a decreasing output voltage. When the cement had set, the voltage dropped to zero.

The working time was taken as the time for the amplitude of oscillation to fall to 95% of its initial value[119], as shown below. This method thus allows a comparison of working times between different cements; the

values are purely arbitrary and cannot be taken as absolute. In practice, the working time can be regarded as the period of time when the cement can be usefully manipulated by the dentist or surgeon in a clinical situation.

3.2.9 Compressive Strength Determination

Cements were mixed as described previously and packed into stainless steel moulds, to give cylindrical specimens of nominal dimensions 6mm length, 4mm diameter. After packing, the ends were enclosed by polyethylene sheets and stainless steel plates. The whole assembly was then clamped and stored in an incubator at 37°C for 1 hour. The samples were then placed in water at 37°C for 24 hours prior to testing.

Immediately before testing, the diameter of each specimen was measured at three points along its length, and a mean determined. Compressive strengths were measured on a Mayes DM30 universal testing machine at room temperature and humidity. The mean of at least five results were recorded for each glass. Compressive strengths were determined using the formula:

$$compressive\ strength = \frac{4P}{\pi d^2}$$

where, P = load in Newtons

d = diameter of cylinder

Again, this test is purely comparative and has little

practical relevance compared to, for instance, flexural strength or fracture toughness[120], since dental materials rarely fail in compression.

3.2.10 Fracture Toughness by Indentation

The fracture toughnesses (K_{IC}) of cast glass samples and glass-ceramics were measured on polished cut disks using the indentation technique[121,122]. Assuming that the scale of the microstructure of the glass-ceramic remains small compared to the size of the crack system, this technique can be used to measure the changes in fracture toughness between glasses and glass-ceramics. Figure 26 overleaf shows a schematic of an ideal indentation fracture pattern for a Vickers geometry.

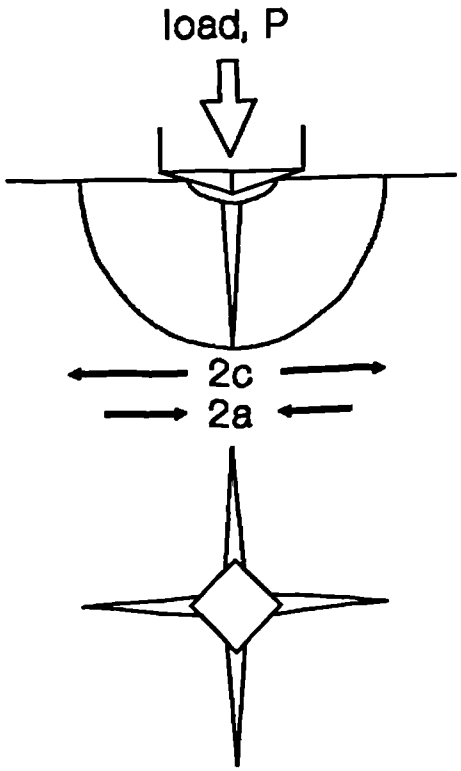

Figure 26 - Fracture Toughness by Indentation

P is the peak load and a and c are characteristic dimensions of the "plastic" impression and the radial/median crack respectively. These parameters are directly related to the fracture toughness of the material by the equation:

$$K_{IC} = \frac{P}{\beta_0 c^{3/2}}$$

where β_0 is a numerical constant.

The technique thus involved measuring the lengths of radial cracks in the sample. Care was taken to avoid chipping of the samples and at least five results were taken for each sample and a mean taken. A Youngs modulus of 120 GPa was assumed for all samples.

4. RESULTS

4.1 EFFECT OF QUENCHING REGIME ON GLASS PROPERTIES

Hill and Wilson[78] have previously shown that the quenching regime was important in determining glass and cement properties for a simple SiO_2-Al_2O_3-CaF_2 glass. In order to look at the effect of quenching in the proposed model system, three batches of the model glass, G280 were prepared, each having the same nominal pre-firing composition, but each being quenched slightly differently. The compositions of the glasses are shown below:

Component	G280/A	G280/B	G280/C
SiO_2	149.96	150.01	150.01
Al_2O_3	127.50	127.49	127.49
$CaCO_3$	124.94	124.99	124.99
CaF_2	97.46	97.49	97.49

Table 5 - Weight (in grams) of G280 Components

The batches were thus assumed to have same pre-firing composition so that any effects observed were concluded to arise from quenching only. Equal weights of all glasses were held at 1350°C for 90 minutes prior to quenching. The first batch, G280/A was quenched by pouring the molten glass onto a steel plate for thirty seconds prior to immersion in water. The second batch, G280/B was poured onto a sloping steel plate and allowed to run into water and the third batch, G280/C was poured directly into water.

The resulting glass frit was then ground down and subjected to X-ray diffraction (XRD) and differential

thermal analysis(DTA).

4.1.1 X-Ray Diffraction

Qualitative XRD produced traces as shown in Figure 27. A quantitative analysis of the amount of crystalline calcium fluoride present in each sample is shown below:

Batch	Crystalline CaF_2
G280/A	1.70
G280/B	0.85
G280/C	not detectable

Table 6 - Amount of Crystalline CaF_2 in each Glass

The quantitative analysis shows that unless the glass is quenched immediately into water, crystalline calcium fluoride will form. Since the best nucleating agent for a crystal phase is a particle of the same phase, any crystallization would obviously restrict the aims of the work which is to bring about the *controlled* crystallization of calcium fluoride from an amorphous glass.

4.1.2 Differential Thermal Analysis

DTA showed for all glasses a characteristic trace as shown in Figure 28. A clear glass transition is seen followed by two exothermic peaks which are attributed to crystallization phenomena. There may be a second glass transition between the two exothermic peaks, but it is not very clear. The data is presented in Table 7 overleaf:

Glass	Tg_1 (°C)	Tp_1 (°C)	Tp_2 (°C)
G280/A	634	692	866
G280/B	639	693	852
G280/C	633	697	866

Table 7 - DTA Data for Three Batches of G280

This data is very inconclusive. The lower peak crystallization temperatures for /A and /B correspond with the glasses being slightly crystalline but there are no real trends for the other features.

Following this work it was decided to quench all the glasses directly into water as the best means of preventing unwanted and uncontrolled crystallization. X-ray diffraction of three subsequent batches of G280, quenched into water confirmed that this procedure would produce a completely glassy material, as shown in Figure 29.

4.2 ANALYSIS OF THE CRYSTALLIZATION MECHANISM OF G280

4.2.1 Qualitative X-ray Diffraction

On the basis of the characteristic DTA trace, a series of samples were placed in a tube furnace which was ramped at 5°C min^{-1} to 930 °C. Samples were removed at temperatures between 650 °C and 930 °C to achieve a series of snapshots of the crystallization process. These samples were then reground and subject to XRD.

The XRD traces of a number of samples are shown in

Figures 30a to 30f. The diffraction pattern of the base glass prior to any heat treatments consists only of a diffuse halo; this shows the glass to be completely amorphous. Above the glass transition at 700 °C, a series of lines appear which on comparison with JCPDS files were found to be due to the crystallization of calcium fluoride. The 111, 220 and 311 lines at 2 theta = 27.9°, 47.0° and 55.4° are clearly visible.

The intensity of these lines increases with increasing temperature until at 870 °C a second series of lines is seen to develop. Once all the calcium fluoride has crystallized from the original glass, the residual glass will have a composition corresponding to anorthite, $CaAl_2Si_2O_8$, and this is seen as the second crystalline phase, (see Table 8). A match for anorthite was not immediately apparent, however, since the most intense lines of anorthite (204, $\underline{0}40$, 220, 004 and 200) overlap with the 111 line from fluorite and the 424 anorthite line overlaps with the 220 fluorite line. The only way of detecting the onset of anorthite crystallization was to monitor the ratios of the various lines.

Because the lattice parameters of fluorite and anorthite are so well matched (as witnessed by the superposition of lines), it may be that anorthite is crystallizing from fluorite nuclei and in effect, this is a self-nucleating system.

A trace amount of gehlenite, $Ca_2Al_2SiO_7$, was also detected; this indicates, as will be shown later, an excess

of calcium in the glass which would arise if the glass had lost a small amount of fluorine.

2 theta (2θ)	**d (Å) expmtl**	d (Å) JCPDS	**I/Io expmtl**	I/Io JCPDS	**phase**
27.96	**3.19**	3.26 3.21 3.20 3.18 3.15 3.12	**100**	55 35 100 75 94 45	**ANOR** **ANOR** **ANOR** **ANOR** **FLUO** **ANOR**
46.64	**1.95**	1.93	**47**	100	**FLUO**
29.27	**3.05**	3.07 3.04	**42**	25 18	**GEHL** **ANOR**
21.89	**4.06**	4.04	**24**	60	**ANOR**
55.42	**1.66**	1.66	**13**	35	**FLUO**
23.85	**3.73**	3.71	**11**	20	**GEHL**
26.38	**3.38**	3.37	**9**	25	**ANOR**
47.39	**1.92**	1.93	**8**	14	**ANOR**
51.59	**1.77**	1.75	**7**	35	**GEHL**
49.35	**1.84**	1.85 1.84	**7**	14 18	**ANOR** **ANOR**
30.39	**2.94**	2.95 2.93	**7**	25 18	**GEHL** **ANOR**
48.42	**1.88**	1.88	**6**	8	**ANOR**
23.01	**3.86**	3.92 3.78	**6**	12 20	**ANOR** **ANOR**
42.07	**2.15**	2.14	**5**	16	**ANOR**
39.36	**2.29**	2.29	**5**	14	**GEHL**
35.90	**2.50**	2.50	**5**	25	**ANOR**
25.63	**3.47**	3.47	**5**	12	**ANOR**
43.09	**2.10**	2.09	**4**	8	**ANOR**
31.61	**2.83**	2.83	**4**	20	**ANOR**
31.33	**2.85**	2.85	**4**	100	**GEHL**

KEY: ANOR = anorthite, GEHL = gehlenite, FLUO = fluorite

Table 8 - X-ray Diffraction Data for G280

It is interesting to note that the lines of maximum intensity of the anorthite and fluorite correspond with the maximum in the scattering for the base glass. One of the previously discussed theories of glass structure is that glasses consist of very small microcrystallites or clusters which have the same structural units as those phases in the equivalent crystal, but which are only a few angstroms in dimension. There is an inverse relationship between crystallite size and the broadening which occurs of diffraction lines. Therefore, small crystallites would produce very diffuse diffraction patterns. Upon crystallization, following a heat treatment, the crystallites would grow in size and the broadening would decrease to give individual sharp lines. It could thus be envisaged that the trace of the largely crystalline material could be reconstituted as the trace of the base glass by assuming massive broadening effects due to small crystallites.

4.2.2 Quantitative X-ray Diffraction

The crystalline calcium fluoride content of the heat treated glasses was then determined quantitatively. The results of the quantitative X-ray diffraction, using an internal standard, are shown in Table 9 overleaf and Figure 31.

Removal Temperature (°C)	CaF_2:NaF ratio	weight% crystalline CaF_2
653	0.00	0.00
680	0.02	0.00
700	0.12	0.37
710	0.21	1.18
720	0.69	5.47
735	1.15	9.53
780	1.44	12.08
802	1.46	12.26
838	1.50	12.61
855	1.46	12.29
870	1.79	15.26
882	1.95	16.68
930	2.27	19.46

Table 9 - Quantatative XRD Data for G280

This data shows quite clearly that the crystallization of calcium fluoride occurs in two distinct stages. This corresponds very well with the two exothermic peaks seen in the DTA thermogram (Figure 28). The much larger second exotherm on the DTA trace is explained by the fact that in addition to fluorite, anorthite (and gehlenite) have crystallised at these higher temperatures.

The extent of calcium fluoride crystallization accounts for 89% of the total amount that was present in the pre-firing composition and assuming at crystallization is not yet complete, it would seem that this glass undergoes relatively little fluorine loss during the

melting procedure.

The apparent two-step crystallization of calcium fluoride is unusual and suggests that the glass could have undergone prior amorphous phase separation. Phase separation has previously been reported in the commercial ionomer glasses[76,77] and in light of this, heat-treated glass frit was examined by SEM for both phase separation and crystallization.

4.2.3 Scanning Electron Microscopy

The micrographs of several heat-treated glass frits are shown in Figures 32a to 32f. There are no distinct features on the base glass or the glass heated to 665 °C. At 680 °C and 690 °C, however, the glass has an inter-connected structure suggesting a spinodal mechanism for liquid-liquid phase separation although this can not be confirmed by SEM alone. At higher temperatures a distinct droplet structure is seen; these droplets coarsen with increasing temperature. At 735 °C, small cubes or rounded cubes can be seen, suggesting crystallization of cubic calcium fluoride.

The last two micrographs show fewer droplets present and this is attributed to the matrix crystallizing to anorthite and becoming less susceptible to the acid etch.

This data agrees well with that obtained by DTA and XRD. The calcium fluoride has been shown to crystallize in two stages; the initial crystallization occurring in the droplet phase whilst the remaining calcium fluoride

together with anorthite is crystallized out of the matrix phase.

Bulk nucleation has previously been shown, by comparing DTA traces of different particle sizes of the glass, to be the dominant mechanism in the crystallization of G280[123].

In many commercial glass systems, nucleating agents are often added to promote bulk crystal nucleation from a large number of internal sites. In G280, however, bulk nucleation arises due to amorphous phase separation and it is doubtful that any nucleating agent would have such well matched lattice parameters as fluorite and anorthite. For these reasons, the addition of nucleating agents has been shown by Goat[124] to be ineffective in bringing about bulk nucleation compared with the phase separation step which the glass undergoes. This indicates that a conventional glass-ceramic route is not necessary for this system.

4.3 DETERMINATION OF ACTIVATION ENERGIES OF CRYSTALLIZATION

4.3.1 The Marotta Method[112]

Heating Rate $^{o}Cmin^{-1}$	Tp_1 (Kelvin)	Tp_2 (Kelvin)
4.1	962	1131
7.0	975	1141
11.0	980	1150
16.0	989	1155
22.0	996	1159

Figure 10 - Activation Energy Data for G280

4.3.2 The Matusita Method[113,114]

This method requires a prior knowledge of the crystallization mechanism. It has been shown that in glass G280, crystallization is via a bulk mechanism and that the nuclei are formed as a result of an instantaneous phase separation; the number of nuclei will thus be constant and the exponent n is set at 3. For a process with n=3, the crystallization kinetics will thus be dominated by growth of pre-existing nuclei and the activation energy obtained will be dominated by the activation energy for growth. The activation energy of the first crystallization step can thus be attributed only to the growth of crystals of fluorite. The second activation energy is a combination of the crystallization of fluorite, anorthite, and gehlenite.

From this data, shown graphically in Figures 33 and 34, the following activation energies were determined:

By the Marotta method:

for the first crystallization process, 402 kJ mol^{-1},

for the second crystallization process, 640 kJ mol^{-1}

By the Matusita method:

for the first crystallization process, 397 kJ mol^{-1},

for the second crystallization process, 633 kJ mol^{-1}

There is thus good agreement between the two sets of values, although reservations remain about the accuracy of the Marotta method[125].

4.4 EFFECT OF SUB-GLASS TRANSITION TEMPERATURE HEAT TREATMENTS

In order to control the properties of commercial glass-ionomer cements, manufacturers often use low temperature heat treatments to alter the reactivity of the glass. These heat treatments can both increase and decrease glass reactivity depending upon glass composition and precise heating regime. There has been no convincing explanation of how the heat treatments work. In order to investigate this phenomenon, samples of G280 of particle sizes <45 um and >45 um were placed in a furnace and heated isothermally for eighteen hours at temperatures between 550 °C and 650 °C. The samples were then reground and a portion used in quantitative XRD and a portion used in rheology experiments aimed at finding the working times of the resulting cements.

4.4.1 X-Ray Diffraction

The results from the quantitative analysis are shown in Figure 35 and Table 11 overleaf. Calcium fluoride was found to crystallise out of the glass, the amounts increasing with increasing temperature in an approximately exponential manner. There is, however, a particle size effect. This indicates that some surface crystallization of fluorite is occurring. This contrasts with the bulk nucleation data described previously:

Isotherm Temperature (°C)	% crystalline CaF_2		working time (seconds)	
	<45µm	>45µm	<45µm	>45µm
550	0.85	-	63	
560	0.73	-	63	
570	0.66	0.69	69	75
580	1.30	1.01	69	105
590	1.75	1.18	81	102
600	2.10	1.80	96	81
610	5.13	2.70	102	129
620	5.06	3.83	117	126
630	8.56	5.03	127	132
640	7.99	7.15	147	156
650	12.42	9.50	150	201

Figure 11 - Effect of Sub-Tg Heat Treatments on G280

The fact that there is significant crystallization *below* the experimentally determined glass transition may suggest that the calcium fluoride exists as discreet entities within holes in the glass network and that the fluorine is not bonded to the glass network. This supports the conclusions of Rabinovich[91] with regard to the role of fluorine in glasses with a large basic content.

However, the glass transition is not an absolute temperature, rather it occurs gradually over a temperature range with a corresponding reduction in viscosity. As the isotherm temperature approaches the glass transition it may well be that the viscosity of the glass reduces enough for calcium and fluorine to become mobile in the glass network and for crystallization to occur.

4.4.2 Rheology of the Cements

As the isotherm temperature increases, so the working times of the cement pastes also increase (Figure 36 and Table 10 above). Again there is evidence of a particle size effect, with the smaller glass particles providing a larger surface area for reaction to occur with, resulting in cements with shorter working times. The rheology results are not straightforward, however, as the available surface area for reaction is dependent both on the extent of surface crystallization and on particle size. However, a plot of crystallinity against working time (Figure 37) still shows that the glass can be deactivated by heat treatment below Tg to produce cements with practical working times.

Surface crystallization would thus readily explain how commercial glasses are deactivated, as opposed to a simple annealing of the glass, which has previously been assumed.

Activation of commercial glasses could be explained by assuming that a heat treatment might result in an amorphous phase separation to give a two phase glass, one phase of which was more reactive than the original glass.

4.5 THE EFFECT OF SUCCESSIVE DSC RUNS ON G280

In order to confirm the analysis of crystallization data, a sample of G280 was heated for six successive runs using a Netzsch High Temperature DSC 404 apparatus. The results of the heat treatments are shown in Figures 38a to 38f. The sample was initially heated to a temperature of

680 °C; that is, above the glass transition temperature, but below the onset of crystallization. A glass transition temperature at 632 °C was detected. A repeat run resulted in a glass transition at a higher temperature, 643 °C, and this is probably attributed to annealing of the glass causing a reduction of free volume. A third run, up to 800 °C, showed the same glass transition and additionally, a crystallization exotherm which peaks at 724 °C; this corresponds to the crystallization of fluorite. A fourth run, again to 800 °C, however, shows no exotherm and two glass transitions at 731 °C and 761 °C; much higher than the original.

This is consistent with fluorite crystallization and suggests that fluorine atoms are bonded to the glass network. The two glass transitions temperatures are attributed to (i) the calcium and fluorine depleted droplet phase and (ii) the residual matrix phases respectively. Assuming a random network model, because the phases are depleted in network modifier, they will have higher glass transitions than the base glass. The combination of the new glass transitions is also thought to account for the possible second glass transition on the DTA trace for G280 (Figure 28).

The fifth run also shows two glass transitions at 738 °C and 762 °C. The increase in the lower glass transition suggests that this transition is associated with a phase which is crystallizing to fluorite whereas the second transition corresponds to the silicon and aluminium rich

phase. This run also showed a large exotherm at 894 °C, not shown on the figure, which is due to crystallization of anorthite in the matrix phase.

A final run up to 940 °C exhibited no distinctive features which suggests the material has now completely crystallized to fluorite and anorthite.

4.6 FLUORINE ANALYSIS

4.6.1 Hydropyrolysis

Samples of G280 from two batches were ground with a flux mixture and subject to hydropyrolysis. The results are shown in Table 12 below:

SAMPLE	ppm fluorine	% CaF_2	% CaF_2
1. <45µm	118.5	24.32	24.73
	122.5	25.14	
1. >45µm	118.0	24.22	25.04
	126.0	25.86	
2. <45µm	96.0	19.70	22.17
	127.0	24.63	
2. >45µm	101.0	20.73	22.18
	127.0	24.63	

Table 12 - Hydropyrolysis Data for G280

Therefore,

the %CaF_2 in G280 [experimental] = 23.65 (s.d. 2.20)

and the %CaF_2 in G280 [theoretical] = 21.91

As can be seen, the amount of calcium fluoride found in the glasses appears to exceed the theoretical maximum. However, there is no statistical difference between these values and the theoretical maximum. The high values are ascribed to the fact that the standards used to produce the calibration line range over such a large scale (three decades on a log scale) that errors are likely when all the samples have values at one end of this scale. The calibration line used is shown in Figure 39.

The author thus has reservations regarding the absolute values obtained by this method. It is, however, encouraging that there is such good agreement between different particle sizes for the same batch, suggesting that this is a good comparative technique.

All being considered, the values obtained suggest that little or no fluorine is being lost during melting. This agrees with the previous data and with the suggestion that a large basic oxide content prevents the formation of silicon tetrafluoride, thus reducing fluorine loss.[90,91]

4.6.2 Differential Thermal Gravimetry

Differential thermal gravimetry (DTG) was used to monitor fluorine loss upon heating the sample to 900°C. The analysis was performed on two samples; G280 and a commercial formulation, G338 (ex LGC) as a comparison. The resulting traces are shown in Figures 40a and 40b, the upper line in both being the DTG curve, the lower line being DTA.

Weight loss in G338 is large, accounting for a reduction in weight of 6% over a temperature range of 1000 °C. To account for such a large loss, silicon is presumably being lost from the melt, along with fluorine through the loss of volatile SiF_4 species, since the simple replacement of an (F^-) by an (OH^-) species would only result in a very small change in weight. In this experiment , the atmosphere is controlled (dry nitrogen), but it can be seen when making a batch of such a glass, upon removal of the crucible from the furnace, SiF4 could react with moisture in the air to produce HF as shown below:

$$SiF_4 + H_2O \longrightarrow Si(OH)_4 + HF$$

This can be seen as 'fuming' from the crucible and moist indicator paper held over the fumes turns instantly red, indicating a pH < 1-2. Such acidity at such high temperatures has great implications with regard to operator safety, and furnace lifetimes, especially upon scaling up to commercial sized batches.

Fluorine loss in G280 is minimal (less than 1% over 900 °C) compared to the commercial formulation. This is again attributed to the basic nature of the glass and provides further supporting evidence to the fact that this glass has a post-firing composition very close to its pre-firing formulation.

G338, however, contains no basic oxide in its prefiring composition and consequently undergoes a much larger weight loss.

4.7 EFFECT OF VARYING THE CALCIUM OXIDE TO CALCIUM FLUORIDE RATIO

G280 is only one of a series of quaternary glasses studied by Wilson et al[40]. They made a number of glasses which had a constant Si:Al ratio but varied the amounts of calcium oxide and calcium fluoride. These glasses have the generic formula given below:

$2SiO_2 . Al_2O_3 . 2(1-x)CaO . 2xCaF_2$ (where x<1)

It was decided to investigate the properties of some of these glasses to see how closely they related to G280. The glasses shown below were investigated:

Glass	x =
G241	0
G278	0.10
G276	0.167
G279	0.25
G280	0.50
G282	0.90

Table 13 - Glasses made by Varying CaO:CaF_2 Ratio

4.7.1 X-Ray Diffraction

The traces for a number of glasses in the G280 series are shown in Figures 41a to 41f. They all show the characteristic amorphous halo, apart from the traces for G241 and for G282.

G241 represents a fluorine free glass (i.e. x=0). An analysis of the peaks showed a very good match with gehlenite ($Ca_2Al_2SiO_7$) and corundum (Al_2O_3) as shown overleaf.

2 Theta 2θ	d (Å) expmtl	d Å) JCPDS	I Io expmtl	I Io JCPDS	phase
31.50	2.840	2.85	100	100	GEHL
29.19	3.059	3.07	36	25	GEHL
35.30	2.543	2.55	33	90	CORU
43.32	2.089	2.09	29	100	CORU
57.49	1.603	1.60	29	80	CORU
51.99	1.759	1.75	14	35	GEHL
25.69	3.467	3.48	14	75	CORU
24.07	3.695	3.71	14	20	GEHL
37.48	2.400	2.40	14	25	GEHL
39.29	2.293	2.29	9	14	GEHL

KEY: GEHL = gehlenite, CORU = corundum

Table 14 - X-ray Diffraction Data for G241

The presence of corundum may indicate that the glass has not been fully melted and the furnace temperature was too low.

G282 represents another extreme case (x=0.9) and was found to consist largely of crystalline calcium fluoride as witnessed by the very intense diffraction lines. Indeed, Wilson[40] reported that this glass was opaque upon quenching from the melt.

4.7.2 Differential Thermal Analysis

The traces of some of the glasses in the G280 series are shown in Figure 42. The glass transition temperatures for each glass were determined and are shown in Table 15 overleaf.

Glass	Glass Transition (°C)
G241	not found
G278	745
G276	750
G279	717
G280	642
G282	636

Figure 15 - Glass Transition Temperatures

No glass transition temperature was found for G241; the material was highly crystalline and the DTA trace was essentially a straight line. The values of glass transition temperature obtained for the other glasses, however, show a trend which can be explained in terms of regarding the fluorine as being bonded to the glass network. The lower x is, the less fluorine there is in the glass and the less disrupted will be the glass network. This results in the crosslink density of the glasses increasing, giving rise to an increasing glass transition temperature with decreasing calcium fluoride content, as shown above.

The traces also display a second exotherm, seen most clearly for G279 but appearing poorly resolved on the other traces. The crystallization of G280 to anorthite was not unexpected since the composition of the residual glass phase, following fluorite crystallization, is that of anorthite. For the other glasses, however, the remaining glassy phase, after crystallization of fluorite, will be

richer in calcium compared with anorthite. The new exotherm is thus attributed to the crystallization of a new phase which would take up the extra calcium. To investigate this phase, a sample of G278 was heated to 930 °C for 20 minutes during which time it crystallized and was subsequently subjected to XRD. The resulting trace is shown in Figure 43 and the analysis of the data is shown in Table 16 overleaf. The diffraction lines show a good match for anorthite, and shows the presence of a smaller amount of calcium fluoride. The dominant features of the trace, however, are the diffraction lines corresponding to crystalline gehlenite. This phase is calcium rich compared to anorthite and its crystallization was again expected in that gehlenite is the principal phase in G241, the next glass in the series of decreasing x values.

2theta (2θ)	**d (Å) expmtl**	d (Å) JCPDS	**I/Io expmtl**	I/Io JCPDS	**phase**
31.42	**2.847**	2.85	**100**	100	**GEHL**
29.18	**3.061**	3.07	**88**	25	**GEHL**
27.88	**3.202**	3.21 3.20 3.18	**83**	35 100 75	**ANOR** **ANOR** **ANOR**
27.22	**3.276**	3.26	**27**	35	**ANOR**
52.62	**1.739**	1.75	**22**	35	**GEHL**
21.90	**4.059**	4.04	**20**	60	**ANOR**
30.96	**2.888**	2.895	**20**	8	**ANOR**
39.36	**2.289**	2.292	**20**	14	**GEHL**
23.95	**3.710**	3.71	**19**	20	**GEHL**
36.93	**2.434**	2.435	**19**	20	**GEHL**
37.49	**2.398**	2.404	**15**	25	**GEHL**
35.53	**2.526**	2.525	**14**	24	**ANOR**
23.49	**3.789**	3.78	**12**	20	**ANOR**
26.47	**3.366**	3.37	**12**	25	**ANOR**
28.25	**3.160**	3.153	**12**	94	**FLUO**
30.68	**2.914**	2.93	**12**	18	**ANOR**
49.26	**1.850**	1.846	**11**	14	**ANOR**
22.93	**3.880**	3.92 3.78	**10**	12 20	**ANOR** **ANOR**
48.14	**1.890**	1.892	**10**	6	**ANOR**
50.29	**1.815**	1.812	**10**	10	**GEHL**
52.16	**1.754**	1.754	**9**	35	**GEHL**
47.30	**1.922**	1.931	**8**	100	**FLUO**
53.27	**1.720**	1.723	**8**	8	**GEHL**
33.67	**2.663**	2.655	**7**	12	**ANOR**
44.31	**2.044**	2.043	**7**	25	**GEHL**
32.92	**2.721**	2.72	**5**	6	**GEHL**

KEY: ANOR = anorthite, GEHL = gehlenite, FLUO = fluorite

Table 16 - X-ray Diffraction Data for G278

4.8 ANALYSIS OF A CURRENT MATERIAL, G338 (ex LGC)

The glasses in current use in commercial dental glass-ionomer cements contain sodium and phosphate ions and are thus more complex than the model glass previously investigated. The role of these species within these glasses is still unclear and before adding them to the model glass, it was decided to undertake a preliminary investigation of the properties of a commercial formulation (see Table 3). This glass is known to suffer from batch to batch variation due to fluorine loss and phase separation.

4.8.1 Thermal Analysis

One way of demonstrating amorphous phase separation is by seeing if the glass has two glass transitions, indicating two glassy phases. Samples were subjected to DTA and DSC using a variety of different apparatus, but using the same reference material and employing the same heating rates, see Table 17 below.

METHOD	Temperatures (°C)			
	Tg_1	Tp_1	Tg_2	Tp_2
1	452		593	
1			621	
2	448		596	
3	456	557	617	740
3	456	556	628	757
4	453		605	
5	456		614	

Table 17 - DTA and DSC of G338 (ex LGC)

KEY:

Method 1 Stanton Redcroft DTA 673/674 at Thames Polytechnic

Method 2 Stanton Redcroft STA 1500

Method 3 Stanton Redcroft DTA 673/674 at Eastmans Dental Hospital

Method 4 Stanton Redcroft DSC 700 (see Figure 44)

Method 5 Netzsch High Temperature DSC 404 (see Figure 45)

The material shows two clear glass transitions at approx. 456 °C and 610 °C. This indicates that this material is indeed phase separated upon quenching from the melt. This phase separation is uncontrolled and is the reason why this material shows inter batch variation. Barry[76,77] and Wasson and Nicholson[46] have also reported that this glass was phase separated. Upon heating, the material was found to crystallise and in order to determine the crystalline phase present, the glass was subject to XRD.

4.8.2 X-ray Diffraction

Three batches of G338 were examined by XRD (Figures 46a to 46c) and were found to be essentially amorphous. There are, however, slight differences in the traces. One of the glasses was then placed in a furnace at 930 °C and heated for 20 minutes, after which it was reground and subject to XRD. The resulting trace is shown in Figure 47 and an analysis of the data given in Table 18.

2 theta (2θ)	**d (Å) expmtl**	d (Å) JCPDS	**I/Io expmtl**	I/Io JCPDS	**phase**
31.88	**2.807**	2.81	**100**	100	**HAP**
33.00	**2.715**	2.71	**76**	60	**HAP**
25.81	**3.452**	3.45	**59**	40	**HAP**
32.16	**2.783**	2.78	**46**	60	**HAP**
49.54	**1.840**	1.84	**29**	40	**HAP**
46.83	**1.940**	1.94	**27**	30	**HAP**
34.03	**2.635**	2.63	**27**	25	**HAP**
26.09	**3.416**	3.42 3.39	**26**	95 100	**MUL** **MUL**
39.91	**2.259**	2.26	**24**	20	**HAP**
28.98	**3.081**	3.08	**18**	18	**HAP**
28.05	**3.181**	3.18	**15**	12	**HAP**
40.76	**2.214**	2.21	**15**	60	**MUL**
50.66	**1.802**	1.80	**15**	20	**HAP**
53.24	**1.725**	1.73	**14**	20	**HAP**
35.24	**2.547**	2.55	**13**	50	**MUL**
51.5	**1.775**	1.77	**12**	12	**HAP**
48.23	**1.887**	1.89	**12**	16	**HAP**
39.26	**2.295**	2.30	**11**	8	**HAP**
16.28	**5.445**	5.44	**11**	50	**MUL**
22.82	**3.897**	3.90	**9**	10	**HAP**
21.79	**4.079**	4.08	**8**	10	**HAP**
42.16	**2.144**	2.14	**7**	10	**HAP**
42.44	**2.130**	2.13	**7**	4	**HAP**
56.08	**1.640**	1.64	**7**	10	**HAP**
57.38	**1.606**	1.61	**6**	8	**HAP**

KEY: HAP = hydroxyapatite, MUL = mullite

Table 18 - X-Ray Diffraction Data for G338

A near perfect match was found for nearly all the lines, the two phases identified being an apatite phase, probably hydroxyapatite ($Ca_{10}(PO_4)_6\ OH_2$ together with mullite, an aluminium silicate $Al_6Si_2O_{13}$). This result is very significant with regards to the excellent biocompatibility of the glass-ionomer cement [22-25]. Forty percent (by weight) of dry bone is made up of inorganic bone mineral which is essentially a complex of tricalcium phosphate and calcium hydroxide in the form of hydroxyapatite crystals. It would not be unreasonable to imagine good bonding between the mineral and the glass across the bone/cement interface as has been reported for commercial apatites and bioglasses [28].

4.8.3 Scanning Electron Microscopy

A rod of glass G338 approximately 110mm long, 20mm diameter was cast and sliced using a diamond wheel. A section through the rod was taken, approx. 5mm in depth. The surface of the glass was then etched in 5% HF for 30 seconds and the sample subjected to SEM. The results are shown in Figures 48a and 48b. There is clear evidence of phase separation, with the droplets having an average size of 0.4-0.5 μm. Two or three appear to have straight edges. When measured using a protractor the angles between the edges were found to be 120°; this suggests the presence of hexagonal crystals of apatite in the cast sample.

4.8.4 Transmission Electron Microscopy

TEM shows clear evidence of phase separation in another sample of G338 glass which had again been cast as a rod, as shown in Figures 49a to 49f. The micrographs are taken from carbon replicas of the glass surface which had been etched in 5%HF for 30 seconds. The micrographs show clearly droplets which appear to have been pulled out of the glass surface by the application of the carbon film. The rings also visible on the glass surface can thus be attributed to the holes in which these droplets sat and which have been etched preferentially. The droplets are very much more electron dense than the background, suggesting that they are calcium rich. Some of them appear hexagonal in shape, which suggests that these correspond to apatite crystals. These micrographs and those from SEM thus imply that crystallization of apatite occurs following prior amorphous phase separation and takes place within the droplet phase.

Following this pilot study, glass G280 was again taken as a base for an investigation of the effects of substituting sodium and phosphorus into the glass. Again, a systematic approach was taken in that the components were added individually: sodium replacing calcium in one series of glasses, phosphorus replacing silicon in another.

4.9 ADDITION OF SODIUM OXIDE TO G280

Sodium oxide was systematically substituted for calcium oxide in G280. Glass compositions were made from the generic system:

$$2\ SiO_2.\ Al_2O_3.\ (1-x)\ CaO.\ x\ Na_2O.\ CaF_2$$

where x was varied between 0 and 0.75

Each glass was placed in the furnace for 90 mins at 1350 °C. All the glasses gave fluid pours, which is not surprising since sodium oxide should reduce the viscosity of the melt. Upon quenching, the glass frit was ground and examined using X-ray diffraction.

4.9.1 X-Ray Diffraction

Only the composition with x = 0.1 Na_2O was found to be essentially amorphous to a large extent, as shown in Figure 50. Quantitative X-ray diffraction demonstrated that the only crystalline phase present in the glasses was calcium fluoride. The amount of calcium fluoride in each composition is shown below in Table 19:

Composition	x =	Crystalline CaF2
G514	0.25	5.10 %
G515	0.10	0.97 %
G516	0.50	19.60 %
G517	0.75	17.70 %

Figure 19 - XRD of Glasses with Various Sodium Contents

The author suspects that sodium ions are conventionally put in ionomer glasses merely to lower melting temperatures and may additionally provide a counter ion for the release of fluoride ions in the oral environment. In the model glasses, sodium oxide incorporation would seem to bring about significant crystallization of calcium fluoride, and the reason for putting sodium in ionomer glasses may at the end of the day simply be historical.

It is perhaps surprising that in glasses with a significant sodium content, CaF_2 is the only phase to crystallise out of the glass. This may again indicate the presence of CaF_2 clusters in the glass.

G516 was found to contain 19.6% crystalline CaF_2 - this again corresponds to ~ 90% of the available amount in the glass and may indicate that the presence of *any* basic oxide (e.g. Na_2O) is important with regards to fluorine retention, although in this composition the presence of the monovalent species seems to result in subsequent crystallization.

4.9.2 Differential Scanning Calorimetry

Traces for the glasses heated at 10°C min^{-1} to 735°C are shown in Figures 51a to 51d. The only one to produce a trace that could be interpreted was G515, the one with the lowest sodium content. Both the glass transition temperature and the peak crystallization temperature are lower than those for G280. This is not surprising since the replacement of a divalent cation by a monovalent cation in

the glass network would be expected to open the glass network by reducing [-O-Si(O)$_2$-O- Ca^{2+} -O-Si(O)$_2$-O-] type bonds which act as a linkage between non-bridging oxygens.

The glasses with a high value of x are similar to fluorine bearing glasses based on jadeite, studied recently by Dupree et al[126]. They studied glasses based on the compositions {$NaAlSi_2O_6$}, {$NaAlSi_2O_6$ +NaF} and {$NaAlSi_2O_6$ +Na_3AlF_6} using MAS NMR. It was found that in addition to the $^{[4]}$Al which was present in fluorine-free jadeite glass, $^{[5]}$Al and $^{[6]}$Al were observed in the fluorine containing compositions. The $^{[5]}$Al was assigned to AlF_5^{2-}, a previously unknown species. No fluorine to silicon bonds were found[127] in these glasses, and Dupree assumed that the fluorine was bonded only onto aluminium sites.

Furthermore, samples of glass G280 supplied by the author, have been subject to the Lentz reaction[128,129]. This essentially involves degrading the glass network fully in acid and then looking at the environment of the silicon atoms by trimethylsilylating the silicate fragments produced to give polysiloxanes which are related to the silicate structure of the original glass. Using this technique, no fluorine containing polysiloxanes were found in either study, which again suggests that there are no Si-F bonds in the glass. In addition, the number of [SiO_4] products was more than that predicted by assuming a random distribution of aluminium sites suggesting a relatively ordered structure and a glass network consisting essentially of alternating [AlO_4] and [SiO_4] tetrahedra.

This method can not, however, tell us if the fluorine is bonded only to aluminium or, as Rabinovich postulates, is sitting as CaF_2 clusters within the glass network. This would be possible for G280 since there is enough Ca present in the glass to maintain network neutrality, and to accommodate fluorine as CaF_2. Rabinovich[91], however has not studied these effects in *alumino*-silicate compositions; the results of Dupree, Zaheer and Martin suggest the presence of Al-F bonds in these glasses.

Looking at the setting reaction of glass-ionomers, Wilson[130] postulated that fluoride was released as AlF_2^+ and AlF^{2+} from ionomer glasses, rather than as the free fluoride ion. Wilson[131] has postulated the existence in the glass of structures such as AlF_6^{3-}, with some F being replaced by O and further postulates that the basicity of the glass would affect the nature of this fluoroaluminium and hence the loss of fluorine from the melt.

It seems, therefore, that in addition to the presence of a basic oxide to prevent fluorine loss, aluminium must also be present to provide a site for the fluoride ion to bond on to . Indeed, in a study on $ZnO-Al_2O_3-SiO_2$ glasses in which ZnF_2 was progressively substituted for ZnO, Lau[132] reported a large fluorine loss (as fuming HF) in those glasses with a low aluminium content, whereas those glasses with sufficient aluminium to 'fix' the fluoride ions appeared to undergo no fluorine loss.

4.10 ADDITION OF PHOSPHOROUS PENTOXIDE TO G280

The other component found in commercial compositions is aluminium phosphate. In modifying the composition of the model glass to incorporate phosphorus, it was decided to add phosphorus pentoxide, rather than aluminium phosphate, since the addition of P_2O_5 would not affect the amount of aluminium in the glass. P_2O_5 plays the same role in the glass as does silica (i.e. it is a network former); initially a series of glasses were made consisting of a systematic substitution of 1 silicon ion by 2 phosphorus ions. This reduces the Si:Al ratio in the glass but provides more network forming cations, i.e. the total ratio of network forming to intermediate cations increases. Glasses of the following generic composition were initially made:

$$\mathbf{(2-x)\ SiO_2.\ x\ P_2O_5.\ Al_2O_3.\ CaO.\ CaF_2}$$

The glasses were labelled using the conventional notation adopted by Workers at the Laboratory of the Government Chemist, and shown below in Table 20:

Glass	x
G280	0
G518	0.25
G521	0.375
G519	0.5
G520	0.75
G526	1.0

Table 20 - Nomenclature of Glasses Containing P_2O_5

Prior to melting, the glass components were placed in a vacuum oven at 90°C for several hours, to prevent moisture contaminating the powder. G518 was melted at 1350 °C for 90 mins and produced an essentially clear glass. However, the melt was viscous and contained lumps. G519 and G520 were then melted at 1380 °C for 120 mins and gave very fluid pours to produce again essentially clear glasses. G521 was heated to 1350 °C for 90 mins but did not pour. It was then remelted at 1400 °C for a further hour; did not pour, and was remelted for another hour at 1450 °C after which the glass poured but was very viscous. At this temperature there was some attack on the crucible and significant fuming. A second batch of this glass was then produced after melting a fresh charge at 1470 °C for 100 mins but again the glass ate through the crucible and there was a large amount of fuming. This emphasizes the problems in making these glasses without prior knowledge of any of the phase diagrams. G521 lies in compositional terms between G518 and G519, both of which melted easily at 1380 °C.

4.10.1 Differential Thermal Analysis

DTA traces for the various phosphate containing glasses are shown in Figures 52a to 52e. Glass transition temperatures and peak crystallisation temperatures are summarized in Table 21 overleaf for glass powders of <45um particle size:

Glass	Tg_1	Tg_2	Tp_1	Tp_2	Tp_3
G280	642		707	876	
G518	631	713	772	834	
G521	631		718	782	801
G519	621		723	814	
G520	662	758	826	878	1037
G526	669	751	818	860	1015

Table 21 - DTA of Glasses Containing P_2O_5

Glass transition temperature will increase with increased crosslink density. In this series of glasses, each Si ion is replaced by two P ions; the network would thus be expected to be more crosslinked and the glass transition temperature to be higher with increased phosphorus pentoxide.

However, the P-O bond is not as strong as the Si-O bond and glasses with a high phosphorus pentoxide content would thus require less thermal energy for the network to become mobile, i.e. the glass transition temperature and crystallization temperatures would be less.

In addition, the aluminium ion, Al^{3+} can maintain local electroneutrality by being closely associated with the phosphorus, P^{5+} ion. Thus, the inclusion of phosphorus in the glasses will result in the release of the calcium, Ca^{2+} ions from a charge balancing role; they are then free to disrupt the glass network.

There are therefore opposing factors affecting glass transition and crystallization temperatures and this may account for the lack of any consistent trends in the data obtained.

4.10.2 X-Ray Diffraction

Diffraction traces of the five phosphate based glasses are shown in Figures 53a-53e. None of the traces show a totally amorphous halo. The trace for G518 shows evidence for very slight crystallization to calcium fluoride, whilst that for G521 shows a more extensive crystallization to apatite. This high degree of crystallization may well be due to the difficulties in producing a sample of this glass. The trace for G519 also shows a very slight crystallization to apatite, as do the traces for G520 and G526.

The glasses G518, G519 and G526 were then subjected to a simple heat treatment (930 °C for 20 mins) and further examined by X-ray powder diffraction.

The phosphate containing glasses were all found to have crystallised to an apatite phase, probably fluorapatite. The other phases present were anorthite and fluorite in G518, mullite ($3Al_2O_3.2SiO_2$) in G519, and an undetermined phase in G526. Diffraction data for glasses G518 and G519 are shown in [Figure 54 and Table 22] and [Figure 55 and Table 23] respectively.

2 theta (2θ)	**d (Å) expmtl**	d (Å) JCPDS	**I/Io expmtl**	I/Io JCPDS	**phase**
27.96	**3.19**	3.21 3.20 3.18 3.17 3.15 3.12	**100**	35 100 75 15 94 45	**ANOR** **ANOR** **ANOR** **APP** **FLUO** **ANOR**
29.34	**3.04**	3.04	**67**	18	**ANOR**
31.85	**2.81**	2.814	**54**	100	**APP**
46.95	**1.93**	1.95 1.94	**38**	100 30	**FLUO** **APP**
27.29	**3.26**	3.26	**32**	55	**ANOR**
32.97	**2.71**	2.72	**31**	60	**APP**
21.88	**4.06**	4.04	**29**	60	**ANOR**
32.13	**2.78**	2.778	**26**	60	**APP**
25.80	**3.45**	3.47 3.44	**26**	12 40	**ANOR** **APP**
49.47	**1.84**	1.85 1.84 1.841	**22**	14 18 40	**ANOR** **ANOR** **APP**
23.56	**3.77**	3.78	**21**	20	**ANOR**
35.67	**2.51**	2.50	**21**	25	**ANOR**
30.27	**2.95**	2.93	**19**	18	**ANOR**
26.45	**3.37**	3.37	**19**	25	**ANOR**
51.61	**1.77**	1.78	**14**	12	**APP**
34.00	**2.63**	2.631	**14**	25	**APP**
42.20	**2.14**	2.14	**13**	16	**ANOR**
39.87	**2.26**	2.262	**12**	20	**APP**
50.68	**1.80**	1.806	**12**	20	**APP**
23.00	**3.86**	3.92 3.78	**11**	12 20	**ANOR** **ANOR**

2 theta (2θ)	**d (Å) expmtl**	d (Å) JCPDS	**I/Io expmtl**	I/Io JCPDS	**phase**
43.22	**2.09**	2.09	**10**	8	**ANOR**
48.16	**1.89**	1.88	**10**	8	**ANOR**
57.39	**1.60**	1.61	**9**	8	**APP**
55.71	**1.65**	1.66 1.644	**9**	35 10	**FLUO** **APP**
52.17	**1.75**	1.72	**8**	20	**APP**
39.31	**2.29**	2.29	**8**	8	**APP**

Table 22 - X-Ray Diffraction of G518

2 theta (2θ)	**d (Å) expmtl**	d (Å) JCPDS	**I/Io expmtl**	I/Io JCPDS	**phase**
31.79	**2.81**	2.814	**100**	100	**APP**
33.01	**2.71**	2.72 2.694	**65**	60 40	**APP** **MUL**
25.82	**3.45**	3.44	**53**	40	**APP**
32.17	**2.78**	2.778	**47**	60	**APP**
27.96	**3.19**	3.17	**45**	12	**APP**
49.45	**1.84**	1.841	**38**	40	**APP**
26.19	**3.40**	3.43 3.39	**35**	95 100	**MUL** **MUL**
34.03	**2.63**	2.631	**29**	25	**APP**
46.74	**1.94**	1.943	**29**	30	**APP**
39.92	**2.26**	2.262	**23**	20	**APP**
40.85	**2.21**	2.206	**23**	60	**MUL**
29.27	**3.05**		**22**		
28.99	**3.08**	3.08	**18**	18	**APP**
35.34	**2.54**	2.542	**18**	50	**MUL**
53.00	**1.73**	1.722	**16**	20	**APP**
50.66	**1.80**	1.806	**15**	20	**APP**
48.14	**1.89**	1.890 1.887	**14**	16 8	**APP** **MUL**
51.50	**1.77**	1.780	**14**	12	**APP**
39.27	**2.29**	2.292 2.296	**13**	20 8	**MUL** **APP**
52.15	**1.75**	1.754	**13**	16	**APP**
21.89	**4.06**	4.07	**12**	10	**APP**
16.38	**5.41**	5.39	**11**	50	**MUL**
22.92	**3.88**	3.88	**11**	10	**APP**
42.53	**2.12**	2.121 2.134	**10**	25 4	**MUL** **APP**
31.05	**2.88**	2.886	**9**	20	**MUL**
42.16	**2.14**	2.148	**9**	10	**APP**
23.57	**3.77**	3.774	**7**	8	**MUL**
55.98	**1.64**	1.644	**6**	10	**APP**

2 theta (2θ)	**d (Å) expmtl**	d (Å) JCPDS	**I/Io expmtl**	I/Io JCPDS	**phase**
57.48	**1.60**	1.599	**6**	20	**MUL**
43.75	**2.07**	2.065	**5**	8	**APP**
48.79	**1.86**	1.871	**5**	6	**APP**
54.02	**1.70**	1.694 1.700	**5**	10 14	**MUL** **MUL**
24.41	**3.64**		**4**		
30.30	**2.95**		**4**		
36.93	**2.43**	2.428	**4**	14	**MUL**
45.24	**2.00**	2.000	**4**	6	**APP**
57.20	**1.61**	1.611	**4**	8	**APP**
58.41	**1.58**	1.578 1.587	**4**	12 4	**MUL** **APP**
16.76	**5.29**		**3**		
18.90	**4.69**		**3**		
58.97	**1.56**	1.564	**2**	2	**MUL**

Table 23 - X-Ray Diffraction of G519

In G526, it appears that apatite is initially formed followed at higher temperatures by the formation of the secondary phase(s). To demonstrate this, G526 was heated to different temperatures, the sintered powder reground and subjected to XRD. The resulting diffraction traces are shown in figures 56a to 56d and Tables 24 to 27.

2 theta (2θ)	**d (Å) expmtl**	d (Å) JCPDS	**I/Io expmtl**	I Io JCPDS	**phase**
31.72	**2.822**	2.81 2.78	**100**	100 60	**APP** **APP**
25.72	**3.463**	3.44	**61**	40	**APP**
32.91	**2.721**	2.72	**51**	60	**APP**
33.94	**2.641**	2.63	**30**	25	**APP**
49.35	**1.846**	1.841	**29**	40	**APP**
21.33	**4.165**	-	**26**	-	**-**
46.64	**1.947**	1.943	**22**	30	**APP**
39.73	**2.268**	2.262	**19**	20	**APP**
52.90	**1.730**	1.722	**17**	20	**APP**
28.89	**3.089**	3.089	**14**	18	**APP**
27.96	**3.191**	3.170	**12**	12	**APP**
35.34	**2.539**	-	**12**	-	**-**
51.96	**1.759**	1.754	**12**	16	**APP**
50.47	**1.808**	1.808	**11**	20	**APP**
22.82	**3.896**	3.880	**10**	10	**APP**
27.12	**3.287**	-	**10**	-	**-**
48.04	**1.893**	1.890	**10**	16	**APP**
51.40	**1.777**	1.780	**10**	12	**APP**
44.28	**2.090**	-	**7**	-	**-**
43.65	**2.073**	2.065	**7**	8	**APP**
55.98	**1.642**	1.644	**7**	10	**APP**
57.38	**1.605**	1.611	**7**	8	**APP**
39.17	**2.299**	2.296	**5**	8	**APP**
40.75	**2.213**	-	**5**	-	**-**
42.07	**2.148**	2.148	**5**	10	**APP**

Table 24 - X-Ray Diffraction of G526 heated to 800 °C

2 theta (2θ)	d (Å) expmtl	d (Å) JCPDS	I/Io expmtl	I/Io JCPDS	phase
31.81	**2.813**	2.810 2.78	**100**	100 60	**APP** **APP**
21.36	**4.160**	-	**94**	-	-
25.65	**3.473**	3.440	**59**	40	**APP**
32.93	**2.720**	2.720	**56**	60	**APP**
49.35	**1.846**	1.841	**33**	40	**APP**
33.96	**2.640**	2.631	**32**	25	**APP**
20.24	**4.388**	-	**27**	-	-
46.65	**1.947**	1.943	**23**	30	**APP**
35.36	**2.538**	-	**22**	-	-
39.83	**2.263**	2.262	**21**	20	**APP**
52.91	**1.730**	1.722	**20**	20	**APP**
22.75	**3.907**	3.880	**18**	10	**APP**
27.98	**3.188**	3.170	**18**	12	**APP**
28.91	**3.087**	3.087	**14**	18	**APP**
50.57	**1.805**	1.806	**14**	20	**APP**
52.06	**1.756**	1.754	**13**	16	**APP**
48.05	**1.893**	1.890	**11**	16	**APP**
51.41	**1.777**	1.780	**11**	12	**APP**
43.66	**2.073**	2.065	**9**	8	**APP**
55.89	**1.645**	1.644	**8**	10	**APP**
39.09	**2.304**	2.296	**7**	8	**APP**
41.98	**2.152**	2.148	**7**	10	**APP**
45.16	**2.007**	-	**5**	-	-
16.69	**5.310**	-	**3**	-	-
57.01	**1.615**	-	**3**	-	-
57.38	**1.605**	1.611	**3**	8	**APP**
19.30	**4.598**	-	**2**	-	-

Table 25 - X-Ray Diffraction of G526 heated to 870 °C

2 theta (2θ)	**d (Å) expmtl**	d (Å) JCPDS	**I/Io expmtl**	I/Io JCPDS	**phase**
31.79	**2.814**	2.81 2.778	**100**	100 60	**APP** **APP**
21.33	**4.165**	-	**99**	-	**-**
32.91	**2.721**	2.72	**60**	60	**APP**
25.63	**3.476**	3.44	**57**	40	**APP**
49.35	**1.846**	1.841	**34**	40	**APP**
33.94	**2.641**	2.631	**31**	25	**APP**
46.64	**1.947**	1.943	**25**	30	**APP**
35.34	**2.539**	-	**24**	-	**-**
20.21	**4.394**	-	**23**	-	**-**
39.83	**2.263**	2.262	**22**	20	**APP**
52.90	**1.730**	1.722	**19**	20	**APP**
28.89	**3.089**	3.08	**16**	18	**APP**
22.73	**3.911**	3.88	**14**	10	**APP**
27.96	**3.191**	3.17	**14**	12	**APP**
50.56	**1.805**	1.806	**14**	20	**APP**
52.06	**1.756**	1.754	**12**	16	**APP**
48.04	**1.893**	1.890	**11**	16	**APP**
51.41	**1.777**	1.780	**11**	12	**APP**
55.89	**1.645**	1.644	**9**	10	**APP**
39.08	**2.305**	2.296	**8**	8	**APP**
43.65	**2.073**	2.065	**8**	8	**APP**
41.97	**2.150**	2.148	**7**	10	**APP**
16.66	**5.320**	-	**5**	-	**-**
45.15	**2.008**	-	**5**	-	**-**
43.18	**2.094**	-	**5**	-	**-**
57.01	**1.615**	1.611	**3**	8	**APP**
19.18	**4.620**	-	**2**	-	**-**

Table 26 - X-Ray Diffraction of G526 heated to 930 °C

2 theta (2θ)	**d(Å) expmtl**	d(Å) JCPDS	**I/Io expmtl**	I/Io JCPDS	**Phase**
31.79	**2.814**	2.810	**100**	100	**APP**
21.33	**4.165**	-	**80**	-	**-**
32.92	**2.721**	2.720	**64**	60	**APP**
32.07	**2.790**	2.778	**54**	60	**APP**
25.62	**3.476**	3.440	**49**	40	**APP**
49.35	**1.846**	1.841	**32**	40	**APP**
33.94	**2.641**	2.631	**31**	25	**APP**
46.73	**1.943**	1.943	**23**	30	**APP**
35.34	**2.539**	-	**20**	-	**-**
39.92	**2.258**	2.262	**20**	20	**APP**
28.89	**3.089**	3.088	**17**	18	**APP**
27.96	**3.191**	3.170	**15**	12	**APP**
52.90	**1.730**	1.722	**14**	20	**APP**
26.09	**3.415**	-	**14**	-	**-**
20.21	**4.394**	-	**13**	-	**-**
50.56	**1.805**	1.806	**13**	20	**APP**
48.14	**1.890**	1.890	**12**	16	**APP**
51.40	**1.777**	1.780	**12**	12	**APP**
22.73	**3.911**	3.880	**11**	10	**APP**
52.15	**1.753**	1.754	**11**	16	**APP**
39.17	**2.299**	2.296	**8**	8	**APP**
40.76	**2.213**	-	**8**	-	**-**
42.07	**2.148**	2.148	**8**	10	**APP**
16.28	**5.442**	-	**7**	-	**-**
43.65	**2.073**	2.065	**7**	8	**APP**
55.98	**1.642**	1.644	**7**	10	**APP**
45.15	**2.008**	2.000	**4**	6	**APP**
18.81	**4.717**	4.720	**2**	4	**APP**
57.10	**1.613**	1.611	**2**	8	**APP**

Table 27 - X-Ray Diffraction of G526 heated to 1050 °C

This data clearly demonstrates the initial formation of the apatite phase, followed by the crystallization of at least one more phase. The principal line of the unknown phase is at 4.16 Å, the intensity of this line increases dramatically to roughly be equal to that of the apatite phase. However, no match could be found for this unknown phase or phases upon comparison with published tables from the JCPDS. The fact that three exotherms were observed by DTA for G526 may suggest that three crystalline phases were present in the sample following heating. This would make identification of the unknown phases very difficult.

4.10.3 Cement Forming Ability

Glass Code	x	Working Time (s)	Setting Time (s)	Compressive Strength (MPa)	S.D	n
G280	0	Too reactive to form a stable cement				
G518	0.25	72	420	12.2	1.9	6
G521	0.375	96	540	23.3	6.0	8
G519	0.5	160	720	19.7	6.0	8
G520	0.75	Did not harden or form a stable cement				
G526	1.0	Did not harden or form a stable cement				

Table 28 - Cement Forming Ability of Various Glasses

G518 and G519 produced cements with reasonable handling characteristics at a powder:liquid ratio of 3:1, as shown if Table 28 above. Glasses with a higher P_2O_5 content, however, did not form hydrolytically stable cements. The rheogram for glass G519 is shown in Figure 57.

There would seem a limiting maximum substitution of silica above which practical cements will not be formed. Of the cements that were hydrolytically stable, G519 and G521 had the highest compressive strength, as shown above.

Unlike G280, the phosphate containing model glasses were nearer in composition to the commercial formulations; but it was additionally possible to look at the glasses in a systematic manner.

4.11 EFFECT OF REDUCING CALCIUM FLUORIDE CONTENT

As the next step it was decided to select one of these compositions and look at the effect of varying the amount of calcium fluoride, whilst keeping the amounts of all other components constant. This should result in glasses with a more crosslinked network. G519 was chosen as the base for this series of formulations since it gave the cement with the best handling characteristics, without the need for subsequent heat treatments or modification. Glasses were then made having the generic formula:

$$1.5\ SiO_2.\ 0.5\ P_2O_5.\ Al_2O_3.\ CaO.\ x\ CaF_2$$

The following glasses, shown in Table 29, were thus made:

Glass	x	Melting Conditions
G519	1	1380°C, 120 min
G527	0.75	1400°C, 120 min
G522	0.5	1470°C, 100 min
G528	0.25	1470°C, 120 min
G523	0	1500°C, 120 min

Table 29 - P_2O_5 Based Glasses with Reduced CaF_2 Content

The most obvious effect of reducing the fluorine content was that the melting temperatures were found experimentally to be progressively higher for each glass. Under these melting conditions, the glasses were quite fluid and in addition to being quenched directly into water, glasses were cast into graphite moulds which had previously been heated to 650 °C. The moulds were then annealed for 1 hr at 650 °C, and then left overnight in the slowly cooling oven. Upon removal from the mould, G519 was found to be very slightly crystalline, with twinned needle-like crystals, although there were extensive regions of clear glass in the sample. The other glasses could be cast to give optically clear homogenous glass rods.

4.11.1 Differential Thermal Analysis

Glass frit was ground and sieved into three particle sizes for each glass. Differential thermal analysis was initially carried out using <45 um particles. The traces are shown in Figs 58a to 58e, and the data summarized in Table 30 below.

Glass	Tg_1	Tg_2	Tc_1 onset	Tc_1 peak	Tc_2 onset	Tc_2 peak	Tc_2 end
G519	621	-	713	723	792	814	829
G527	640	-	732	761	910	943	978
G522	668	-	789	815	952	987	1009
G528	717	834	-	-	1036	1079	1140
G523	819	922	-	-	1037	1095	1140

Table 30 - DTA Data for Glasses with Reduced CaF_2 Content

Glass transition temperatures were observed to rise as fluorine content was reduced and this is again consistent with calcium fluoride acting as a network modifier in the glass, disrupting the glass and producing non-bridging oxygens and fluorines. The less calcium fluoride in the glass, the more cross-linked is the glass and the higher would be the glass transition, as seen above. There was also an apparent change in crystallization behaviour, glasses with a high fluorine content exhibited two sharp exotherms whilst those with low or no fluorine content, crystallized with a single broad exotherm. The two glasses with low fluorine content (G528 and G523) appeared to exhibit two glass transition temperatures , suggesting they had undergone amorphous phase separation, and only one broad crystallization exotherm, whilst the other glasses have one glass transition temperature and two exotherms. There thus appear to be two mechanisms by which crystallization is occurring.

4.11.2 X-Ray Diffraction

XRD was carried out on the base glasses. The resulting traces are shown in Figures 59a to 59e, and show that the glasses produced by reducing the fluorine content were amorphous. G527 and G528 were examined using a Phillips 1812 XRD apparatus. Patel[133] has subsequently shown that following heat treatment, all the fluorine containing glasses again crystallised to an apatite phase and to mullite. Only the fluorine free glass crystallized to

different phases, the principle phase found was anorthite with a trace amount of apatite also present. Patel[133] has found that the apatite phase was again the initial phase to crystallise in these glasses followed at higher temperatures by the crystallization of anorthite or mullite. The composition with no fluorine is similar to that of bone china which also crystallises to principally an anorthite phase[134].

4.11.3 Cement Forming Ability

Glass	x	Working Time(s)	Setting Time(s)	Compressive Strength (MPa)	S.D	n
G519	1.0	160	720	19.7	6.0	8
G527	0.75	124	540	35.1	2.3	6
G522	0.5	200	780	39.8	5.9	8
G528	0.25	170	780	39.5	5.6	8
G523	0	-	-	16.4	5.6	8
G338	**-**	**-**	**-**	**51.0**	**19**	**7**

Table 31 - Cement Forming Ability of Various Glasses

A reduction in the amount of calcium fluoride in the glass produced cements with increasing strength, as shown above in Table 31. However, the glass with no calcium fluoride gave the weakest cement and was difficult to mix, since the cement paste was very dry and only set after an hour or so. To compare the compressive strength of the experimental cements to that of a commercial material, test specimens were made from G338, the glass studied in section

4.8. None of the experimental cements achieved a compressive strength comparable to that of the commercial formulation, which itself gave a low value, compared to quoted values[135], and this is attributed to the fact that the poly(acrylic acid) used in this study had a lower molecular weight than that used commercially. Hill and Wilson[136] have shown that the mechanical properties of glass-ionomer cements decrease with decrease in molecular weight of the polyacid.

4.12 ABILITY OF GLASSES TO FORM GLASS-CERAMICS

4.12.1 Differential Thermal Analysis

Initially, the glasses in the above system were examined using DTA. Three particle sizes were chosen to indicate whether the glasses crystallized by bulk or surface crystallization. Traces for each glass are shown in Figures 60 to 64 and are tabulated in Tables 32a to 32e.

Particle Size (μm)	Tg_1 (°C)	Tc_1 (°C)	Tc_2 (°C)
< 45	621	721	818
> 45, < 125	624	724	818
> 125	625	726	820

Table 32a - DTA of Glass G519

Particle Size (μm)	Tg_1 (°C)	Tc_1 (°C)	Tc_2 (°C)
< 45	640	761	943
> 45, < 125	644	755	963
> 125	644	757	964

Table 32b - DTA of Glass G527

Particle Size (μm)	Tg_1 (°C)	Tc_1 (°C)	Tc_2 (°C)
< 45	664	816	987
> 45, < 125	664	876	1015
> 125	662	923	1037

Table 32c - DTA of Glass G522

Particle Size (μm)	Tg_1 (°C)	Tc_1 (°C)	Tc_2 (°C)
< 45	717	834	1079
> 45, < 125	708	856	1096
> 125	718	-	1086

Table 32d - DTA of Glass G528

Particle Size (μm)	Tg_1 (°C)	Tc_1 (°C)	Tc_2 (°C)
< 45	819	922	1095
> 45, < 125	803	955	1148
> 125	802	971	1169

Table 32e - DTA of Glass G523

G519 and G527 undergo bulk crystallization, whilst in the others, crystallization is occurring in part by a surface mechanism.

4.12.2 Fracture Toughness

Glass	Base Glass K_{IC} ($MNm^{-3/2}$)	S.D. (n=5)	Glass-Ceramic K_{IC} ($MNm^{-3/2}$)	S.D. (n=5)
G527	0.85	0.09	1.07	0.15
G522	0.79	0.07	1.33	0.23
G528	0.93	0.04	-	-
G523	1.13	0.16	1.26	0.16

Table 33 - K_{IC} of Glasses and Resulting Glass-Ceramics

Following a crude one step heat treatment, the fracture toughness of the glass ceramic samples was in all cases higher than that of the base glass, as shown above in Table 33.

4.12.3 Scanning Electron Microscopy

SEM of cerammed discs of G519 which had been etched in 5% HF for 30 seconds showed the presence of an interlocking needle microstructure as shown in the Figures 65a to 65d. The heat treatment used was a crude one stage heating cycle at 10 °C min^{-1}.

4.12.4 Transmission Electron Microscopy

TEM of glass G527 also showed the presence of an interlocking needle microstructure (see Figure 66). The white phase appears to be mullite, which would be expected to be more resistant to the acid etch than an apatite phase. The mullite needles are apparently pierced by cavities and it is possible that these have been formed following the dissolution of the apatite phase. The mullite needles have an aspect ratio of roughly three to one whilst the apatite needles seem to be finer with a much higher aspect ratio.

The presence of an interlocking needle microstructure may account for the increase in fracture toughness of the cerammed disc compared to the base glass, although the effect of composition and heat treatment produces very different microstructure and needs to be studied in further depth.

4.13 COMPUTER MODELLING OF GLASS STRUCTURE

As stated previously, the most intense line in the X-ray diffraction patterns for glass-ceramics appeared to correspond to the maximum in the amorphous scattering halo of the base glass. Zanotto[137] has postulated the idea of multicomponent glasses consisting of microcrystallites of the components. The glasses will then readily crystallise to these component phases with a minimal amount of structural rearrangement being necessary.

Because the X-ray diffraction data was collected using a computer driven step-counting procedure, the original diffraction patterns obtained were of high accuracy. The data could thus be used in an attempt to model the amorphous scattering from the glass in terms of a microcrystallite model and a line broadening approach.

The simulation attempted was kept as simple as possible; the program written in BASIC for a BBC Master microcomputer is shown in Appendix A. No factors relating to strain broadening were included and relative crystallite sizes of different phases were assumed to have been the same. The model essentially consisted of looking at samples which were highly crystalline and simulating their diffraction patterns by overlaying individual peaks until the pattern is built up. Each simulated peak consisted of the positive half of a sine wave which was described as a function of nominal position (the d spacing) and intensity (both taken from the original diffraction data) and in addition, a broadening factor which has an arbitrary value. The same broadening factor was used for each peak in a given simulation. Each peak was saved as a separate file and files then merged together to produce the final simulated diffraction pattern.

A broadening factor of ten produced a simulation nearly identical to that of the original trace for heat treated G519 (as seen in Figures 67a and 67b respectively). The next part of the simulation involved progressively increasing the broadening factor at the expense of

intensity, whilst maintaining a constant peak area, in an attempt to produce a simulation equivalent to the trace of an amorphous glass. Broadening factors of one hundred and two hundred gave the simulations shown in Figures 68a and 68b along with the original amorphous pattern for G519 (shown as the dashed line). The data suggests that there is a difference between the simulation and the experimental results in that there seems to be a different distribution of bonds at higher values of 2 theta between the two patterns. In order to determine crystallite (or cluster) size for the amorphous material, more work needs to be done in correlating different broadening factors with crystallite size, but the author believes that it would be possible to then extrapolate these values to the angstrom scale.

5. CONCLUSIONS

As a result of this study, there is for the first time an understanding of the processes of phase separation and crystallization that occur within ionomer glasses.

Amorphous phase separation has been shown to occur in model glass compositions, prior to crystallization, possibly by a spinodal decomposition mechanism. Crystallization subsequently occurs in two or more stages, depending upon the precise glass composition.

Crystallization can also occur below the glass transition temperature to deactivate the glasses, and produce cements with controllable setting properties. Surface crystallization would seem to be the dominant process in this case.

Commercial manufacturers often use low temperature heat treatments to modify the setting characteristics of ionomer glasses, and these can now be explained in terms of deactivation of the glasses by crystallization. Activation of glasses would similarly be explained by assuming that the heat treatment results in amorphous phase separation to produce a more reactive and a less reactive phase.

Furthermore, there is now an understanding of the role of fluorine in these glasses and also of how fluorine can be retained in model glass formulations. It would seem that for fluorine to be retained in a glass, the glass must (1) have a large basic oxide content to prevent the formation of silicon tetrafluoride in the melt and (2) contain sufficient aluminium to provide sites for the fluorine to

be accommodated in the glass network. By using this knowledge, it is now possible to produce glasses which have essentially the same pre- and post-firing compositions and for the first time to systematically design glasses for specific applications.

A commercial glass was examined and was found to have two glass transition temperatures, indicating that the glass had undergone amorphous phase separation. Following a simple heat treatment regime, the glass crystallized to apatite and mullite. The presence of apatite may explain the excellent biocompatability of the glass ionomer cement, in terms of bonding across the enamel (or bone) to glass interface, since the mineral phase of bone and enamel is also apatite.

Thermal gravimetric Analysis, however, showed that this glass lost silicon tetrafluoride quite readily and difficulty in making reproducible glasses of this composition is well known.

Glasses based on the model compositions but incorporating sodium and phosphate ions have also been produced. The glasses containing sodium were found to crystallise straight from the melt, the crystalline phase in all cases being calcium fluoride. There appears again to be little fluorine loss in these glasses which supports the evidence regarding the role of the basic oxide.

The phosphate glasses are similar to commercial formulations and were found to readily produce cements which showed useful working characteristics. The phosphate

glasses were found upon heating to again crystallize, following prior amorphous phase separation, initially to an apatite phase [of general formula $Ca_{10}(PO_4)_6(OH/F)_2$].

Selected compositions were additionally found to crystallise to mullite [$2SiO_2.3Al_2O_3$] and the microstructure of these glass-ceramics consisted of interlocking needles of the two phases. The fracture toughness of these glass-ceramics measured by indentation was found to be significantly greater than that of the base glasses. In addition these glasses were easily castable into preheated graphite moulds to produce optically clear homogenous glass rods. There thus exists the possibility that these materials could find use as either a bone substitute material or as a crown or inlay material. The latter is particularly attractive since there exists the possibility of using a glass ionomer cement to fix the ionomer glass-ceramic crown to the remaining tooth material or post.

6. REFERENCES

1. J. Charnley, J. Bone Joint Surgery, 52B, (1970), p340

2. G.J. Benke, 'Cash's Textbook of Orthopaedics and Rheumatology for Physiotherapists', ed. by P.A. Downie, pub. by Faber and Faber, London, (1984)

3. G. Lewis, J. Mater. Educ., 11, (1989), p429

4. E. Ebramzadeh, M. Mina-Araghi, I.C. Clarke and R. Ashford, 'Corrosion and Degradation of Implant Materials: Second Symposium', ASTM STP859, ed by A.C. Fraker and C.D. Griffin, pub. by American Society for Testing and Materials, Philadelphia, (1985), p373-379

5. Link Medical Implants Programme, Produced for the LINK Secretariat by the Department of Trade and Industry, (December 1990)

6. P. Ducheyne, S. Radin, and J.M. Cucker, 'Bioceramics', Vol. 1, ed. by H. Oonishi, H Aoki and K. Sawai, pub. by Ishiyaku EuroAmerica, Inc., Tokyo, St. Louis, (1989), p365

7. S.F. Hulbert, F.A. Young, R.S Matthews, J.I. Klawitter, C.D. Talbot and F.H. Stelling, J. Biomed. Mater. Res.,4,(1970), p433

8. M. Jarcho, C.H. Bolen, M.B. Thomas, J. Bobich, J.F Kay, and R.H. Doremus, J. Mater. Sci., 11, (1976), p2027

9. D. Anderson, G.W. Hastings, S Morrey & C. Rich, 'Bioceramics', Vol. 2, ed. by G. Heimke, pub. by Deutsche Keramische Gesellschaft e.V., Cologne, (1990), p251

10. H. Carrerot, J. Rieu, G. Bousquet & A. Rambert, 'Bioceramics', Vol. 2, ed. by G. Heimke, pub. by Deutsche Keramische Gesellschaft e.V., Cologne,(1990), p211

11. A. Green, Nursing Times, 85, (1989), p32

12. G.W. Hastings, 'Biocompatability of Implant Materials, Part IV', ed. by D. Williams, pub. Sector Publishing Ltd., London

13. R.M. Pilliar, R. Blackwell, I. McNab & H.V. Cameron, J. Biomed. Mater. Res., 10, (1976), p893

14. A. Murakami, J.C. Behiri & W. Bonfield, J. Mater. Sci., 23, (1988), p2029

15. H. Oonishi, S. Kushitani, M. Aono, K. Maeda, E. Tsuji & H. Ishimaru, 'Bioceramics', Vol. 1, ed. by H. Oonishi, H Aoki and K. Sawai, pub. by Ishiyaku EuroAmerica, Inc., Tokyo, St. Louis,(1989), p102

16. R.L. Strausberg and R.P. Link, Biotechnology, February 1990, Vol. 8

17. T. Kokubo, S. Yoshihara, N. Nishimura, T. Yamamuro and T. Nakamura, J. Amer.Ceram. Soc., 74 (7),(1991), p1739

18. J. C. Behiri,M. Braden, S.N. Khorasani, D. WiWattanadate and W. Bonfield, 'Bioceramics 4', ed. by W. Bonfield, G.W. Hastings and K.E. Tanner, pub. by Butterworth-Heinemann Ltd., (1991), p301

19. A.D. Wilson & B.E. Kent, Brit. Pat. No. 1,316,129

20. D.C. Smith, Br. Dent. J., 125, (1968), p381

21. J. Perek and R.M. Pilliar, Proceedings 9th European Conference on Biomaterials, Chester, (September 1991)

22. L.M Jonck, C.J. Grobbelaar & H. Strating, Clinical Materials, 4, (1989), p85

23. L.M Jonck, C.J. Grobbelaar & H. Strating, Clinical Materials, 4, (1989), p201

24. I.M. Brook, G.T. Craig and D.J. Lamb, Clinical Materials, 7, (1991), p295

25. I.M. Brook, G.T. Craig and D.J. Lamb, Biomaterials, 9, (1989), p171

26. P.J. Doherty, Clinical Materials, 7, (1991), p335

27. T. Masuda and J.E. Davies, Biomaterials, 9, (1989), p454

28. L.L. Hench, R.J. Splinter, W.C. Allen, T.K. Greenlee, J. Biomed. Mater. Res. Symp., 2, (1971), 117

29. E.W Skinner & R.W. Philips, 'The Science of Dental Materials', 6th Edn., pub. by Saunders, Philadelphia / London, (1967), p60

30. R.S. Sanderson, Dental Record, (February 1908)

31. P. Steenbock, Brit. Pat. No.'s 15,176 & 15,181, (1904)

32. F. Schoenbeck, US Pat. No. 897,160, (1907)

33. A.D. Wilson & R.F. Batchelor, J. Dent. Res., 46, (1967), p1025

34. A.D. Wilson, B.E. Kent, D. Clinton & R.P. Miller, J. Mater. Sci., 7, (1972), p220

35. H.J. Prosser, C.P. Richards & A.D. Wilson, J. Biomed. Mater. Res., 16, (1982), p431

36. S. Crisp, B.E. Kent, B.G. Lewis & A.D. Wilson, J. Dent. Res., 59, (1980), p1055

37. J. Ellis, PhD Thesis, Thames Polytechnic, (1989)

38. M. Kajiwara, J. Mat. Sci. letters, 4, (1985), 1178

39. B.E. Kent, B.G. Lewis & A.D. Wilson, J. Dent. Res., 58, (1979), p1607

40. A.D. Wilson, S. Crisp, H.J.Prosser, B.G. Lewis & S.A. Merson, Ind. Eng. Chem. Prod. Res. Dev., 19, (1980), p263

41. M. Wilson and E.C. Combe, Clinical Materials, 7, (1991), 15

42. A.D. Wilson, S. Crisp & A.J. Ferner, J. Dent. Res., 55, (1976), p489

43. S. Crisp & A.D. Wilson, J. Dent. Res., 55, (1976), p1023

44. S. Crisp & A.D. Wilson, J. Dent. Res., 53, (1974), p1408

45. S. Crisp, M.A. Pringuer & D. Wardleworth, J. Dent. Res., 53, (1974), p1414

46. E.A. Wasson and J.W. Nicholson, Clinical Materials, 7 (1991), p289

47. T. Masuda & J.E. Davies, Biomaterials, 8, (1987), p275

48. H. Kawahara, Y. Imanishi & H. Oshima, J. Dent. Res., 58, (1979), p1080

49. 'Concise System of Orthopaedics and Fracture, part 1', Chapter 6, ed. by A.G. Apley and L. Solomon, pub. by Butterworths, (1988)

50. J. Zarzycki, 'Glasses and the Vitreous State', Cambridge Solid Science Series, ed. by R.W. Cahn, E.A. Davies and I.M. Ward, pub. by Cambridge University Press, (1991)

51. G.O. Jones, 'Glass (2nd edition)', pub. by Chapman and Hall, London, (1971)

52. T.G. Fox and P.J. Flory, J. Appl. Phys., 21, (1950), 581

53. T.G. Fox and P.J. Flory, J. Phys. Chem., 55, (1951),221

54. T.G. Fox and P.J. Flory, J. Polymer Sci., 14, (1954), 315

55. M.H. Cohen and D. Turnbull, J. Chem. Phys., 31, (1959), 1164

56. W.H. Zachariasen, J. Am. Ceram. Soc., 54, (1932), 3841

57. V.M. Goldschmidt, Geochemische Verteilungsgesetze der Elemente viii, Vid, Akad, (1926)

58. A.A. Appen, J Appl. Chem., 25 , (1952), 12

59. L.A. Balewick and J.E. Shelby, J. Am. Ceram. Soc., 72, (1989), 1751

60. W. Lowenstein, Am. Mineral., 39, (1954), 92

61. G. Engelhardt, M. Nofz, K. Forkel, F.G. Wihsmann, M. Mägi, A. Samoson and E. Lippmaa, Phys. Chem. Glasses, 26, (1985), 157

62. B.E. Warren, H. Krutter, O.J. Morningstar, J. Am. Ceram. Soc., 19, (1936),287

63. N. Ray, 'Ionic Polymers', Chapter 8, ed. by L. Holliday, Applied Science Publishers, London

64. G.M. Bartenev, 'The Structure and properties of Inorganic glasses', pub. by Wolters-Noordhoff Publishing, (1970)

65. E.A. diMarzio and J.H. Gibbs, J. Polymer Sci., 40, (1959), 121

66. J.T. Randall, H.P. Rooksby, B.S. Cooper, J. Soc. Glass Technol., 14, (1930), 219

67. J.T. Randall, H.P. Rooksby, B.S. Cooper, J. Soc. Glass Technol., 15, (1931), 54

68. J.T. Randall, H.P. Rooksby, B.S. Cooper, J. Soc. Glass Technol., 17, (1933), 287

69. C.H.L. Goodman, Phys. Chem. Glasses, 26, (1985),1

70. P.H. Gaskell, M.C. Eckersley, A.C. Barnes and P. Chieux, Nature, vol. 350, (1991), 675

71. D. Turnbull and M.H. Cohen, J. Chem. Phys.,29,(1958),1049

72. D. Turnbull and M.H. Cohen, 'Modern Aspects of the Vitreous state, Vol. 1', ed. by JD Mackenzie, pub. by Butterworths, London, (1960)

73. D. Turnbull and M.H. Cohen, Nature, 189, (1961), 131

74. D.R. Uhlmann, J. Non. Cryst. Solids, 7, (1972), 337

75 D. Turnbull, 'Solid State Physics', ed. by F. Seitz and D. Turnbull, pub. by Academic Press, New York, (1956)

76. T.I. Barry, D.I. Clinton & R. Morrel, NPL Report No. 91/10/486, (1972)

77. T.I. Barry, D.I. Clinton & A.D. Wilson, J. Dent. Res., 58, (1979), p1072

78. R.G. Hill & A.D. Wilson, Glass Technology, 29, (1988), p150

79. P.F. James, J. Mat. Sci., 10, (1975), 1802

80. J.W. Cahn, J. Chem. Phys., 42, (1961), 93

81. J.W. Cahn and R.J. Charles, Phys. Chem. Glasses, 6, (1965), 181

82. J.W. Cahn and J.E. Hilliard, J. Chem. Phys., 28, (1958), 258

83. J.W. Cahn and J.E. Hilliard, J. Chem. Phys., 31, (1959), 688

84. J.W. Cahn and J.E. Hilliard, Acta Met., 9, (1961),795

85. J.W. Cahn and J.E. Hilliard, Acta Met., 10, (1962),179

86. D.R. Uhlmann, Discussion Remarks, Trans. Faraday Soc., 11b, (1970)

87. G.M. Singer and M. Tomozawa, Phys. Chem. Glasses, 30, (1989), 86

88. G.M. Singer and M. Tomozawa, Phys. Chem. Glasses, 30, (1989), 95

89. G.M. Singer and M. Tomozawa, Phys. Chem. Glasses, 30, (1989), 102

90. D. Kumar, R.G. Ward and D.J. Williams, Discuss. Faraday Soc., 32,(1961), 147

91. E.M. Rabinovich, Phys. Chem. Glasses, 24, (1983), 54

92. J.M. Parker and G.F. West, Materials Science Forum, 7, (1986), 297

93. J.E. Shelby, J. Am. Ceram. Soc., 68, (1985),551

94. J. Coon and J.E. Shelby, J. Am. Ceram. Soc., 71, (1988), 354

95. J.E. Shelby, C.M. Shaw and M.S. Spess, J. Appl. Phys., 66, (1989), 1149

96. J.E. Shelby and C.E. Loro, J. Am. Ceram. Soc., 73, (1990), 750

97. P.W. McMillan, 'Glass Ceramics, 2nd edition', pub. by Academic Press, London, (1979)

98. W. Vogel and W. Höland, 'Advances in Ceramics, volume 4', ed. by J.H. Simmons, D.R. Uhlmann and G.H. Beall, American Ceramic Society, Westerville, (1982), 125

99. S.P. Mukherjee and P.S. Rogers, Phys. Chem. Glasses, 8, (1967),81

100. Y.E. Roginskaya, N.M. Pavlushkin, P.D. Sarkisov, T.S. Matveev, G.P. Livorskaya and N.S. Chernyak, Inorg. Mater., 11, (1975), 115

101. I. Gutzow, S. Zlateva, S. Angelov and S. Levy, J. Mat. Sci., 24, (1989), 1281

102. P.D. Has and L.N. Stelian, Brit. Pat 848,447 , (1960)

103. L.L. Hench, J. Am. Ceram. Soc., 74, (1991), 1487

104. T. Kokubo, M. Shigematsu, Y. Nagashima, M. Tashiro, T. Nakaura, T. Yamamuro and H. Higashi, Bull. Inst. Chem. Red. Kyoto Univ., 60, (1982), 260

105. G.J.H. Beall, M.R. Montierth and P. Smith, Barbeithare. Glasheramik Umschau, 42, (1972), 468

106. D.G. Grossman, US Pat. 3839055, (1974)

107. W. Vogel, W. Höland, K. Naumann and J. Gummel, J. Non-Cryst. Solids, 80, (1986), 34

108. H. Bromer, K. Deutscher, B. Blenke, E. Pfeil and V. Strunz, Sci. Ceram., 9, (1977), 219

109. T. Kokubo, S. Ito, S. Sakko and T, Yamamuro, J. Mat. Sci, 21, (1986), 536

110. B.E. Kent, B.G. Lewis and A.D. Wilson, J. Dent. Res., 58, (1979), 1607

111. M.H. Lewis, 'Glasses and Glass-ceramics', Chapman & Hall, London, (1989)

112. A. Marotta, A. Buri, F. Branda & S. Saiello, 'Advances in Ceramics 4', (1982), Edited by J.H. Simmonds, D.R. Uhlmann & G.H. Beall, Amer. Ceram. Soc., (Columbus), p146

113. K. Matusita & S. Sakka, J. Non Cryst. Solids, 38, (1980), p741

114. K. Matusita, S. Sakka and Y. Matsui, J. Mat Sci., 10, (1975), 961

115. R. Meddes, BSc Final Year Project, (1987), Thames Polytechnic

116. L. Alexander & H.P. Klug, Anal. Chem., 20, (1948), p886

117. Newman, The Analyst, 93, (1968), 827

118. C. G. Plant, J.I. Jones, H.J. Wilson, Br. Dent. J., 133, (1972), 21

119. A.D. Wilson, S. Crisp and A.J. Ferner, J. Dent. Res., 55, (1976),489

120. A.D. Wilson, Clinical Materials, 7, (1991), 275

121. G.S. Anstis, P. Chantikal, B.R. Lawn and D.B. Marshall, J. Am. Ceram. Soc., 64, (1981), 533

122. B.R. Lawn and R. Wilshaw, J. Mat. Sci., 10, (1975), 1049

123. D.J. Wood, BSc Final Year Project Report, Thames Polytechnic, 1988

124. C. Goat, MSc Project Report, Thames Polytechnic, 1988

125. M. Weinberg, J. Am. Ceram. Soc., August, 1991

126. R. Dupree, S.C. Cohn, M.G. Mortuza and D. Holland, 'The Physics of Non-Ccrystalline Solids', ed. by L.D. Pye, W.C. La Course and H.J. Stevens, pub. by Taylor and Francis, London, 1992

127. R. Dupree, private communication

128. F. Zaheer, MSc Project report, Thames Polytechnic, 1989

129. C.S. Martin, BSc Final Year Project Report, Thames Polytechnic, 1992

130. S. Crisp and A.D. Wilson, J. Dent. Res., 55, (1976), 1023

131. A.D. Wilson, private communication

132. K. Lau, MSc Project report, Thames Polytechnic, 1991

133. M. Patel, MSc Project report, Thames Polytechnic, 1991

134. K. Webster, BSc Final Year Project Report, Thames Polytechnic, 1992

135. 3M Dental Products, 3M Health Care, 3M House, Morley Street, Loughborough, Leicestershire,LE11 1EP

136. R.G. Hill, A.D. Wilson and C.P. Warrens, J. Mat. Sci, 24, (1989), 363

137. E.D. Zanotto, private communication

7. LIST OF FIGURES

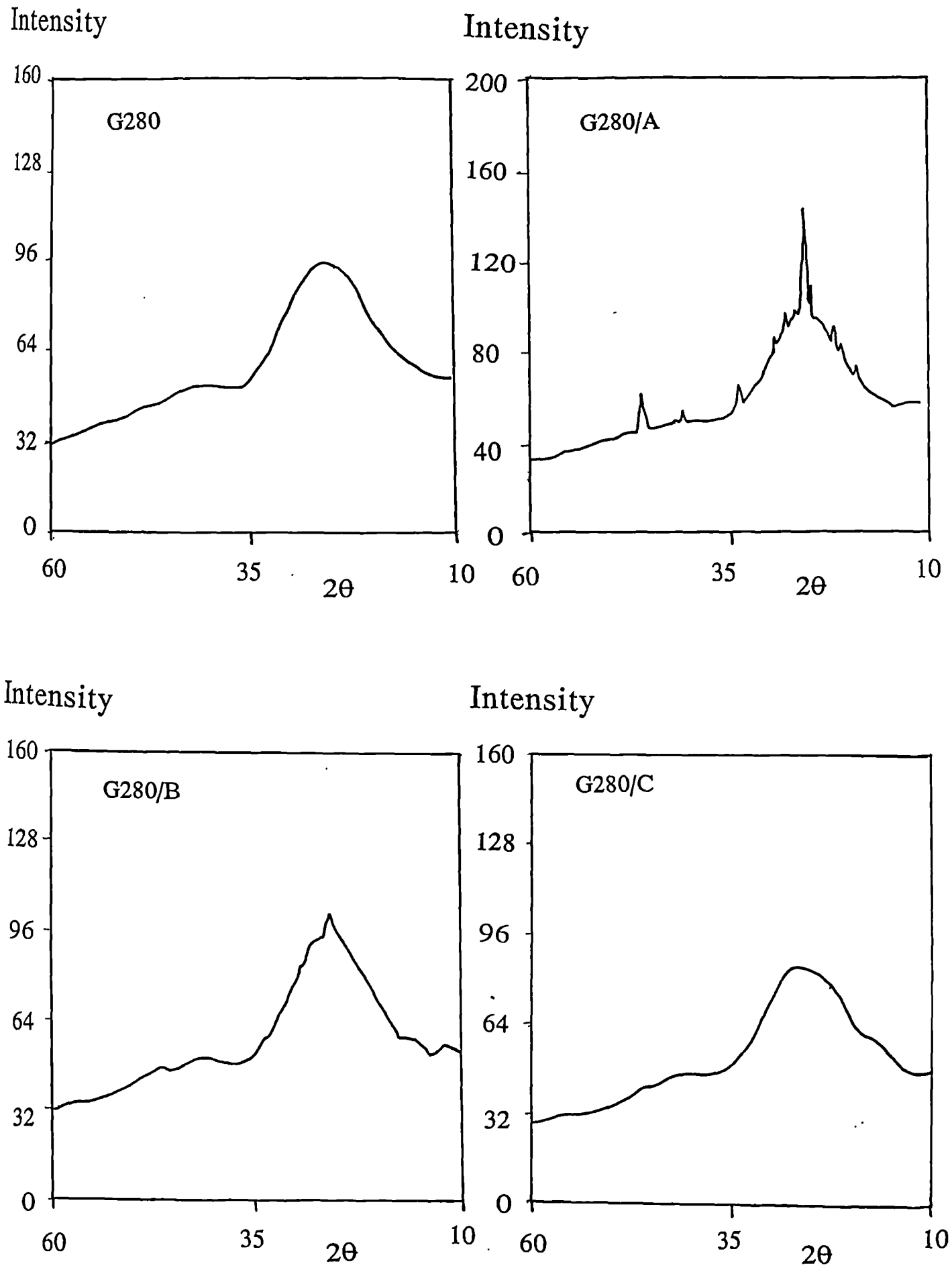

Figure 27 - XRD of 4 batches of G280

Figure 28 - DTA of G280

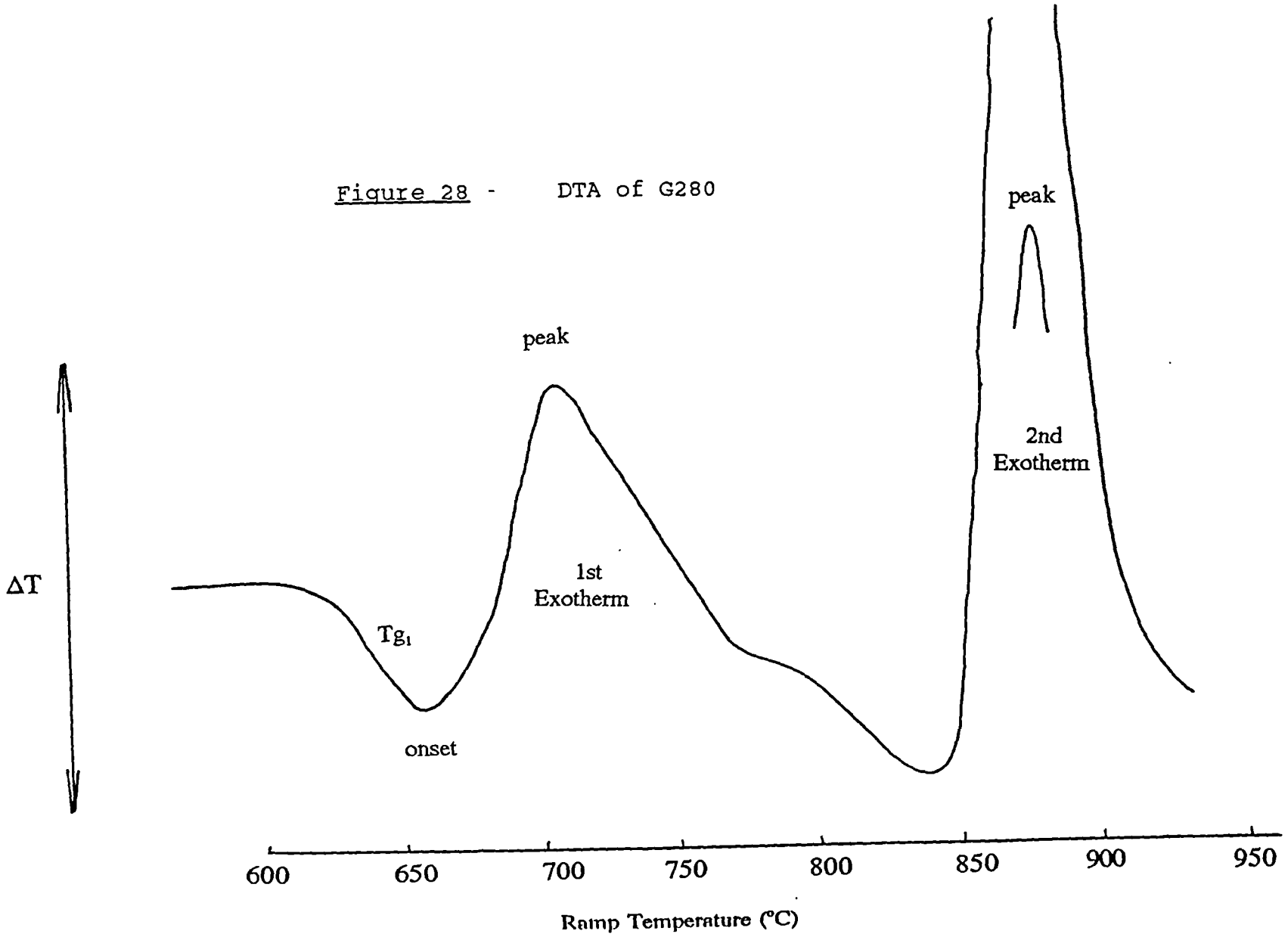

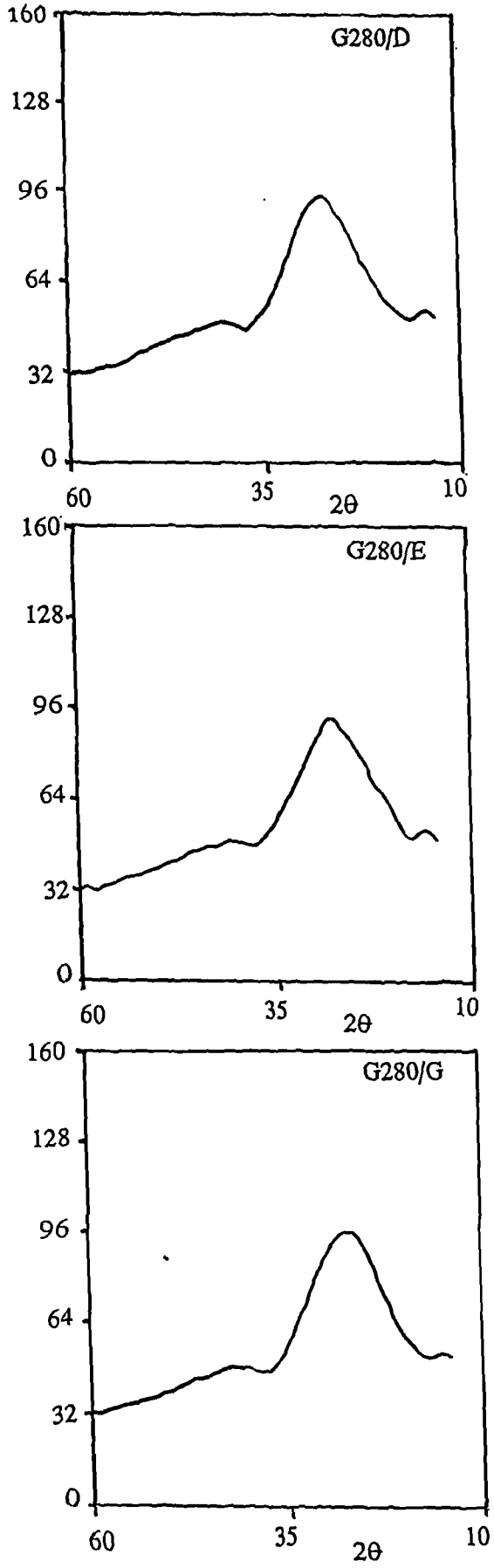

Figure 29 - XRD of G280/D, G280/E and G280/G

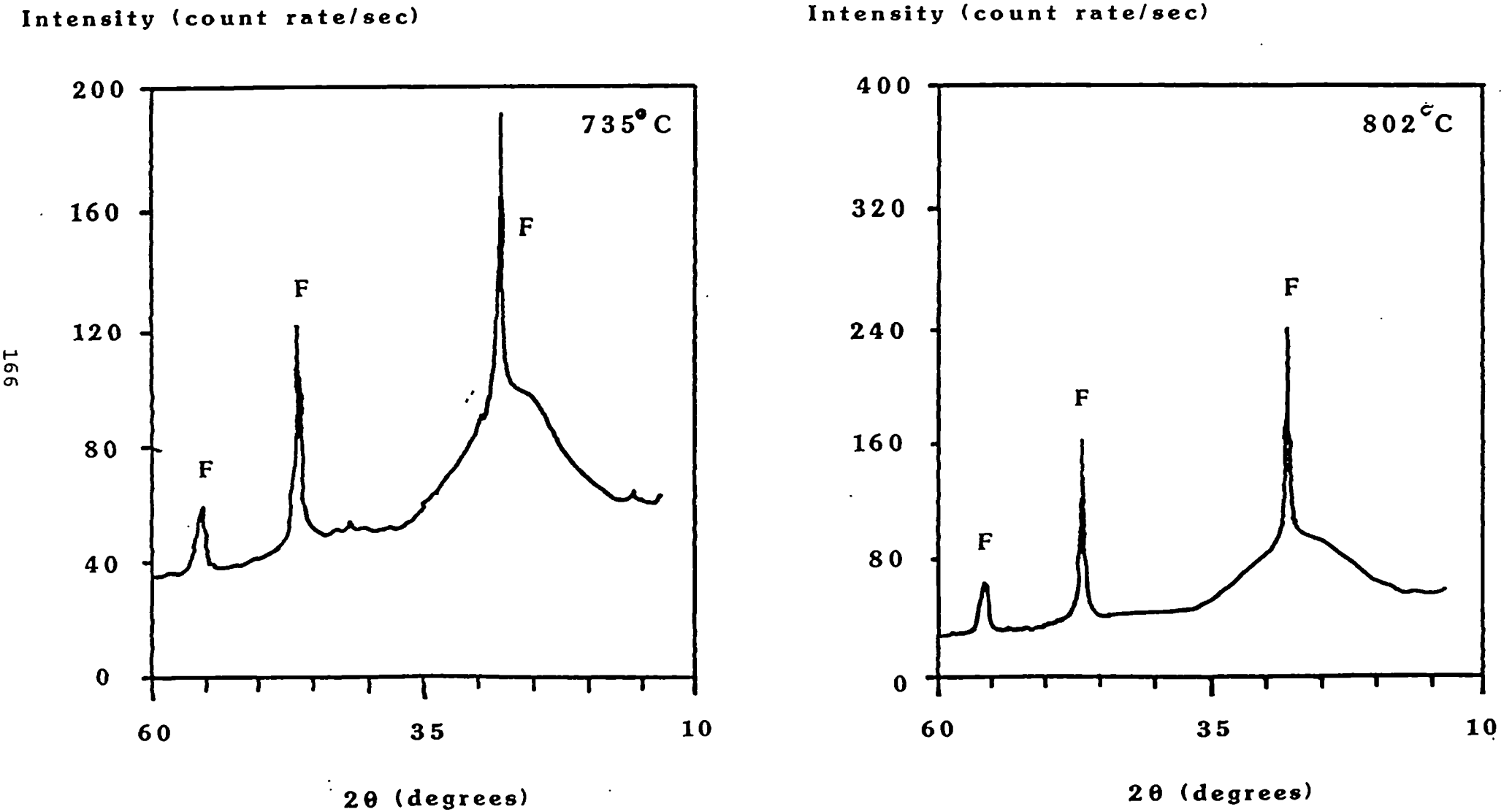

Figure 30 - XRD of Heat Treated G280

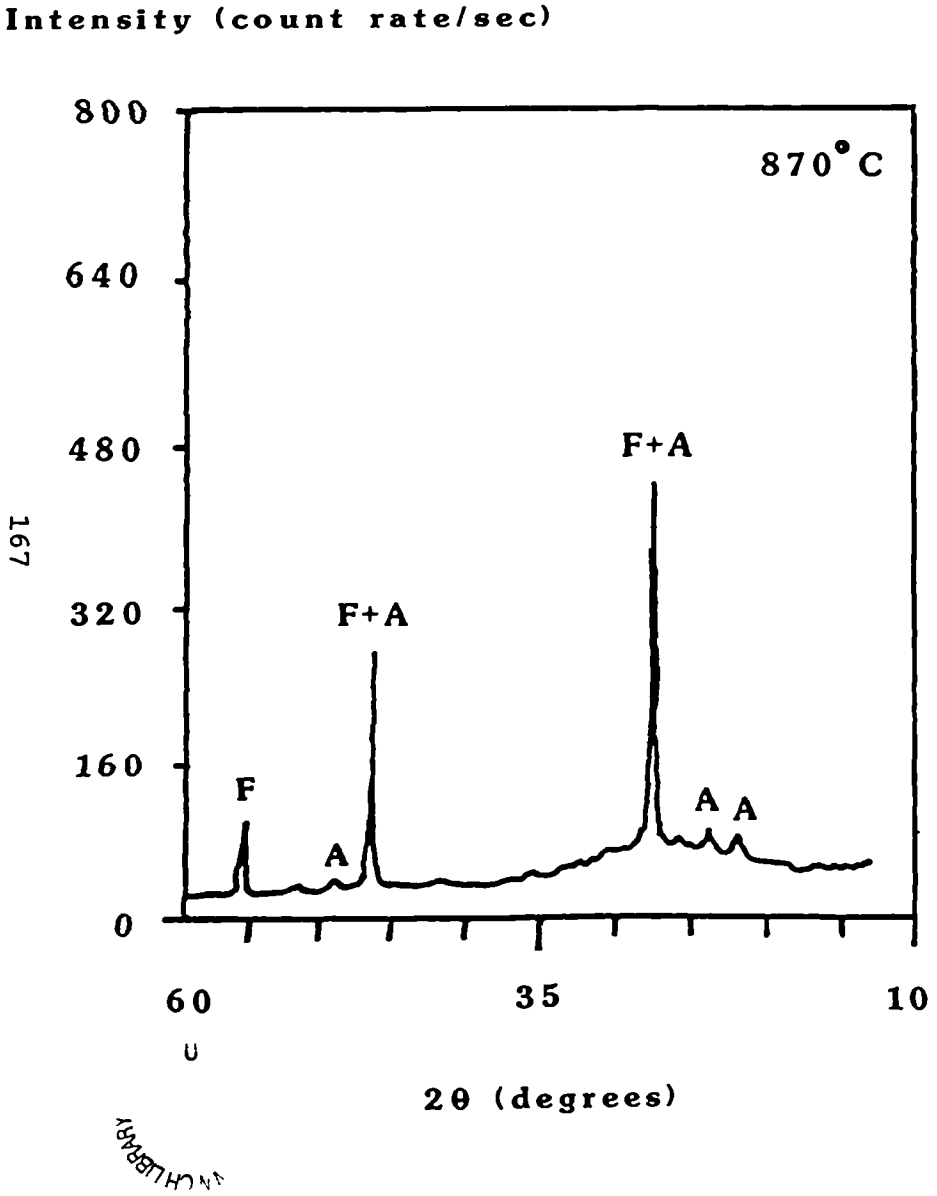
Intensity (count rate/sec)
800
640
480
320
160
0
870°C
F+A
F+A
F
A
A
A
60
35
10
2θ (degrees)

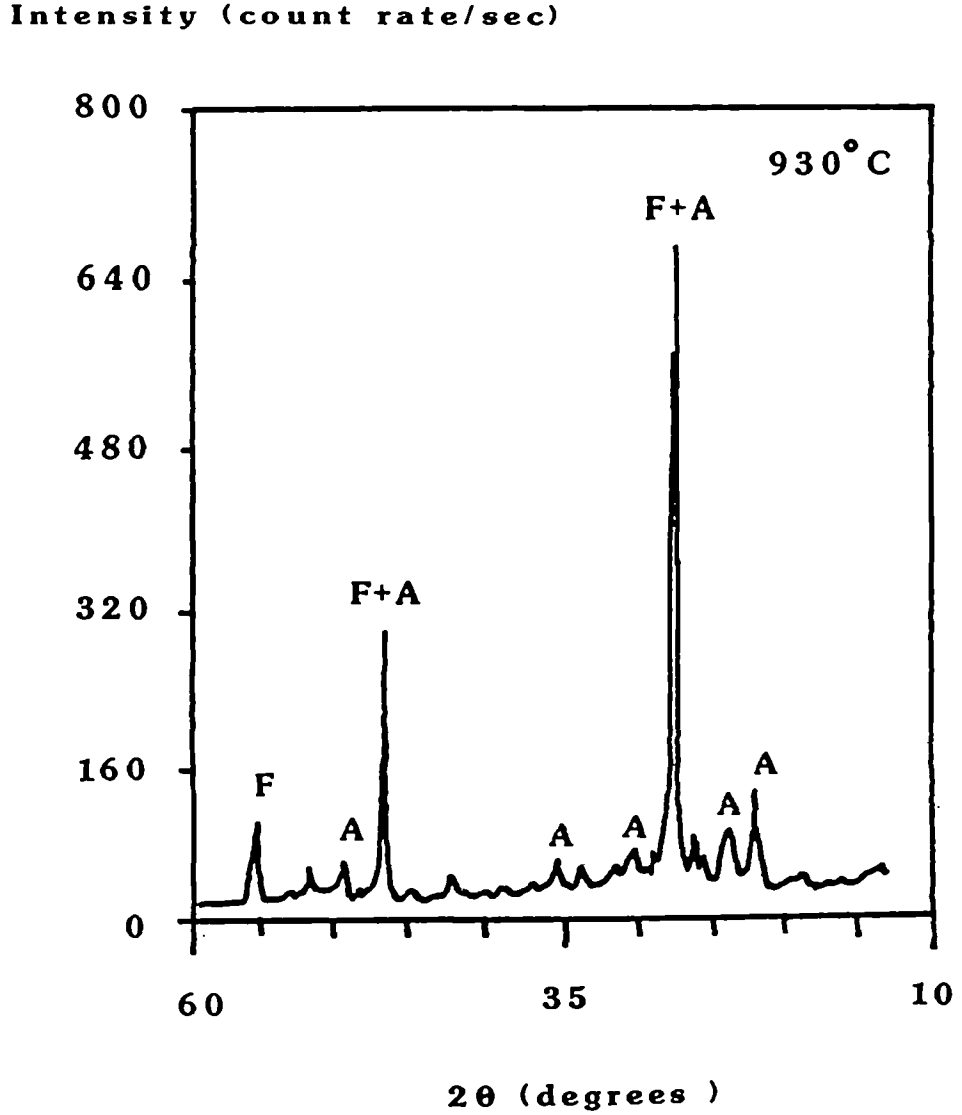
Intensity (count rate/sec)
800
640
480
320
160
0
930°C
F+A
F+A
F
A
A
A
A
A
60
35
10
2θ (degrees)

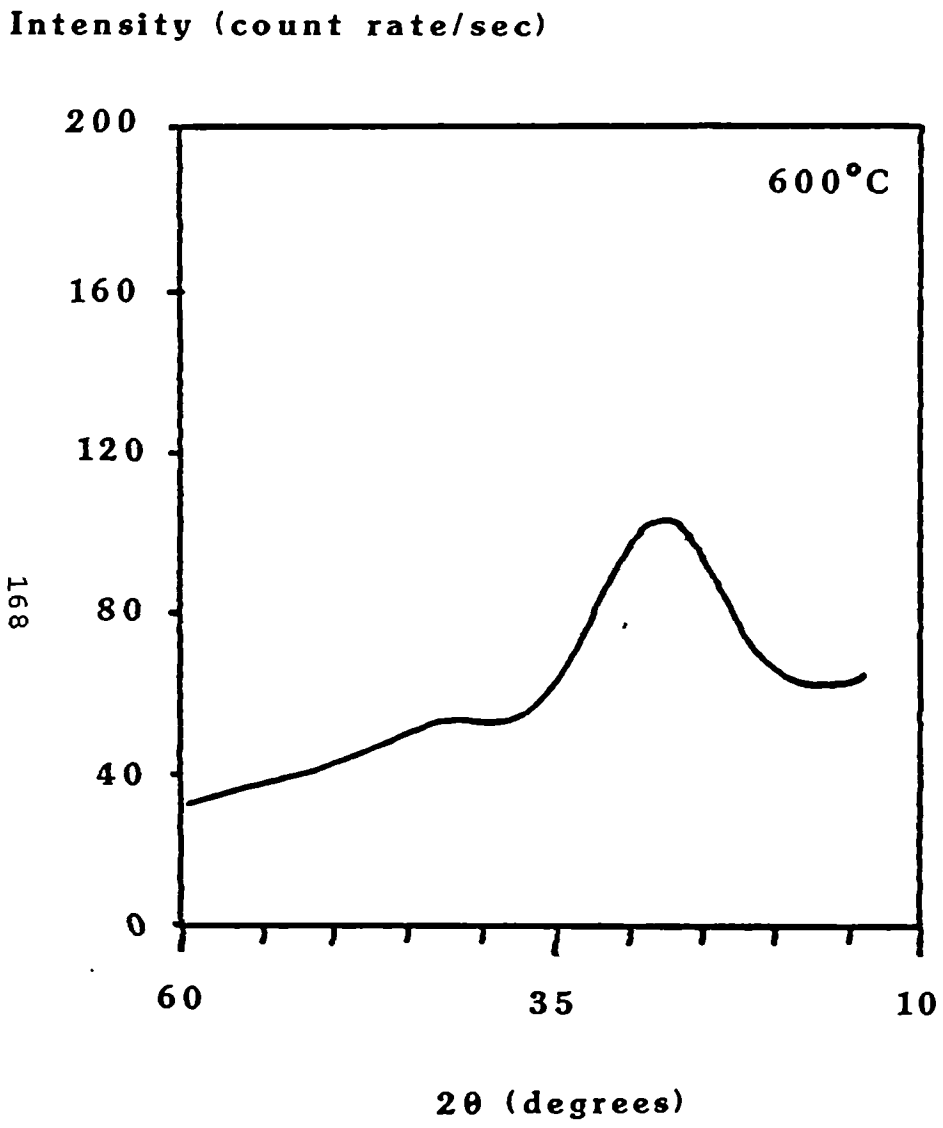
Intensity (count rate/sec)
200
160
120
80
40
0
600°C
60
35
10
2θ (degrees)

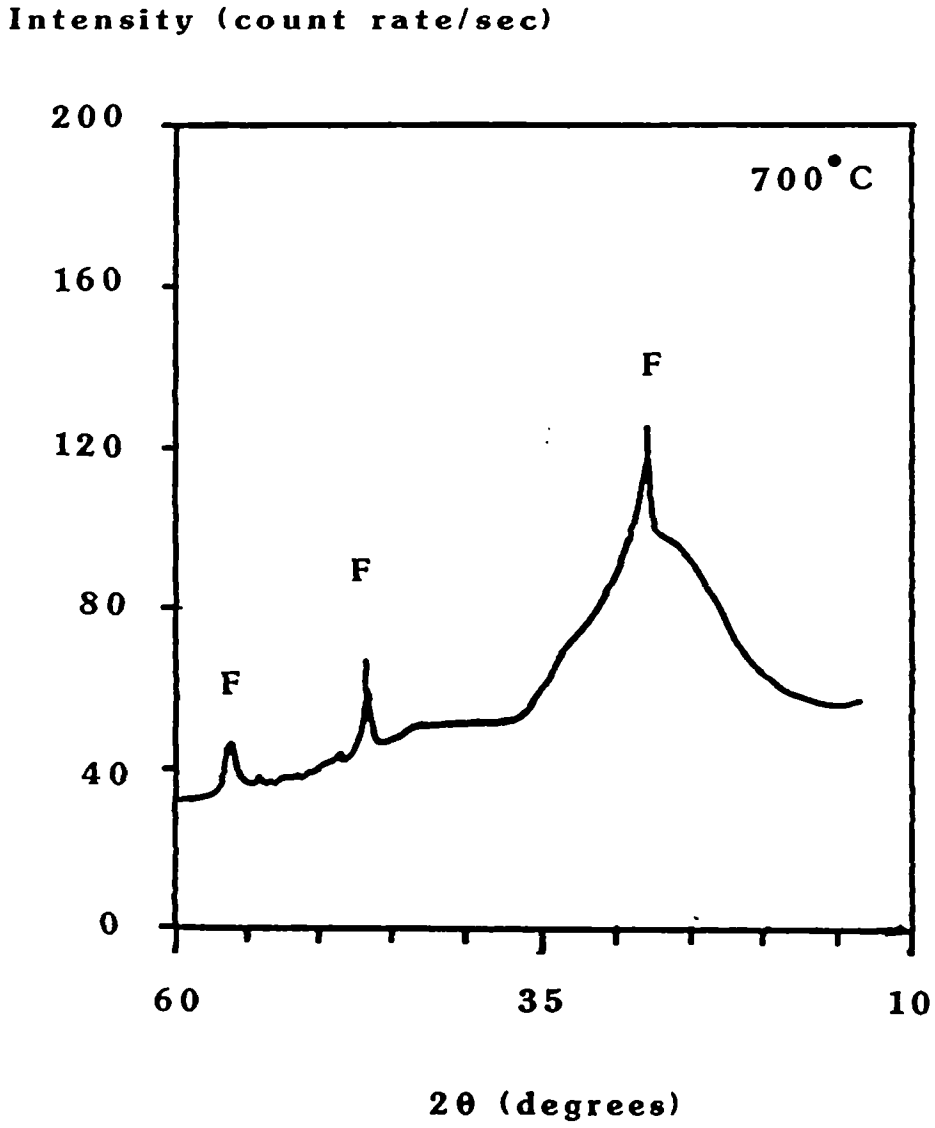
Intensity (count rate/sec)
200
160
120
80
40
0
700°C
F
F
F
60
35
10
2θ (degrees)

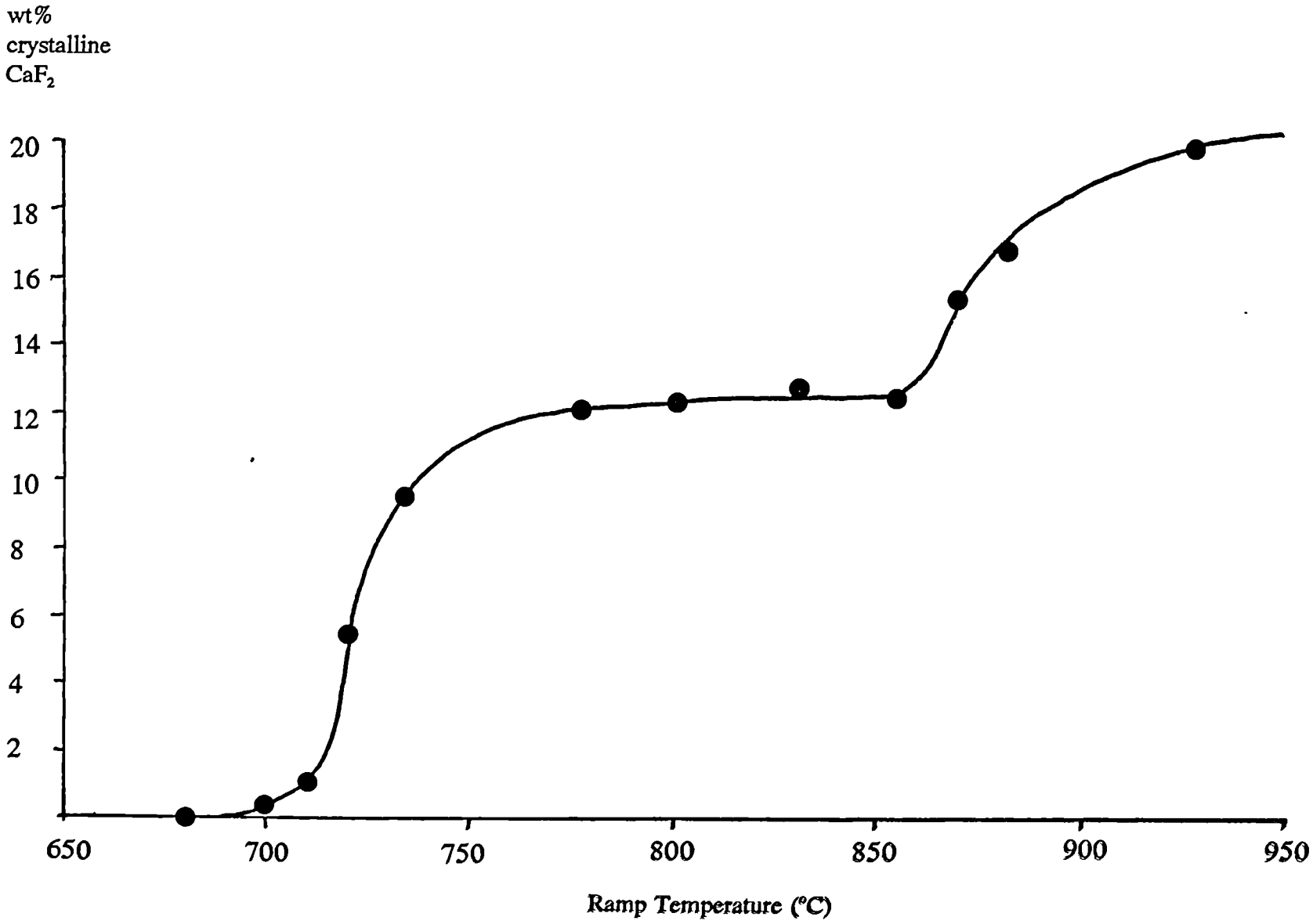

Figure 31 - CaF_2 Crystallization as a Function of Temperature

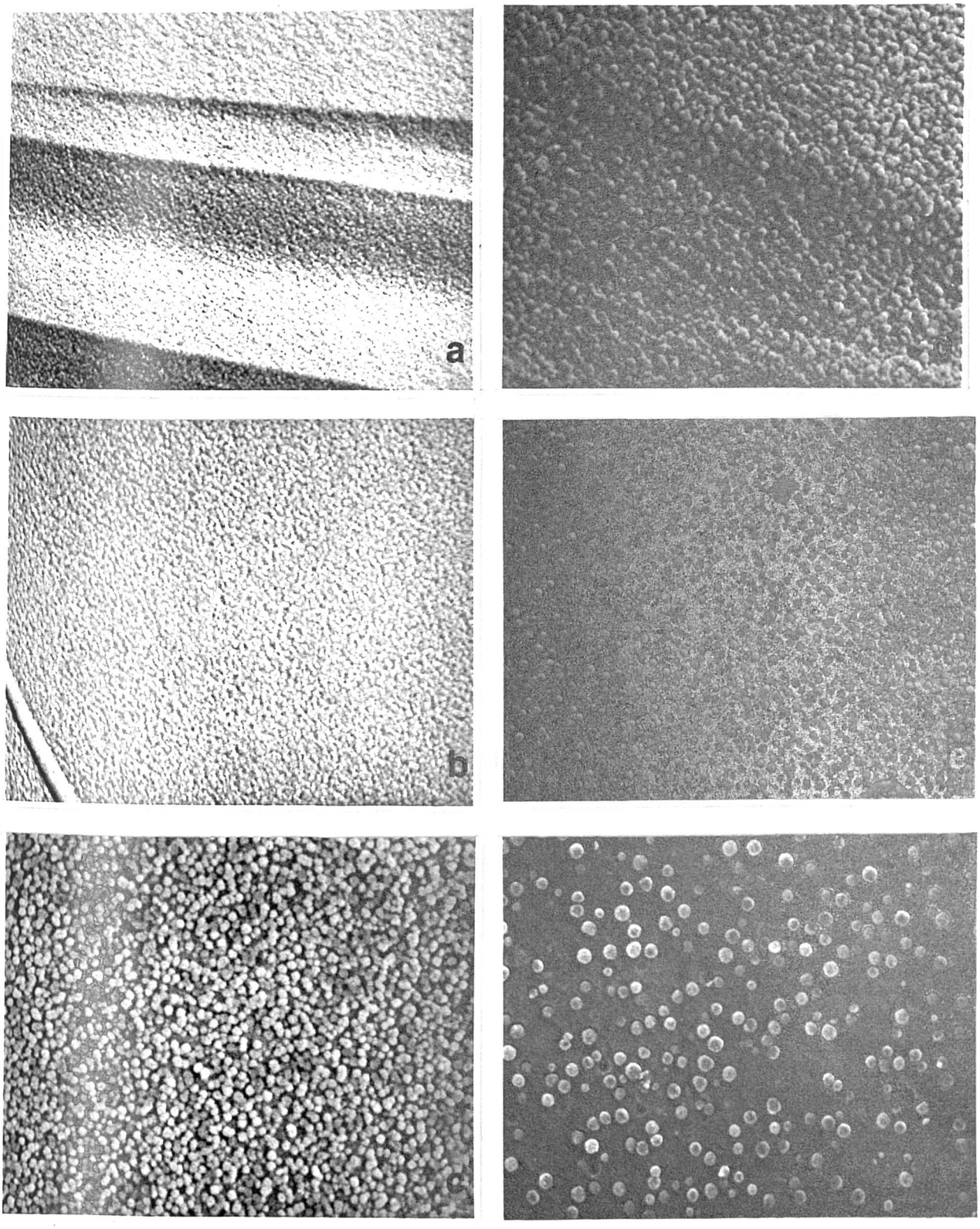

Figure 32 - SEM of Heat Treated G280

Figure 33 - Marotta plot of Activation Energy

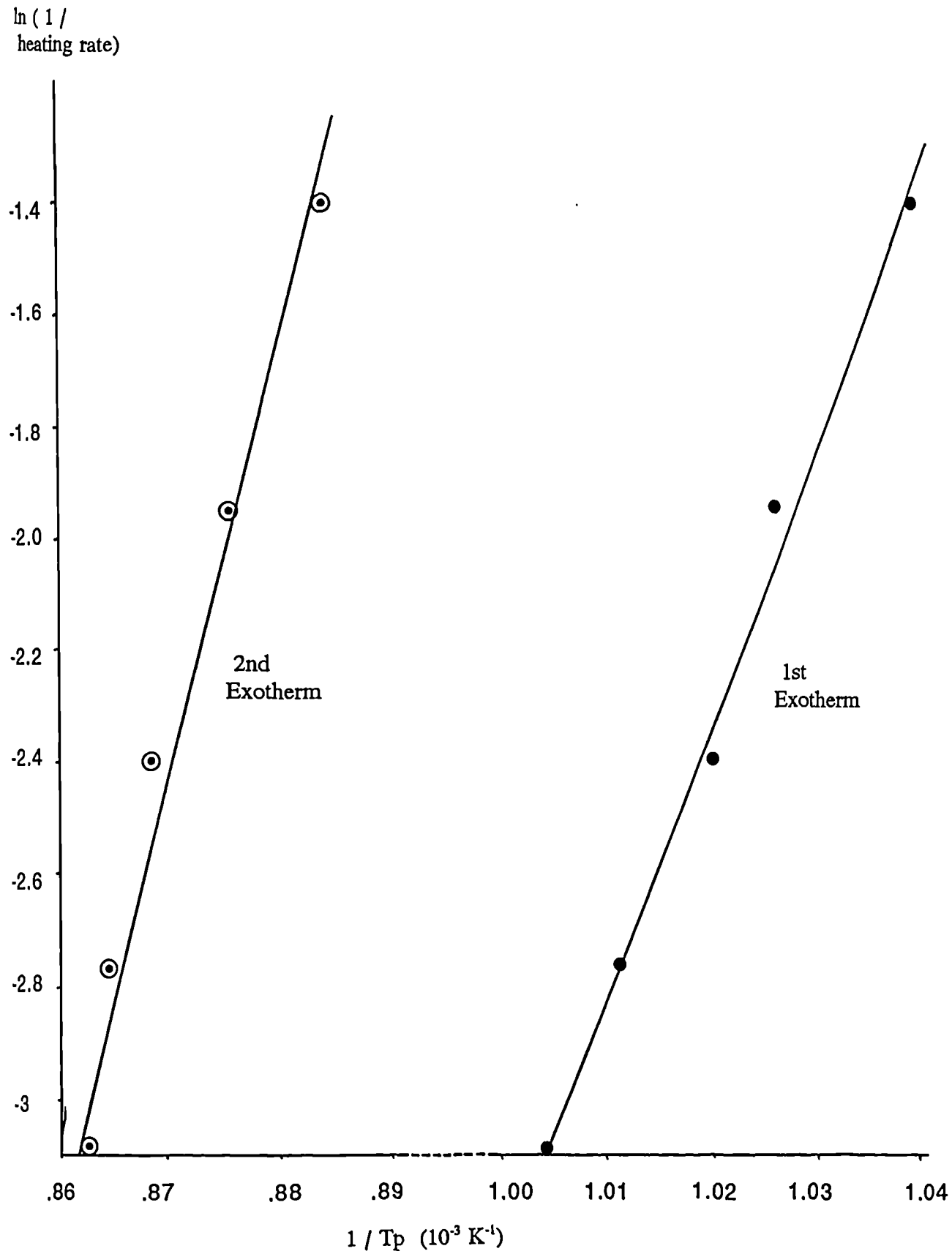

Figure 34 - Matusita plot of Activation Energy

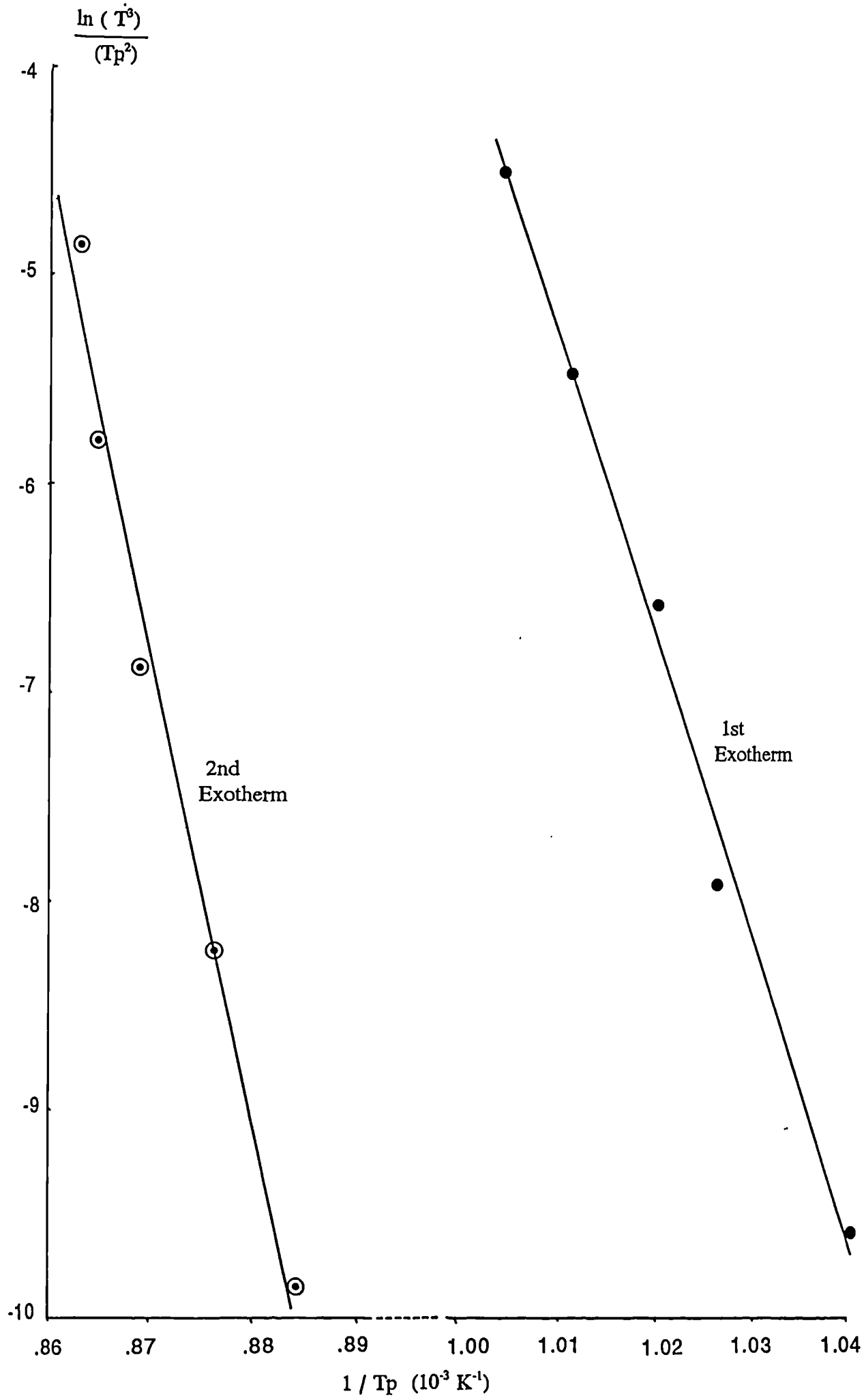

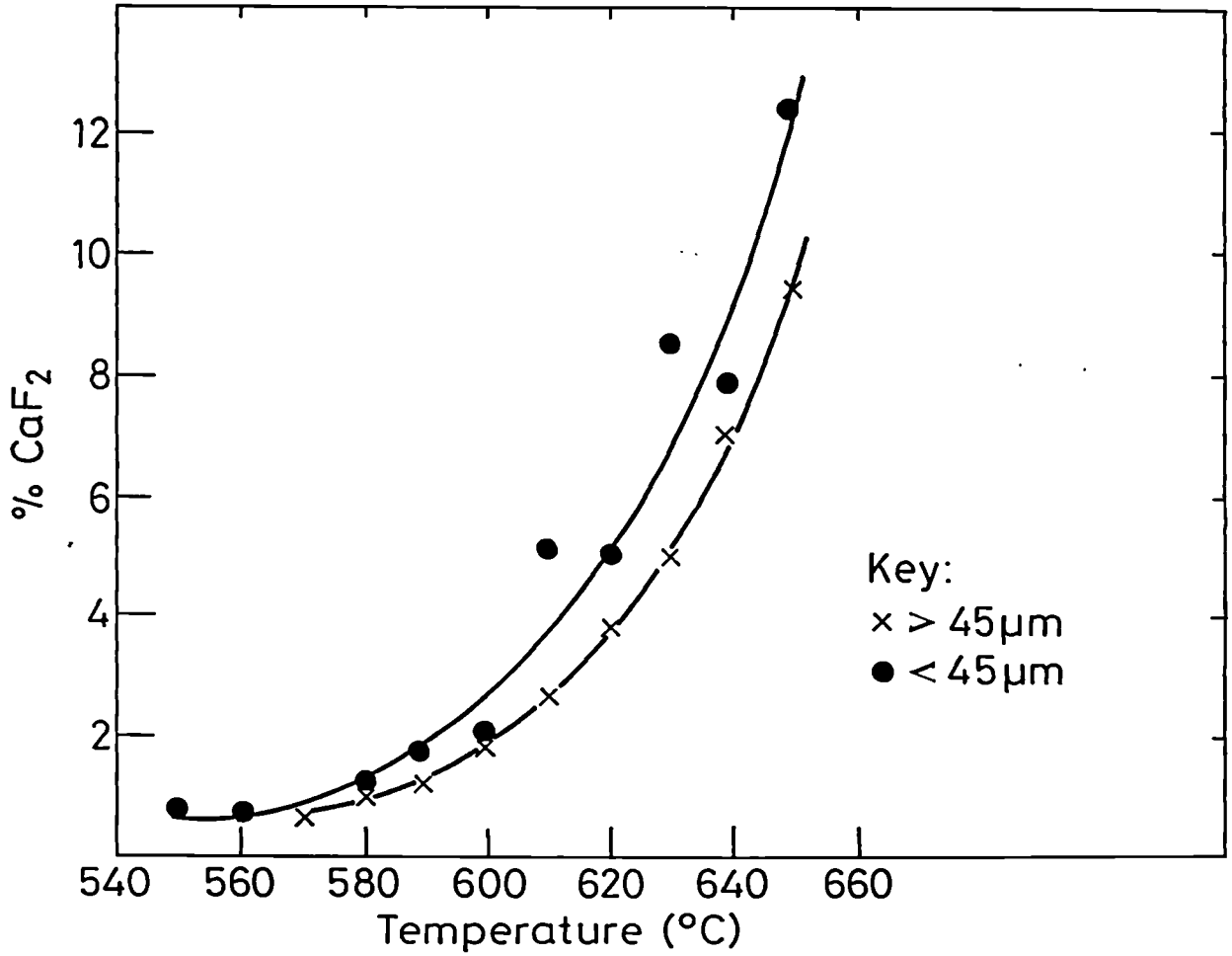

Figure 35 - % Crystalline CaF_2 in G280 heated to various temperatures below Tg for 18 hours

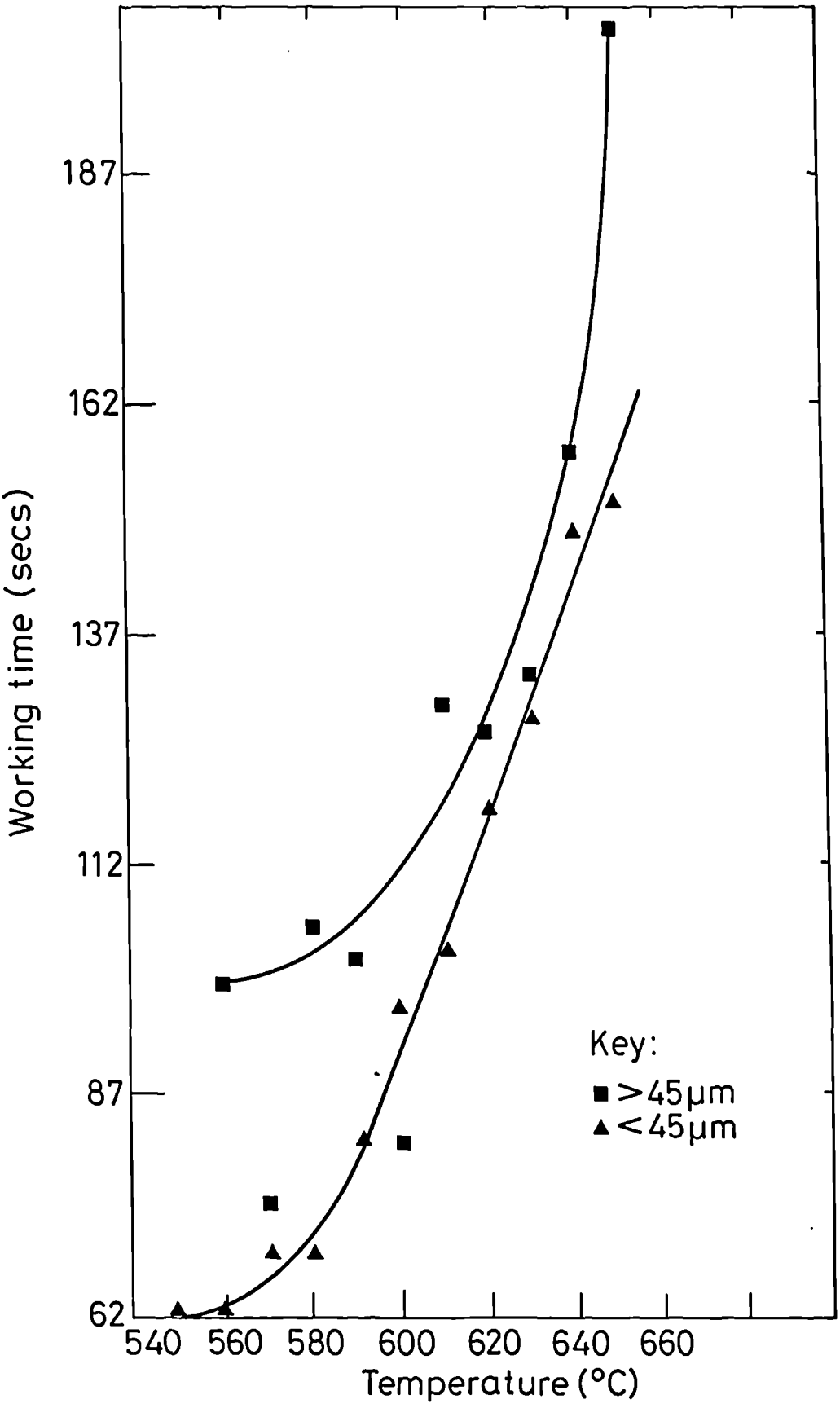

Figure 36 - Variation in working time of cement with isotherm temperature

Figure 37 - Plot of CaF_2 Crystallization vs Working Time

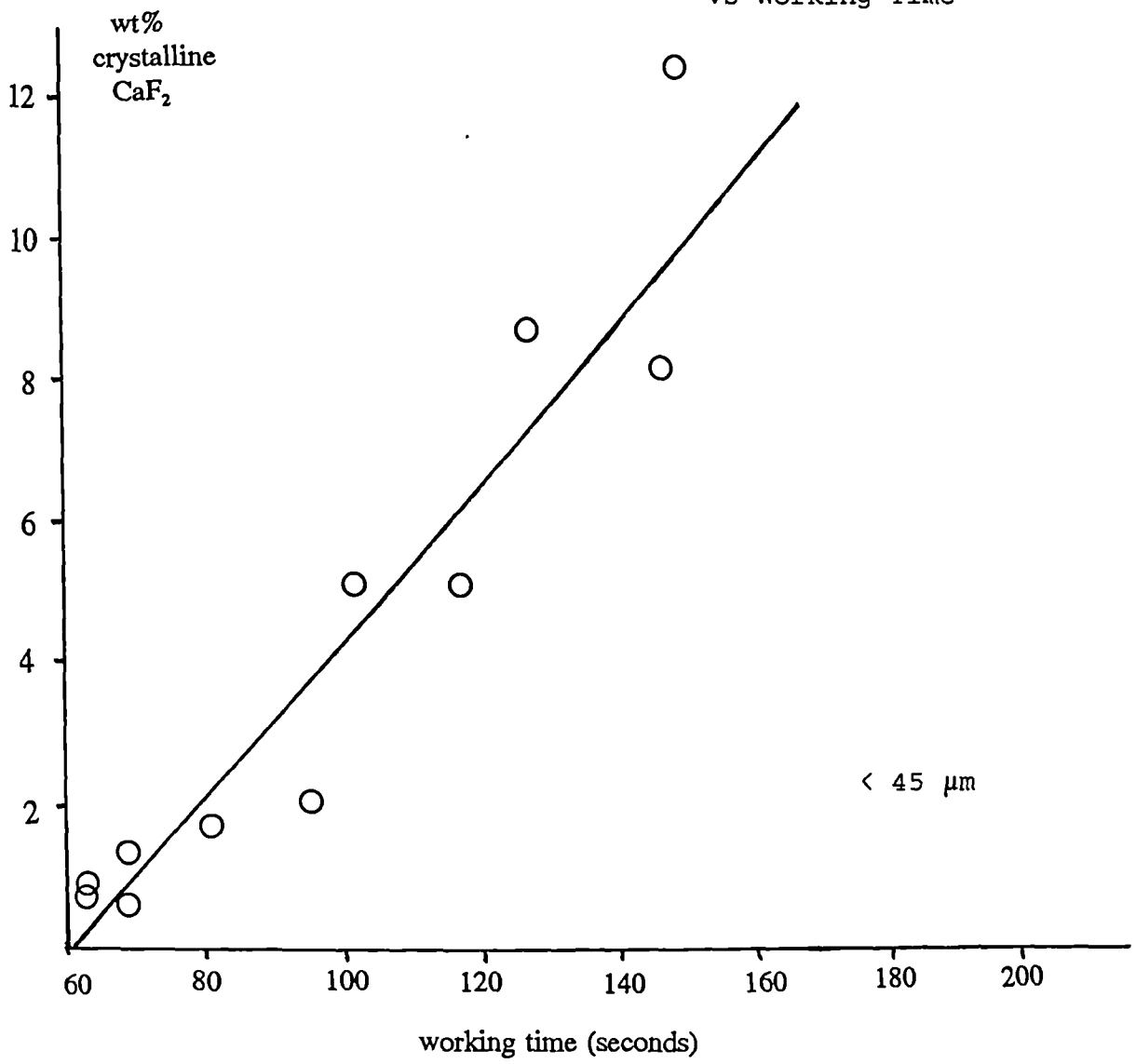

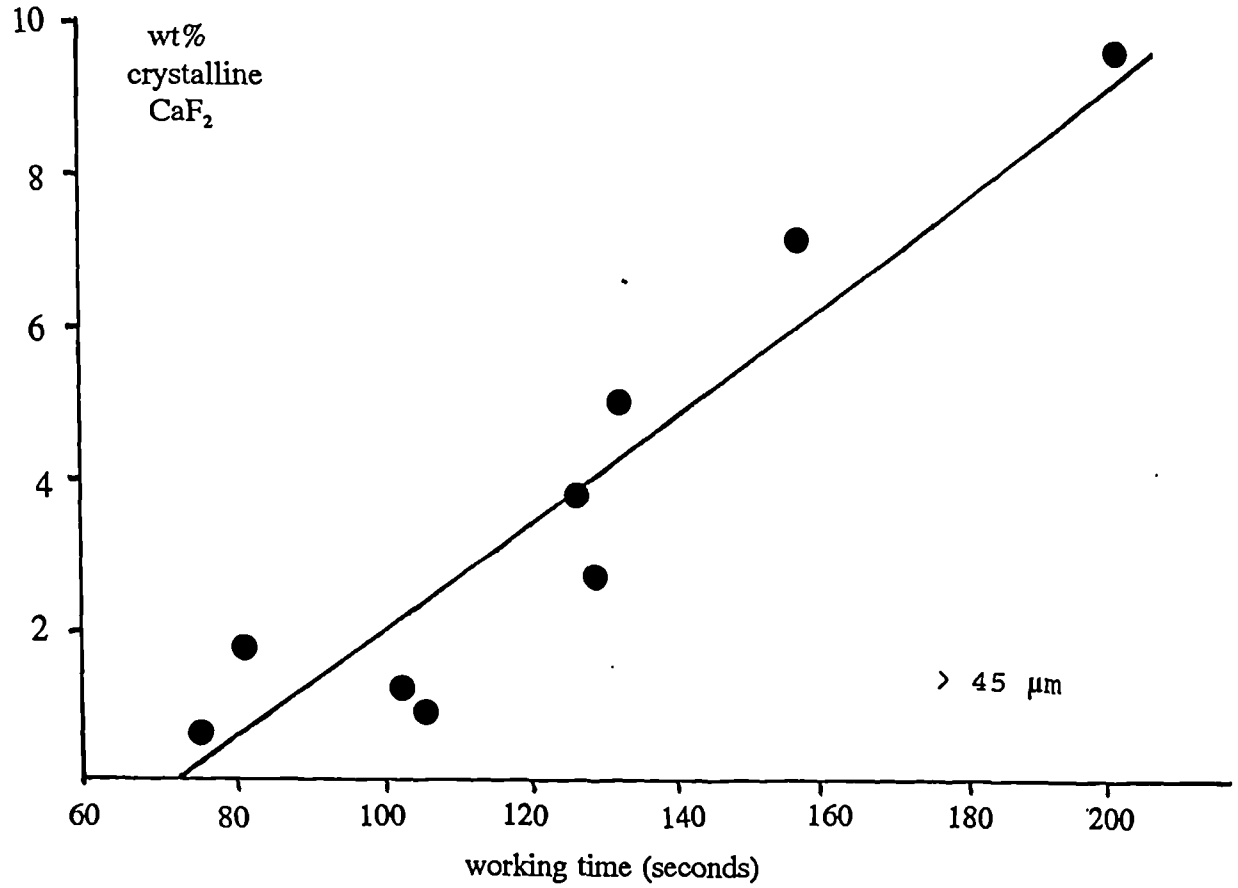

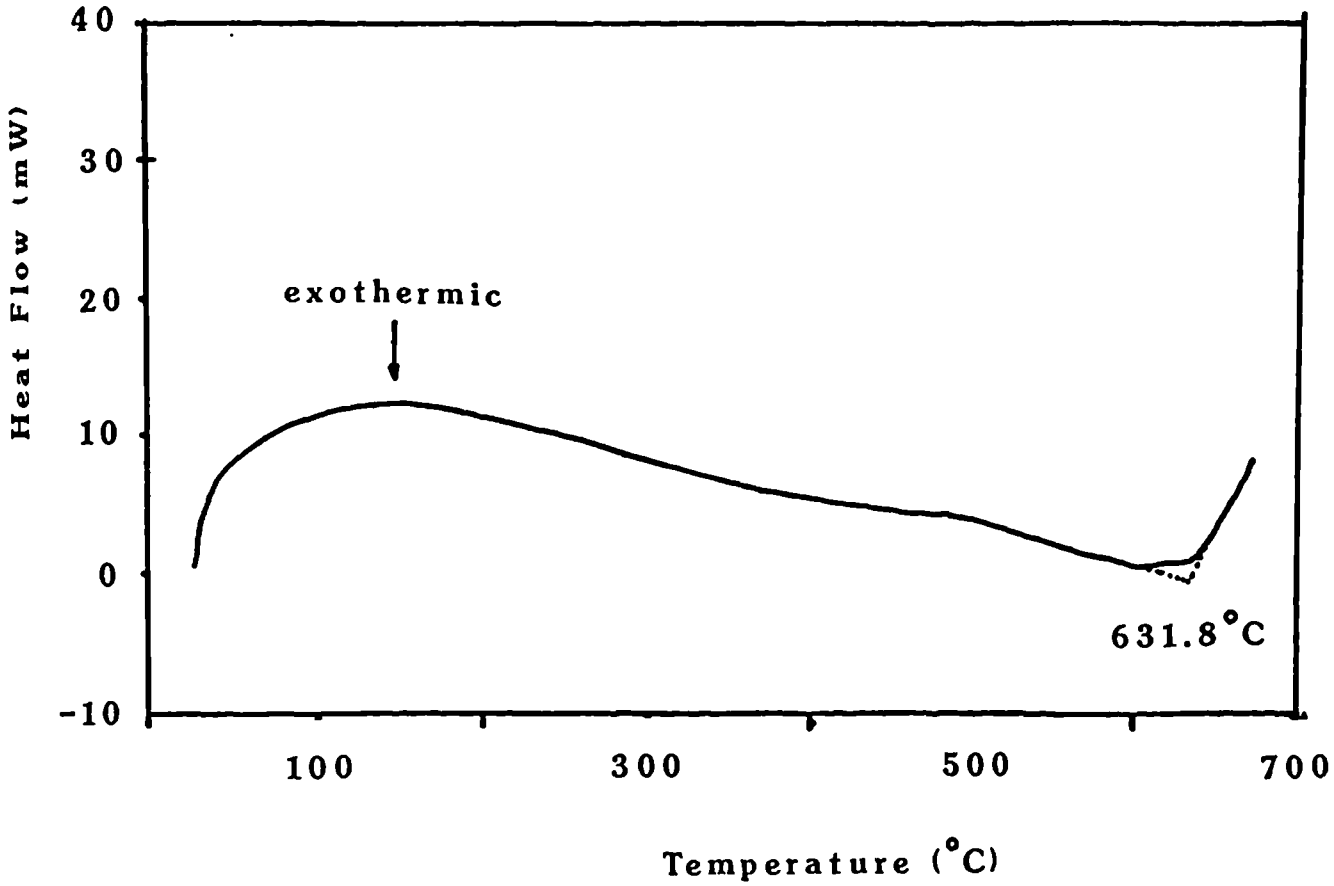

Figure 38 - Six Successive DSC Runs

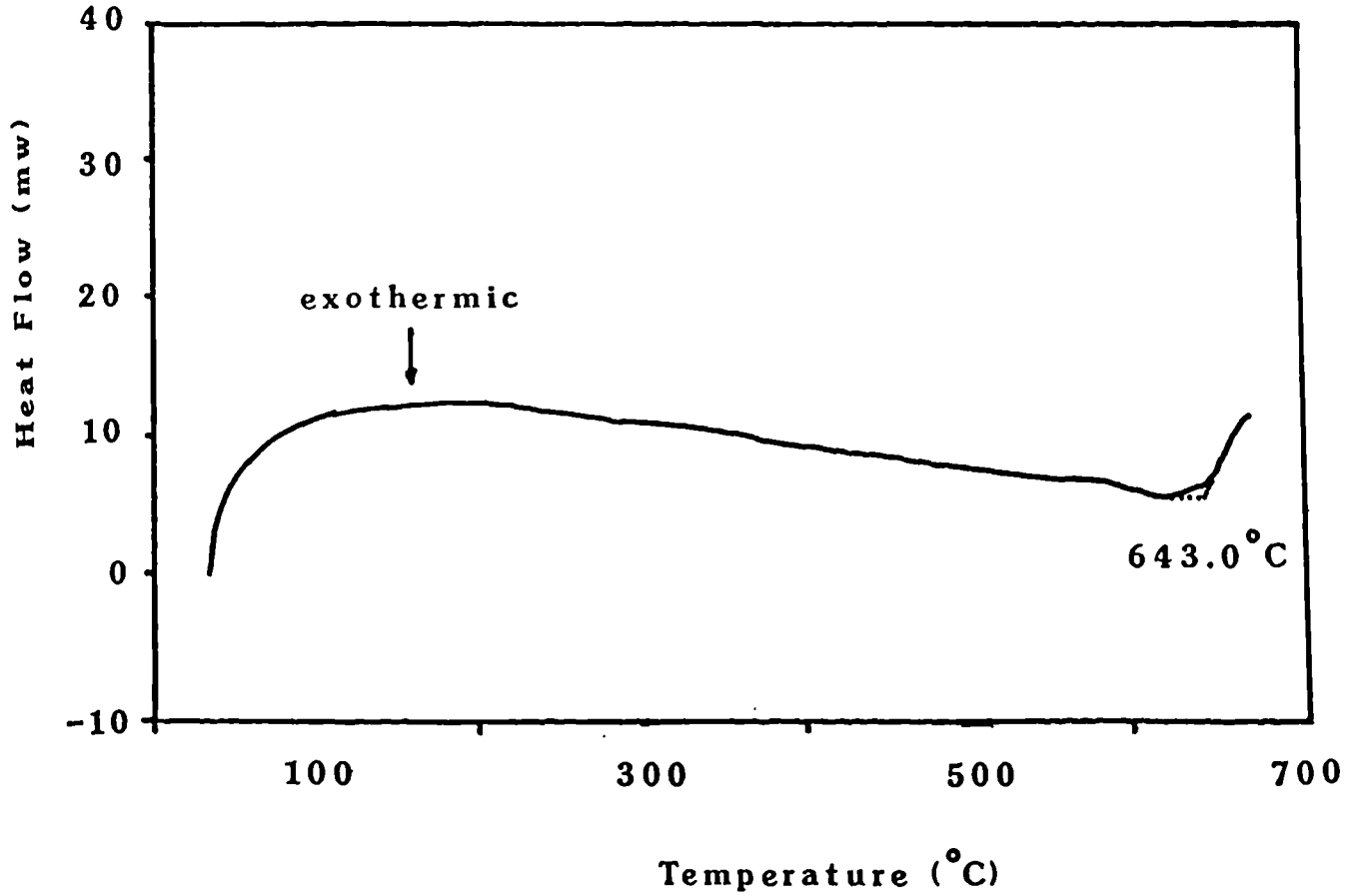

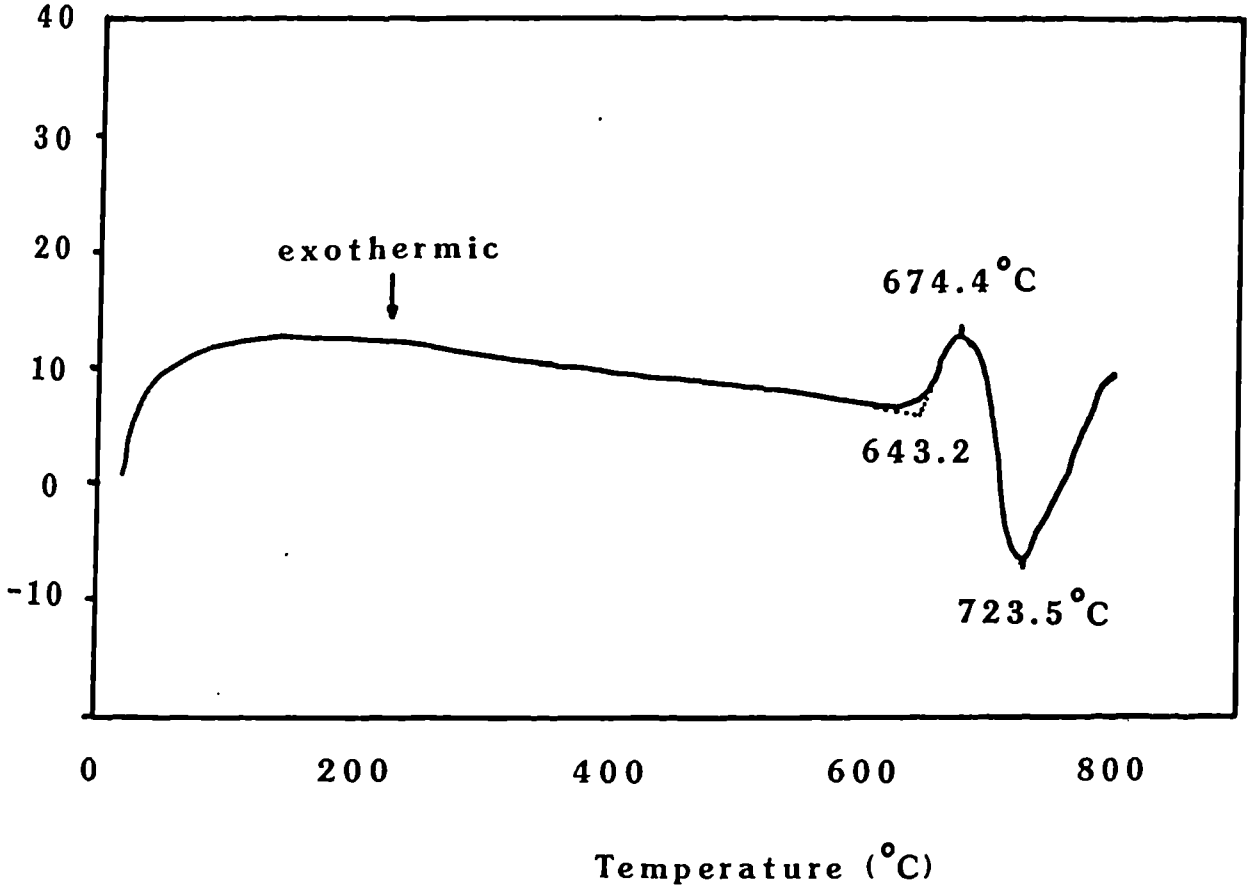
40
30
20
10
0
-10
exothermic
674.4°C
643.2
723.5°C
0
200
400
600
800
Temperature (°C)

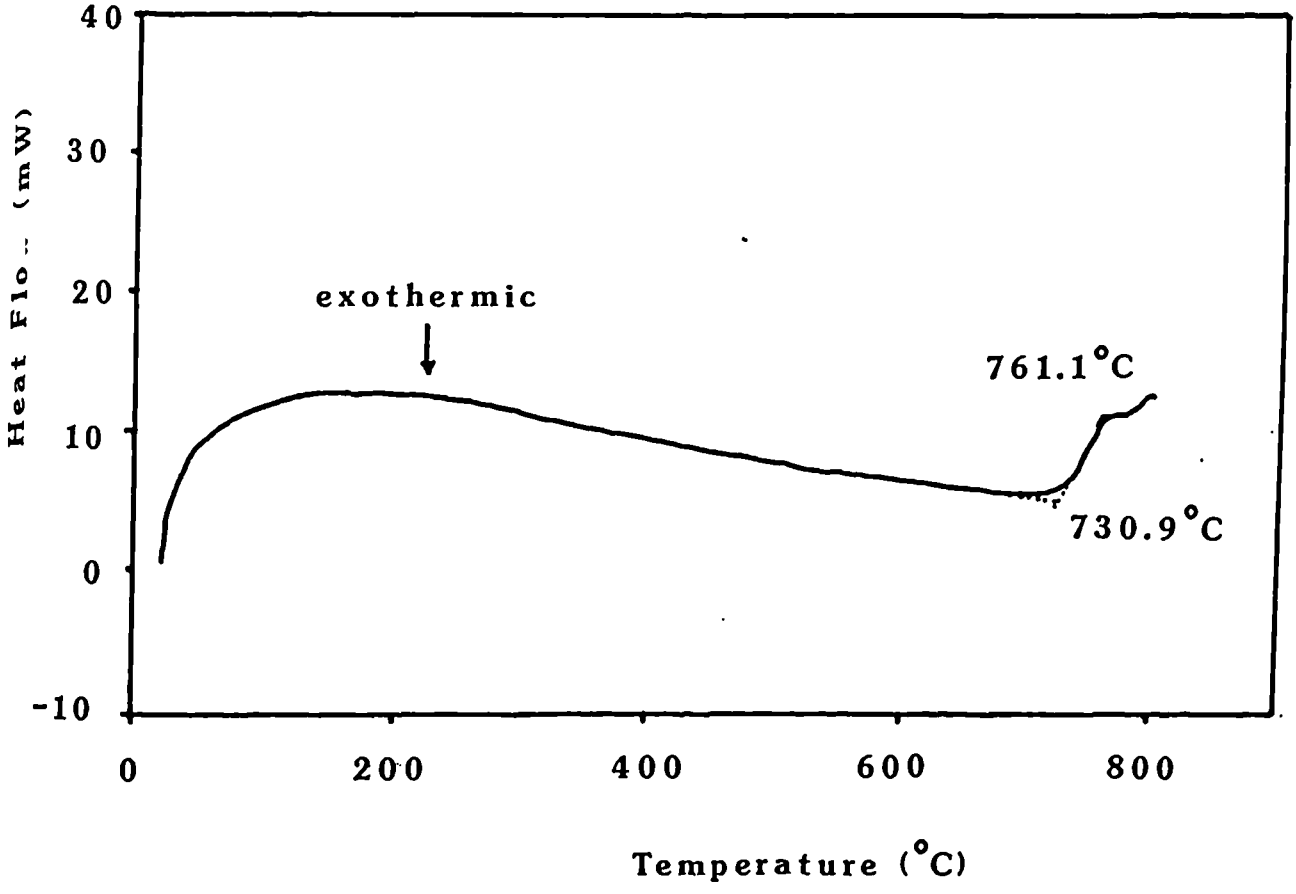
Heat Flo.. (mW)
40
30
20
10
0
-10
exothermic
761.1°C
730.9°C
0
200
400
600
800
Temperature (°C)

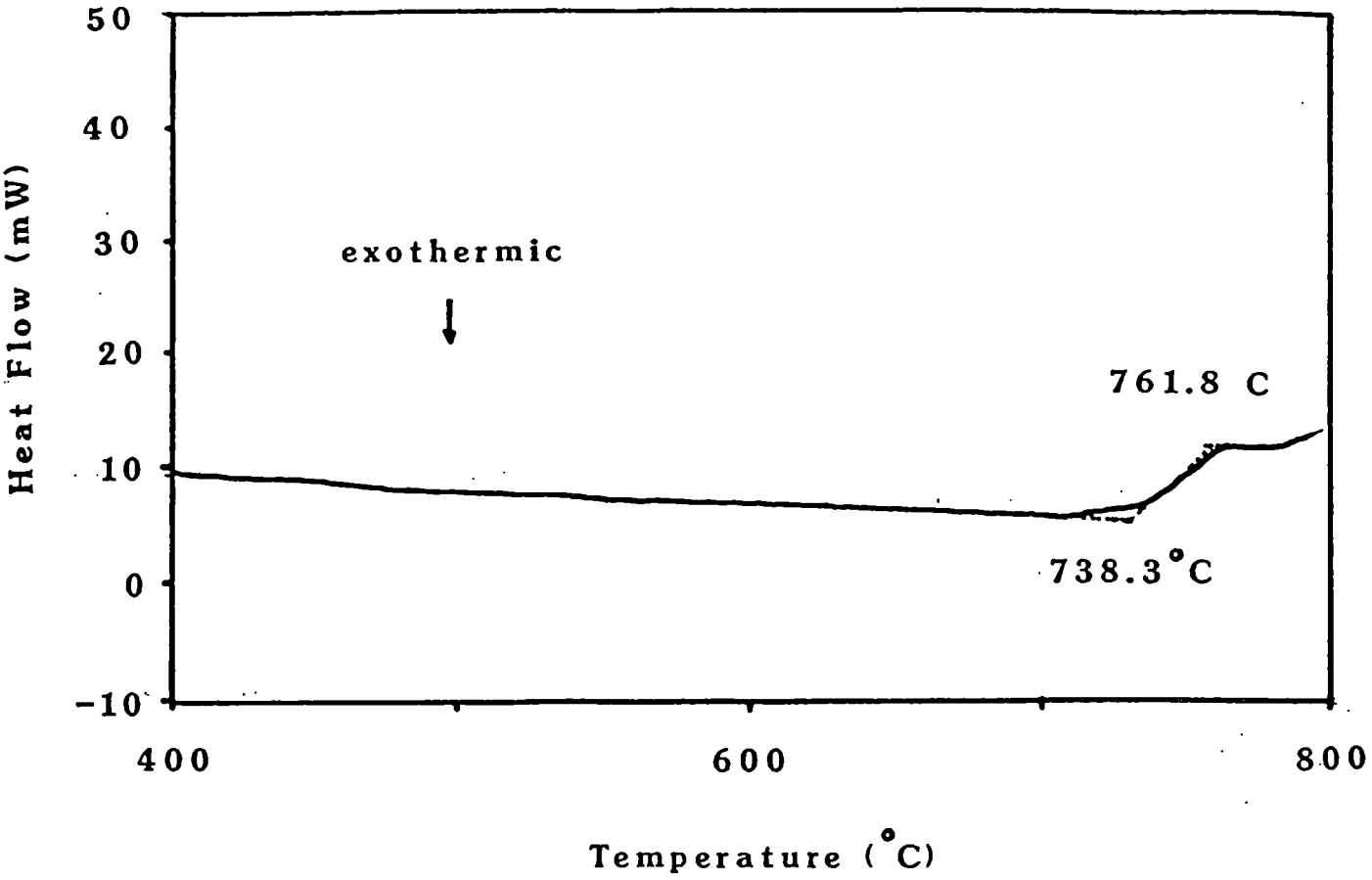
50
40
30
20
10
0
-10
Heat Flow (mW)
exothermic
761.8 C
738.3°C
400
600
800
Temperature (°C)

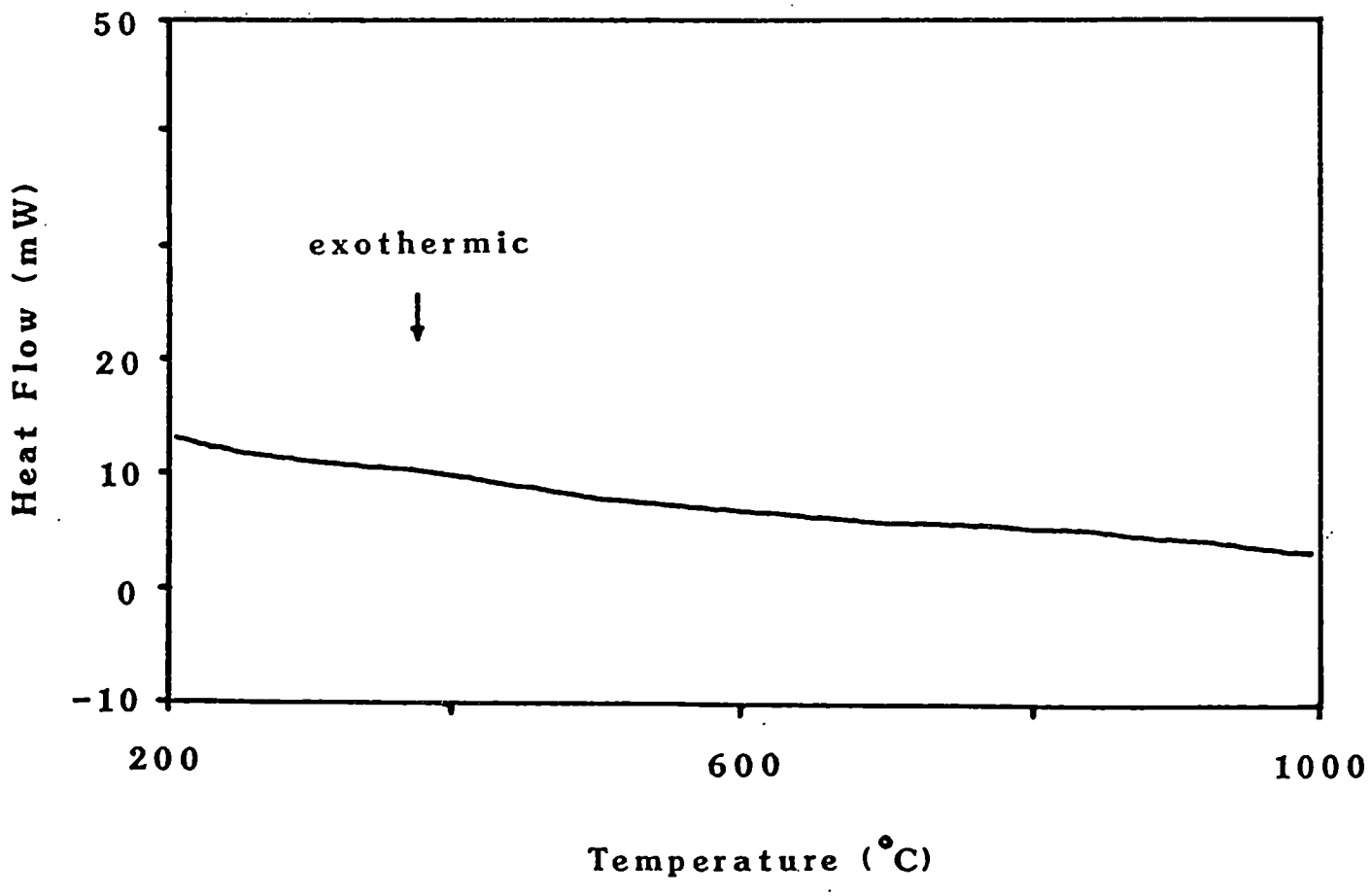
50
20
10
0
-10
Heat Flow (mW)
exothermic
200
600
1000
Temperature (°C)

Figure 39 - Calibration Line for Hydropyrolysis

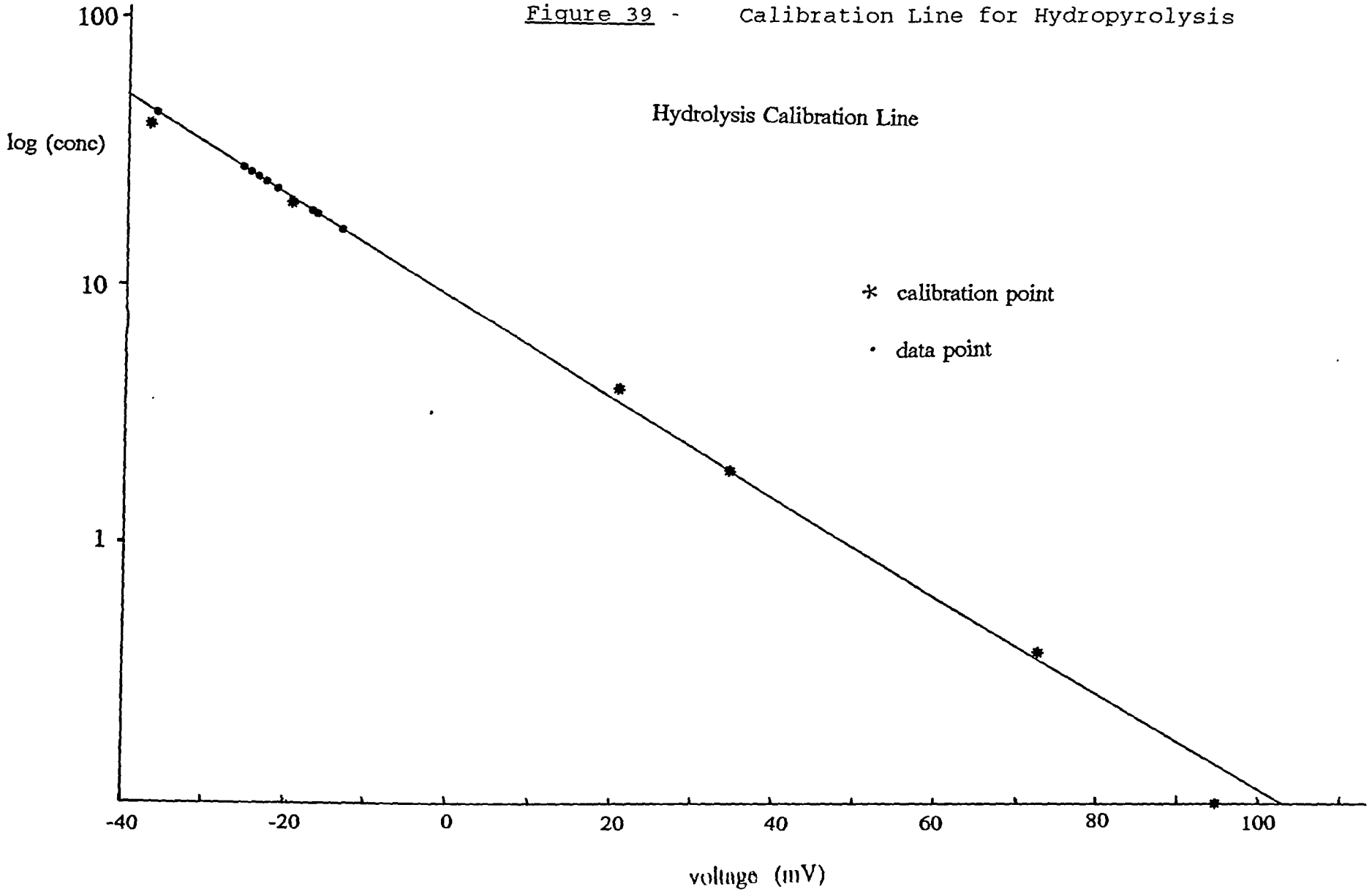

Figure 40 - DTG of G338 and G280

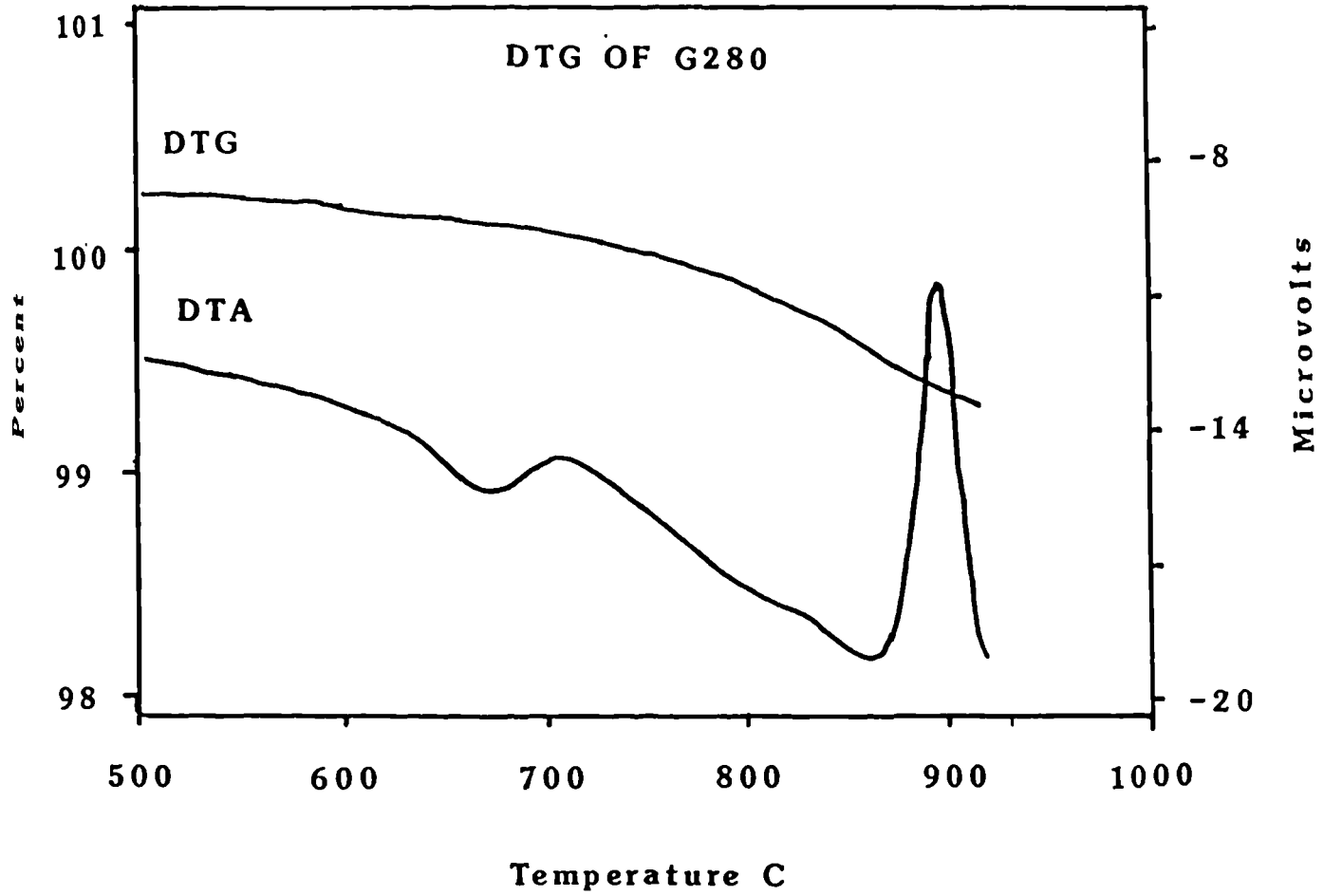

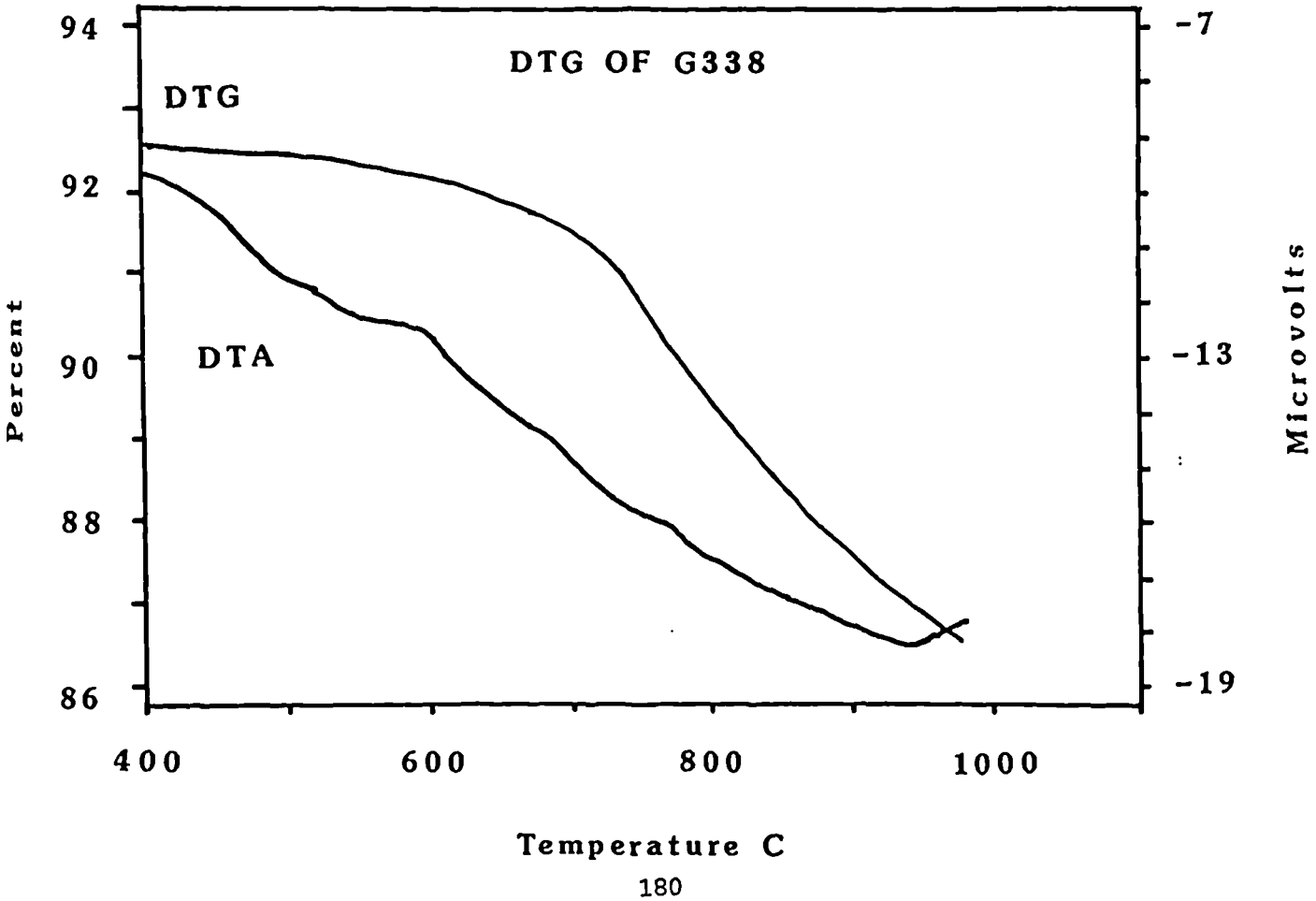

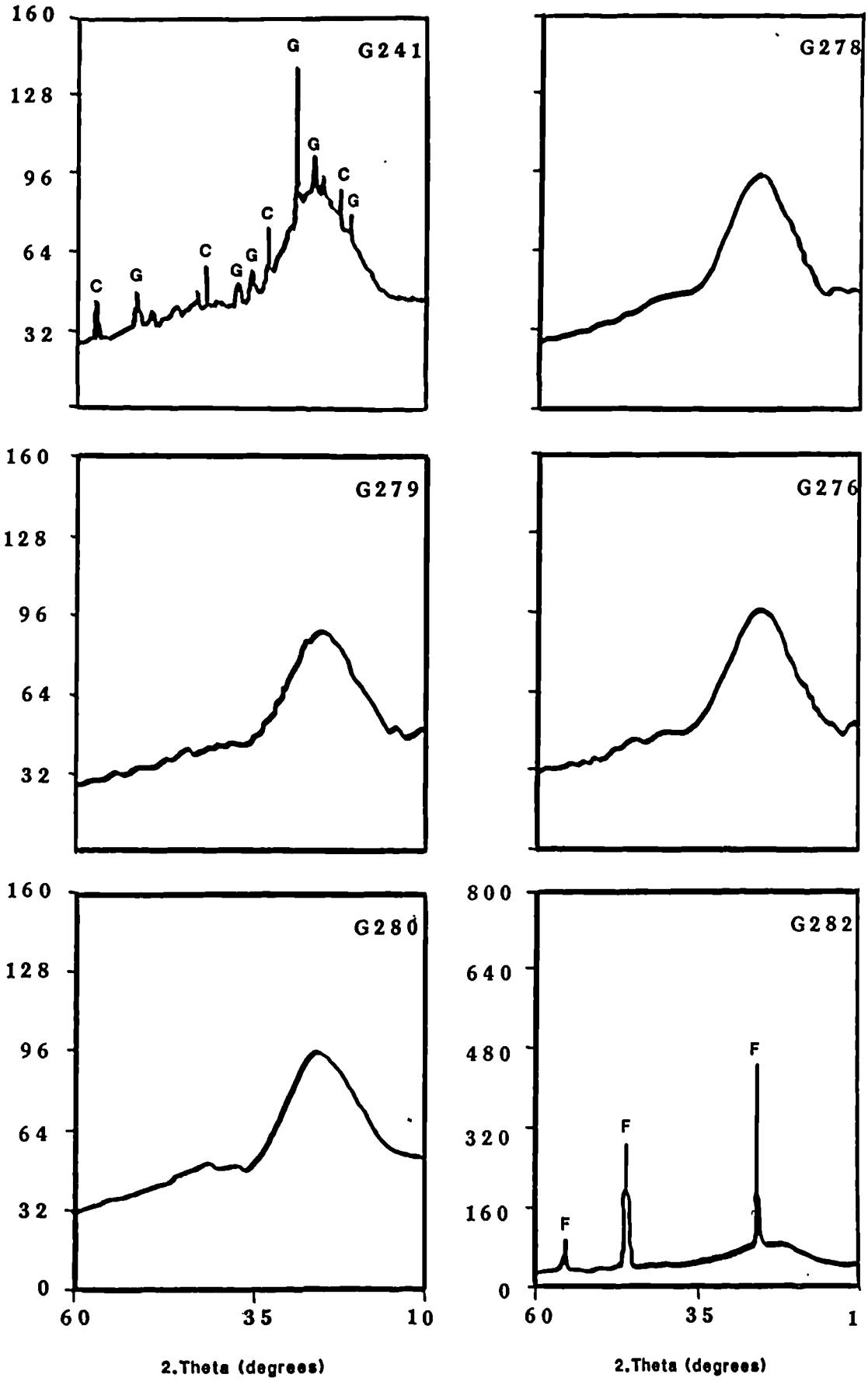

Figure 41 - XRD of Glasses in G280 Series

Figure 42 - DTA of Glasses in G280 Series

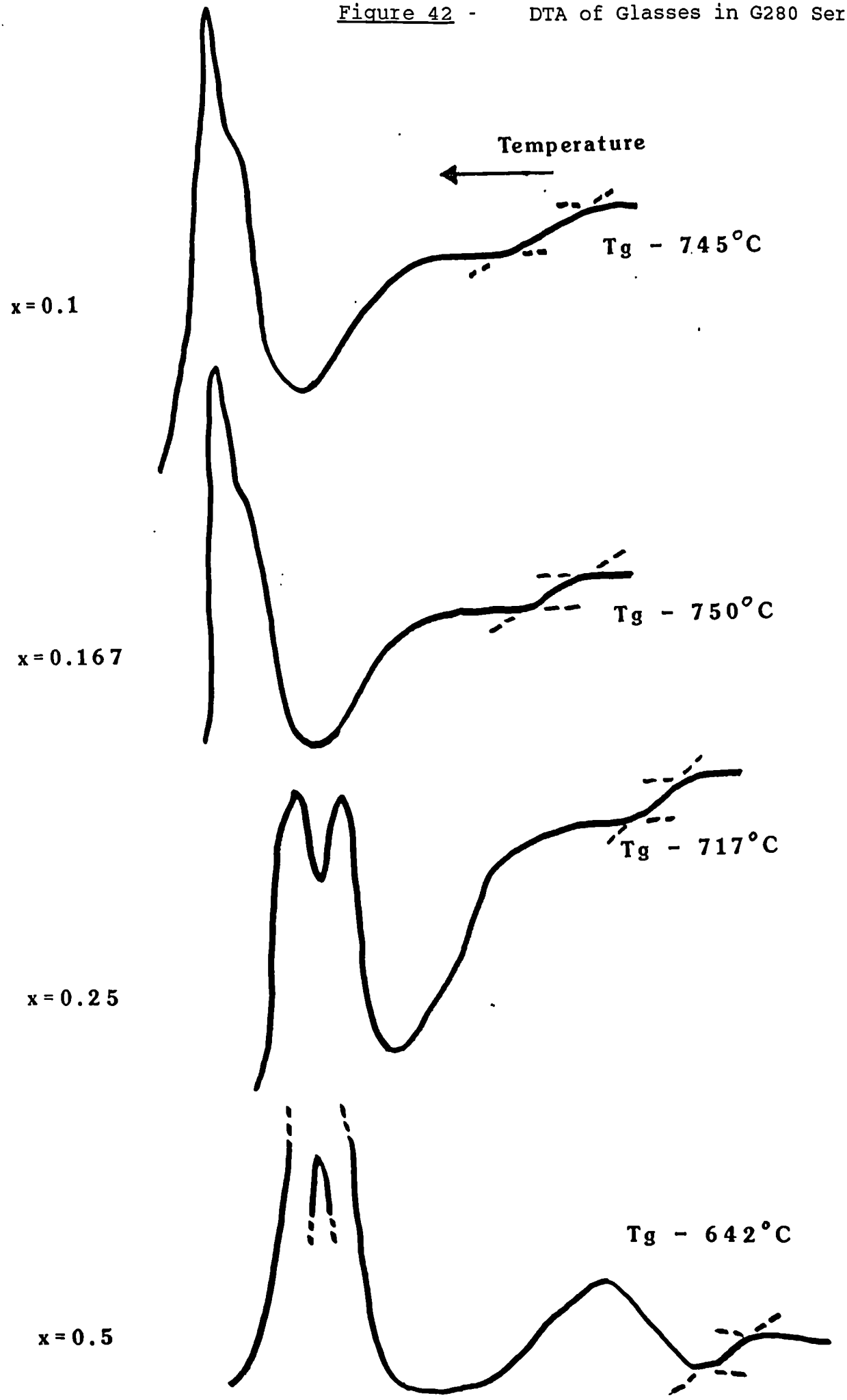

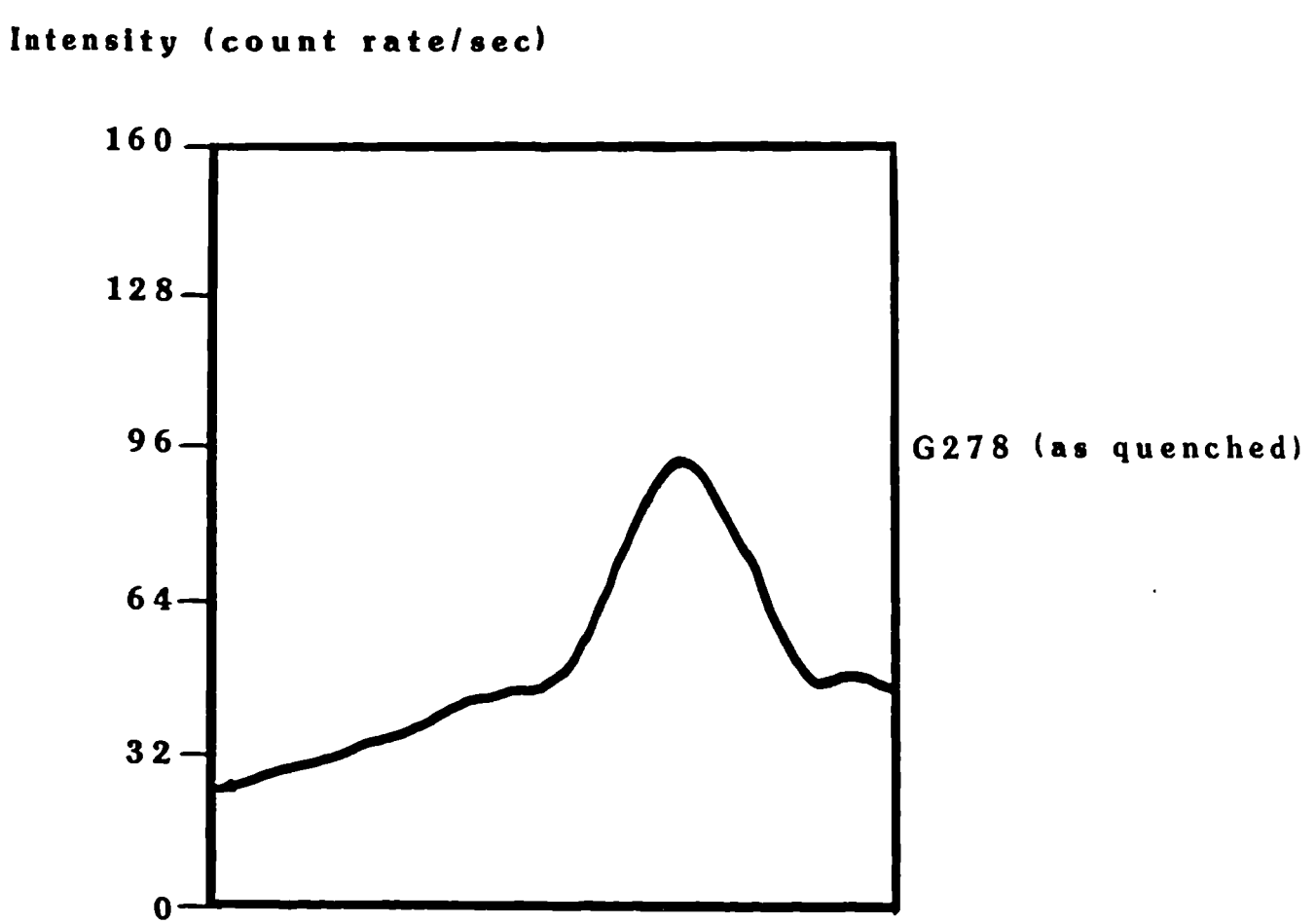

Figure 43 - XRD of Heat Treated G278

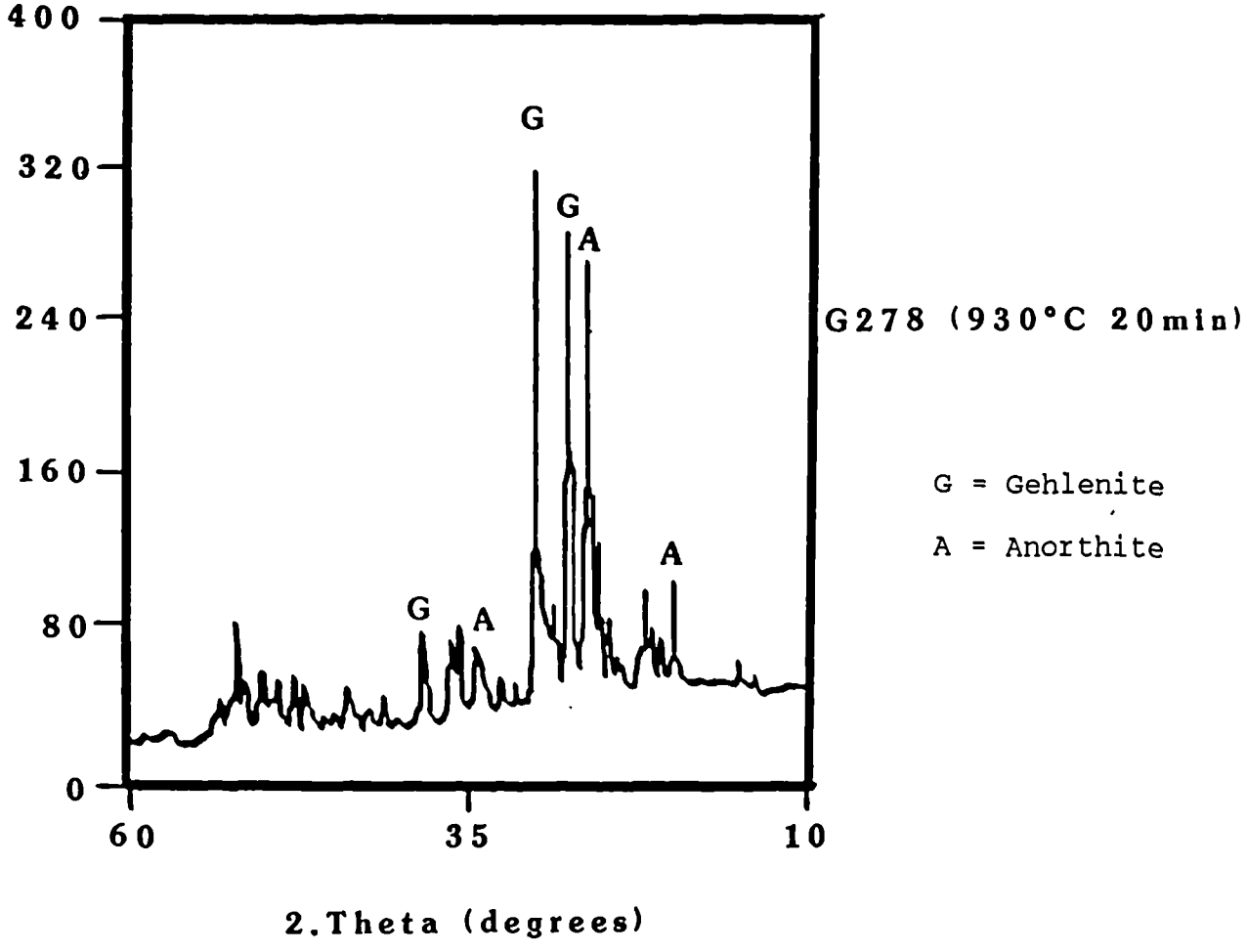

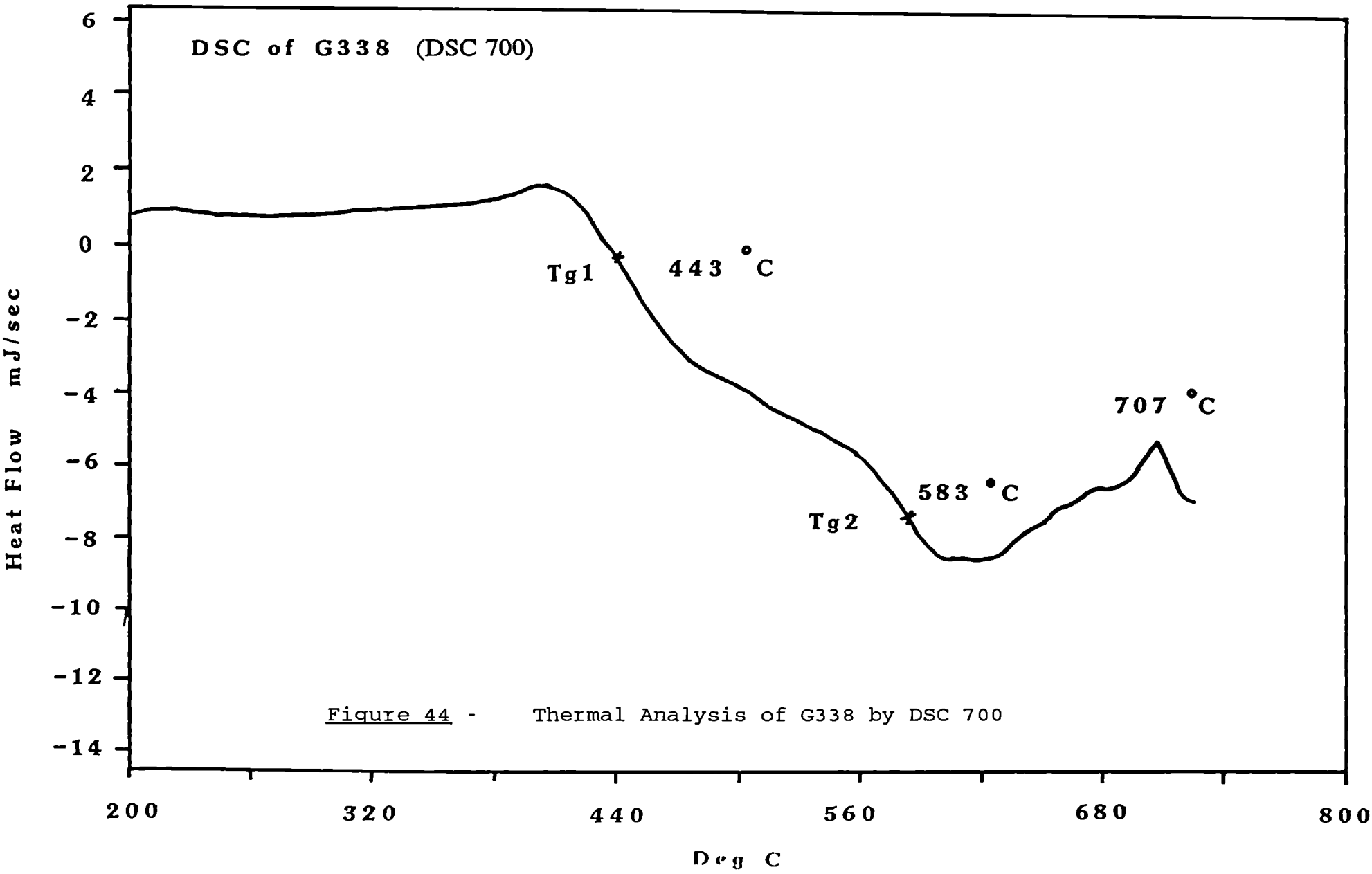

Figure 44 - Thermal Analysis of G338 by DSC 700

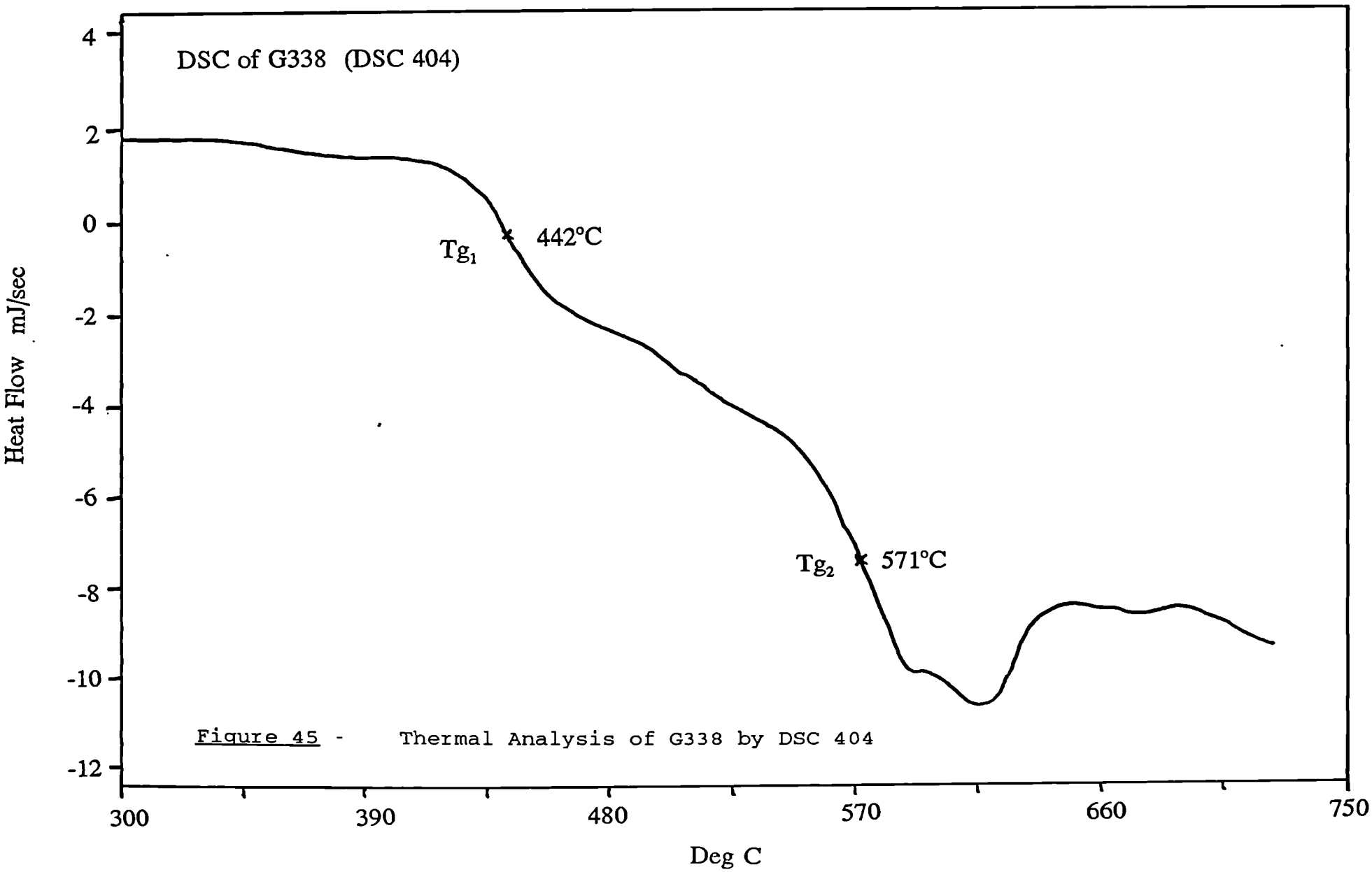

Figure 45 - Thermal Analysis of G338 by DSC 404

Figure 46 - XRD of three batches of G338

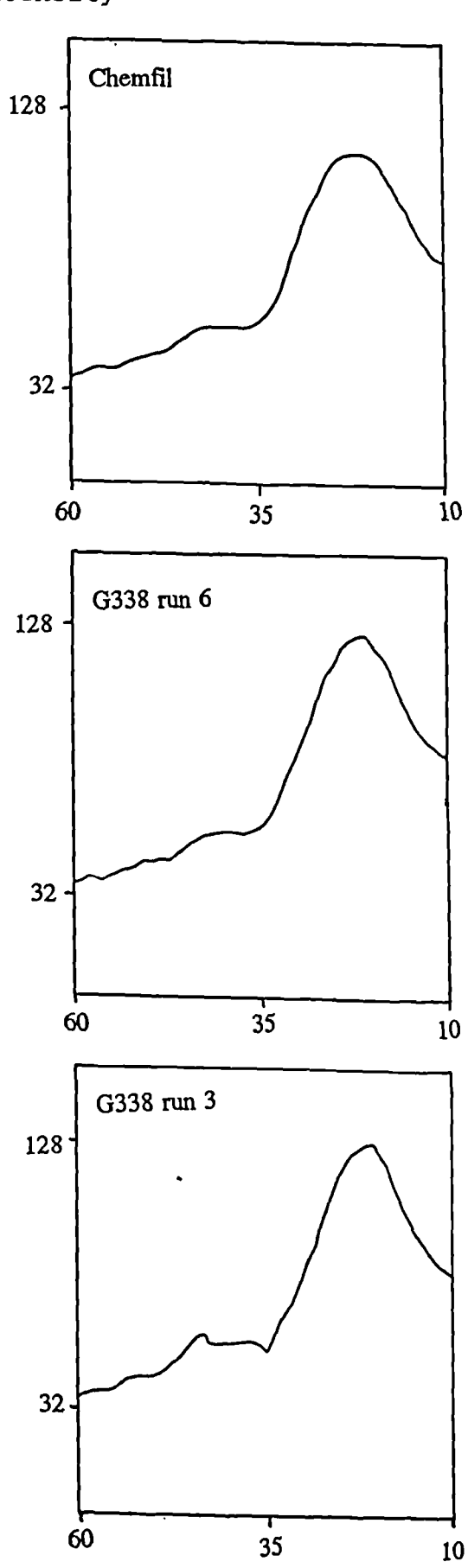

Figure 47 - XRD of Heat Treated G338

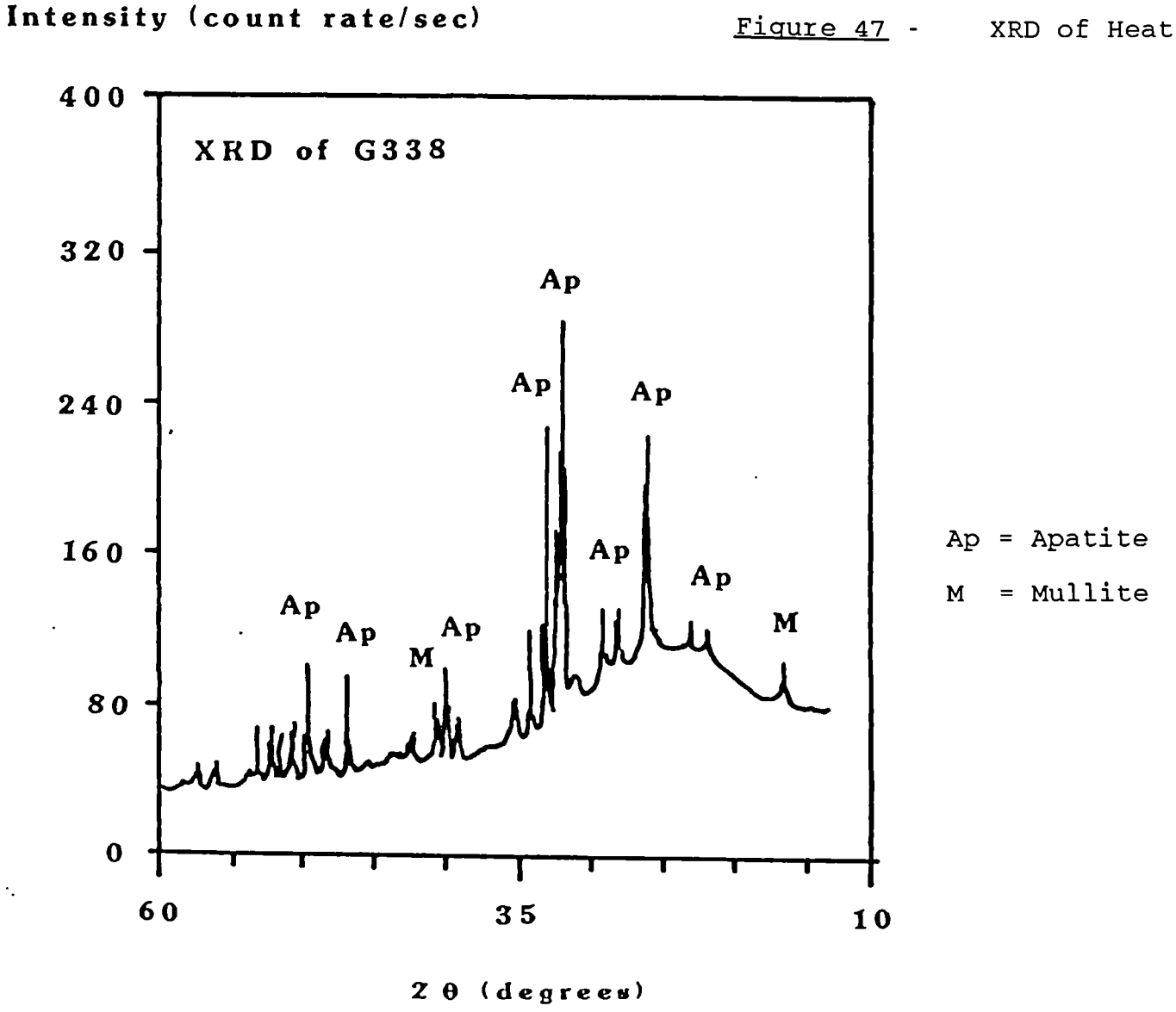

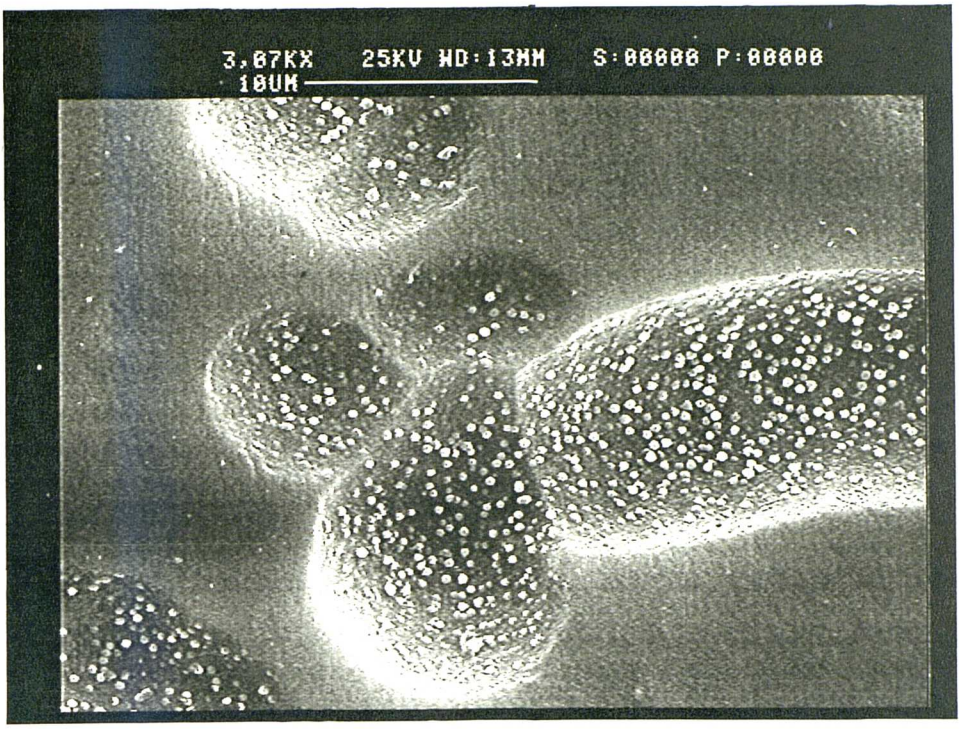

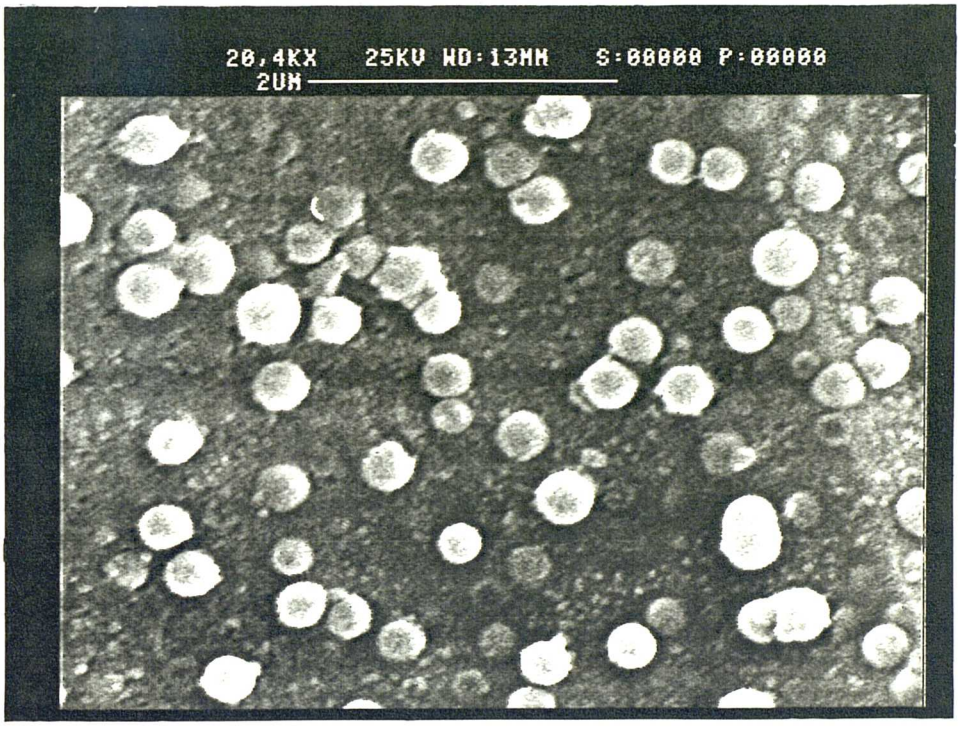

Figure 48 - SEM of G338

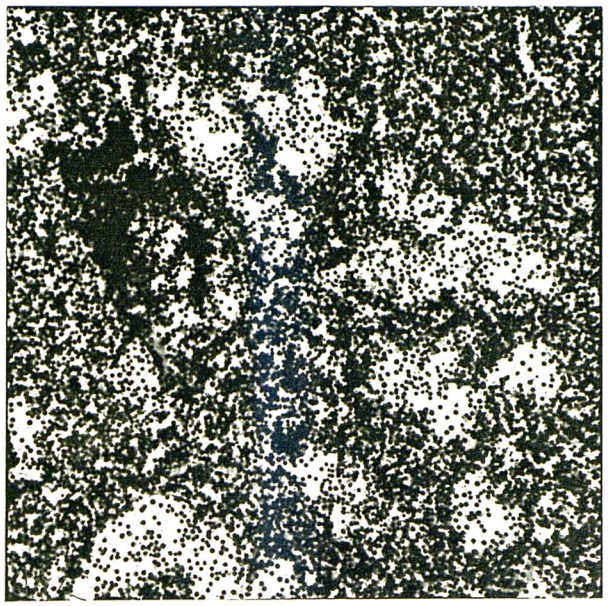

1 cm = 6.3 μm

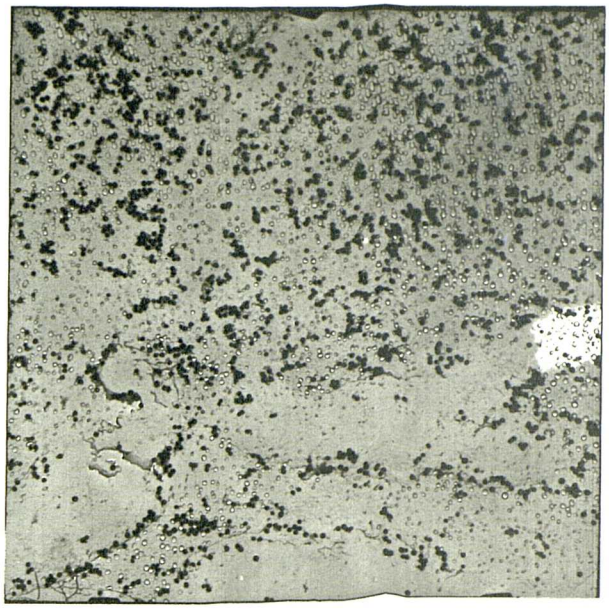

1 cm = 6.3 μm

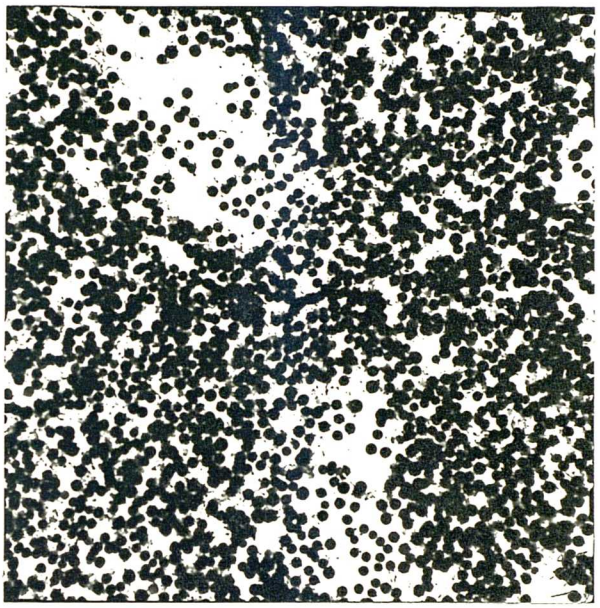

1 cm = 2.5 μm

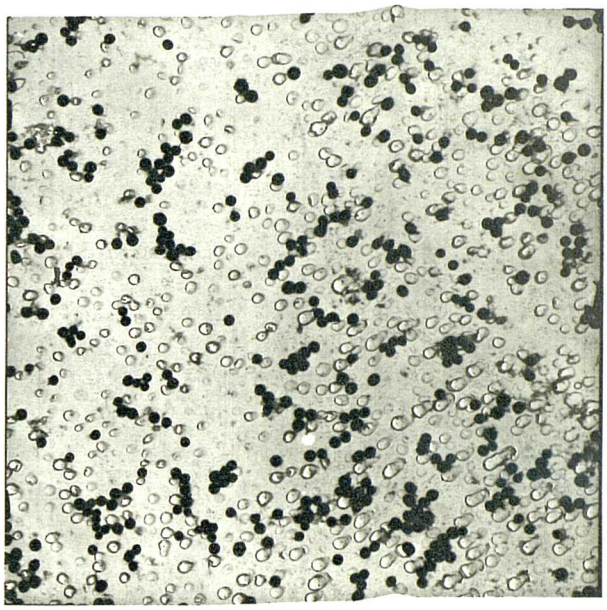

1 cm = 2.5 μm

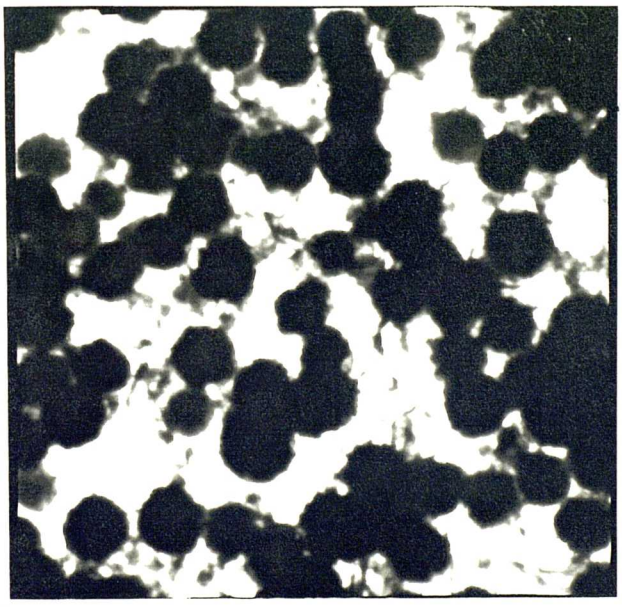

1 cm = 0.4 μm

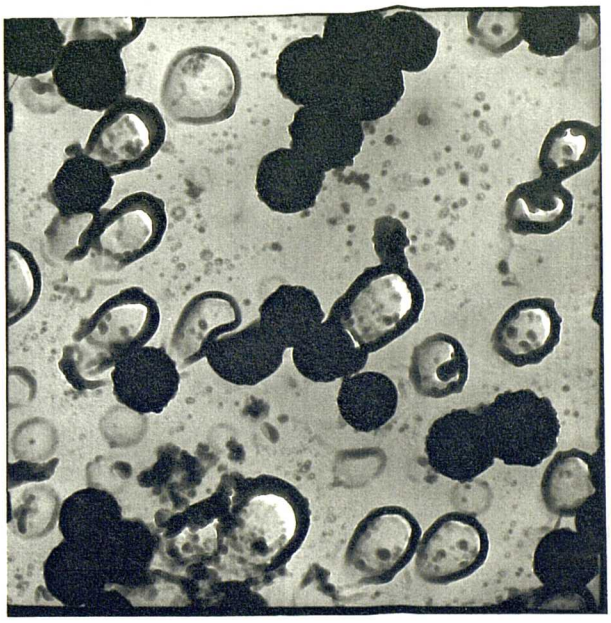

1 cm = 0.4 μm

Figure 49 - TEM of G338

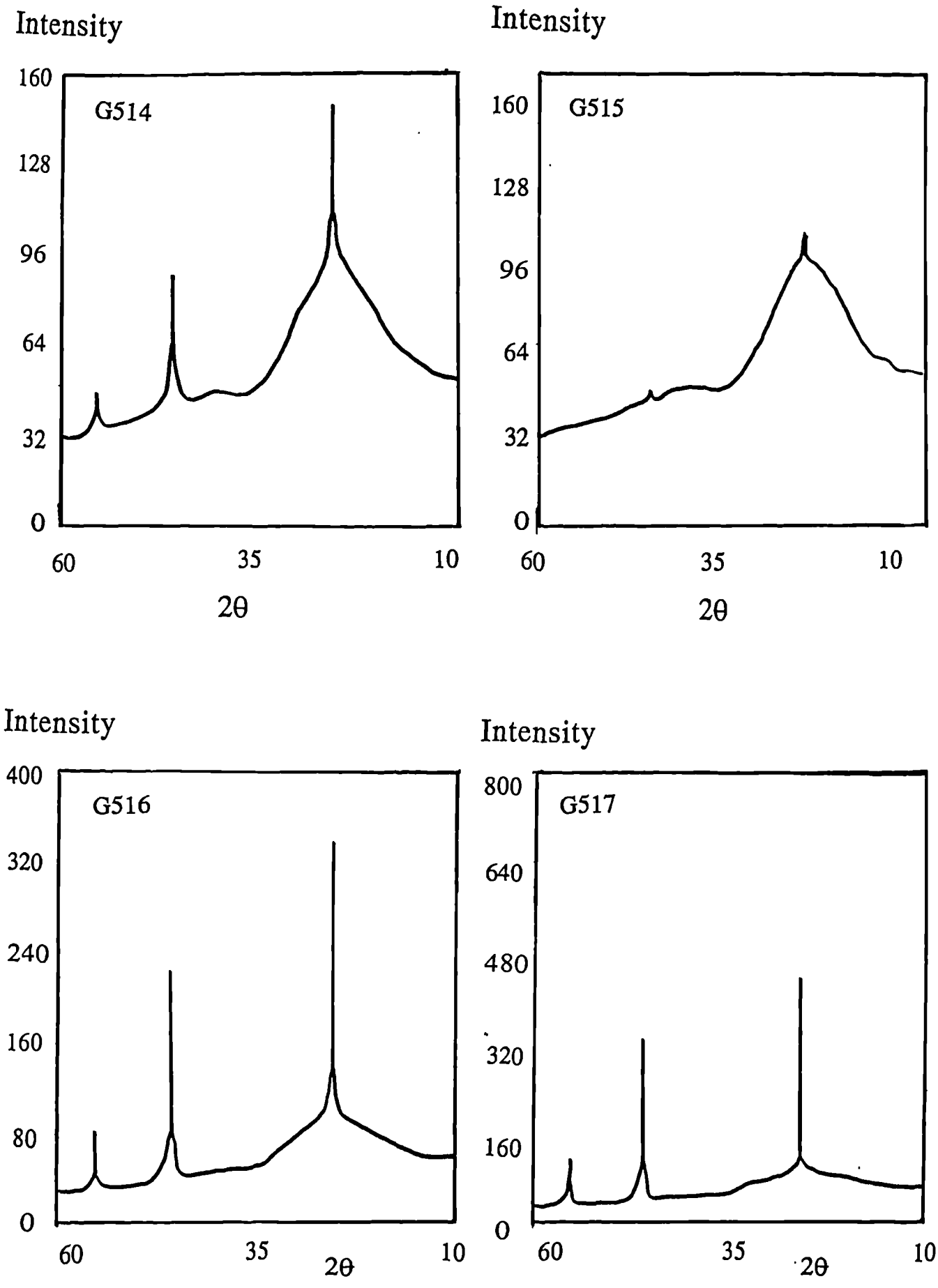

Figure 50 - XRD of Sodium Containing Glasses

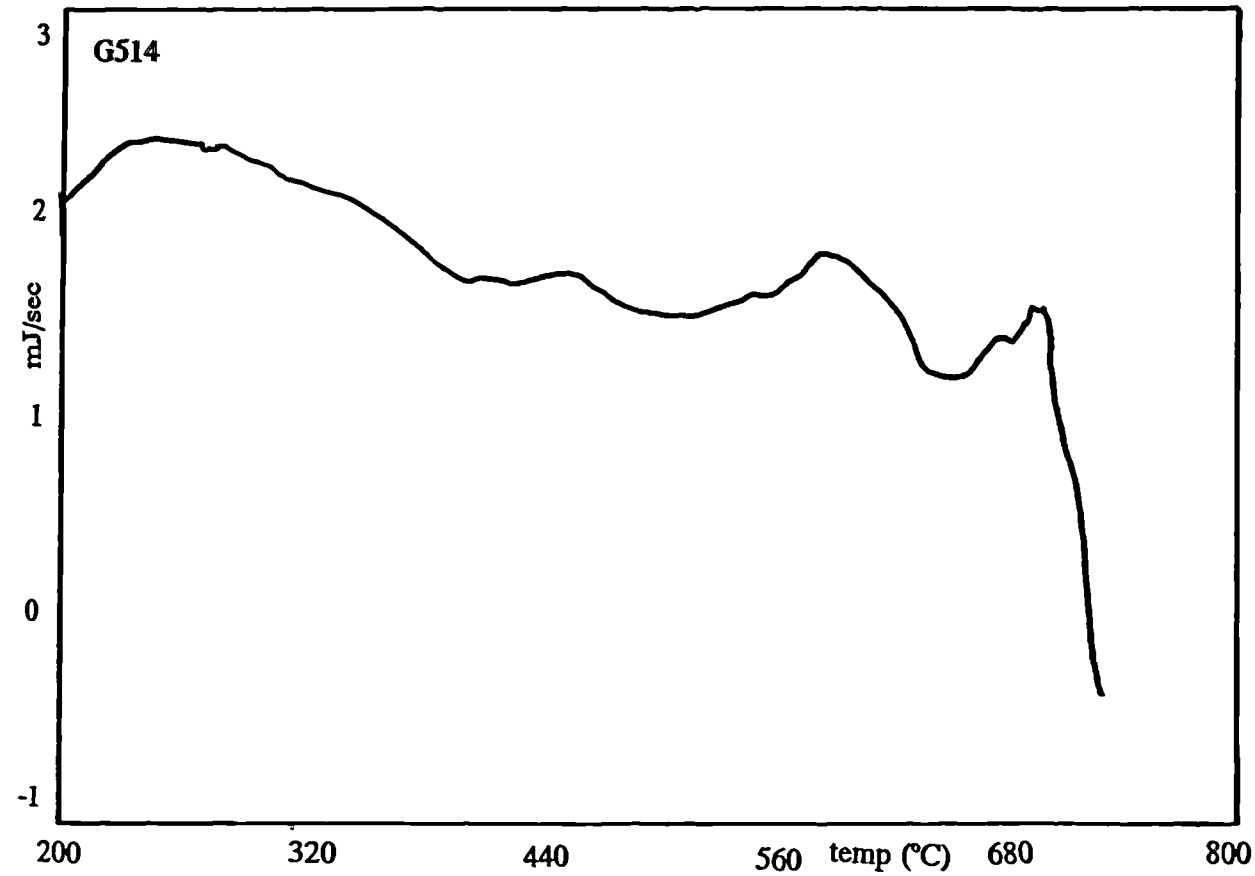

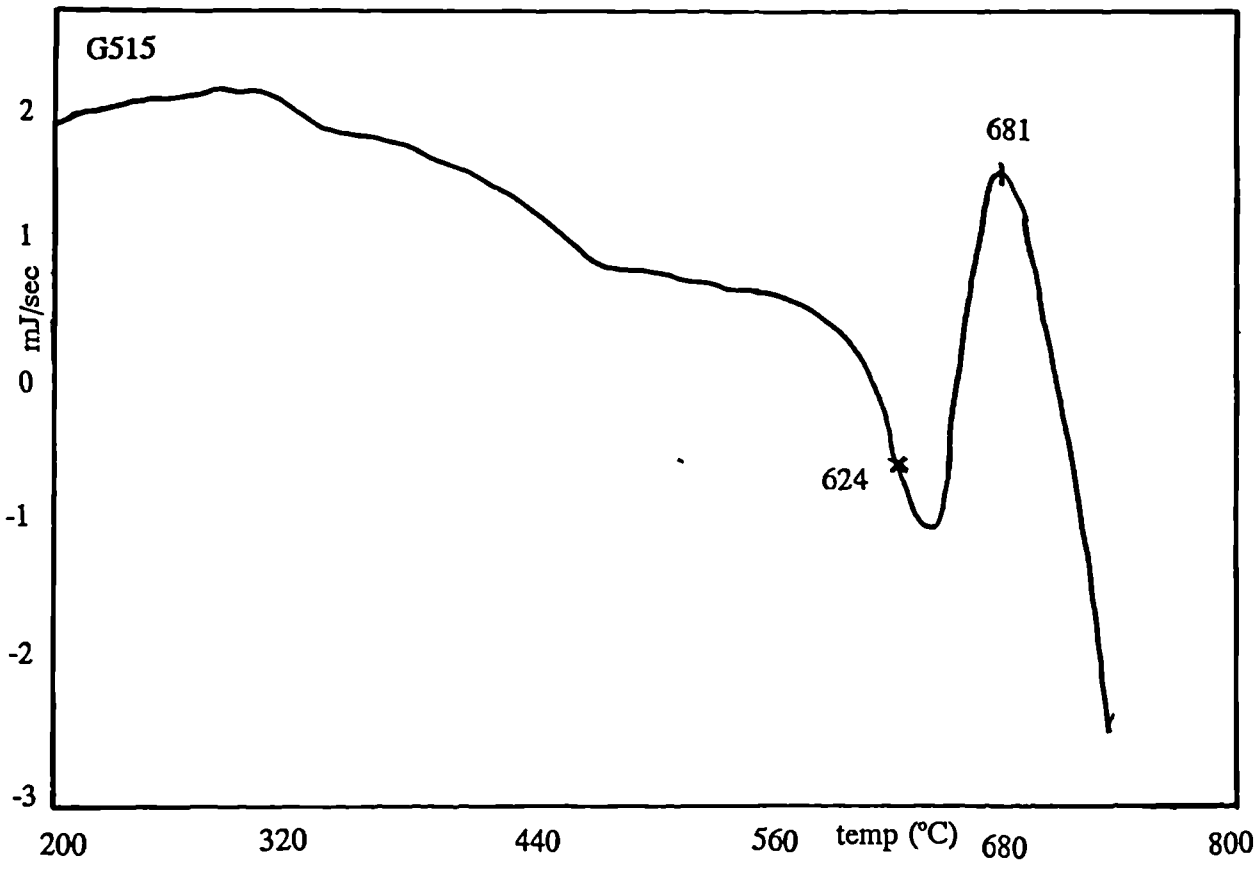

Figure 51 - DSC of Sodium Containing Glasses

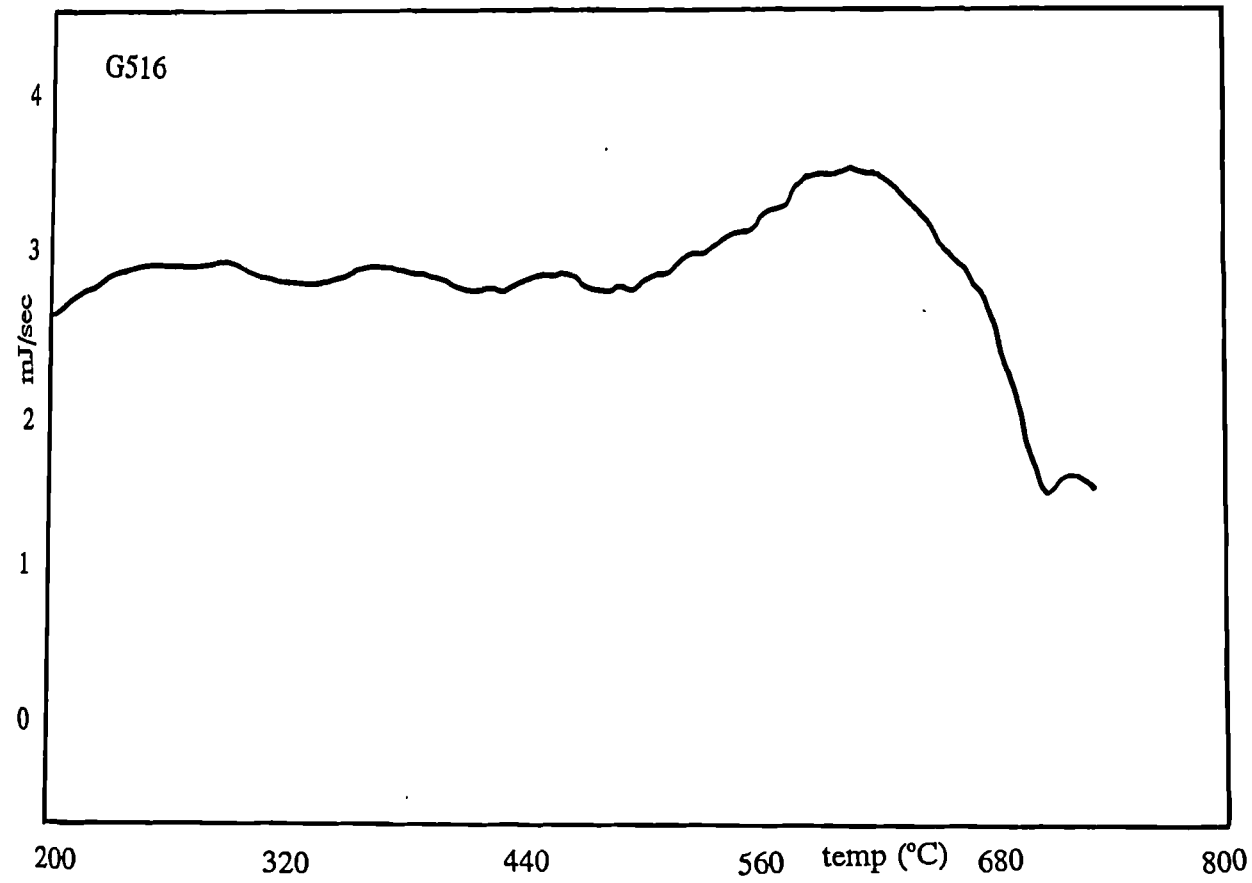
G516
4
3
2
1
0
mJ/sec
200
320
440
560
temp (°C)
680
800

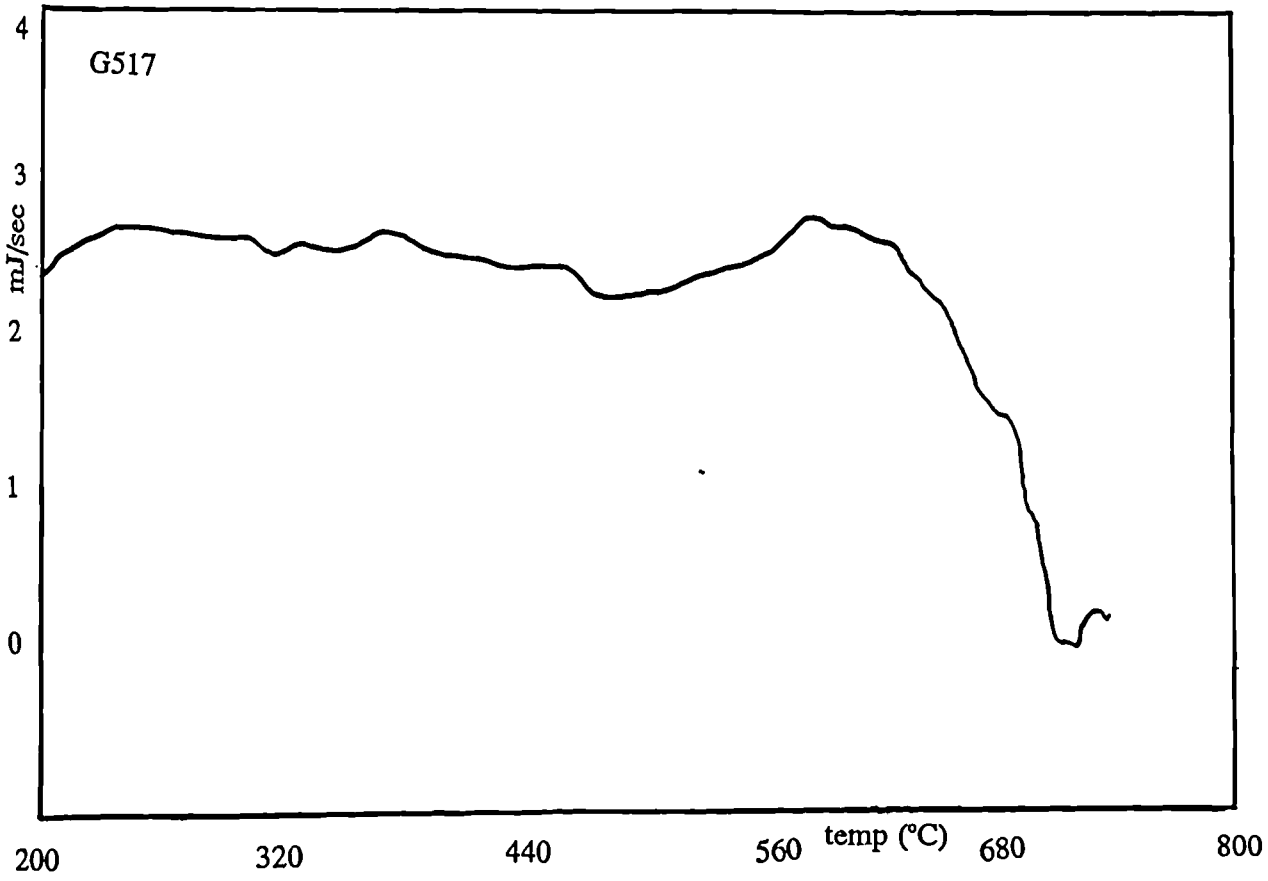
G517
4
3
2
1
0
mJ/sec
200
320
440
560
temp (°C)
680
800

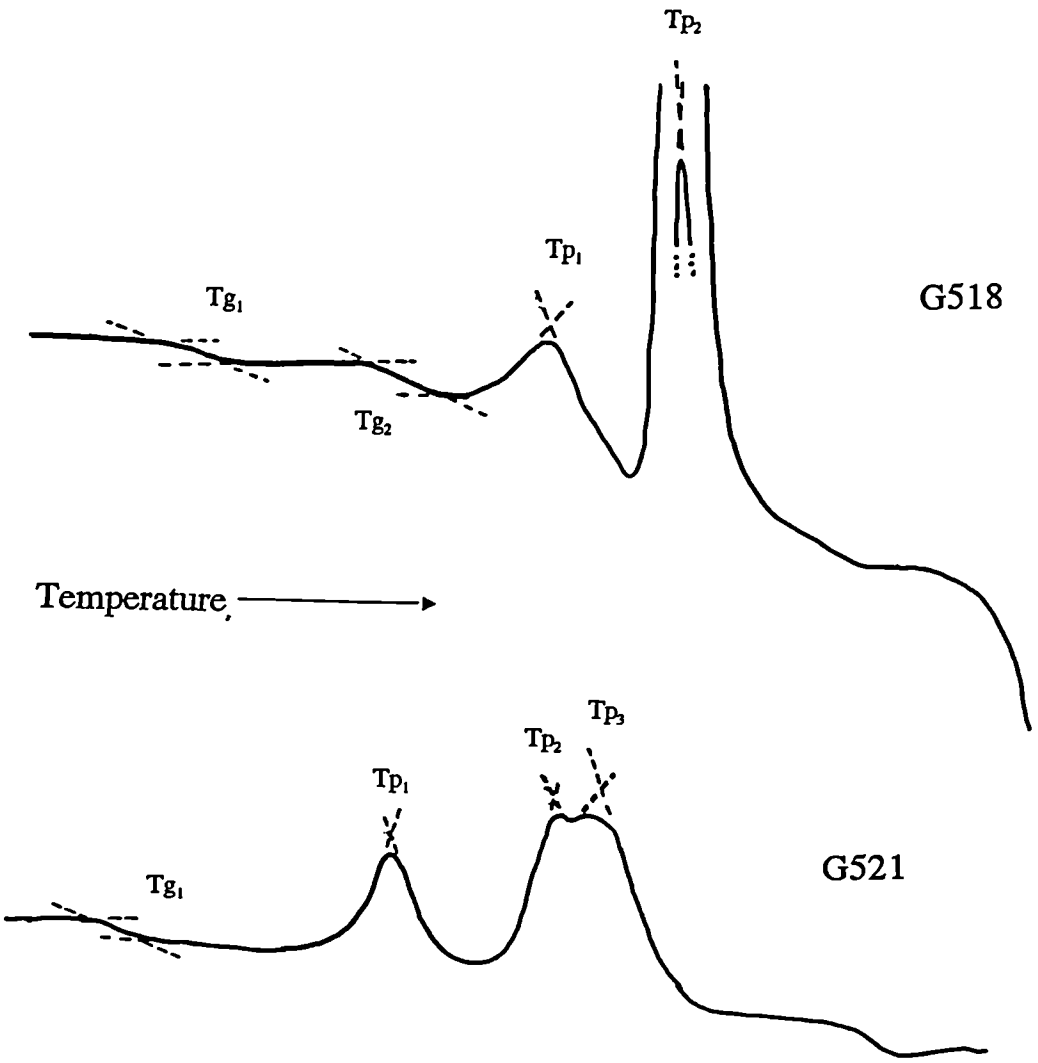

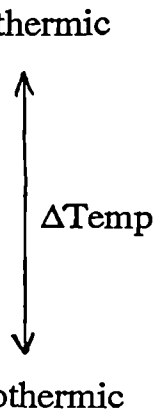

Glass	Tg_1	Tg_2	Tp_1	Tp_2	Tp_3
G518	631	713	772	834	
G521	631		718	782	801

Figure 52 - DTA of Phosphate Containing Glasses

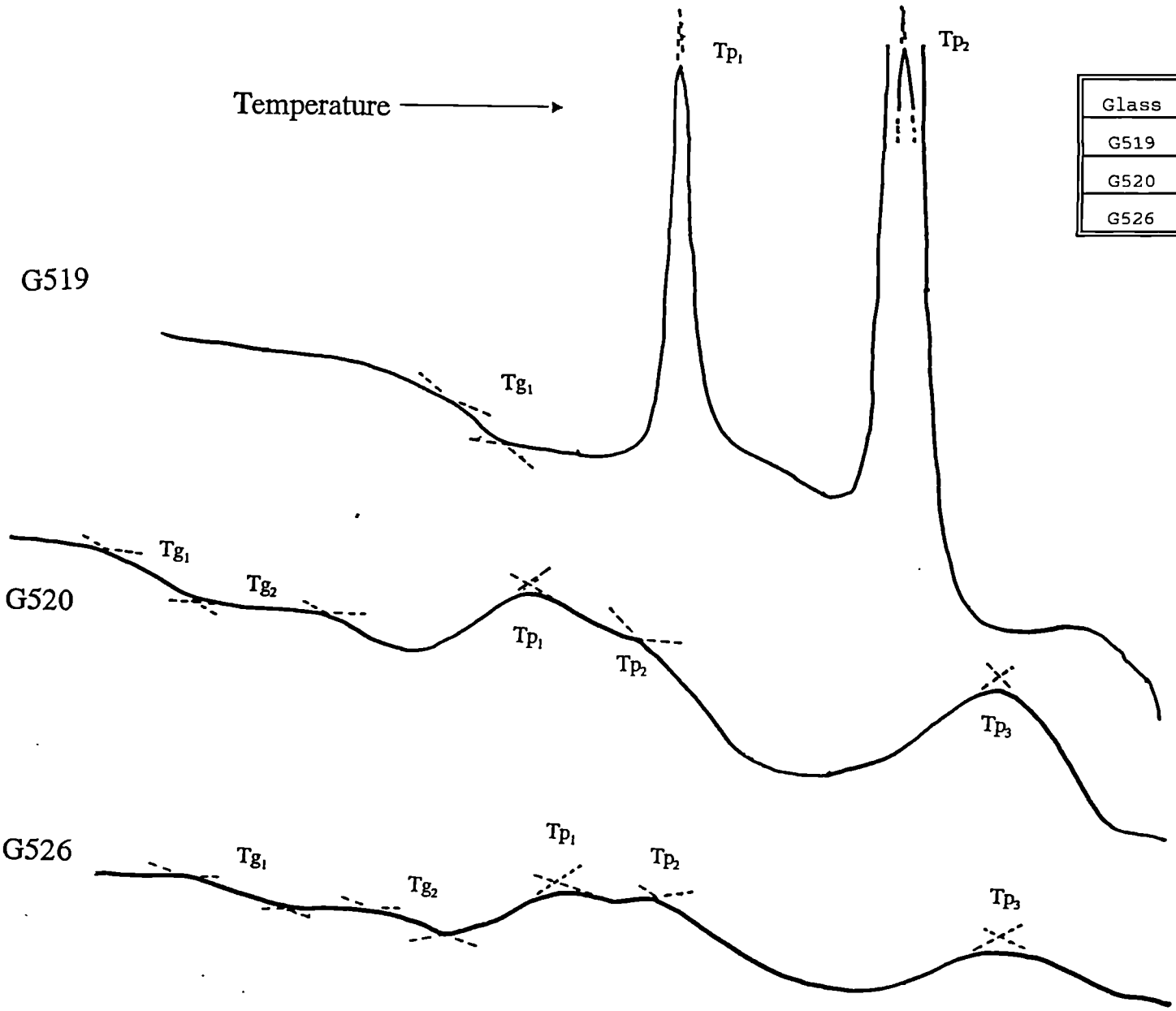

Glass	Tg_1	Tg_2	Tp_1	Tp_2	Tp_3
G519	621		723	814	
G520	662	758	826	878	1037
G526	669	751	818	860	1015

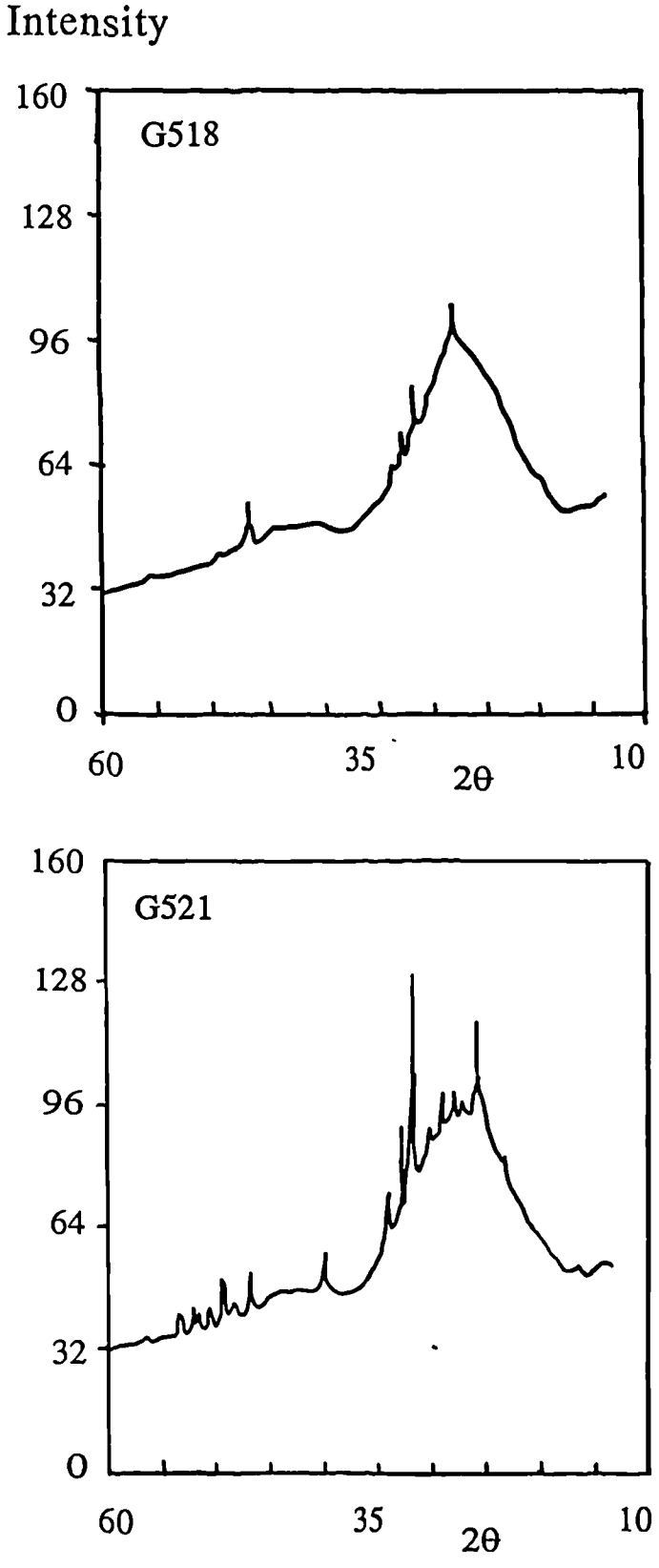

Figure 53 - XRD of Phosphate Containing Glasses

Intensity

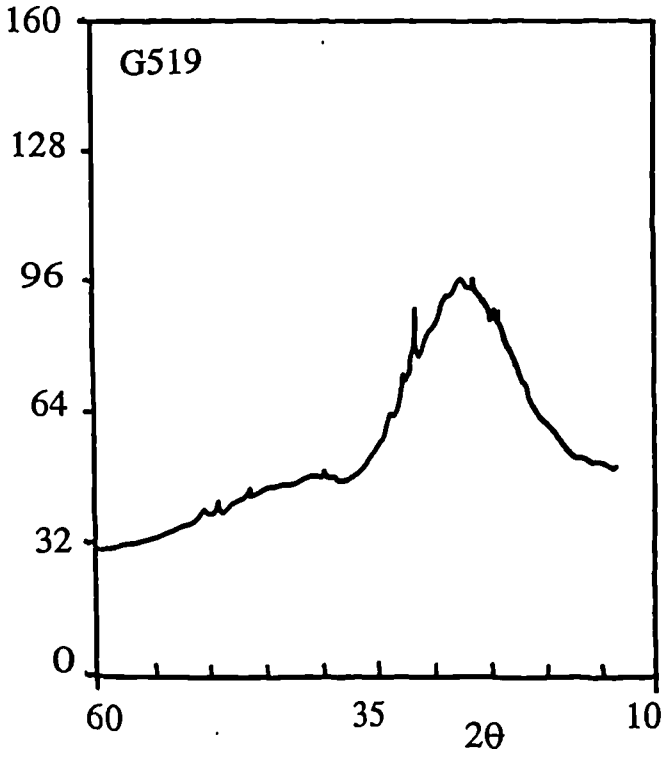
G519
160
128
96
64
32
0
60
35
10
2θ

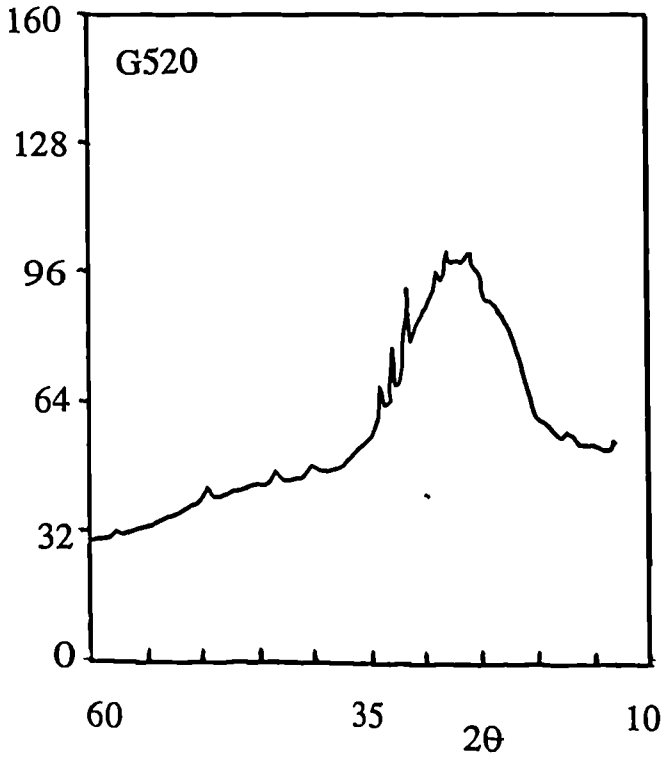
G520
160
128
96
64
32
0
60
35
10
2θ

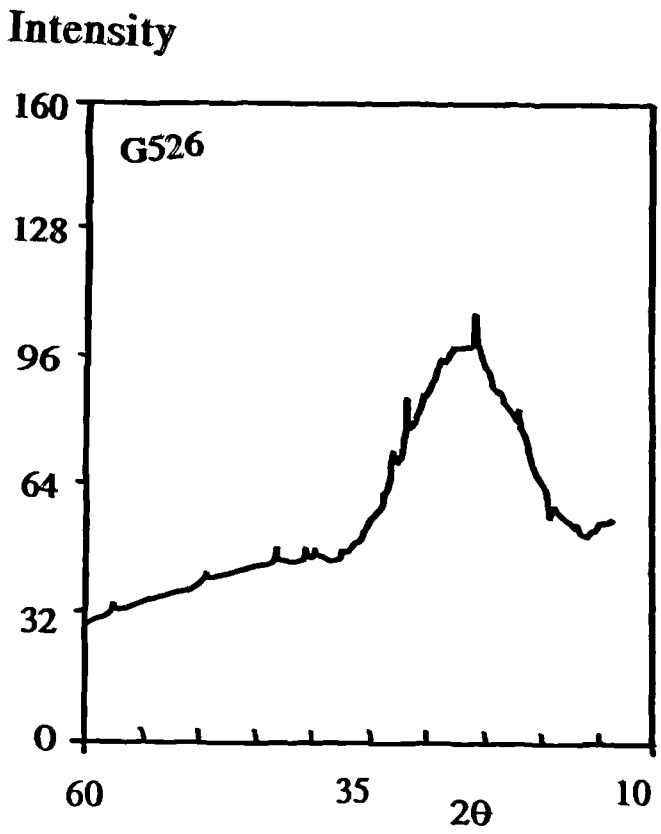
Intensity
160
G526
128
96
64
32
0
60
35
2θ
10

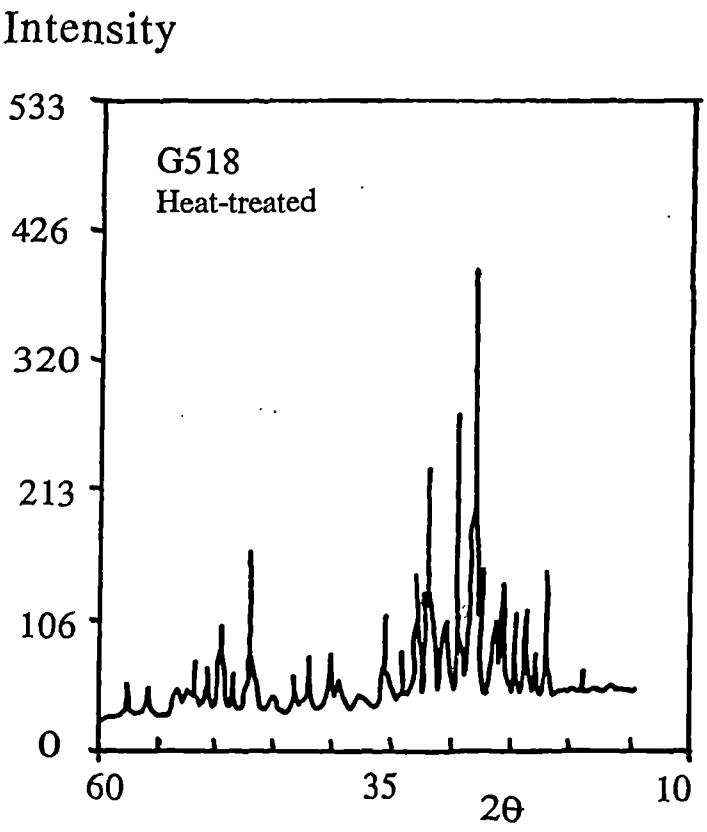

Figure 54 - XRD of Heat Treated G518

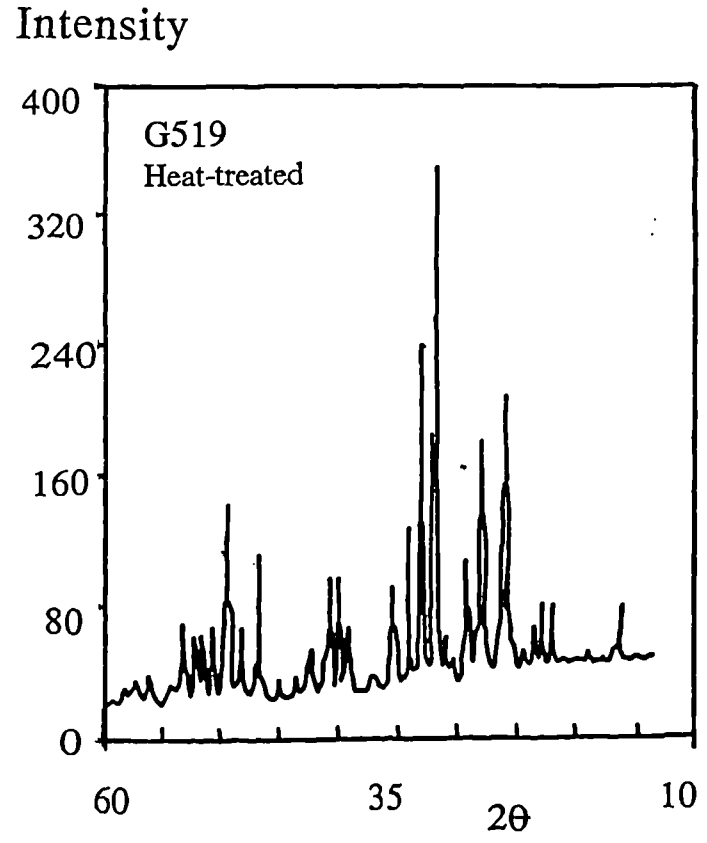

Figure 55 - XRD Of Heat Treated G519

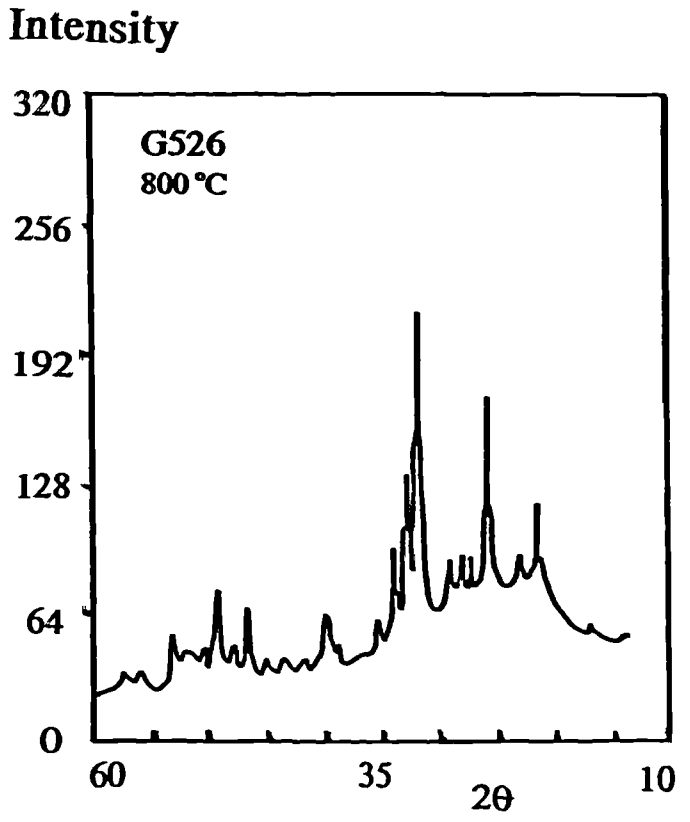

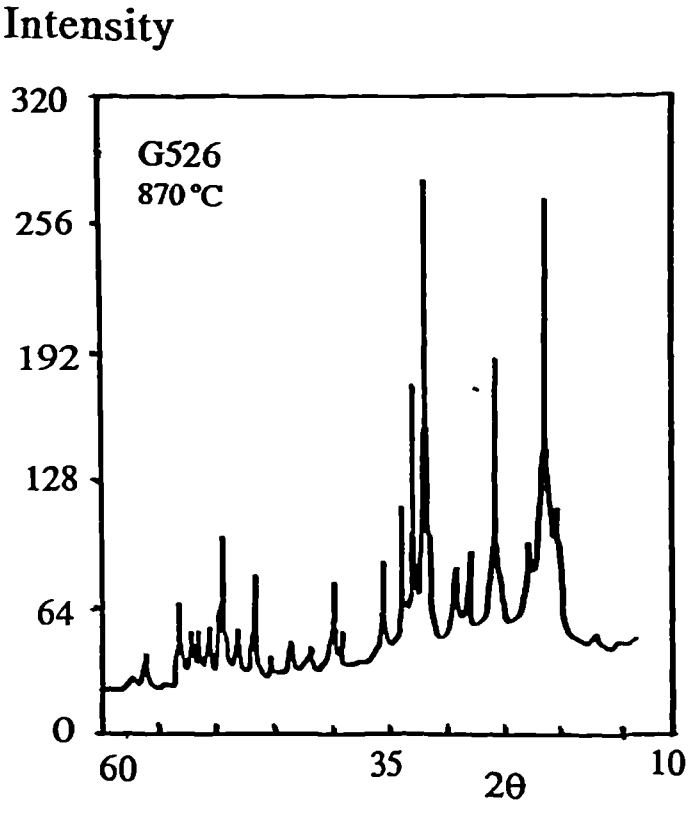

Figure 56 - XRD Of Heat Treated G526

Intensity

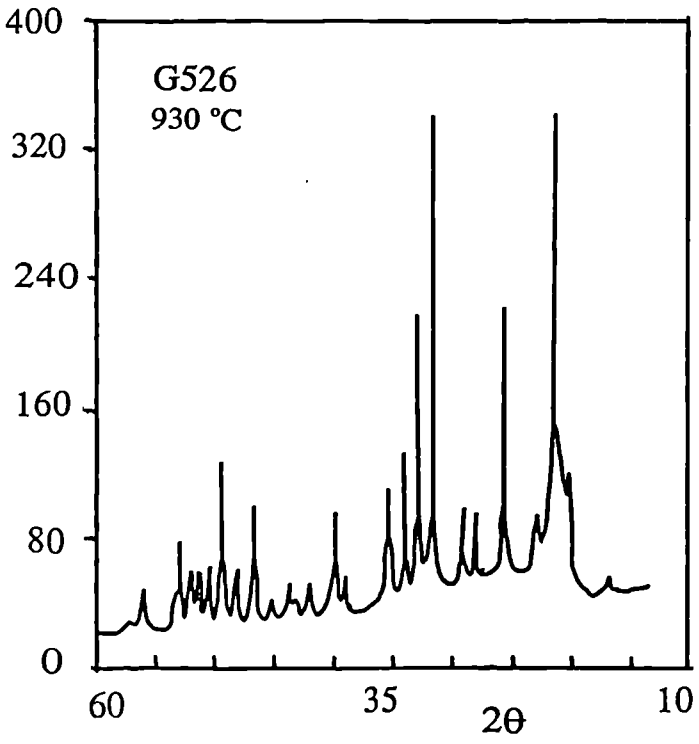

Intensity

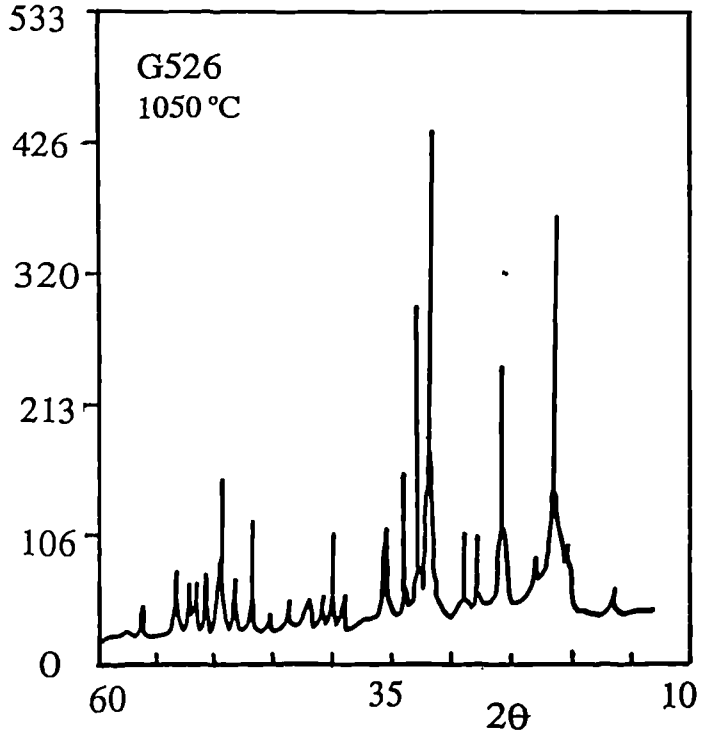

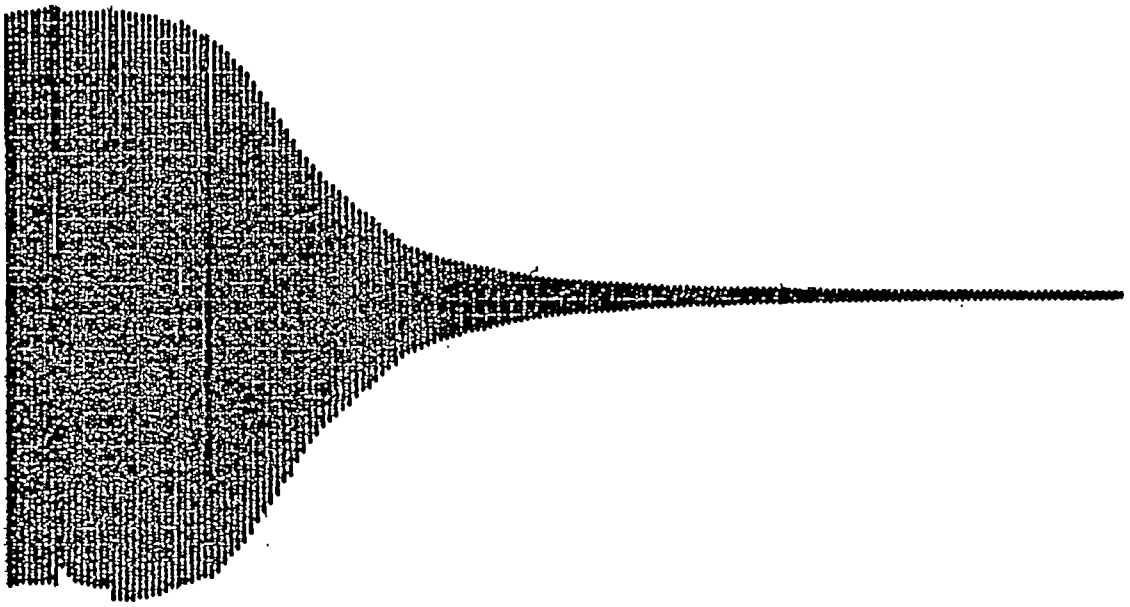

Rheogram of a G519 cement
powder : liquid ratio 3 : 1
Chart speed 10mm / min

Figure 57 - Rheogram of G519 Glass Ionomer Cement

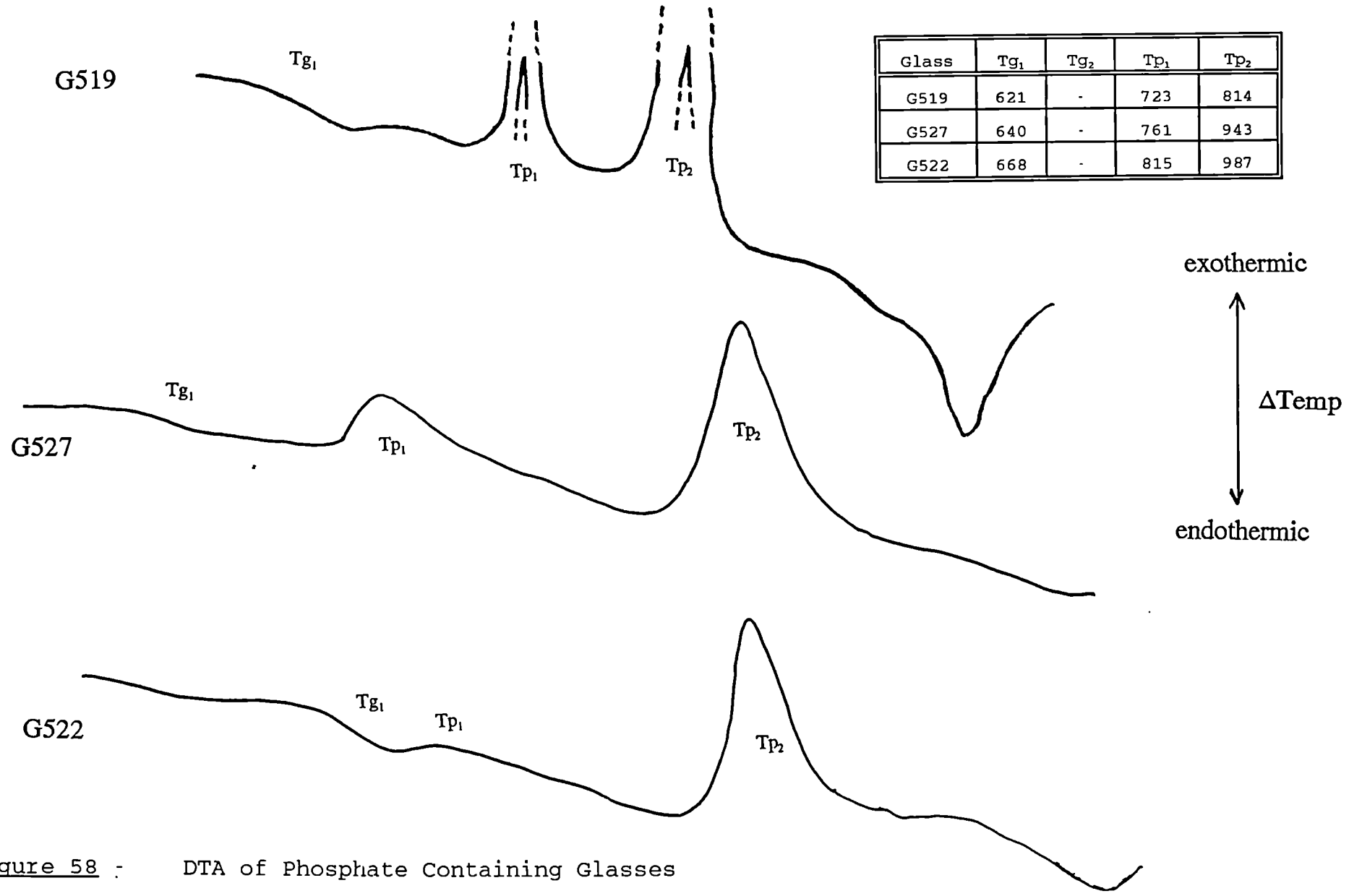

Glass	Tg_1	Tg_2	Tp_1	Tp_2
G519	621	-	723	814
G527	640	-	761	943
G522	668	-	815	987

Figure 58 - DTA of Phosphate Containing Glasses

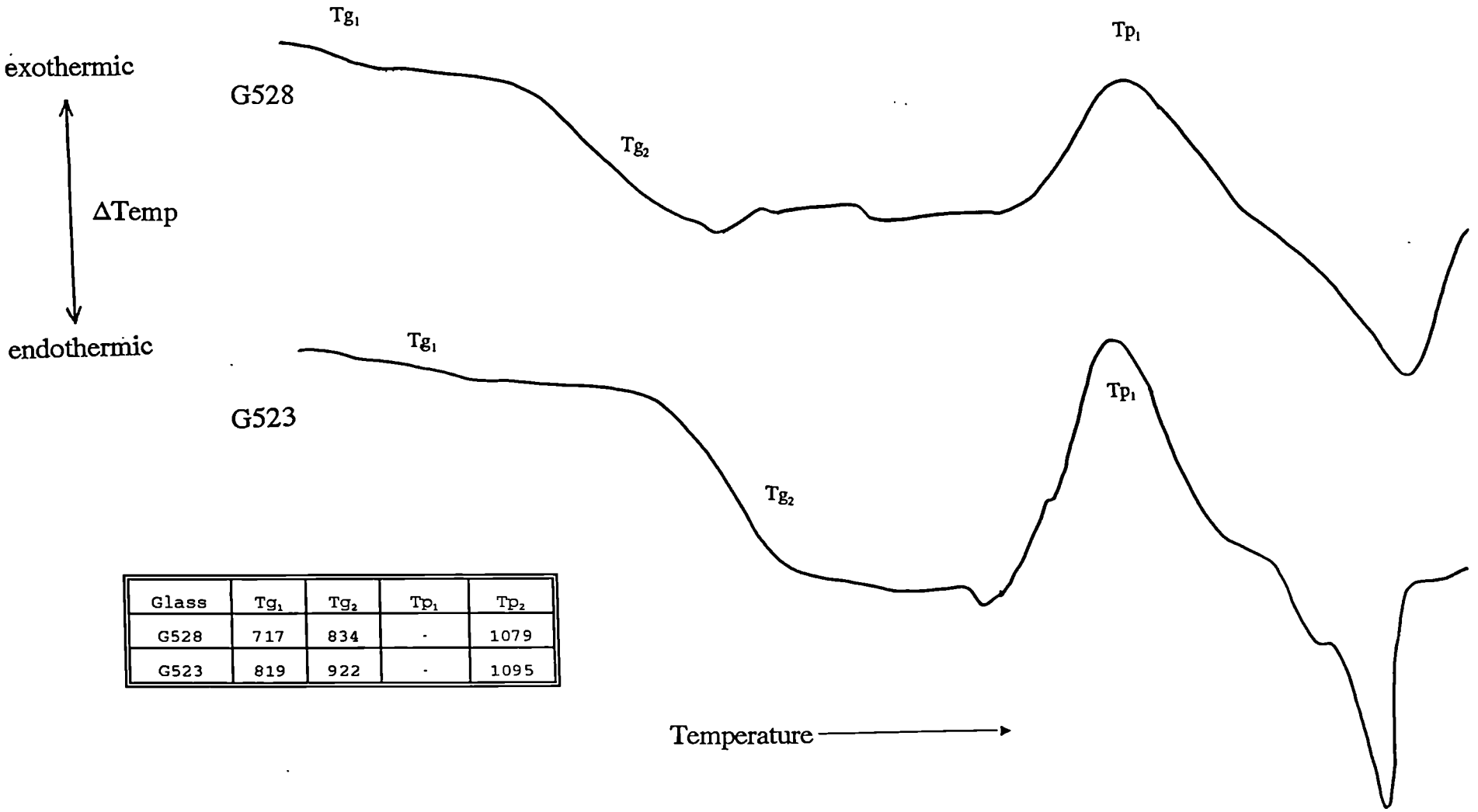

Glass	Tg_1	Tg_2	Tp_1	Tp_2
G528	717	834	-	1079
G523	819	922	-	1095

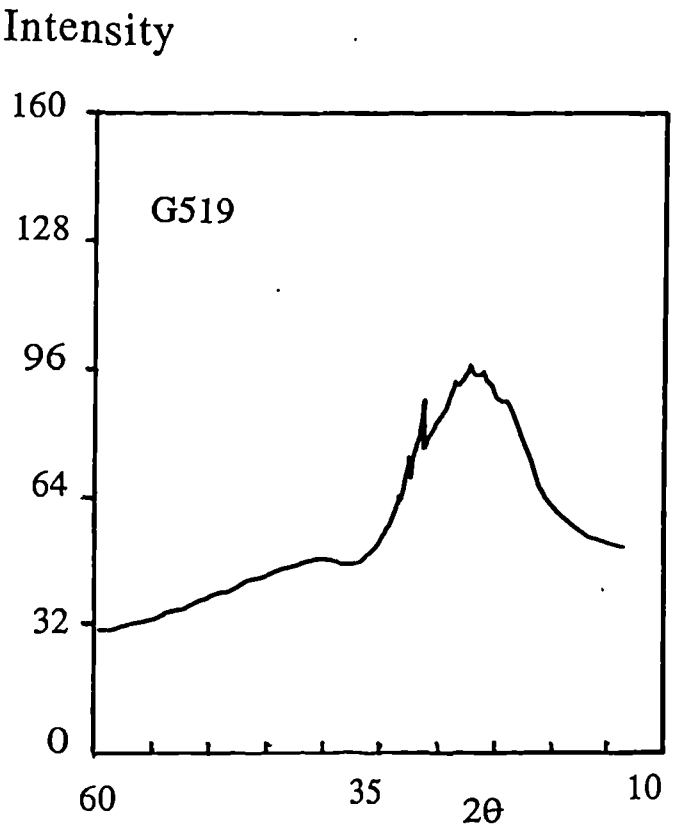

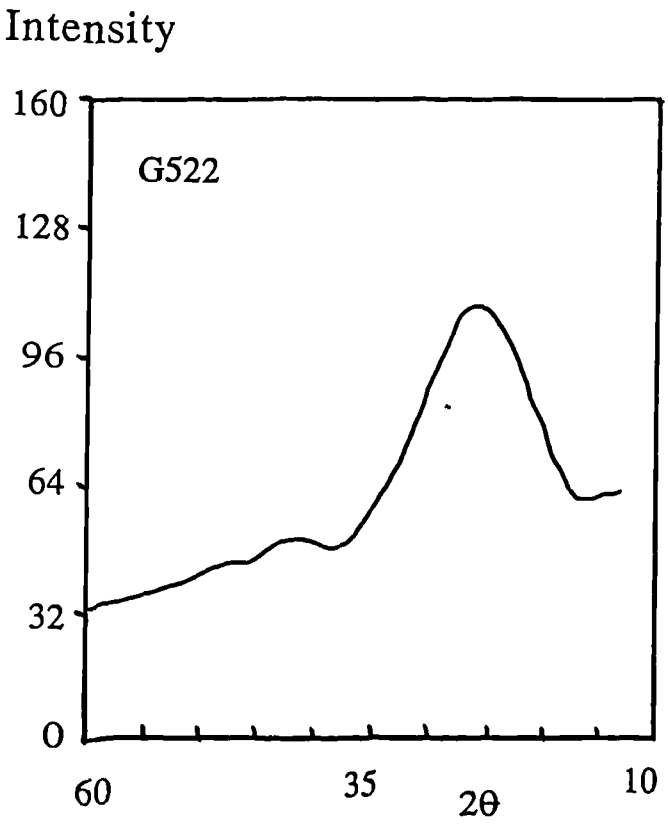

Figure 59 - XRD of Phosphate Containing Glasses

Intensity

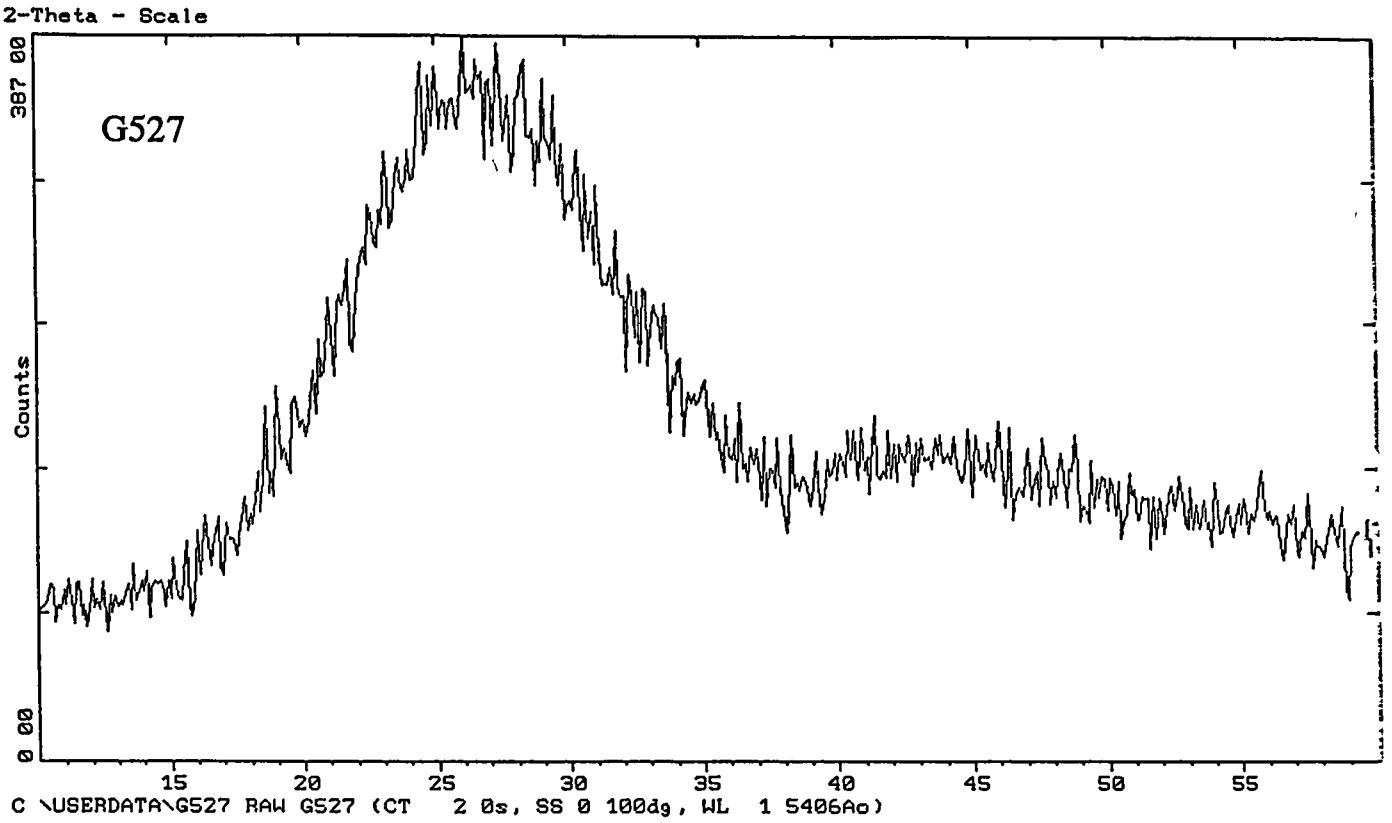

2θ

Intensity

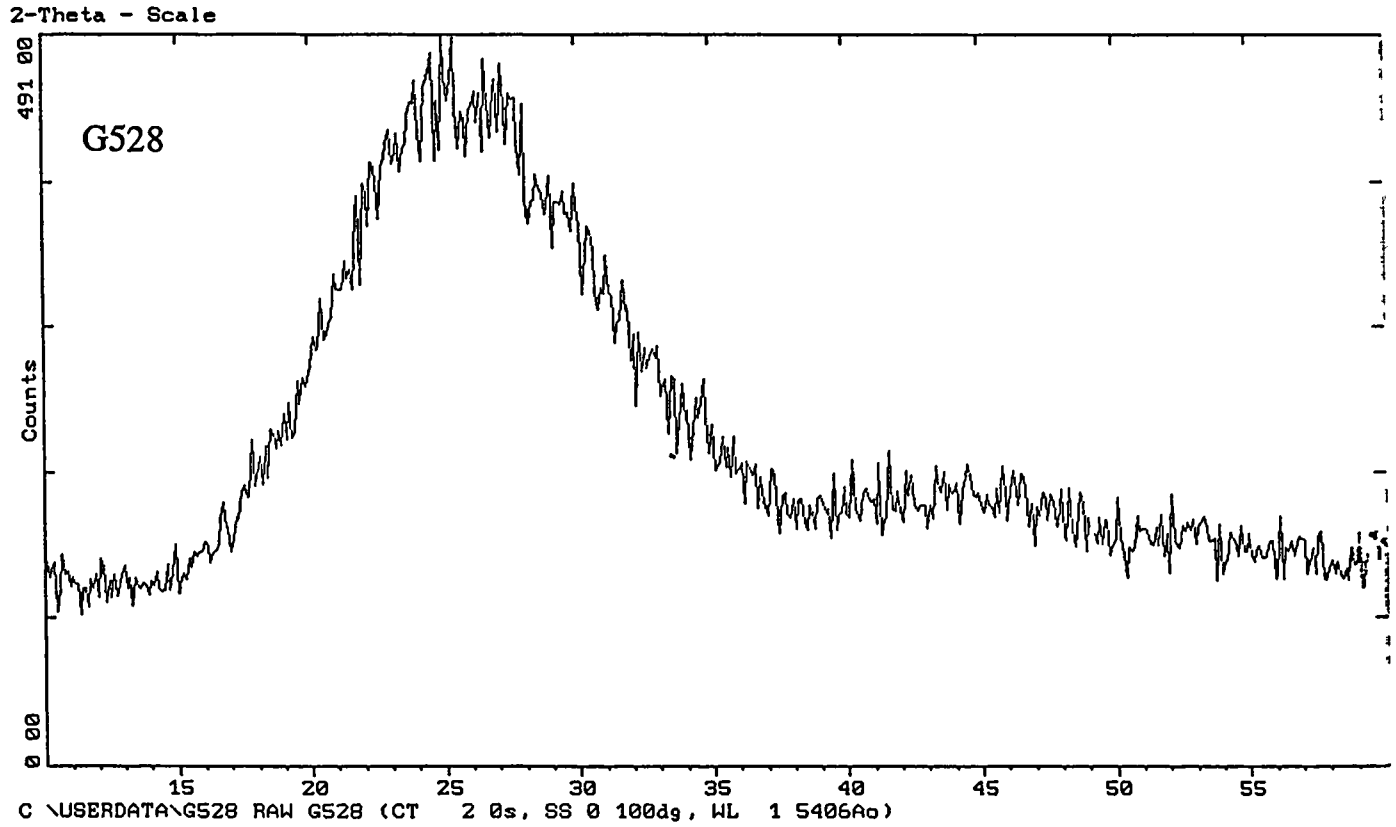

2θ

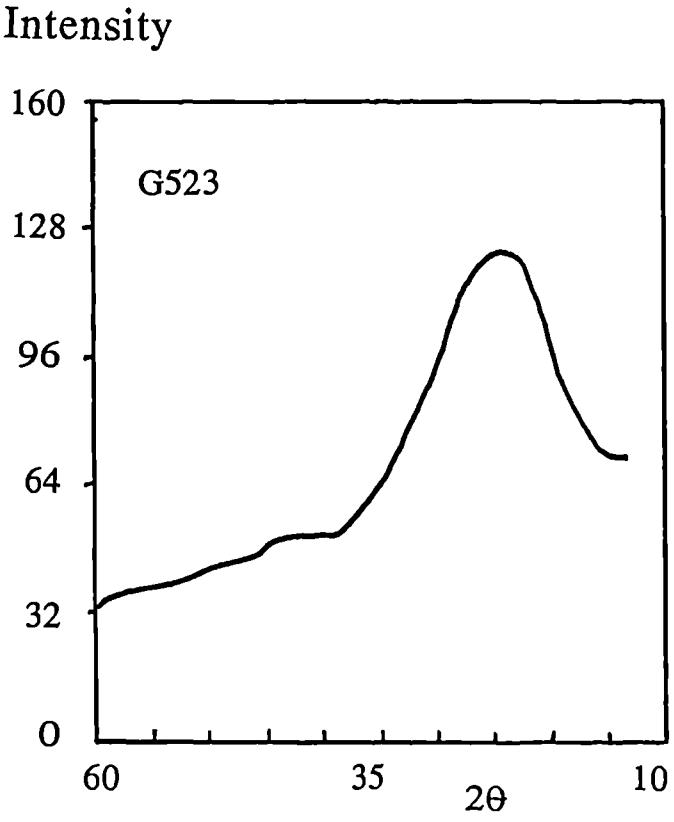
Intensity
160
128
96
64
32
0
G523
60
35
10
2θ

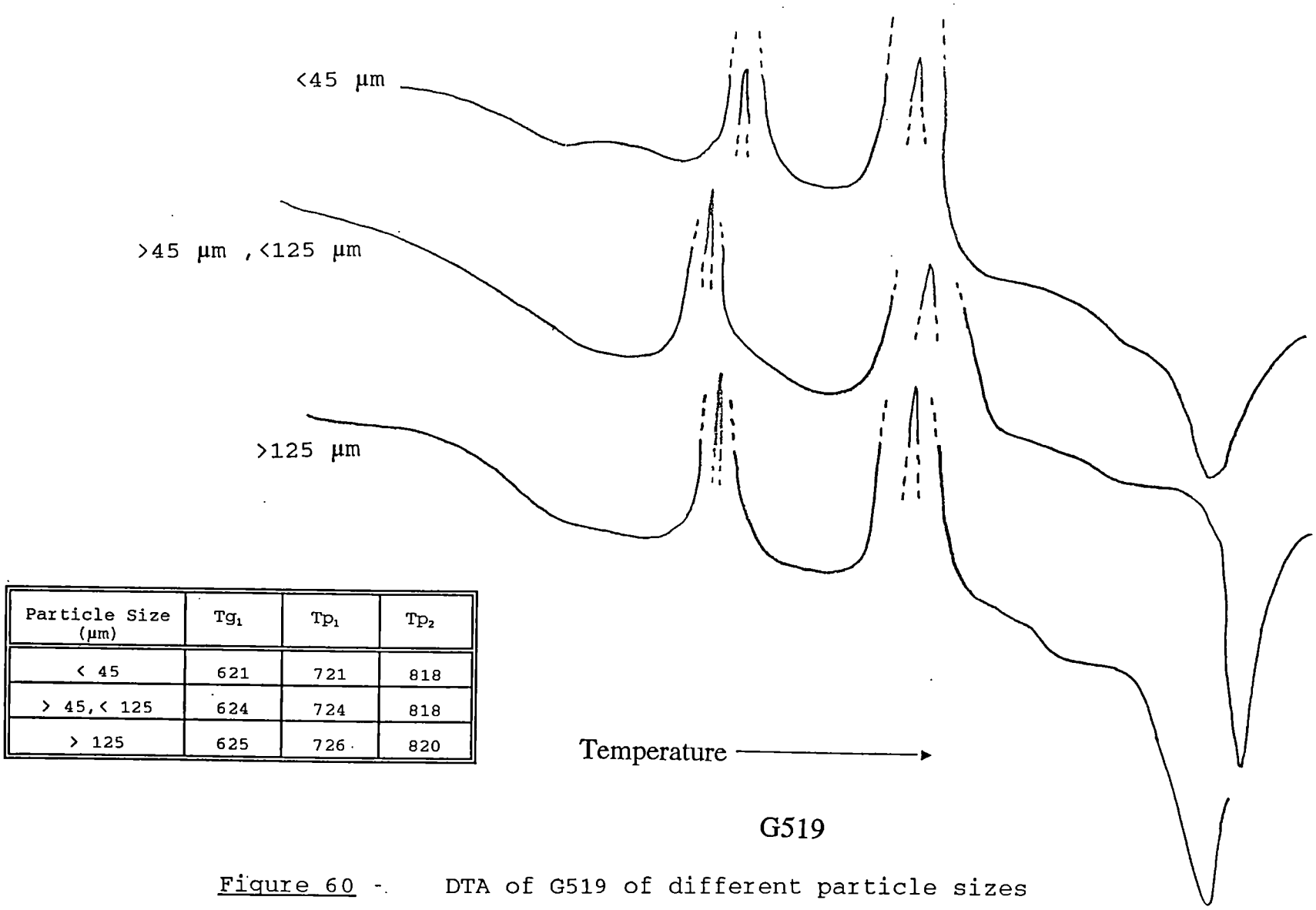

Particle Size (µm)	Tg_1	Tp_1	Tp_2
< 45	621	721	818
> 45, < 125	624	724	818
> 125	625	726	820

Figure 60 - DTA of G519 of different particle sizes

Figure 61 - DTA of G527 of different particle sizes

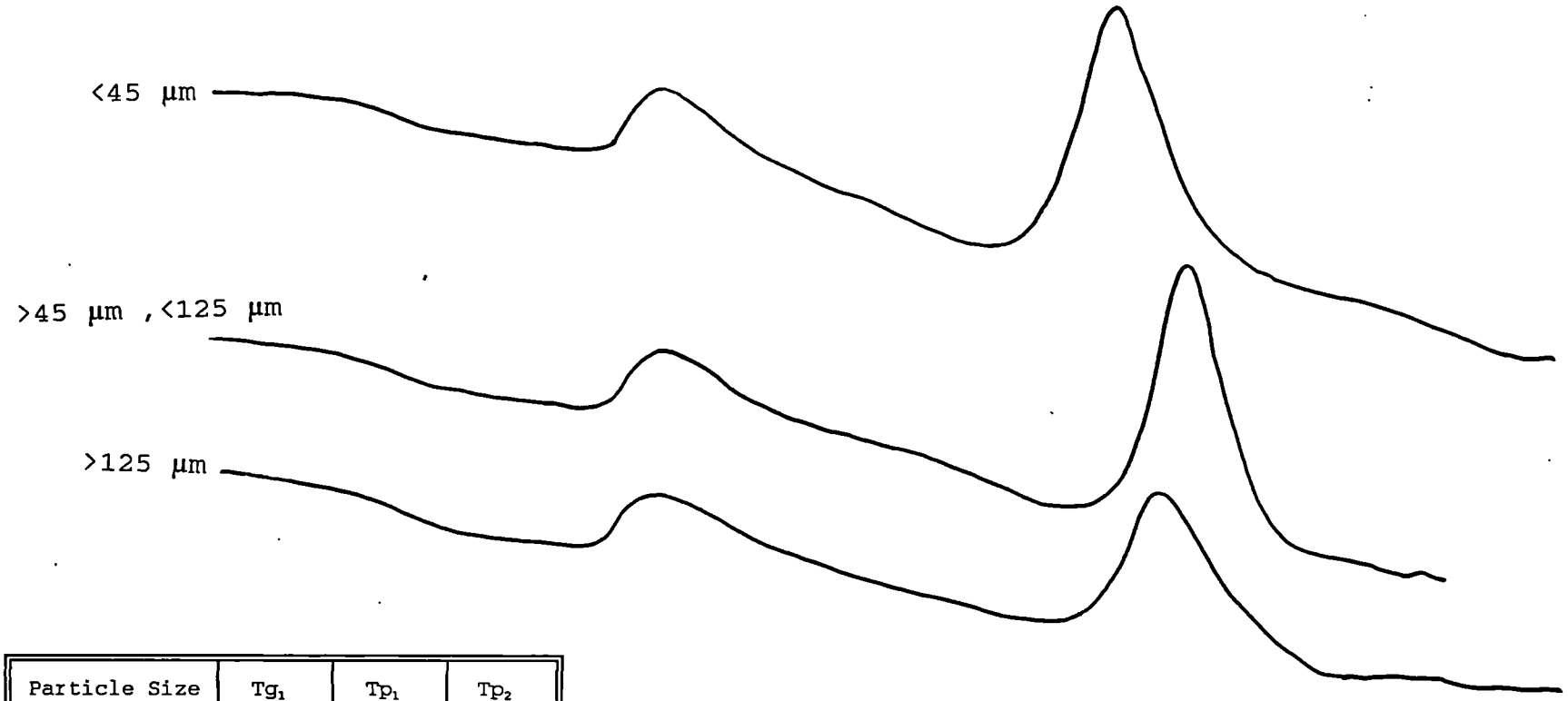

Particle Size (µm)	Tg_1	Tp_1	Tp_2
< 45	640	761	943
> 45, < 125	644	755	963
> 125	644	757	964

G527

Figure 62 - DTA of G522 of different particle sizes

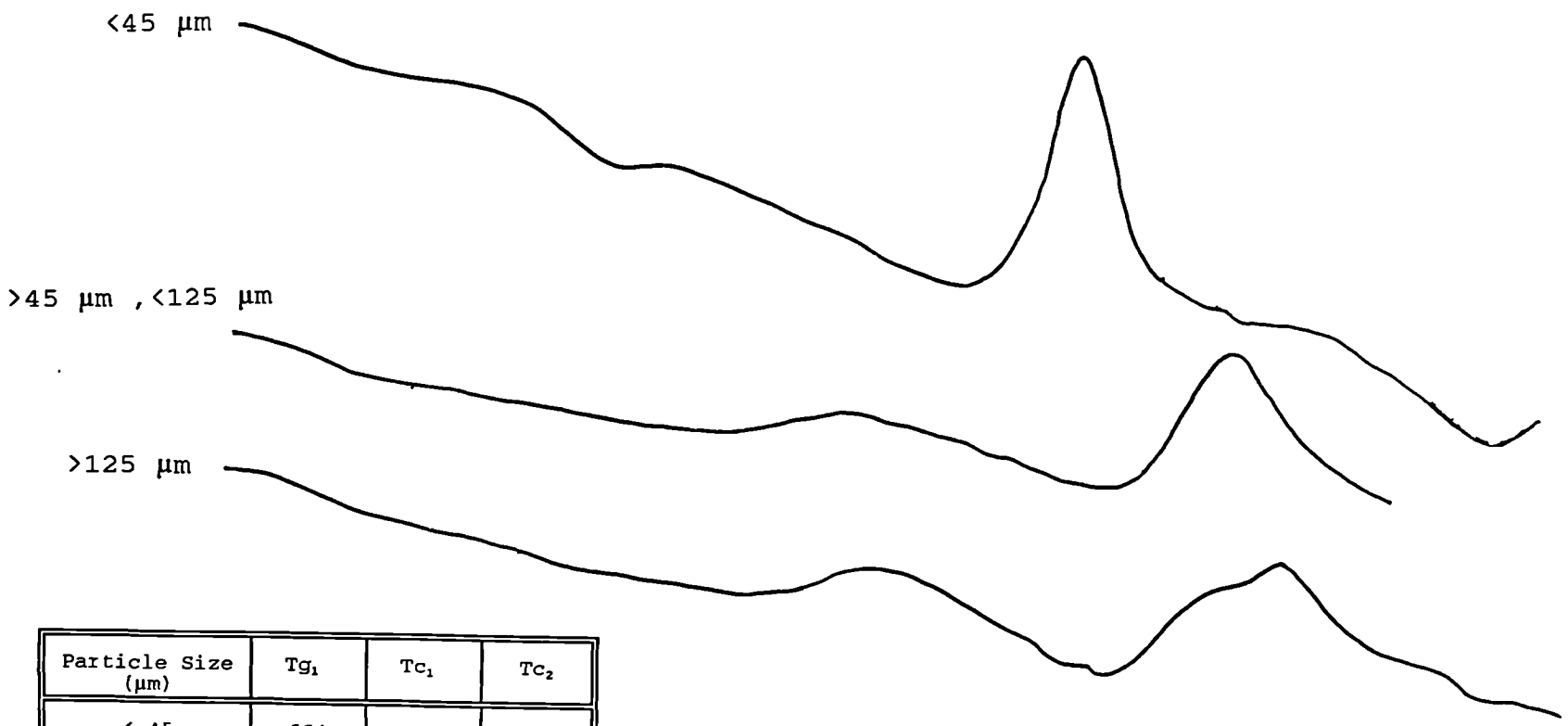

Particle Size (µm)	Tg_1	Tc_1	Tc_2
< 45	664	816	987
> 45,< 125	664	876	1015
> 125	662	923	1037

Figure 63 - DTA of G528 of different particle sizes

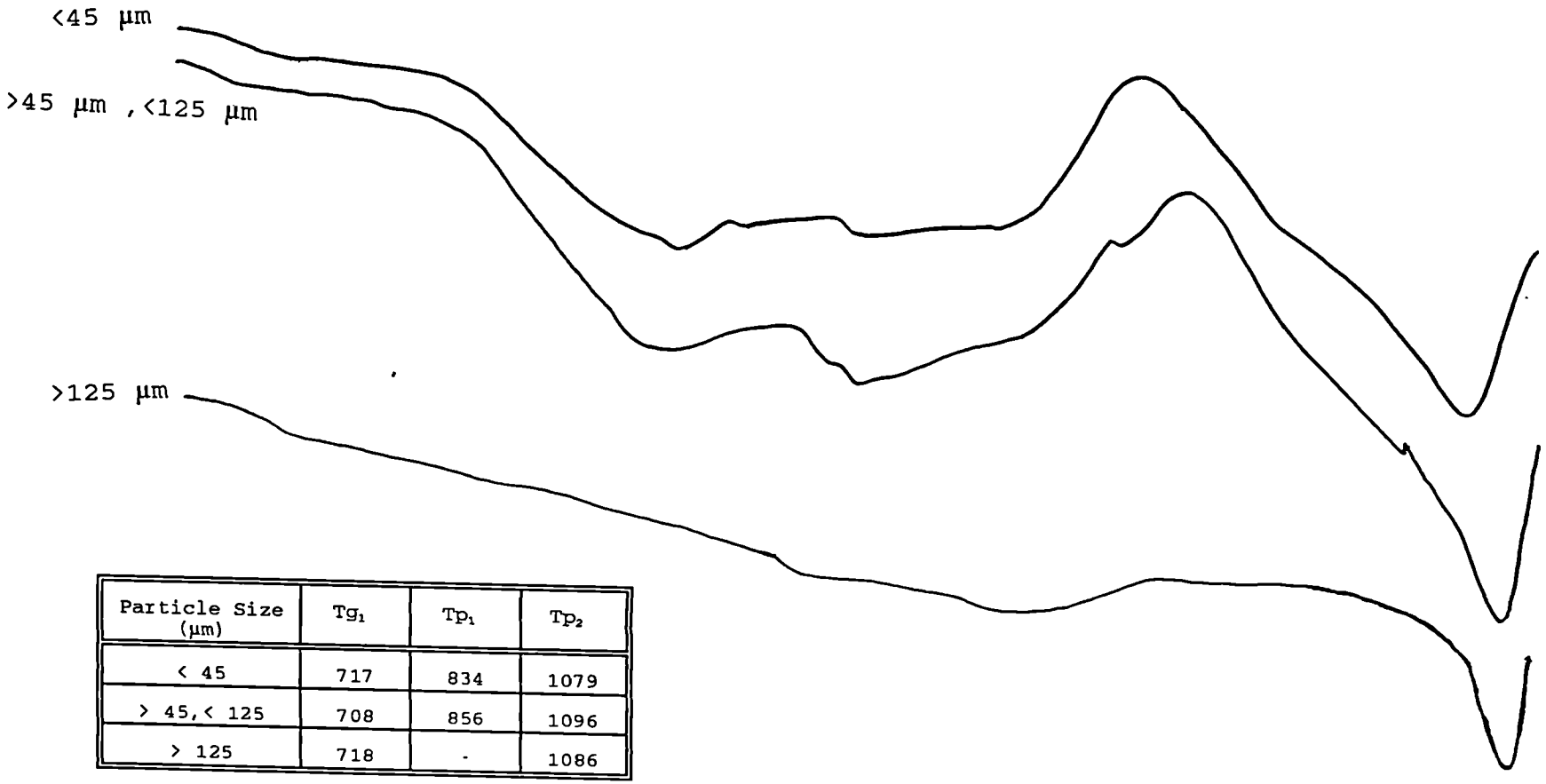

Particle Size (µm)	Tg_1	Tp_1	Tp_2
< 45	717	834	1079
> 45, < 125	708	856	1096
> 125	718	-	1086

G528

Figure 64 - DTA of G523 of different particle sizes

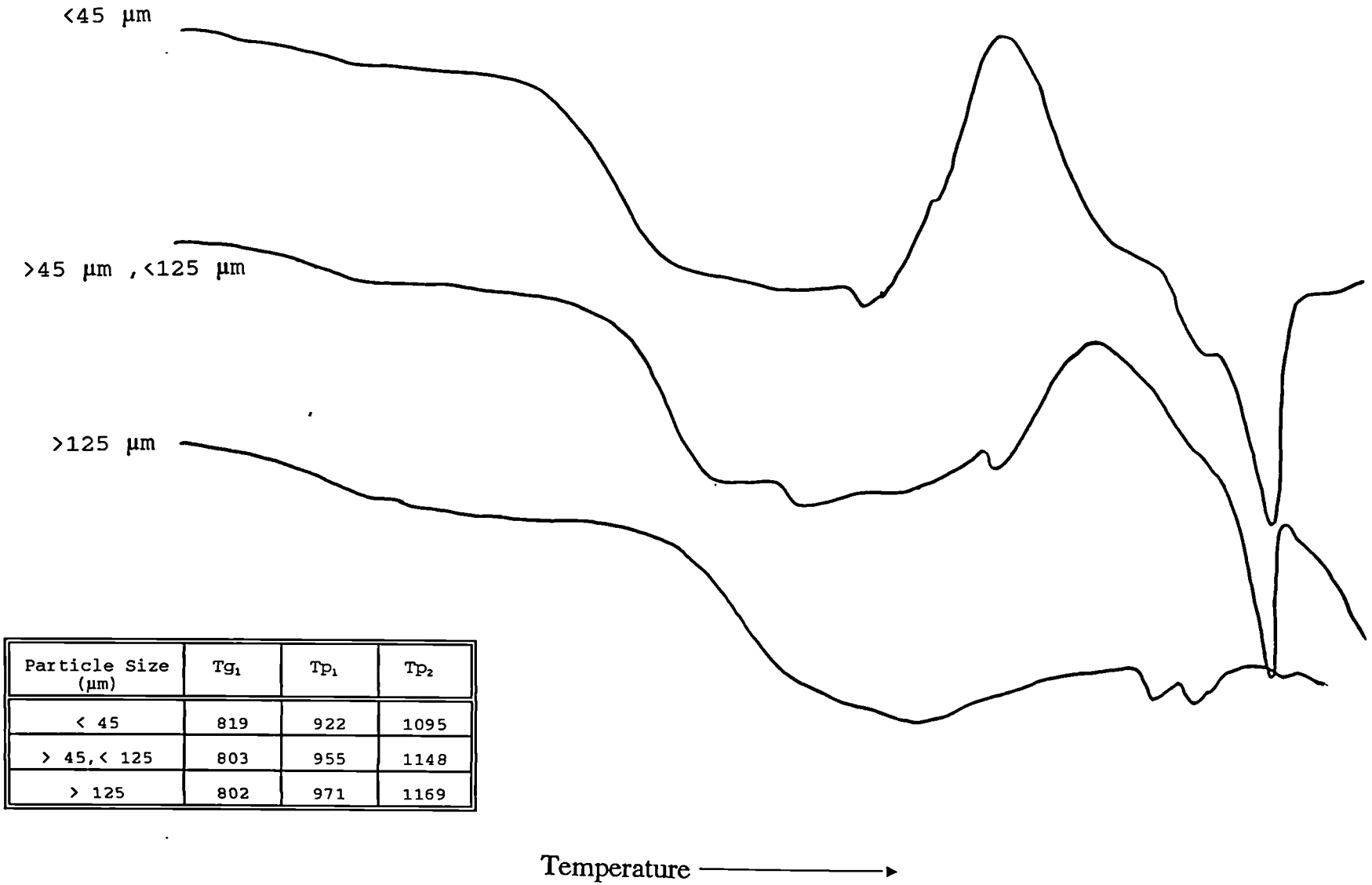

Particle Size (µm)	Tg_1	Tp_1	Tp_2
< 45	819	922	1095
> 45, < 125	803	955	1148
> 125	802	971	1169

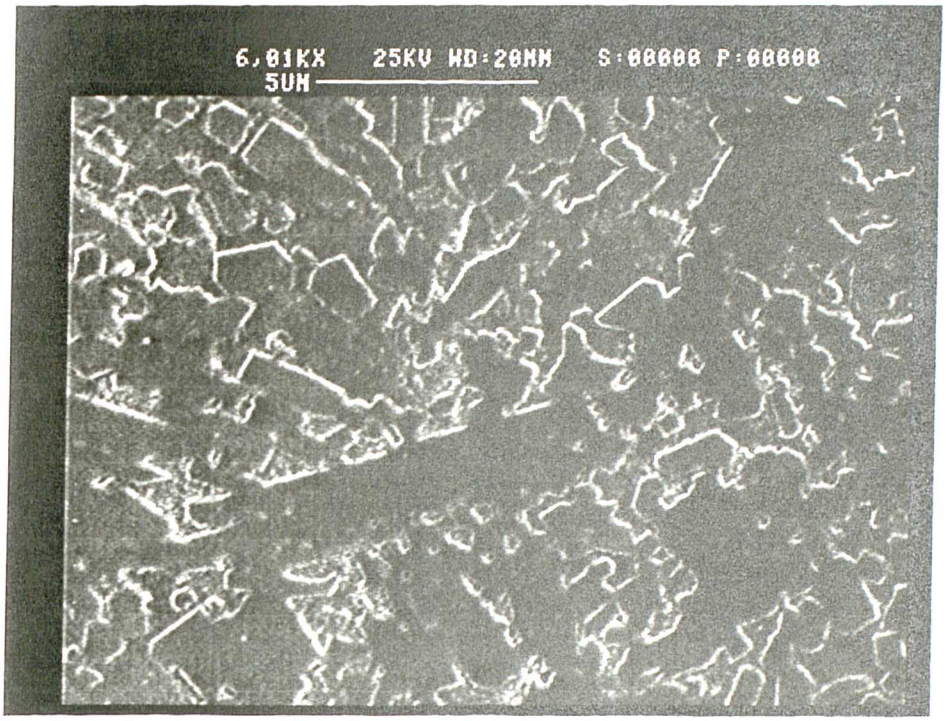

Figure 65-SEM Micrograph of G519

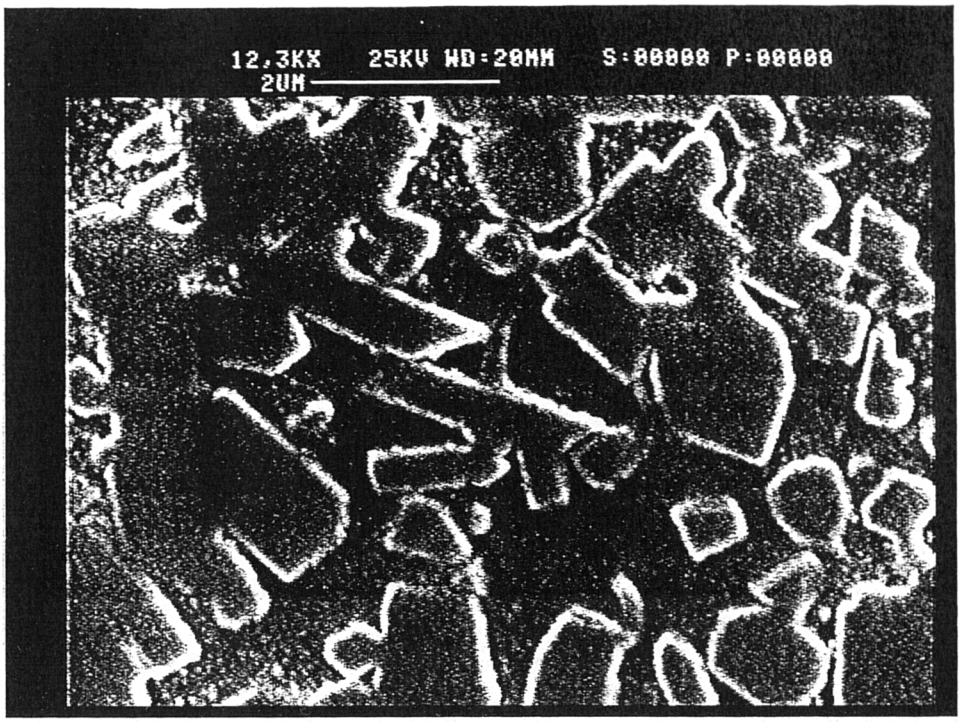
12,3KX 25KV WD:20MM S:00000 P:00000
2UM

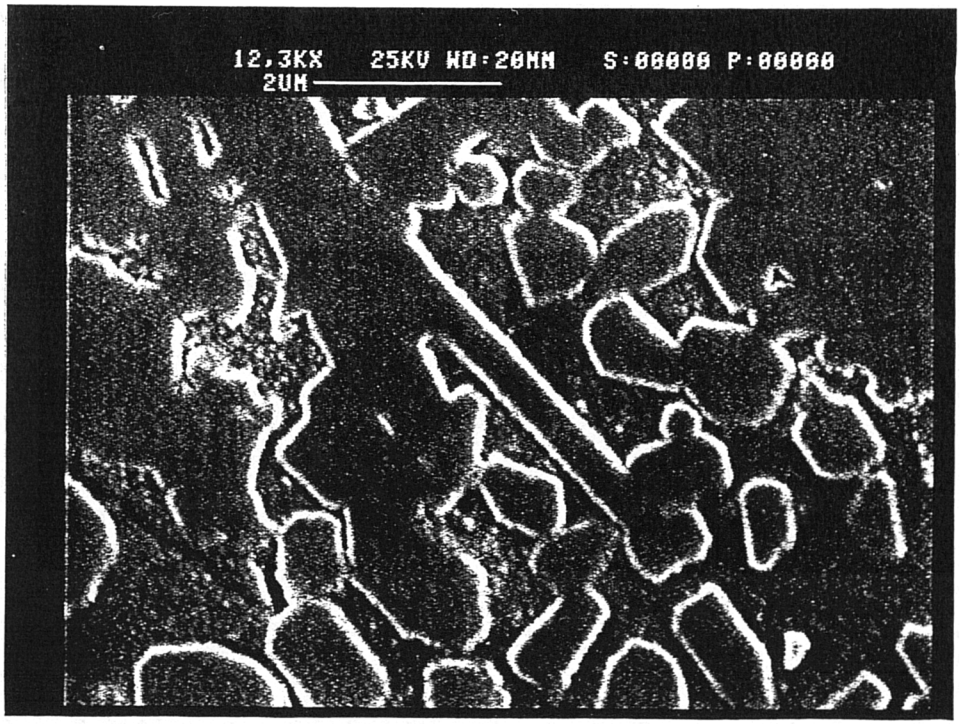
12,3KX 25KV WD:20MM S:00000 P:00000
2UM

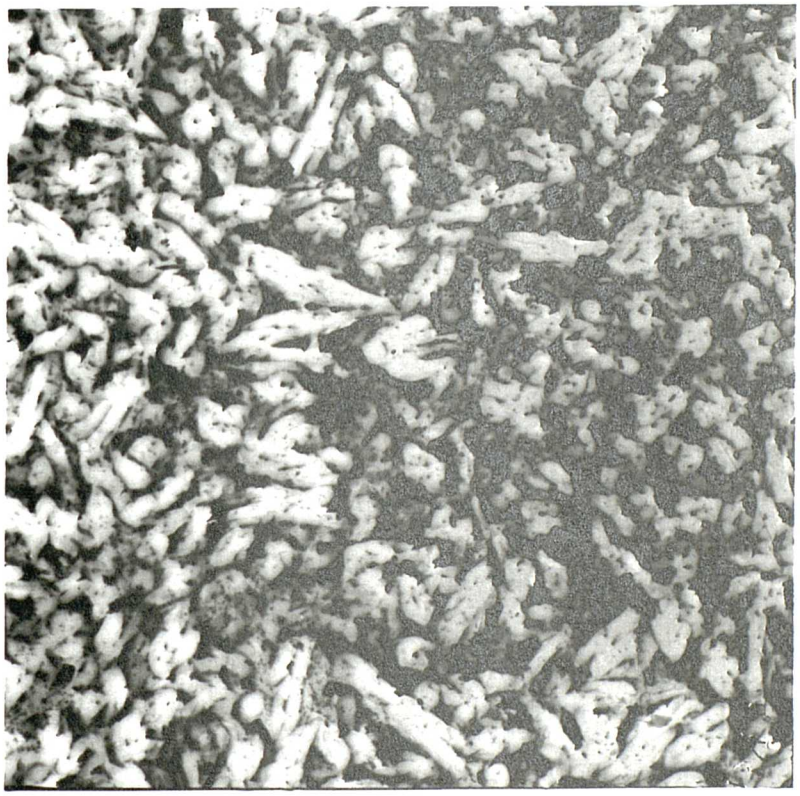

Figure 66-TEM Micrograph of G527

Intensity

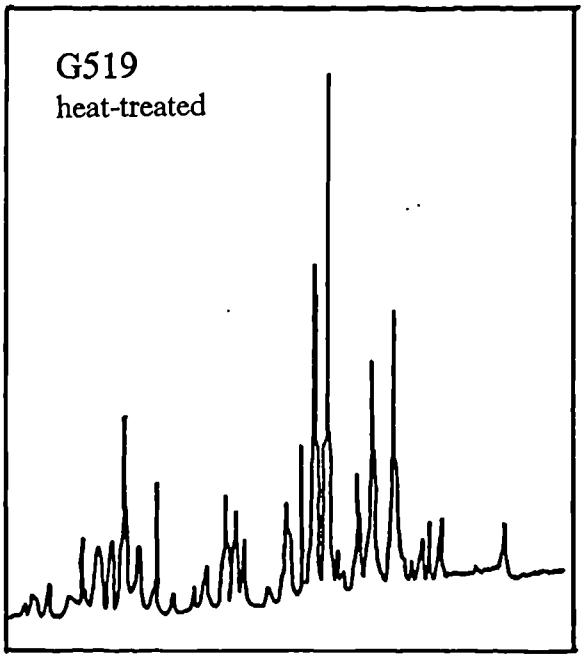

2θ

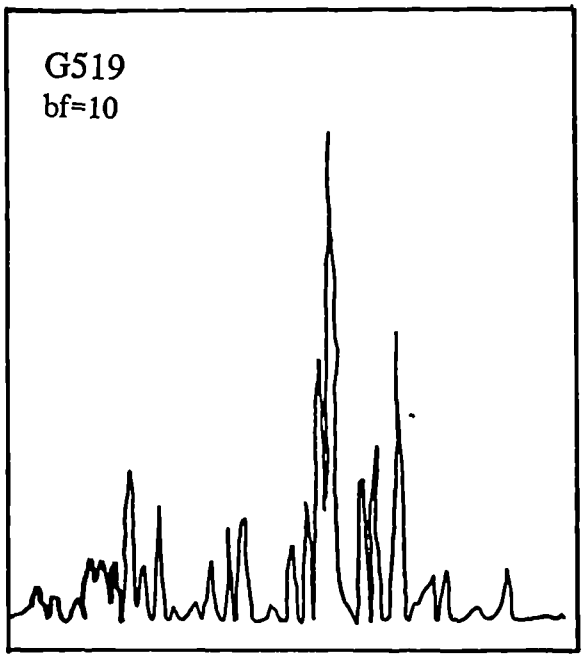

2θ

Figure 67 - Simulation of Heat Treated G519 (bf=10)

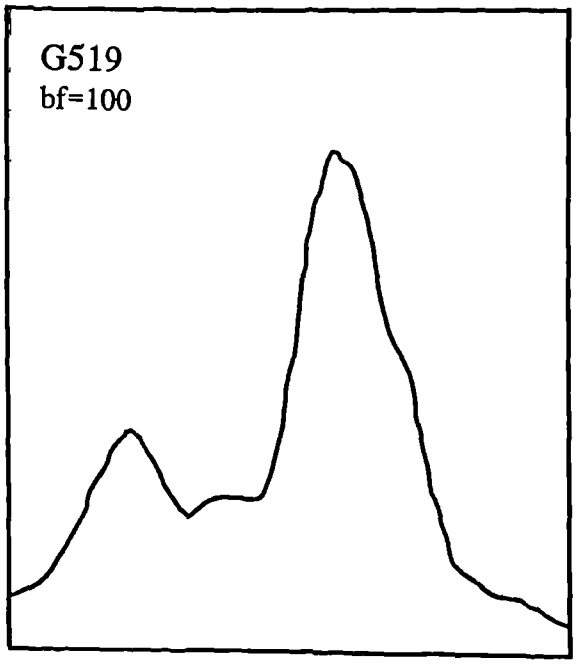

Figure 68 - Simulation of Heat Treated G519

(bf=100 and bf=200)

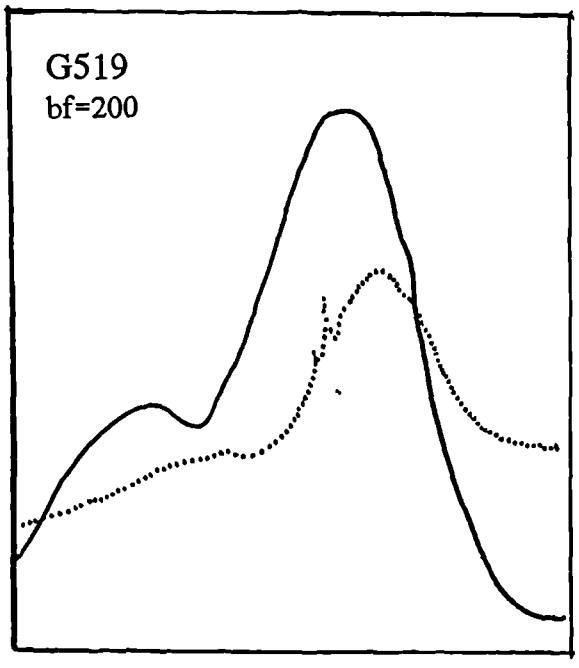

Appendix A

```
REM PROGRAM ZXC
LEAR:CLS
MODE4
PROCTITLES
X=0
REM COMPUTER SIMULATION OF X-RAY DIFFRACTION
REM PROGRAM 1 - PLOTS A SINGLE PEAK AND SAVES
REM IT AS A 500 DATA POINT FILE
REM WRITTEN BY DAVID WOOD
REM LAST MODIFIED 6/8/90
CLS:CLEAR
DIM HEIGHT(501)
INPUT "INPUT THE d SPACING";DS
X=0
Q=1.54/(2*DS)
PP=ASN(Q)
PP=DEG(PP)
PP=2*PP
INPUT "BROADENING FACTOR (0-500)";BF
INPUT "RELATIVE INTENSITY (1-100)";RI
PB=500-((PP-10)/0.1)
Z=180
SP=PB-(BF/2)
FP=PB+(BF/2)
IF SP>0 THEN Y=(-SP*(180/BF)): GOTO320
IF FP>500 THEN Z=(500-(FP*(180/BF)))
FOR B=0 TO SP
HEIGHT(X)=0
X=X+1
NEXT B
Y=0
VG=100
FOR B=Y TO Z STEP (180/BF)
HEIGHT(X)=(SIN(RAD(B))*RI)
X=X+1
IF X = 500 THEN GOTO410
NEXT B
FOR B=X TO 500
HEIGHT(X)=0
X=X+1
NEXT B
PROCAREA
INPUT "FILENAME";F$
Y=OPENOUT F$
PRINT #Y,F$
VG=100
PRINT #Y,VG
PRINT #Y,TOTAL_AREA
FOR X=0 TO 500
PRINT #Y,HEIGHT(X)
NEXT X
CLOSE #Y
INPUT "ANOTHER d SPACING";P$
IF P$= "Y" THEN GOTO100
IF P$="N" THEN PROCCHOICE
IF P$<>"Y" OR P$<>"N" THEN END
DEFPROCAREA
PRINT:PRINT:PRINT
FOR B=0 TO 500
AREA=(((HEIGHT(B))+ (HEIGHT(B+1)))/2)*0.1
TOTAL_AREA=TOTAL_AREA +AREA
NEXT B
PRINT "TOTAL AREA =";TOTAL_AREA
ENDPROC
DEFPROCASD
REM PROGRAM TO MERGE DATA FILES FOR
```

```
REM X-RAY DIFFRACTION SIMULATION
REM LAST MODIFIED 10/8/90
DIM HEIGHT1(501)
PRINT:PRINT:"ENTER INITIAL FILE"
PROCCALLFILE
A=TOTAL_AREA
Y=0
FOR X=O TO 500
HEIGHT1(X)=HEIGHT(X)
NEXT X
PRINT:PRINT"ENTER FILE TO MERGE"
PROCCALLFILE
PROCMERGE
GOTO 760
DEFPROCCALLFILE
INPUT"FILENAME";F$
IF F$="FINISH" THEN PROCSAVEDATA
Y=OPENIN F$
INPUT #Y,F$
INPUT #Y,VG
INPUT #Y,TOTAL_AREA
FOR X=0 TO 500
INPUT #Y,HEIGHT(X)
NEXT X
CLOSE #Y
ENDPROC
DEFPROCMERGE
FOR X-0 TO 500
HEIGHT1(X)=HEIGHT1(X)+HEIGHT(X)
NEXT X
A=A+TOTAL_AREA
ENDPROC
DEFPROCSAVEDATA
INPUT "FILENAME";F$
P=OPENOUT F$
PRINT #P,F$
PRINT #P,VG
PRINT #P,A
FOR X=0 TO 500
PRINT #P,HEIGHT1(X)
NEXT X
CLOSE #P
PRINT "CUMULATIVE AREA =";A
PRINT:PRINT:INPUT"DISPLAY TRACE";T$
IF T$="Y" THEN PROCQW
IF T$<> "Y" THEN GOTO 1230
ENDPROC
ENDPROC
DEFPROCTITLES
PRINT" ************************"
PRINT" * COMPUTER SIMULATION *"
PRINT" *          OF          *"
PRINT" *  X-RAY DIFFRACTION   *"
PRINT" *                      *"
PRINT" * WRITTEN BY D.J.WOOD *"
PRINT" ************************"
FOR T =1 TO 5000:NEXT T
CLS
PRINT" DO YOU WISH TO:"
PRINT" 1. CREATE NEW FILES ?"
PRINT" 2. MERGE FILES TOGETHER ?"
PRINT" 3. LOOK AT MERGED FILES ON SCREEN ?"
PRINT" 4. END ?"
PRINT:INPUT "INPUT C,M,L OR E";Z$
IF Z$="C" THEN CLS:GOTO 100
IF Z$="M" THEN CLS:DIMHEIGHT(501):PROCASD
IF Z$="L" THEN CLS:PROCQW
```

```
IF Z$="E" THEN END
IF Z$<>"C" OR Z$<>"M" OR Z$<>"L" OR Z$<>"E" THEN GOTO1280
ENDPROC
DEFPROCQW
CLS
REM GRAPH
DIMXRD(500)
S1=10:S2=60:S4=0.1
PROCRECALL
PF=0
CLS
PRINT" LOWEST ANGLE =";S1:PRINT"HIGHEST ANGLE =";S2
PRINT" ANGLE INTERVAL =";S4
INPUT" PROCESS DATA FROM (LOW ANGLE)=";ST
INPUT" PROCESS DATA TO (HIGH ANGLE)=";FI
INPUT" PLOT POINTS Y/N";PP$
INPUT" GRAPH VERTICAL MAGNIFIER 1,2,3 ETC. =";VG
PROCGRAPHSCALE
PROCPOINT
MOVE 0,800:PRINT" HARD"
MOVE 0,700:PRINT" COPY"
MOVE 0,600:PRINT" OF"
MOVE 0,500:PRINT"GRAPHICS"
MOVE0,400:INPUT"Y/N";GO$
IF GO$="Y" THEN GOTO 1580
CLS
GOTO 1480
PROCGRAPHSCALE
PROCPOINT
PROCSCREENDUMP
CLS
DEFPROCRECALL
PRINT:PRINT
PRINT TAB(5);"**********************"
PRINT TAB(5);"LOADING DATA FROM DISC"
PRINT TAB(5);"**********************"
PRINT:PRINT:PRINT
INPUT" ENTER DATA FILE NAME (7 LETTERS MAX)";F$
PRINT:PRINT:PRINT" * RECEIVING DATA *"
X= OPENIN F$
INPUT #X,F$
Z=501
INPUT #X,S3
DIMXRD(1000)
FOR I=0 TO (Z-1)
INPUT #X,XRD(I)
NEXT I
CLOSE #X
ENDPROC
DEFPROCPOINT
IF PP$ <>"Y" THEN PLOT 69,250,XRD(INT(((S2-FI)/S4)+1))+128
FOR Q=1 TO (Z-1)
G=(((S2-FI)/S4)+Q)
IF PP$="Y" THEN PLOT 69,((1000/((FI-ST)/S4))*Q)+250, XRD(G)*VG/10)+168
IF PP$<>"Y" THEN DRAW((1000/((FI-ST)/S4))*Q)+250, XRD(G)*VG/10)+168
IF G=(Z-1) THEN GOTO 1880
NEXT Q
ENDPROC
DEFPROCGRAPHSCALE
VDU5:REM WRITE TEXT AT GRAPHICS CURSER
REM SCALES AXES AND PUTS THEM ON GRAPH
FOR I=250 TO 1250 STEP 100
MOVE I,128
DRAW I,113
DRAW I,140
NEXT I
FOR I=250 TO 1250 STEP 500
```

```
MOVE I,128
DRAW I,102
DRAW I,928
MOVE I+3,128:DRAW I+3,102
MOVE I-280,80:PRINT FI-(INT(((FI-ST)/10)*((I-250)/10))/10)
NEXT I
FOR I=128 TO 928 STEP 160
MOVE 250,I
DRAW 235,I
DRAW 262,I:IF I=928 THEN DRAW 1250,I
MOVE -90,I+10
NEXT I
MOVE 250,128:DRAW 250,928
MOVE 250,128:DRAW 1250,128
MOVE 500,30
PRINT "2. THETA(DEGREES)"
MOVE 0,1000
PRINT" INTENSITY(COUNT RATE PER SECOND)"
ENDPROC
DEFPROCSCREENDUMP
LOCALX%,Y%,Z%,M%
VDU2
VDU1,27,1,ASC"1",1,10;0;
FOR Z%=0 TO 312 STEP 8
VDU1,27,1,ASC"K",1,1;:REM ASC"L" FOR CONDENSED
FOR Y%= 9920 TO 0 STEP -320
M%=&5800+Y%+Z%
FOR X%=7 TO 0 STEP-1
VDU1,M%?X%
NEXT:NEXT:VDU1,10;0;
NEXT:VDU1,27,1,ASC"@";0;:VDU3
ENDPROC
ENDPROC
DEFPROCCHOICE
PRINT:PRINT"DO YOU WISH TO MERGE FILES ?"
PRINT:PRINT"OR LOOK AT A FILE ?"
PRINT:PRINT"OR END ?"
INPUT"M,L OR E";C$
IF C$="M" THEN CLS:PROCASD
IF C$="L" THEN CLS:PROCQW
IF C$="E" THEN END
IF C$<>"M" OR C$<>"L" OR C$<>"E" THEN GOTO 2430
ENDPROC
```

APPENDIX B

D. Wood and R. Hill, Biomaterials, 12, (1991), 164

David Wood and Robert Hill, Clinical Materials, 7, (1991), 301

R.G. Hill, M. Patel and D.J. Wood, 'Bioceramics 4', pub. by Butterworth-Heinemann, London, (1991), 79

Robert G. Hill, Christopher Goat and David Wood, J. Am. Ceram. Soc., 75, (1992),778